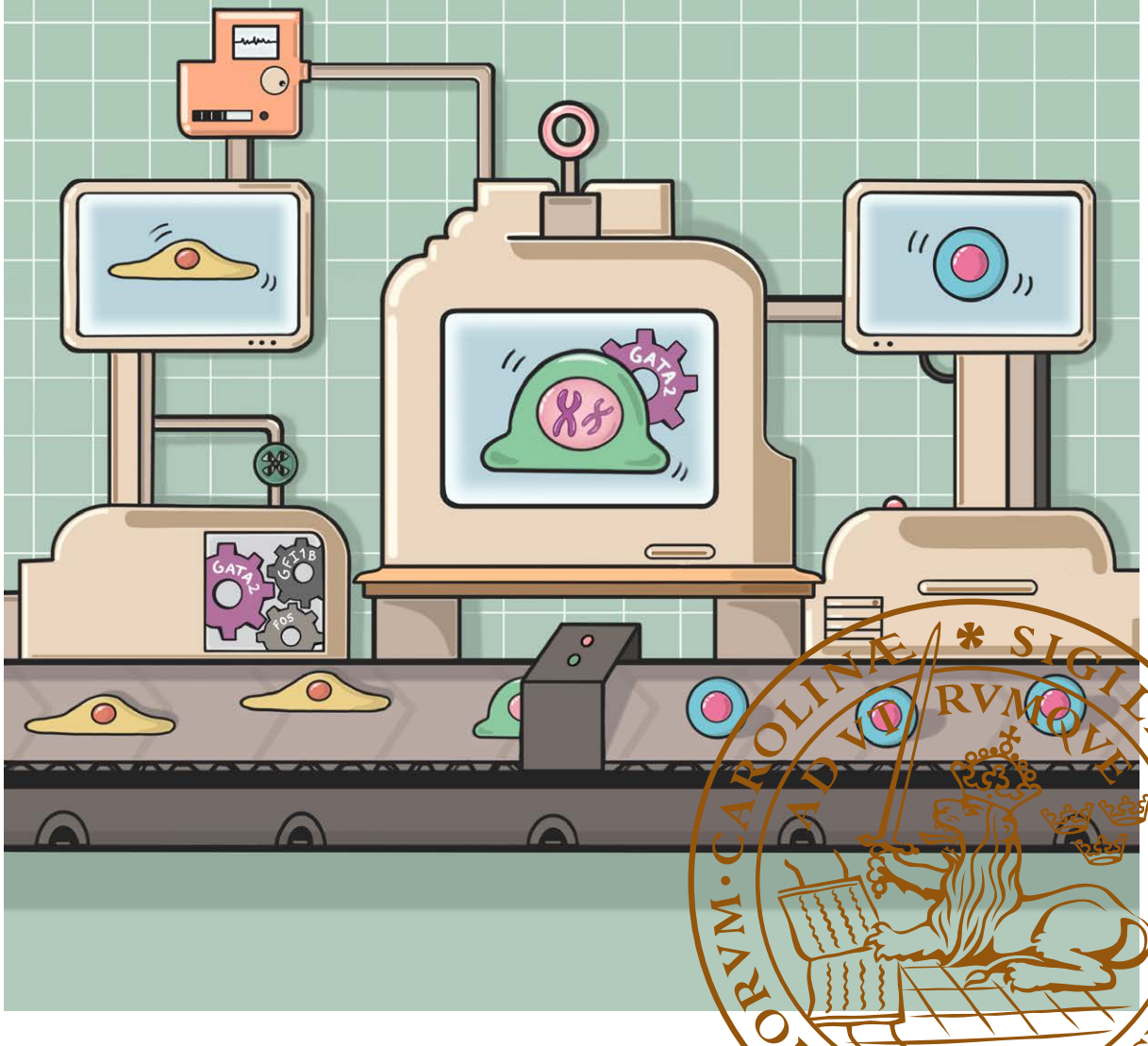


# Mechanisms Underlying the Specification of Definitive Hematopoiesis

RITA ALVES

DEPARTMENT OF LABORATORY MEDICINE | FACULTY OF MEDICINE | LUND UNIVERSITY





## Mechanisms Underlying the Specification of Definitive Hematopoiesis



# Mechanisms Underlying the Specification of Definitive Hematopoiesis

Rita Alves



**LUND**  
UNIVERSITY

1 2



9 0

**UNIVERSIDADE D**  
**COIMBRA**

DOCTORAL DISSERTATION

Doctoral dissertation for the degree of Doctor of Philosophy (PhD) at the Faculty of Medicine at Lund University to be publicly defended on November 3<sup>rd</sup> 2023, at 9.00 in Segerfalksalen, BMC A10, Lund, Sweden

*Faculty opponent*  
Professor Kenneth Zaret  
University of Pennsylvania, USA

**Organization:** LUND UNIVERSITY, Faculty of Medicine, Department of Laboratory Medicine, Division of Molecular Medicine and Gene Therapy

**Document name:** DOCTORAL DISSERTATION

**Date of issue:** 2023-11-03

**Author:** Rita Alves

**Title and subtitle:** Mechanisms Underlying the Specification of Definitive Hematopoiesis

**Abstract:**

Hematopoietic stem cells (HSCs) maintain blood through self-renewal and differentiation. Although HSC transplantation is the only cure for various blood disorders, generating and maintaining HSCs *in vitro* remains challenging, partly due to a limited understanding of the cellular and molecular mechanisms underlying human HSC ontogeny. In embryos, definitive HSCs arise from hemogenic endothelium via an endothelial-to-hematopoietic transition (EHT) in the aorta-gonad-mesonephros (AGM) region and placenta. In humans, limited access to embryos hinders the study of this process. Exploring new methods to mimic hematopoietic development *in vitro* may shed light on the regulators and mechanisms of human HSC specification *in vivo*.

In my thesis, I outlined a protocol for generating hemogenic-like cells with hematopoietic potential from human dermal fibroblasts (HDFs) through direct cell reprogramming. HDFs were transduced with lentiviruses encoding GATA2, GFI1B, and FOS transcription factors (TFs). These three TFs activate hemogenic and hematopoietic transcriptional programs in HDFs, recapitulating EHT and leading to the generation of hematopoietic progeny capable of short-term engraftment in mice. Notably, I showed that the three TFs induce the expression of the HSC marker CD9 at early stages of reprogramming. Thus, human hemogenic reprogramming offers a tractable platform for identifying new markers and regulators of human HSC development.

I then combined hemogenic reprogramming with CRISPR/Cas9 knockout screening to identify regulators. I transduced HDFs with lentivirus encoding Cas9 and a single guide RNA library targeting over 100 genes related to HSC function. In parallel, I optimized the delivery of the three TFs in a single polycistronic vector at a defined stoichiometry, where high levels of GATA2 and GFI1B induced reprogramming efficiently. After Cas9-edited cells underwent hemogenic reprogramming, my colleagues and I isolated both successfully and unsuccessfully reprogrammed cells based on the expression of CD49f and CD9 for next-generation sequencing. Surprisingly, we identified two markers of hemogenic endothelium and HSCs, CD34 and CD44, as barriers to hemogenic reprogramming, while STAG2 was uncovered as a facilitator of the process. These results suggest that commitment to human hemogenic and hematopoietic identity may benefit from time-wise inhibition of CD34 and CD44 signaling.

Finally, I set out to uncover a less appreciated role of TFs *in vivo* using definitive hematopoiesis as a model. Several TFs remain bound to chromatin during mitosis and mark specific genomic sites – a mechanism termed “mitotic bookmarking”. Mitotic retention and bookmarking have been associated with the maintenance of pluripotency, cell reprogramming, and the preservation of somatic lineages *in vitro*, but the relevance for lineage commitment *in vivo* remains to be addressed. Here, I assessed the mitotic retention of hemogenic reprogramming TFs using fluorescent fusion proteins and subcellular protein quantification. Live-cell imaging and western blotting showed that GATA2 remains bound to chromatin in mitosis via C-terminal zinc finger-mediated DNA binding, as opposed to GFI1B and FOS. Moreover, GATA2 bookmarks a subset of its interphase sites with a higher density of GATA2 motifs, which include key regulators of hematopoietic fate. To uncover the role of GATA2 at mitotic exit *in vivo*, we generated a mouse model with the mitosis-degradation domain of cyclin B1 inserted upstream the *Gata2* gene. Remarkably, homozygous mice died during development, partially phenocopying *Gata2* null mice, which die at the onset of definitive hematopoiesis. Interestingly, removing GATA2 at mitosis-to-G1 transition impacts AGM and placental hematopoiesis but not yolk sac hematopoiesis. Altogether, these findings implicate GATA2 as a mitotic bookmarker critical for definitive hematopoiesis and underscore a dependency on bookmarkers for *in vivo* lineage commitment.

Overall, my thesis provides new insights on the molecular mechanisms underlying the specification of definitive hematopoiesis. In the future, harnessing these mechanisms may enable the faithful generation of patient-tailored HSCs to meet clinical demands.

**Key words:** Mitotic bookmarking, TFs, GATA2, hemogenic reprogramming; HSCs, EHT

**Language:** English

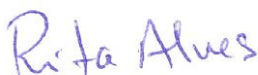
**ISSN:** 1652-8220

**Number of pages:** 111

**ISBN:** 978-91-8021-468-1

I, the undersigned, being the copyright owner of the abstract of the above-mentioned dissertation, hereby grant to all reference sources permission to publish and disseminate the abstract of the above-mentioned dissertation.

Signature



Date 2023-09-21

# Mechanisms Underlying the Specification of Definitive Hematopoiesis

Rita Alves

Cell Reprogramming in Hematopoiesis and Immunity Lab  
Division of Molecular Medicine and Gene Therapy  
Department of Laboratory Medicine  
Faculty of Medicine, Lund University, Sweden

&

Cell Reprogramming in Hematopoiesis and Immunity Lab  
Center for Neuroscience and Cell Biology  
University of Coimbra, Portugal



**LUND**  
UNIVERSITY



UNIVERSIDADE D  
**COIMBRA**

Cover art by Rita Alves, inspired by an image generated using Microsoft Bing Image Creator,  
powered by DALL-E

Copyright pp 1-111: Rita Alves

Paper 1 © Journal of Visualized Experiments (JoVE)

Paper 2 © by the Authors (Manuscript unpublished)

Paper 3 © Nature Communications

Reproduced with permission from Springer Nature and JoVE

ISSN 1652-8220

ISBN 978-91-8021-468-1

Lund University, Faculty of Medicine Doctoral Dissertation Series 2023:126

Printed in Sweden by Media-Tryck, Lund University

Lund 2023



Media-Tryck is a Nordic Swan Ecolabel  
certified provider of printed material.  
Read more about our environmental  
work at [www.mediatryck.lu.se](http://www.mediatryck.lu.se)

**MADE IN SWEDEN** 



To my husband, João

*“Happiness (is) only real when shared.”*

From the movie *Into the Wild*

# Table of Contents

<b>Acknowledgments</b> .....	<b>10</b>
<b>List of Papers</b> .....	<b>13</b>
Papers included in this thesis .....	13
Papers not included in this thesis .....	14
<b>Author’s contribution to the papers</b> .....	<b>15</b>
<b>Abbreviations</b> .....	<b>16</b>
<b>Abstract</b> .....	<b>19</b>
<b>Resumo em Português</b> .....	<b>21</b>
<b>Lay Summary</b> .....	<b>23</b>
<b>Populärvetenskaplig sammanfattning</b> .....	<b>25</b>
<b>Hematopoiesis</b> .....	<b>27</b>
The hematopoietic hierarchy.....	27
<b>The waves of developmental hematopoiesis</b> .....	<b>29</b>
The first wave – Primitive hematopoiesis.....	29
The second wave – Pro-definitive hematopoiesis.....	30
The third wave – Definitive hematopoiesis .....	31
Transcriptional control of developmental hematopoiesis .....	33
<b>GATA2 role in normal and malignant hematopoiesis</b> .....	<b>35</b>
<b>Hematopoietic Stem Cells</b> .....	<b>38</b>
Isolation of hematopoietic stem cells.....	39
Functional assessment of hematopoietic stem and progenitor cells .....	41
Clinical applications of hematopoietic stem cells.....	42
<i>In vitro</i> approaches to generate definitive hematopoietic stem cells ..	43
<b>Cell fate reprogramming</b> .....	<b>45</b>
Direct cell reprogramming by transcription factors.....	46
Direct cell reprogramming towards hematopoietic fates .....	47

<b>The CRISPR/Cas9 system .....</b>	<b>50</b>
Discovery and mechanism of CRISPR/Cas complexes.....	50
Applications of CRISPR/Cas9.....	52
Genetic models.....	52
Gene therapy .....	52
Genomic screenings .....	53
<b>Transmission of cell fates through mitosis.....</b>	<b>55</b>
Mitotic retention and bookmarking by transcription factors .....	56
Transcription factor binding (un)specificity during mitosis .....	58
Methods to study mitotic retention and bookmarking .....	59
<b>Aims of the thesis.....</b>	<b>62</b>
<b>Summary of results .....</b>	<b>63</b>
Study I – Hemogenic Reprogramming of Human Fibroblasts by Enforced Expression of Transcription Factors .....	63
CD9 is a prospective marker of human hemogenic precursor cells....	63
Study II – Identifying Novel Regulators of Hemogenic Reprogramming with CRISPR/Cas9 Knockout Screening.....	65
Optimization of a CRISPR/Cas9 lentiviral delivery system for gene knockout during human hemogenic reprogramming. ....	65
CRISPR/Cas9 screening identifies regulators of human hemogenic reprogramming .....	68
Study III – GATA2 Mitotic Bookmarking is Required for Definitive Hematopoiesis.....	71
GATA2 is retained in mitotic chromatin through C-terminal zinc finger-mediated DNA binding .....	71
GATA2 bookmarks regulators of hematopoietic stem and progenitor cell development and function .....	74
GATA2 is necessary at mitosis-to-G1 transition for definitive hematopoiesis <i>in vivo</i> .....	76
<b>Discussion and future directions.....</b>	<b>80</b>
<b>References .....</b>	<b>87</b>

# Acknowledgments

Doing a PhD is like riding a roller-coaster (but the track is on fire). Although there were many ups and downs, being surrounded by the right people made the ride much more memorable.

I would like to start by thanking my supervisor, **Filipe Pereira**, for giving me the opportunity to continue doing science alongside him. Thank you for your guidance and for creating an exciting environment that has allowed me to grow. I am especially thankful for our brainstorming sessions and for granting me the freedom to explore my own ideas. Your vision and ambition have continuously inspired me to overcome the challenges in my path. Thank you for recognizing the curiosity-driven scientist in me and for supporting my decisions.

I would also like to thank my co-supervisor, **Jonas Larsson**, for sharing his knowledge with me and for always being available to provide feedback on my work, as well as for handling somewhat boring bureaucratic tasks when needed. The same kind of appreciation can be extended to my co-supervisor at the University of Coimbra, **João Ramalho Santos**.

To my Pereira Lab mates – **Abigail, Alex, Beatriz, Camila, Daniel, Diogo, Ervin, Evelyn, Gabriela, Ilia, Inês, Lavínia, Luís, Malavika, Mariana, Nejc, Olga, Pedro, Radha, Rita, Robin, Stefanie, Susana** and **Tomasso** - thank you all for being an amazing team and for helping me get where I am today. I am truly glad to be surrounded not only by colleagues but, more importantly, friends. It pains me to think that I will eventually part from this incredible group of people. In particular, I would like to thank **Ilia** for his precious help during this time. If I was able to publish and complete this thesis, it is largely thanks to you. Thank you for always answering my questions about sequencing data, even the less smart ones. I want to extend my thanks to **Olga**, for teaching me to seize the day and for showing me that there is more to Sweden than meets the eye. It might not sound like much, but you made me enjoy the Swedish summer, and in doing so, you made me miss Portugal a little bit less. **Cami**, I see you as a role model in both science and life. You encouraged me to be fearless and true to myself. Thank you for believing in me when I found it hard to do so. Thank you, **Abby, Luís** and **Ervin** for brightening my days with your sense of humor, making stressful times more manageable and helping me feel laid-back, while still taking lab work seriously. Working long hours is easier with friends. “We’re all in this together” after all. Also, thank you so much for the amazing

barbecues. Thank you, **Nejc**, for your insightful comments and suggestions, and **Evelyn**, for always being there to lend a hand, even when you were busy. Thanks to the no-longer master's students, **Diogo** and **Malavika**, for helping me recall the basics that can sometimes be forgotten. **Inês**, thank you for listening to my rants and indecisions, and for your support during tough situations, despite going through hard times yourself. Thank you for the sharing and caring, as well as for our talks about the future. I am really glad we became friends after knowing each other for so long. I am also thankful for all your creative input into my projects. Don't ever lose that artistic side of yours. Finally, **Gabi**, thank you for being my long-lasting companion on this journey. We have laughed and cried together, had our ups and downs and ups again, and now we are both finally approaching the finish line. I couldn't be prouder of us. Thank you for your honesty, understanding and unbreakable friendship.

To two very important past lab members who embarked on this adventure alongside me, **Cristiana** and **Fábio**, thank you for these years. **Cris**, your laughter and enthusiasm are truly contagious. You always recognized the strengths of my work when I couldn't see them myself. Thank you for reminding me of my achievements. **Fábio**, besides the scientific discussions of each other's work, you gave me some of my funniest memories outside the lab. Thank you for always making it a great time when we are together. You are an example of hard work, determination, and humility, one I strive to follow.

I want to thank my former students, **Jakob**, **Nina**, **Aida**, and **Louise**, for not only directly contributing to this work but also for showing me what is expected from a mentor in the lab. You taught me patience and helped me understand the responsibility of guiding young, critical minds.

Thanks to all my **A12 colleagues** who have made the BMC a collaborative yet casual workplace, especially **Pavan** for his friendship, and **Anna R.**, with whom I had the pleasure of working and learning. Also, thanks to the PIs who contributed with suggestions to my research and provided advice for the future, particularly **Jörg**, **Niels-Bjarne**, and **Mattias**. I want to express my gratitude towards **Xiaojie** and **Ineke** for always showing me where things are, even after all these years, and for keeping the A12 on track.

This project couldn't be completed without the help of a few people outside A12. Thank you, **Zhi** and **Anna F.**, for the troubleshooting and patience when I wasn't so lucky during my sorting or flow cytometry experiments. Thank you, **Rosa-Linda**, for always handling and caring for my mice, making my life easier. Special thanks to **Javier** and **Rafael** for the great partnership and openness to informal discussions and lab visits, as well as to **Marella** for her extraordinary scientific insights and cooperation. Special thanks to **Amanda Fisher** and group members for welcoming me to their lab for a brief period, providing me with the opportunity to experience a distinct yet highly enriching scientific and cultural environment.

*Um grande agradecimento aos meus **pais** que me viram voar para longe e que, apesar da distância, me continuaram a apoiar incondicionalmente. Quero agradecer especialmente à minha **mãe e irmã** por me continuarem a aturar, mesmo que por telemóvel, e por nunca me deixarem desanimar. Às minhas amigas **Rita, Nádia e Vânia**, obrigado por estarem presentes nos momentos mais importantes e por me fazerem sentir que também faço parte das vossas vidas.*

Lastly, I would like to thank the most important person in my life - my then boyfriend and now husband, **João** - for everything. Six years ago, I asked you to come with me to Sweden, and you never looked back. You have contributed to this work more than I can put into words. You gave me courage to face my fears and doubts. You patiently listened to me talk about my research, even though you couldn't understand a word of it, and yet you read it and helped me improve it. You made Sweden our home. This has been the most challenging journey I've endured, and you kept me grounded and sane through it all. I couldn't have done this without you by my side. From the bottom of my heart, thank you.

# List of Papers

## Papers included in this thesis

### *Paper I*

**Silvério-Alves, R.**, Gomes, A.M., Kurochkin, I., Moore, K.A., Pereira, C.F. Hemogenic Reprogramming of Human Fibroblasts by Enforced Expression of Transcription Factors. *J. Vis. Exp.* (153), e60112, doi: 10.3791/60112 (2019)

### *Paper II*

Vazquez-Echegaray, C., **Silvério-Alves, R.**, Kurochkin, I., Lipjankic, N., Bäckström, A., Žemaitis, K., Larsson, J., Pereira, C.F. Identifying Novel Regulators of Hemogenic Reprogramming with CRISPR/Cas9 Knockout Screening. Manuscript (2023)

### *Paper III*

**Silvério-Alves, R.**, Kurochkin, I., Rydström, A., Vazquez Echegaray, C., Haider, J., Nicholls, M., Rode, C., Thelaus, L., Lindgren, A. Y., Ferreira, A. G., Brandão, R., Larsson, J., de Bruijn, M. F. T. R., Martin-Gonzalez, J., & Pereira, C. F. GATA2 mitotic bookmarking is required for definitive haematopoiesis. *Nature communications*, 14(1), 4645, doi: 10.1038/s41467-023-40391-x (2023)

## Papers not included in this thesis

Soboleva, S., Kurita, R., Ek, F., Åkerstrand, H., **Silvério-Alves, R.**, Olsson, R., Nakamura, Y., Miharada, K. Identification of potential chemical compounds enhancing generation of enucleated cells from immortalized human erythroid cell lines. *Commun Biol* 4, 677, doi: 10.1038/s42003-021-02202-1 (2021)

Zimmermannova, O.\*, Ferreira, A. G.\*, Ascic, E.#, Santiago, M. V.#, Kurochkin, I.#, Hansen, M., Met, O., Caiado, I., Shapiro, I. E., Michaux, J., Humbert, M., Soto-Cabrera, D., Benonisson, H., **Silvério-Alves, R.**, Gomez-Jimenez, D., Bernardo, C., Bauden, M., Andersson, R., Höglund, M., Miharada, K., Nakamura, Y., Hugues, S., Greiff, L., Lindstedt, M., Rosa, F. F., Pires, C. F., Bassani-Sternberg, M., Svane, I. M., Pereira, C.-F., Restoring tumor immunogenicity with dendritic cell reprogramming. \*equal contribution, #equal contribution. *Science Immunology* 8, doi: 10.1126/sciimmunol.add4817 (2023)



# Author's contribution to the papers

## *Paper I*

Conceptualization and experimental design. Data collection, analysis, and interpretation. Writing and revision of the published work.

## *Paper II*

Data collection, analysis, and interpretation. Writing of the manuscript.

## *Paper III*

Conceptualization and experimental design. Data collection, analysis, and interpretation. Writing and revision of the published work.

# Abbreviations

ACE	Angiotensin-converting enzyme
AGM	Aorta-gonad-mesonephros
AML	Acute myeloid leukemia
APC	Antigen-presenting cells
BFU-E	Burst-forming unit-erythroid
C-ZF	C-terminal ZF
Cas	CRISPR-associated
cDC1	Conventional dendritic cell type 1
CDK	Cyclin dependent kinases
CFU	Colony-forming unit
CFU-E	CFU-erythroid
CFU-G	CFU-granulocyte
CFU-GEMM	CFU-granulocyte/erythrocyte/macrophage/megakaryocyte
CFU-GM	CFU-granulocyte/macrophage
CFU-M	CFU-macrophage
ChIP-seq	Chromatin immunoprecipitation followed by sequencing
CLP	Common lymphoid progenitor
CMP	Common myeloid progenitor
CRISPR	Clustered Regularly Interspaced Short Palindromic Repeats
crRNA	CRISPR RNA
DA	Dorsal aorta
DBD	DNA-binding domain
DSG	Disuccinimidyl glutarate

E	Embryonic day
EHT	Endothelial-to-hematopoietic transition
EMP	Erythro-myeloid progenitor
ESC	Embryonic stem cell
FACS	Fluorescence-activated cell sorting
FRAP	Fluorescence recovery after photobleaching
GMP	Granulocyte/macrophage progenitor
GVHD	Graft-versus-host disease
HDR	homology-directed repair
HLA	Human leucocyte antigen
HSC	Hematopoietic stem cell
HSPC	Hematopoietic stem and progenitor cell
IAHC	Intra-aortic hematopoietic cluster
iPSC	Induced PSC
KI	Knock-in
KO	Knockout
Lin	Lineage
LTC-IC	Long-term culture initiating cell
M-G1	Mitosis-to-G1
MAC	Mycobacterium avium complex
MD	Mitosis-specific degradation
MDS	Myelodysplastic syndrome
MEP	Megakaryocyte/erythrocyte progenitor
MMP	Multipotent progenitor
MOI	Multiplicity of infection
mRNA	Messenger RNA
N-ZF	N-terminal ZF
NHEJ	Non-homologous end-joining
NK	Natural killer

NLS	Nuclear localization signal
P-Sp	Para-aortic splanchnopleure
PAM	Protospacer-adjacent motifs
pre-HSC	Pre-definitive HSC
PSC	Pluripotent stem cell
PURO	Puromycin
RBC	Red blood cell
Rho	Rhodamine-123
Sca1	Stem cell antigen 1
SCD	Sickle Cell Disease
SCNT	Somatic cell nuclear transfer
scRNA-seq	Single-cell RNA-sequencing
sgRNA	Single guide RNA
siRNA	Small interfering RNA
SLAM	Signaling lymphocyte activating molecule
tracrRNA	Trans-activating crRNA
VEC	Vascular endothelial cadherin
WT	Wild-type
ZF	Zinc finger

# Abstract

Hematopoietic stem cells (HSCs) maintain blood through self-renewal and differentiation. Although HSC transplantation is the only cure for various blood disorders, generating and maintaining HSCs *in vitro* remains challenging, partly due to a limited understanding of the cellular and molecular mechanisms underlying human HSC ontogeny. In embryos, definitive HSCs arise from hemogenic endothelium via an endothelial-to-hematopoietic transition (EHT) in the aorta-gonad-mesonephros (AGM) region and placenta. In humans, limited access to embryos hinders the study of this process. Exploring new methods to mimic hematopoietic development *in vitro* may shed light on the regulators and mechanisms of human HSC specification *in vivo*.

In my thesis, I outlined a protocol for generating hemogenic-like cells with hematopoietic potential from human dermal fibroblasts (HDFs) through direct cell reprogramming. HDFs were transduced with lentiviruses encoding GATA2, GFI1B, and FOS transcription factors (TFs). These three TFs activate hemogenic and hematopoietic transcriptional programs in HDFs, recapitulating EHT and leading to the generation of hematopoietic progeny capable of short-term engraftment in mice. Notably, I showed that the three TFs induce the expression of the HSC marker CD9 at early stages of reprogramming. Thus, human hemogenic reprogramming offers a tractable platform for identifying new markers and regulators of human HSC development.

I then combined hemogenic reprogramming with CRISPR/Cas9 knockout screening to identify regulators. I transduced HDFs with lentivirus encoding Cas9 and a single guide RNA library targeting over 100 genes related to HSC function. In parallel, I optimized the delivery of the three TFs in a single polycistronic vector at a defined stoichiometry, where high levels of GATA2 and GFI1B induced reprogramming efficiently. After Cas9-edited cells underwent hemogenic reprogramming, my colleagues and I isolated both successfully and unsuccessfully reprogrammed cells based on the expression of CD49f and CD9 for next-generation sequencing. Surprisingly, we identified two markers of hemogenic endothelium and HSCs, CD34 and CD44, as barriers to hemogenic reprogramming, while STAG2 was uncovered as a facilitator of the process. These results suggest that commitment to human hemogenic and hematopoietic identity may benefit from time-wise inhibition of CD34 and CD44 signaling.

Finally, I set out to uncover a less appreciated role of TFs *in vivo* using definitive hematopoiesis as a model. Several TFs remain bound to chromatin during mitosis and mark specific genomic sites – a mechanism termed “mitotic bookmarking”. Mitotic retention and bookmarking have been associated with the maintenance of pluripotency, cell reprogramming, and the preservation of somatic lineages *in vitro*, but the relevance for lineage commitment *in vivo* remains to be addressed. Here, I assessed the mitotic retention of hemogenic reprogramming TFs using fluorescent fusion proteins and subcellular protein quantification. Live-cell imaging and western blotting showed that GATA2 remains bound to chromatin in mitosis via C-terminal zinc finger-mediated DNA binding, as opposed to GFI1B and FOS. Moreover, GATA2 bookmarks a subset of its interphase sites with a higher density of GATA2 motifs, which include key regulators of hematopoietic fate. To uncover the role of GATA2 at mitotic exit *in vivo*, we generated a mouse model with the mitosis-degradation domain of cyclin B1 inserted upstream the *Gata2* gene. Remarkably, homozygous mice died during development, partially phenocopying *Gata2* null mice, which die at the onset of definitive hematopoiesis. Interestingly, removing GATA2 at mitosis-to-G1 transition impacts AGM and placental hematopoiesis but not yolk sac hematopoiesis. Altogether, these findings implicate GATA2 as a mitotic bookmarker critical for definitive hematopoiesis and underscore a dependency on bookmarkers for *in vivo* lineage commitment.

Overall, my thesis provides new insights on the molecular mechanisms underlying the specification of definitive hematopoiesis. In the future, harnessing these mechanisms may enable the faithful generation of patient-tailored HSCs to meet clinical demands.

# Resumo em Português

As células estaminais hematopoiéticas têm a capacidade de se autorrenovarem e produzir sangue através de um processo de diferenciação. Embora o transplante de células estaminais hematopoiéticas seja a única cura para várias doenças sanguíneas, a produção e manutenção destas células *in vitro* continua a ser um desafio, em parte devido à escassez de conhecimento relativamente aos mecanismos celulares e moleculares envolvidos na sua ontogenia no ser humano. No embrião, as células estaminais hematopoiéticas definitivas originam-se a partir de endotélio hemogénico, através de uma transição endotelial-hematopoiética, na aorta-gónadamesonefros e na placenta. No entanto, o acesso limitado a embriões dificulta o estudo deste processo no ser humano. O estudo de novos métodos para replicar o desenvolvimento hematopoiético *in vitro* pode ajudar a descobrir moléculas e mecanismos reguladores envolvidos na especificação das células estaminais hematopoiéticas humanas *in vivo*.

Na minha tese, delineei um protocolo para gerar células com características semelhantes a células hemogénicas, com potencial hematopoiético, a partir de fibroblastos humanos, através da reprogramação direta de células. Os fibroblastos foram transduzidos com lentivírus que codificavam três fatores de transcrição: GATA2, GFI1B e FOS. Estes fatores foram anteriormente descritos como sendo suficientes para ativar programas de transcrição hemogénica e hematopoiética em fibroblastos, imitando a transição endotelial-hematopoiética e gerando progenitores hematopoiéticos capazes de enxertar murganhos a curto prazo. Para mais, demonstrei que os três fatores induzem a expressão do marcador de células estaminais hematopoiéticas CD9, o qual ainda não tinha sido associado à reprogramação hemogénica. Assim, a reprogramação hemogénica oferece uma plataforma viável para identificar novos marcadores e reguladores do desenvolvimento das células estaminais hematopoiéticas no ser humano.

Consequentemente, combinei este sistema com um processo de triagem de genes, usando a tecnologia CRISPR/Cas9, de forma a definir genes reguladores da reprogramação hemogénica. Numa primeira instância, transduzi fibroblastos de origem humana com o lentivírus para a proteína Cas9 e uma biblioteca de “single guide RNA” direcionada a mais de 100 genes relacionados com a função das células estaminais hematopoiéticas. Em paralelo, otimizei a entrega dos três fatores num único vetor policistrónico numa estequiometria definida, em que níveis elevados de GATA2 e GFI1B induziram eficazmente a reprogramação. Após as células editadas

com Cas9 passarem pelo processo de reprogramação, eu e os meus colegas isolámos células reprogramadas e não-reprogramadas, de acordo com os níveis de expressão de CD49f e CD9, que foram submetidas a um processo de sequenciação. Inesperadamente, identificámos as proteínas CD34 e CD44, que são dois marcadores importantes do endotélio hemogénico e das células estaminais hematopoiéticas, como barreiras para a reprogramação hemogénica, enquanto a proteína STAG2 foi apresentada como facilitadora do processo. Esses resultados sugerem que a especificação das linhagens hemogénicas e hematopoiéticas em humanos pode beneficiar da inibição das vias de sinalização controladas pelas proteínas transmembranares CD34 e CD44, em contraste com as funções previamente relatadas.

Finalmente, propus-me a descobrir um papel menos valorizado dos fatores de transcrição *in vivo*, usando a hematopoiese definitiva como modelo. Atualmente sabe-se que vários fatores permanecem ligados à cromatina durante a mitose e marcam locais genómicos específicos - um mecanismo denominado "bookmarking" mitótico. A retenção mitótica e o "bookmarking" têm sido associados à manutenção da pluripotência, à reprogramação celular e à preservação de linhagens somáticas *in vitro*, mas a relevância para a especificação de linhagens celulares *in vivo* ainda não tinha sido abordada. Aqui, avalei a retenção mitótica dos fatores de reprogramação hemogénica usando proteínas de fusão de fluorescência e quantificação de proteínas ao nível subcelular. As imagens de células não fixadas e análises de membranas de "western blot" mostraram que o GATA2 permanece ligado à cromatina durante a mitose através da ligação ao ADN mediada pelo domínio "zinc-finger" do C-terminal, ao contrário do GFI1B e do FOS. Além disso, o GATA2 marca um subgrupo de regiões genómicas no ADN, com um maior número de regiões de ligação ao GATA2, que incluem reguladores-chave da linhagem hematopoiética. De forma a descobrir o papel do GATA2 durante a saída mitótica *in vivo*, nós gerámos um modelo de murganho em que inserimos o domínio de degradação da mitose da ciclina B1 a montante do gene *Gata2*. Para nossa surpresa, os murganhos homozigóticos para o domínio de degradação morreram durante o desenvolvimento, copiando parcialmente o fenótipo dos murganhos sem *Gata2*, os quais morrem no início da hematopoiese definitiva. De notar que a deleção do GATA2 na transição mitose-G1 tem um impacto específico na hematopoiese da aorta-gónada-mesonefros e da placenta, mas não na hematopoiese do saco vitelino. Ao todo, estes resultados implicam o GATA2 como um marcador mitótico crucial para a hematopoiese definitiva e destacam uma dependência de "bookmarkers" para o estabelecimento de linhagens celulares *in vivo*.

Em resumo, a minha tese oferece novas perspetivas sobre os mecanismos subjacentes à especificação da hematopoiese definitiva. O conhecimento coletivo apresentado na minha tese pode, no futuro, possibilitar a produção fidedigna de células estaminais hematopoiéticas, a partir de células de pacientes, para atender às necessidades clínicas.



# Lay Summary

Hematopoietic stem cells (HSCs) reside in the bone marrow and generate every type of blood cells in our body, such as white and red blood cells. In many blood-related disorders and cancers, HSC transplantation is the only available treatment. However, lack of suitable donors, the low numbers of HSCs obtained from hematopoietic cell sources, and challenges in generating these cells in the lab, hamper their use in the clinics. During mammalian development, HSCs form from specialized cells in different embryonic tissues. Nevertheless, limited access to human embryos hinders the study of this process in the human system. Understanding how HSCs are generated and how their identity is kept as cells divide will allow the establishment of new approaches to efficiently generate them in the lab or expand them for therapeutic purposes.

In my thesis, I have described the necessary steps to generate the precursors of HSCs in culture using three specific proteins called transcription factors (TFs). These were GATA2, GFI1B and FOS. Together, they converted skin cells into blood precursor cells that expressed the novel surface marker CD9. Furthermore, my colleagues and I used a powerful gene-editing tool called CRISPR/Cas9 to identify molecules that regulate the cell-conversion or reprogramming process. We introduced the editing protein Cas9 into these cells and targeted over 100 genes linked to the function of HSCs. We also made sure the cells had just the right amounts of three specific TFs to achieve the best reprogramming efficiency. Surprisingly, our analysis showed that two proteins, CD34 and CD44, which are usually associated with blood-forming cells, actually hindered the conversion process, while another molecule called STAG2 seemed to make the process easier. These findings suggest that by blocking the activity of CD34 and CD44, we might be able to improve the development of blood-forming cells.

During the life cycle of a cell, TFs bind to DNA and control the production of many other proteins important for the normal function of cells. It was previously thought that when cells divided – in a process called mitosis – most factors would detach from DNA, making cells become “inactive”. However, more recently, scientists found that actually many factors remained bound and marked mitotic DNA just like bookmarks mark the last page read from a book. These “mitotic bookmarking” factors helped cells to be easily “reactivated” after mitosis.

GATA2 is a TF essential for the normal development and function of HSCs. Without it, there are no HSCs nor blood production. For that reason, we hypothesized that HSC generation and the preservation of their identity relied on mitotic bookmarking by GATA2. Interestingly, we show that GATA2 remains bound to DNA throughout mitosis and bookmarks important genes for the development of HSCs. To assess the significance of GATA2 in living organisms, we created a mouse model in which GATA2 could be removed during cell division. To our surprise, removing this factor during that phase of the cell cycle in mice was lethal. These mice never developed HSCs and died from anemia before birth, similar to mice without any GATA2 at all. These results underscore the critical role of GATA2 for proper blood cell development. Collectively, these findings highlight, for the first time, the importance of mitotic bookmarking factors for the establishment of cellular lineages *in vivo*.

In summary, my thesis contributes to our understanding of how HSCs are generated during development. This research could have significant implications for generating customized HSCs for the treatment of blood disorders in the future.

# Populärvetenskaplig sammanfattning

Hematopoetiska stamceller (HSC) finns i benmärgen och kan bilda alla typer av blodceller i kroppen, som vita och röda blodkroppar. Vid många blodsjukdomar och cancerformer är en HSC-transplantation den enda tillgängliga behandlingen. Brist på lämpliga donatorer, det låga innehållet av HSC i hematopoetiska vävnader, samt utmaningar att generera dessa celler i laboratoriet, begränsar deras användning i kliniken. I däggdjur bildas HSC från specialiserade celler i olika embryonala vävnader. Begränsad tillgång till mänskliga embryon försvårar studier av hur denna process styrs i människor. Att förstå hur HSC bildas och hur deras identitet bevaras när celler delar sig kan bidra till utveckling av nya metoder för att effektivt generera dem i laboratoriet eller expandera dem för terapeutiska ändamål.

I min avhandling har jag beskrivit hur GATA2, GFI1B och FOS, tre specifika proteiner som kallas transkriptionsfaktorer (TF), kan omvandla hudceller till föregångare till HSC. Dessutom använde jag och mina kollegor den användbara gensaxen som kallas CRISPR/Cas9 för att hitta gener som styr omprogrammering. Vi säkerställde också att cellerna hade exakt rätt mängd av de tre specifika TF för att optimera omprogrammeringen. Förvånande nog visade vår analys att två proteiner, CD34 och CD44, som vanligtvis associeras med blodbildande celler, faktiskt hindrade omvandlingsprocessen, medan ett annat protein, STAG2, verkade underlätta processen. Dessa resultat tyder på att genom att blockera aktiviteten hos CD34 och CD44 kan vi möjligen förbättra utvecklingen av blodbildande celler.

Transkriptionsfaktorer binder till DNA och styr produktionen av många andra proteiner som är viktiga för cellens normala funktion. Tidigare trodde man att när celler delade sig - en process som kallas mitos - lossnar de flesta faktorer från DNA, vilket gjorde att celler blev "inaktiva". Ny forskning har visat att många faktorer fortsatte vara bundna och märkte mitotiskt DNA precis som bokmärken markerar den sista sidan som lästs i en bok. Dessa mitotiska bokmärkningsfaktorer hjälper celler att lätt "återaktiveras" efter mitos.

GATA2 är en TF som är viktig för den normala utvecklingen och funktionen av HSCs. Utan den bildas inga HSC och inget blod. Vår hypotes var därför att bildandet av HSC och bevarande av deras identitet förlitar sig på mitotisk bokmärkning av GATA2. Intressant nog visar vi att GATA2 binder till DNA under hela mitosen och märker gener som är viktiga för utvecklingen av HSC. För att studera detta under embryoutvecklingen skapade vi en musmodell där GATA2 kunde avlägsnas under

mitosen. Vi fann att dessa möss inte bildade HSC och dog av anemi före födseln, och liknade därmed möss som helt saknar GATA2. Dessa resultat framhäver hur viktig GATA2s roll är för en korrekt utveckling av blodceller. Sammantaget belyser våra resultat för första gången vikten av mitotiska bokmärkningsfaktorer för etablering av celllinjer in vivo.

Sammanfattningsvis bidrar min avhandling till en ökad förståelse av hur HSC genereras under embryoutveckling. Denna forskning kan ha stor betydelse för att generera HSC för behandling av blodsjukdomar i framtiden.

# Hematopoiesis

Hematopoiesis, in simple terms, the formation of blood, is a complex multicellular process by which new blood cells are produced to replace old cells to ensure the proper function of the whole organism. Different components of the blood serve specific purposes in the body. Red blood cells or erythrocytes, for example, are specialized in supplying oxygen to tissues and disposing of carbon dioxide waste resultant from metabolism, while platelets promote blood clotting, and white blood cells or leukocytes, such as granulocytes and lymphocytes are the body's gatekeepers, protecting us against pathogen infections (1). The continuous replenishing of billions of mature short-lived blood cells every day throughout adult life is dependent on a rare population of cells that reside in the bone marrow, the hematopoietic stem cells (HSCs) (2). HSCs are multipotent cells that give rise to all differentiated blood cell lineages: erythroid, myeloid and lymphoid. These cells also have the ability to self-renew, meaning they can generate copies of themselves and this way preserve their numbers over time. Consequently, a hallmark of HSCs is their ability to reconstitute the hematopoietic system of immunocompromised recipients.

## The hematopoietic hierarchy

For decades, hematopoiesis was seen as a stepwise process where HSCs relate to their progeny in a tree-like shaped roadmap, with HSCs seating at the top of the hierarchy (**Figure 1A**) (3,4). According to this model, HSCs successively differentiate in a branch manner into less potent, and consequently more restricted progenitors, with progressively reduced self-renewal capacity, until the mature cell type stage is reached. Multipotent HSCs, give rise to multipotent progenitors (MMPs), which lack self-renewal capacity, and further differentiate into oligopotent (lineage-restricted) common myeloid progenitors (CMPs) and common lymphoid progenitors (CLPs). CLPs originate lymphocytes, including T cells, B cells and natural killer (NK) cells. CMP further diverge to megakaryocyte/erythrocyte progenitors (MEPs), which produce megakaryocytes and erythrocytes, and to granulocyte/macrophage progenitors (GMPs), which give rise to basophils, eosinophils, neutrophils (granulocytes) and macrophages. Dendritic cells, however, can be originated from both myeloid and lymphoid progenitors (**Figure 1A**) (5).

Recently, with the advent of single-cell omics, previously homogeneous HSC populations started to segregate into heterogeneous HSC pools with different molecular signatures, epigenetic landscapes and transcription factor expression profiles that translated into unequal self-renewal and multipotency abilities (6,7). This led several groups to abandon the classical view of the hematopoietic tree-like hierarchy and suggest a reshape of the hematopoietic landscape to a more continuous and fluid process where HSCs and progenitors progressively acquire distinct lineage affiliations down multiple routes, instead of differentiating in an organized stepwise manner (**Figure 1B**) (8–11). Even though cytokine-cytokine receptor interactions can instruct specific lineages at early stages of hematopoiesis, the regulation of this process for cell fate decisions is still unclear (7).

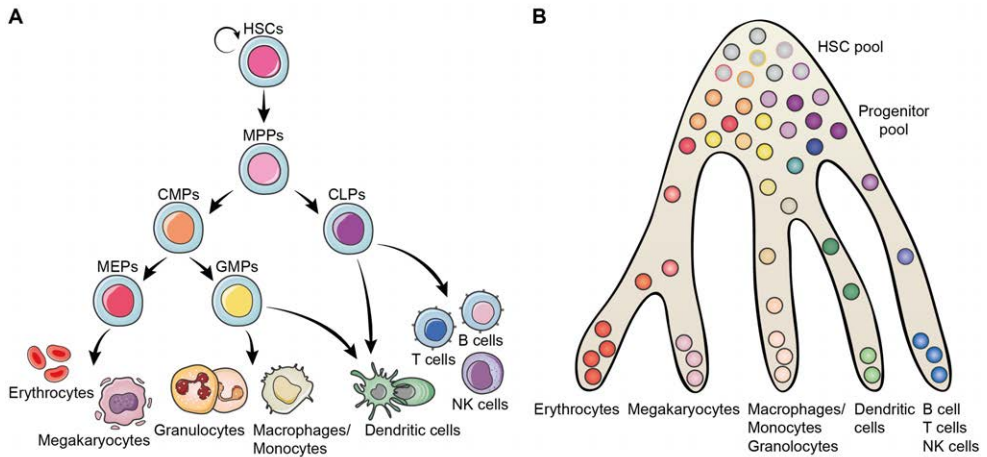


**Figure 1. Models of hematopoiesis. A**, Schematic representation of the classic hematopoietic hierarchy. A homogeneous population of hematopoietic stem cells (HSCs) give rise to all mature blood cell lineages. Multipotent progenitors (MPPs) branch into common myeloid progenitors (CMPs) and common lymphoid progenitors (CLP). CLPs differentiate into lymphocytes, including T cells, B cells and natural killer (NK) cells, as well as into subsets of dendritic cells. CMPs, on the other hand, further diverge to produce megakaryocyte/erythrocyte progenitors (MEPs), which generate erythrocytes and megakaryocytes, and to granulocyte/macrophage progenitors (GMPs), which differentiate into granulocytes, macrophages and dendritic cells. **B**, Revised hematopoietic landscape. Hematopoiesis is shown as a continuum of differentiation, where heterozygous lineage-primed populations of HSCs gradually lose their self-renewal capacity while giving rise to successively more restricted progenitors along a differentiation trajectory represented by different colors. In this model, progenitors are more versatile to change to a different lineage, although closely related. Figure 1B was adapted from Laurenti *et al.*, 2018.

# The waves of developmental hematopoiesis

Even though HSCs are at the top of the hematopoietic hierarchy, the establishment of the hematopoietic system during ontogeny (or embryonic development) starts before the first HSCs are originated. In the vertebrate embryo, blood is formed in three temporally and spatially overlapping waves: first, a primitive, then a pro-definitive and finally a definitive wave, where each generates cells with increased hematopoietic lineage potential (12). Due to the transitory and intercalating nature of the waves, finding individual contributors to adult hematopoiesis remains a challenge.

## The first wave – Primitive hematopoiesis

The developing embryo is a fast-growing mass of cells which begin to form organized tissues. The metabolic demands of the growing organism need to be met to assure survival, which is dependent on oxygen supply to the tissues. The embryo meets these needs by starting the production of transient blood cells.

In the mouse, the first embryonic wave starts in the extra-embryonic mesoderm-derived blood islands of the yolk sac, between embryonic day (E) 7.0 and E7.5 (13). During the primitive wave, only short-lived bi- and unipotent progenitors that give rise to primitive erythrocytes, megakaryocytes and macrophages are generated (**Figure 2**) (13,14). Primitive erythrocytes, contrary to adult red blood cells (RBCs), are large, nucleated cells that express embryonic-specific hemoglobin (15) and are responsible for the diffusion of oxygen throughout the whole embryo. Megakaryocytes and macrophages, on the other hand, are important for sustaining tissue integrity and remodeling during vascular development (14,16). Additionally, primitive macrophages travel to the embryo proper via blood circulation (from E8.5 to E10 in the mouse), and colonize several tissues, becoming tissue-resident macrophages (17,18). In the brain, tissue-resident macrophages were found to establish the microglia through *in vivo* lineage tracing studies (19), making them one of the best examples of embryonic HSC-independent cells persisting into adulthood.

In the human system, although the ethical and technical challenges hinder research at specific stages of development, the presence of primitive erythrocytes, megakaryocytes and macrophages has been reported already in the 70s (20,21), and more recently, single-cell RNA-sequencing (scRNA-seq) studies of human microglia have confirmed its embryonic HSC-independent origin (22).

## The second wave – Pro-definitive hematopoiesis

Shortly after the first wave, a second wave of hematopoietic progenitors arise in the yolk sac and embryo proper, predominantly at the para-aortic splanchnopleure (P-Sp) region (**Figure 2**), from a specialized subpopulation of endothelial cells that express RUNX1 termed hemogenic endothelium (23–25). These cells go through an endothelial-to-hematopoietic transition (EHT), during which they round up, changing their cellular identity to hematopoietic cells that bud off from the endothelial layer to arterial lumina. Definitive erythro-myeloid progenitors (EMPs) are generated during this wave between E8.25 and E10, before homing the fetal liver at E10.5, from where they sustain hematopoiesis until birth (26–28).

EMPs are multipotent progenitors that give rise to definitive myeloid and erythroid cells but lack the long-term potential characteristic of HSCs (29). In the liver, EMPs undergo rapid differentiation towards megakaryocytes, enucleated erythrocytes with fetal-type hemoglobin (15), and monocytes that migrate to different organs to become tissue-resident macrophages (30). Starting from E12.5, the EMP-derived macrophages gradually replace those generated during the primitive wave, making up the majority of tissue-resident macrophages present at birth, with the exception of the brain (31–33). In this context, the blood-brain barrier may protect microglia from being replaced (19,30). Additionally, EMPs also give rise to granulocytes, particularly neutrophils, a cell type that is not produced during the first wave (29). From E10.5 onwards, there is a decrease (but not a total absence) in the number of EMPs in circulation, concordantly with their colonization of the fetal liver.

Other types of progenitors are also produced during this wave. In the P-Sp region of the embryo and yolk sac, lymphoid-restricted progenitors were found as early as E8.5 (34,35), and in the yolk sac at E9.5 both lymphoid-restricted progenitors and lympho-myeloid progenitors were found (35,36). Like EMPs, these cells possibly originate from hemogenic endothelium and migrate to the fetal liver (37). Whether this population of cells arise sequentially from a common pool of hemogenic endothelial cells or from separate subsets is still under debate (38).

While human pro-definitive progenitors are yet to be characterized in detail, hematopoietic progenitors found in the yolk sac and fetal liver prior to HSC emergence or fetal liver colonization are thought to resemble EMPs and lymphoid progenitors found in the mouse (39).



## The third wave – Definitive hematopoiesis

In mice, adult or definitive hematopoiesis initiates at embryonic day E10.5, when HSCs autonomously appear in the aorta-gonad-mesonephros (AGM) region (originated from the P-Sp), vitelline and umbilical arteries, and shortly after in the placenta (**Figure 2**) (40–42). In the AGM region, intra-aortic hematopoietic clusters (IAHCs) containing budding HSCs and progenitors are mainly found in the ventral wall of the dorsal aorta, although a few clusters have been observed in the dorsal wall (43). Similar to the generation of EMPs, HSCs arise from an intermediate endothelial precursor with hemogenic potential, through an EHT (44–47). This transition is dependent on the expression of RUNX1, which orchestrates the transcriptional network responsible for the cell fate conversion (23,24).

The emergence of *bona fide* HSCs from hemogenic endothelium is not a static process. It involves multiple steps, starting with the production of pre-definitive HSCs (pre-HSCs) subpopulations that lack stem cell activity when measured by transplantation and can be distinguished by the sequential expression of cell surface markers, including VE-Cadherin, CD41, CD43 and CD45 in the mouse (48–50). Despite some precursors already start their maturation to HSCs inside the IAHCs, at E11.5 pre-HSCs and HSCs enter circulation and migrate to the fetal liver to further mature and expand their numbers (51,52). By E12.5, the liver is the primary hematopoietic organ, homing hematopoietic cells from both the pro-definitive and definitive waves, and being responsible for the majority of blood output in the embryo. At this developmental stage, lineage-tracing methods have shown that HSCs are highly proliferative and can regenerate after injury, but display negligible contributions to embryonic lymphomyelopoiesis, compared to pro-definitive progenitors (27). Finally, around E16.5, mature HSCs colonize the bone marrow from where they sustain hematopoiesis throughout adult life (39,53).

In humans, HSCs emerge first in the dorsal aorta of the AGM region, between the fourth and fifth post-conception week, and only later in the yolk sac, placenta and liver (54–56). Contrary to mice, human IAHCs were found exclusively in the ventral side of the dorsal aorta (54,55). Although HSC precursors have only been characterized in mice, the human AGM region also gives rise to precursor cells capable of generating hematopoietic colonies before definitive HSCs arise, but with no long-term engraftment ability (57,58).

Current studies are utilizing single-cell data to accurately map and identify transcriptionally distinct cell populations from both mouse and human hemogenic endothelium towards HSCs, that due to their rare and transient nature, prove challenging to identify merely based on surface markers and functional studies (59–62). These efforts are now contributing greatly to our understanding of this complex developmental process and will facilitate the *in vitro* manipulation of developmental hematopoiesis for therapeutic purposes.

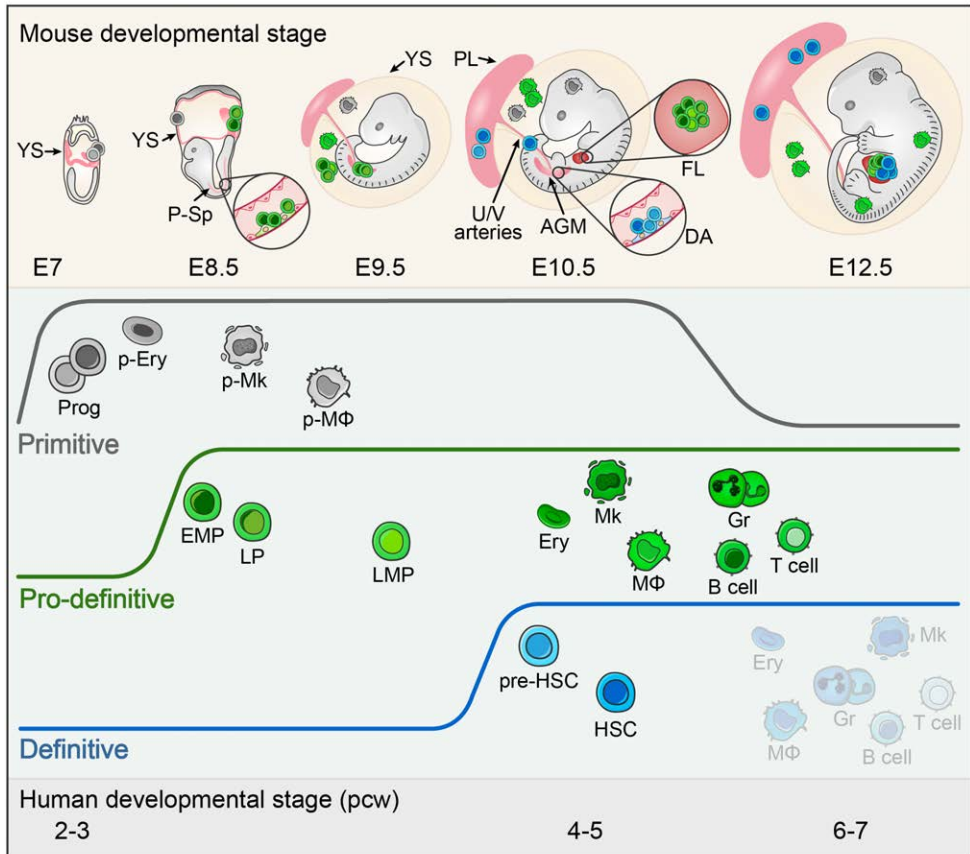


**Figure 2. The waves of hematopoiesis.** Hematopoietic development occurs in three distinct yet overlapping waves: primitive (in grey), pro-definitive (in green), and definitive (in blue). In each wave, unique hematopoietic progenitors are generated. These progenitors are depicted in the upper panel which illustrates their origin within the embryo and their subsequent migration to specific hematopoietic sites at different developmental stages. Primitive progenitors (Prog) arise in the yolk sac (YS) from embryonic day (E) 7 and differentiate into primitive erythrocytes (p-Ery), primitive macrophages (p-MΦ) (which colonize the embryo until adulthood), and primitive megakaryocytes (p-Mk). The second or pro-definitive wave generates erythromyeloid progenitors (EMPs), as well as lymphoid-restricted progenitors (LPs) and lympho-myeloid progenitors (LMPs) in the YS and embryo proper at the para-aortic splanchnopleure (P-Sp) region. These pro-definitive progenitors travel to the fetal liver (FL) at 10.5 and sustain embryonic hematopoiesis until birth, including erythrocytes (Ery), megakaryocytes (Mk), macrophages/monocytes (MΦ), granulocytes (Gr), and B and t cells. From E10.5, the definitive and last developmental hematopoietic wave takes place at the dorsal aorta (DA) of the aorta-gonad-mesonephros (AGM) region, umbilical (U) and vitelline (V) arteries, and placenta (PL), and produces pre-HSCs followed by HSCs. Pre- and definitive HSCs migrate to the FL and mature. HSC minimal contribution to embryonic hematopoiesis is represented by blue cells with transparency. HSC-dependent hematopoiesis becomes more relevant after colonization of the bone marrow at E16.5. EMP-derived MΦ migrate to the embryo and replace most primitive MΦ in the tissues except for the brain. The corresponding human developmental stages in post-conception weeks (pcw) are shown at the bottom. Adapted from Canu & Ruhrberg, 2021 and Dzierzak & Bigas, 2018.

## Transcriptional control of developmental hematopoiesis

As any other developmental process, the process by which cells within the early embryo commit to the hematopoietic lineage, is tightly regulated by molecular signals. These signaling pathways subsequently lead to the activation of key TFs that trigger the expression of hematopoietic genes down the line, which in turn reflect the different cell fates (12).

TAL1 (also known as SCL) and LMO2 TFs are involved in the production of blood in the early stages of hematopoiesis, particularly during the primitive and pro-definitive waves. Mutations resulting in loss-of-function of these factors cause embryo lethality before E10.5, due to yolk sac failure (63,64).

RUNX1 is necessary for the formation of both EMPs and HSCs from hemogenic endothelium (24,65). Knockout (KO) studies reported that mice lacking *Runx1* die by E12.5 with severe anemia from the lack of definitive progenitors and consequent decline in fetal liver hematopoiesis (66,67). These mice never develop HSCs. Studies using pluripotent stem cell (PSC) differentiation protocols have shown that during *in vitro* EHT, endothelial programs are downregulated, while hematopoietic programs are upregulated via the downstream activity of RUNX1 targets GFI1 and GFI1B (68,69). In the absence of RUNX1, GFI1 and GFI1B alone are sufficient to drive the loss of endothelial identity in hemogenic cells, leading to the observed morphological alterations that occur during EHT (68). Even though both HSCs and EMPs emerge from RUNX1<sup>+</sup> hemogenic endothelium, the molecular pathways driving these two cell lineage transitions are distinct (70,71).

While HSC specification is dependent on NOTCH signaling, EMP formation does not require this pathway (72–74). Briefly, the NOTCH signaling pathway is composed of transmembrane receptors (Notch receptors) and ligands (Delta and Jagged ligands) that bind through cell-cell interactions to initiate cell fate-related gene expression in several tissues (78). During definitive hematopoiesis, RUNX1 works in parallel with other pivotal TF – GATA2, which is also a direct target of the NOTCH pathway (73,74).

GATA2 is required during the second and third waves of hematopoietic development, as *Gata2* gene KO affects the generation of both pro-definitive progenitors and HSCs, causing embryo lethality derived from severe anemia between E10.5 and E11.5 (76). In both *Runx1* and *Gata2* KO mice, vasculature and primitive hematopoiesis are not impaired (66,67,76). Despite the apparent functional overlap between these two TFs, their roles are in fact distinct.

Chen *et al.*, beautifully clarified the requirement of RUNX1 in a study where they abolished *Runx1* expression in either hemogenic cells (positive for vascular endothelial cadherin, VEC) or HSC-committed cells (cells expressing *Vav1*, an early gene expressed in HSCs) (77). Deleting RUNX1 exclusively in hemogenic

cells impaired their progression through EHT and IAHC formation, including HSC emergence. However, deletion of the TF after the EHT stage, in HSC-committed cells, had minimal impact on HSC function. In contrast, GATA2 is required not only for the specification of HSCs from hemogenic endothelium, but also for their survival and function (76,78–80). A study that mirrored previous research, where GATA2 was depleted from VEC<sup>+</sup> or Vav<sup>+</sup> cells instead of RUNX1, validated that only GATA2 was necessary beyond the point of HSC emergence for the maintenance of HSCs (76), this way reaffirming its pivotal role in definitive hematopoiesis. In agreement, imaging studies confirmed GATA2 expression in the P-Sp and AGM regions at E9.5 and E10.5, respectively, and later in the E12.5 fetal liver (81), as well as in HSCs and most progenitors at those sites, and in bone marrow (82).

Importantly, the dynamics of *Gata2* expression at single-cell resolution during EHT has been described (83). The levels of *Gata2* oscillate from lower average levels in hemogenic endothelium that progressively increased until the formation of IAHCs. Interestingly, GATA2 shows a pulsatile behavior in single cells, going up and down with time, suggesting gene expression instability as cells transit between cell fates (83). These observations highlight how important the tight control of GATA2 levels is for the development of HSCs. In fact, HSC function is highly dependent on GATA2 dosage, as either overexpression or haploinsufficiency (situation when only one allele or copy of a gene is active) can result in significant decline of the HSC pool, accompanied by increased quiescence, and a reduction in HSC reconstitution capacity (79,84,85). RUNX1 haploinsufficiency, on the other hand, has milder outcomes, resulting in the premature appearance of HSCs in the embryo (67) and in the reduction of the HSC numbers, but with increased engraftment potential and no significant impact to blood lineage differentiation (86). Nevertheless, the cooperative action of GATA2 and RUNX1 is crucial for the specification of HSCs, as *Gata2*<sup>+/-</sup>:*Runx1*<sup>+/-</sup> double heterozygous mice die during development, despite individual mutants (*Gata2*<sup>+/-</sup> or *Runx1*<sup>+/-</sup>) produce viable mice (although with inherent hematopoietic deficits) (87).

Recently, genome-wide approaches, such as chromatin immunoprecipitation followed by sequencing (ChIP-seq) and single-cell transcriptomics, have enabled a more comprehensive study of the TF networks governing blood development and hematopoietic stem and progenitor cell (HSPC) function, facilitating the discovery of novel regulators and protein complexes associated with hematopoiesis (87–91). In particular, a combinatorial interaction between seven TFs, namely TAL1, LYL1, LMO2, GATA2, RUNX1, ERG, and FLI1 was described in an immortalized mouse cell line resembling embryonic multipotent hematopoietic precursors (87,92). These HSPC-related TFs targeted genes associated with transcriptional control, signaling, apoptosis, and cell cycle.

# GATA2 role in normal and malignant hematopoiesis

GATA2 (GATA-binding protein 2) is a member of the GATA family of TFs named after the consensus nucleotide sequence (A/T)GATA(A/G) which they bind to through two highly conserved zinc finger (ZF) domains (93,94). The N-terminal ZF (N-ZF) is responsible for stabilizing DNA-protein complexes and providing specificity to DNA binding, whereas the C-terminal ZF (C-ZF) recognizes and binds to GATA consensus sequences (95–97). Also, both ZFs are critical for the interaction of GATA2 with multiple partner proteins which drive lineage-specific gene expression (98). In addition to the ZFs that compose the DNA-binding domain (DBD), GATA2 has two transactivation domains, a nuclear localization signal (NLS) and a negative regulatory domain (**Figure 3**) (98,99). GATA2 is highly expressed in the immature hematopoietic cell compartment, especially in HSCs, where it controls cell quiescence, self-renew, and proliferation (78–80,99). In downstream progenitors, GATA2 is responsible for the regulation of GMP function and differentiation (100), and for the fate decisions between erythroid and megakaryocyte lineages (101,102). While GATA2 downregulation by GATA1 is necessary for erythropoiesis, increased GATA2 levels are required for megakaryocyte development (102). Fate decisions within the myeloid lineage are dependent on the interplay between GATA1, GATA2 and PU.1. PU.1 inhibits erythroid differentiation by interfering with GATA1's ability to bind to DNA (103), and simultaneously downregulates GATA2 to drive terminal macrophage differentiation (104). Conversely, generation of mast cells requires the cooperative and additive functions of GATA2 and PU.1 (104).

In the absence of GATA2 there is no definitive or adult hematopoiesis (76). *Gata2*<sup>+/-</sup> mice are viable but have reduced numbers of functional bone marrow HSPCs, and reduced ability to generate hematopoietic colonies in colony-forming unit (CFU) assays from bone marrow and embryonic hematopoietic tissues (78,85). Furthermore, the decrease in the number of hematopoietic colonies results from a selective decline in the GMP numbers and function, caused by disruption in the expression of the NOTCH target and HSPC regulator *Hes-1* gene (100). Surprisingly, peripheral blood cell counts and bone marrow cellularity in the adult mice are normal (85), suggesting that lower levels of GATA2 (2-fold decrease in the immature cell compartment of the bone marrow) are still sufficient to support

adult hematopoiesis in the mouse. Nevertheless, the same is not observed in the human system.

Heterozygous autosomal dominant or sporadic germline mutations in the human GATA2 gene resulting in haploinsufficiency lead to GATA2-deficiency syndrome (105,106). This syndrome is characterized by three clinical manifestations: 1) a propensity to develop pre-leukemia, also known as myelodysplastic syndrome (MDS), which may progress to acute myeloid leukemia (AML) (107); 2) Emberger syndrome (108); and 3) MonoMAC and dendritic cell, B and NK lymphoid deficiency (109–112). MDS and AML are characterized by an exceeding number of immature myeloid progenitors that cannot differentiate into mature blood cells, causing anemia and increased risk for bleeding and infections. Emberger syndrome involves localized tissue swelling caused by defects in the lymphatic system (lymphedema) and MDS/AML. MonoMAC syndrome is an immunodeficiency disorder characterized by a profound reduction in the numbers of monocytes (monocytopenia) and a higher susceptibility to infections, particularly by a group of bacteria known as *Mycobacterium avium* complex (MAC). This syndrome is also associated with decreased numbers of dendritic cells, B cells and NK cells. The mutations giving rise to these manifestations are mainly composed of two types: N-terminal frameshift mutations that lead to the early termination of GATA2 protein synthesis, and missense mutations resulting in amino acid substitution in the ZFs, with the majority occurring in the C-ZF (**Figure 3**) (113). Contrary to germline GATA2 mutations, somatic mutations found in the ZFs of adult AML patients happen preferentially in the N-ZF (113,114) and are associated with a better clinical outcome (115).

Considering the role of dendritic cells in initiating adaptive immune responses by presenting pathogenic antigens to T cells, and the fact that this population is severely reduced in GATA2-deficiency syndrome, a recent study aimed to determine the role of GATA2 in dendritic cell development (116). Since either non-conditional or conditional KOs result ultimately in embryo lethality before birth (76,78,117) and heterozygous KO mice (*Gata2*<sup>+/-</sup>) do not exhibit alterations in mature blood cell types (85), Onodera *et al.* used an inducible conditional KO system where *Gata2* expression was inactivated in adult mice *in vivo* or in specific isolated cell types *in vitro* (116). *Gata2* deletion *in vivo* led to a decrease in the dendritic cell population, and impaired dendritic cell generation *in vitro* from LSK cells, CMPs, and common dendritic cell precursors, but not from CLPs, suggesting that GATA2 plays a role in the myeloid route of dendritic cell differentiation. However, none of the mice developed MDS or AML and therefore, there is a strong need of more comprehensive mouse models to mimic the complexity of GATA2-deficiency syndrome, in pre-clinical settings.

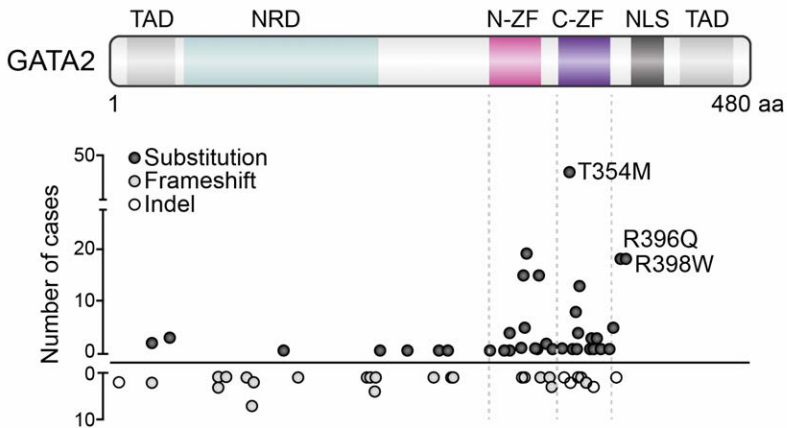


**Figure 3. Domain composition of the canonical GATA2 protein and most frequent mutations associated with GATA2-deficiency syndrome.** GATA2 is a 480-amino acid (aa) long TF that contains two zinc finger (ZF) domains: an N-terminal ZF (N-ZF) and a C-terminal ZF (C-ZF) that form the DNA binding domain. Additionally, GATA2 has two transactivation domains (TADs), a nuclear localization signal (NLS) and a negative regulatory domain (NRD). The type and frequency of GATA2 mutations are shown. The most frequent aa substitution mutations include the replacement of a threonine (T) with a methionine (M) at residue 354, an arginine (R) with a glutamine (Q) at residue 396, and an R with tryptophan (W) at residue 398. Also, insertion and deletion (Indel) mutations have been reported. Adapted from Rodrigues *et al.*, 2012 and Collin *et al.*, 2015.

# Hematopoietic Stem Cells

HSCs are a rare population of multipotent, self-renewing cells that reside in the bone marrow and give rise to all differentiated blood cell types, through hematopoiesis. The identification of these cells came after a series of studies, published by Till and McCulloch in the 1960s, provided evidence of a putative long-lasting blood progenitor (118–120). They showed that the spleen of irradiated mice receiving bone marrow transplants contained hematopoietic colonies of clonal (or unicellular) origin, which proliferated and exhibited multi-lineage differentiation potential. However, cells giving rise to spleen colonies were a mixture of stem and progenitor populations (121). In the 1990s, single-cell transplantation experiments irrefutably proved the existence of self-renewing HSCs with the ability to reconstitute the hematopoietic system of irradiated recipients for prolonged periods of time (122).

Typically, bone marrow HSCs reside in a quiescence or inactive cell cycle state to protect the stem cell pool from exhaustion, and prevent the occurrence of genetic mutations that could contribute to the development of blood malignancies (123,124). Exit from quiescence and re-entry into the cell cycle are defined by leaving the inactive G0 phase and progressing through the cell cycle interphases (G1, S, and G2), during which cells grow and duplicate their DNA, and ultimately undergo cell division (also known as mitosis or M phase). Cell cycle engagement can be triggered by intrinsic (e.g., TFs) and extrinsic (e.g., inflammatory signals) stimuli to induce symmetric (two HSCs or two progenitor daughter cells) or asymmetric (one HSC and one progenitor cell) cell divisions, this way promoting self-renewal or differentiation towards blood (125). However, the predisposition to enter cell cycle, the degree of self-renewal (reflected by the number of symmetrical divisions), and repopulation capacity vary among HSCs, thus dividing the HSC pool into two main subpopulations: the long-term HSCs (LT-HSCs) and the short-term HSCs (ST-HSCs), which are accompanied by differential expression of defined surface and molecular markers in mouse and human (126–130). LT-HSC are slow to re-start cell cycle and complete a total of only four symmetric divisions during a mammals' lifetime, until they reach a point of complete dormancy (131). When challenged, these cells are capable of sustaining blood production for over 16 weeks in primary transplantation assays and can continue to repopulate mouse recipients in subsequent rounds of transplantation (127,129). In other words, these HSCs exhibit a robust ability to persist and replenish blood over an extended period, demonstrating their long-term regenerative potential. LT-HSCs give rise to ST-



HSCs which are quick to enter cell cycle and respond to hematopoietic demand, being the main contributors to blood production. These, however, have a more restricted self-renewal capacity consistent with their ability to reconstitute the hematopoietic system of immuno-ablated mice for shorter periods (126). Regardless of their behavior, HSCs possess remarkable therapeutical potential, making the hematopoietic system one of the most regenerative systems in the human body.

## Isolation of hematopoietic stem cells

Identification of HSC subsets and downstream progeny can be achieved by the detection of specific surface proteins (or markers) that distinguishes the different cells populations. Flow cytometry is one of the most commonly used methodology to study hematopoietic cells (132). It enables the analysis of single cells or other entities, like chromosomes, nuclei, and beads, according to their optical and fluorescent characteristics. Fluorescent dyes can bind to cellular components like DNA or RNA, and antibodies attached to fluorescent dyes can target specific proteins on cell membranes or inside cells. As labeled cells pass by a light source, the fluorescent molecules get excited and emit energy at higher wavelengths which is detected by the flow cytometer. Therefore, cell populations can be separated based on their size, organelle complexity, and immune phenotype when fluorescent-conjugated antibodies are used (132). Consequently, identification of specific HSPC populations by combining the detection of several surface markers allows their isolation through fluorescence-activated cell sorting (FACS) (130,133,134).

CD34, a transmembrane glycoprotein, was the first cell surface marker to be identified in human immature hematopoietic cells (135,136). Since its discovery, CD34 has been extensively used to obtain HSPCs for both research and clinical applications (137). Nevertheless, CD34 alone is not sufficient to purify LT-HSCs, which led to the identification of other markers to enrich this rare cell population (138). The marker CD90, also known as Thy1, was identified in CD34<sup>+</sup> mobilized peripheral blood HSPCs, within the cell population that lacks the expression of mature hematopoietic markers (such as Gr1, B220, CD3, and Ter119), referred to as lineage negative (Lin<sup>-</sup>). Lin<sup>-</sup>CD34<sup>+</sup>CD90<sup>+</sup> cells displayed improved engraftment and higher potential for multi-lineage differentiation in recipients (139). Negative selection for the progenitor-related marker CD38 and the T lymphocyte marker CD45RA, further enriched the HSC subset (140–143). However, obtaining pure multipotent HSCs capable of long-term engraftment is still a challenge. Addition of the adhesion molecule CD49f enabled the isolation of single cells capable of generating long-term multi-lineage grafts with high efficiency. Therefore, the most commonly employed marker combination for efficiently isolating HSCs from progenitors is CD34<sup>+</sup>CD38<sup>-</sup>CD45RA<sup>-</sup>CD90<sup>+</sup>CD49f<sup>+</sup>. Nonetheless, both long-term and short-term HSCs share the same surface phenotype (130). Separation of these

two subsets can be made based on the efflux of the mitochondrial dye rhodamine-123 (Rho) and expression of cell cycle cyclin dependent kinases (CDK), where high efflux (and thus low levels of Rho) and lack of CDK6 are predominant in LT-HSCs (128–130). Interestingly, Anjos-Afonso *et al.* characterized a rare self-renewing CD34<sup>-</sup> population (Lin<sup>-</sup>CD34<sup>-</sup>CD38<sup>-</sup>CD93<sup>hi</sup>) with robust repopulation capacity, characterized by NOTCH signaling pathway activation and quiescence, indicating the existence of an immature HSC population, distinct from CD34<sup>+</sup> cells, that may be placed on top of the HSC hierarchy (144).

In mice, bone marrow HSCs and MPPs are characterized as Lin<sup>-</sup>Sca1<sup>+</sup>c-Kit<sup>+</sup> cells since they lack lineage markers but express stem cell antigen 1 (Sca1) and the stem cell factor receptor c-Kit. For that reason, they are commonly referred to as LSK cells (145,146). Negative expression of the cytokine tyrosine kinase receptor Flt3, and positive or negative expression of signaling lymphocyte activating molecule (SLAM) family members, CD150 and CD48 were found to enrich for LT-HSCs (127,147,148). Currently, mouse LT-HSC subset can be defined by the immunophenotype Lin<sup>-</sup>Sca1<sup>+</sup>c-Kit<sup>+</sup>CD34<sup>-</sup>CD150<sup>+</sup>CD48<sup>-</sup>Flt3<sup>-</sup>. Additional markers include the endothelial protein C receptor, and similarly to the human counterparts, high Rho efflux (149).

Other HSC surface markers which are not routinely used include the tetraspanin CD9 and angiotensin-converting enzyme (ACE). A study conducted by Karlsson and colleagues showed that mouse CD48<sup>-</sup>Flt3<sup>-</sup>LSK fractions where CD9 expression was high contained all HSCs with long-term multi-lineage engraftment potential, including cells that did not fit the typical immunophenotypic profile of LT-HSCs, such as CD150<sup>-</sup> or CD34<sup>+</sup> cells (150). Moreover, CD9 is expressed in CD34<sup>+</sup>CD38<sup>+/-</sup> umbilical cord blood cells and is implicated in their ability to home the bone marrow (151). When it comes to ACE, this marker is expressed in emerging HSCs in the AGM region, in the surrounding hemogenic endothelium and adjacent mesodermal cells, as well as in primitive hematopoietic cells in fetal liver, and in CD34<sup>+</sup> umbilical cord blood (152–154). Interestingly, ACE<sup>+</sup> mesodermal pre-hematopoietic cells, localized ventrally to the dorsal aorta, are negative for CD45 (pan-hematopoietic surface marker present in all nucleated hematopoietic cells (155)), positive for CD49f and in the earliest stages of AGM development, negative for CD34 (152,154), suggesting the presence of a ACE<sup>+</sup>CD34<sup>-</sup>CD45<sup>-</sup>CD49f<sup>+</sup> mesodermal precursor that gives rise to HSCs emerging in the ventral part of the dorsal aorta, in the AGM region, through an EHT.

## Functional assessment of hematopoietic stem and progenitor cells

Several assays can be performed to evaluate HSPC function *in vitro* and *in vivo*. A frequent method used to address hematopoietic progenitor function *in vitro* is the CFU assay. This method provides information regarding the type and frequency of progenitor cells, according to their ability to differentiate and generate lineage-specific colonies in a methylcellulose-based semisolid medium, supplemented with hematopoietic cytokines. After 6 to 12 days in culture, colonies are scored under a microscope to assess colony number and type. Based on their morphology, colonies can be classified as burst-forming unit-erythroid (BFU-E), CFU-erythroid (CFU-E), CFU-granulocytes/macrophages (CFU-GM), or individual CFU-M or CFU-G, and mixed colonies of CFU-granulocytes/erythrocytes/macrophages/megakaryocytes (CFU-GEMM).

The long-term culture initiating cell (LTC-IC) assay is an extension of the CFU assay, aimed at evaluating the proliferative potential of cells over an extended period in culture. This assay is more powerful in quantifying immature HSCPs since they can survive longer *in vitro* than CFU progenitors. Individual cells are plated onto irradiated bone marrow or stromal cells that serve as feeder layers to support the growth of immature cells. By culturing the cells for 5 to 8 weeks, the resulting cells can be assessed for their capacity to generate CFUs, enabling the quantification of primitive hematopoietic progenitors in the original tested cell population (156). Nevertheless, the stem cell properties of *bona fide* HSCs can only be truly investigated by performing *in vivo* transplantation assays.

LT-HSCs are the only cells capable of long-term and multi-lineage engraftment of the bone marrow. HSCs' ability to reconstitute the hematopoietic system can be assessed in primary transplantations, while self-renewal can only be evaluated through consecutive transplantations into secondary or tertiary recipients (157). Prior to transplantation, recipients usually undergo an irradiation procedure to promote myeloablation, thereby reducing a possible rejection of the graft, and to create space for donor cells. Failure to reconstitute recipients can indicate decline in HSC function or numbers in the transplant source.

In competitive transplantation assays, the same number of HSCs from a mouse model of interest and from a control mouse (normally wild-type) are transplanted together into a lethally irradiated recipient mouse (158). To help withstanding the procedure, recipient mice usually receive a defined amount of own whole bone marrow cells that serve as support. There, input cells will compete, and only the fittest will home the bone marrow of the recipient and generate hematopoietic progeny with the same genetic background. If the test cells are functionally equivalent to the control cells, then the percentage of engraftment will be similar. Engraftment and contribution to blood can be assessed through the collection of

cells from the peripheral blood and bone marrow of recipient mice, and can be distinguished by the expression of CD45 isoforms, CD45.1 or CD45.2. In the case that control cells are CD45.1<sup>+</sup> and test cells are CD45.2<sup>+</sup>, the recipient mice can be positive for both isoforms, CD45.1 and CD45.2, since CD45.1<sup>+</sup>CD45.2<sup>+</sup> cells will appear as a separate population in flow cytometry analysis (**Figure 4**). Likewise, the study of human HSC function *in vivo* has been possible due to the development of immunodeficient mice strains (159,160).

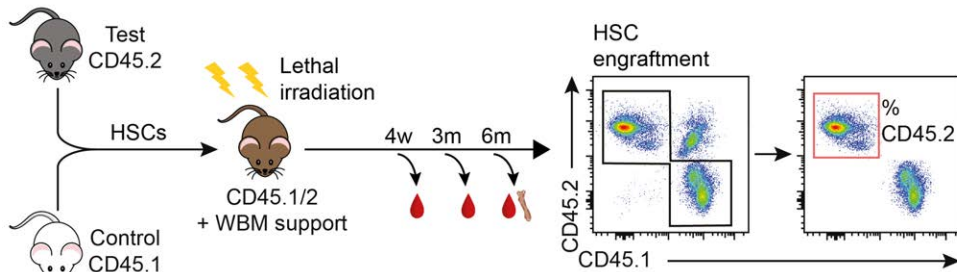


**Figure 4. Schematic representation of a competitive transplantation assay.** Sorted HSCs from a competitor/control CD45.1 mouse and from a CD45.2 test strain are mixed 1:1 and injected into lethally irradiated CD45.1/2 recipients, together with support whole bone marrow (WBM) cells. Blood can be collected for flow cytometry analysis at different time points to address short-term – 4 weeks (w) and 3 months (m) – or long-term (6m) engraftment and evaluate the percentage of test/donor contribution (% CD45.2<sup>+</sup> cells). Adapted from Silvério-Alves *et al.*, 2023.

## Clinical applications of hematopoietic stem cells

The first HSC transplantation in a clinical setting (or more precisely, bone marrow transplantation) was performed by Edward Thomas in 1957. While HSCs and downstream progenitors were not well characterized at the time, the bone marrow was already recognized as the primary site for hematopoiesis and was known for its ability to regenerate irradiated animals (161). In his first attempt, six patients that had been receiving radiation and chemotherapy were treated intravenously with healthy bone marrow (162). Unfortunately, only two showed engraftment and no patient survived passed three months. In 1959, Thomas reported two cases where infant leukemic patients received bone marrow from their identical twin, but still with limited success (163). At that time, little was known about donor-recipient matching, as methods to identify human leucocyte antigen (HLA) complexes, associated with the distinction between “non-self” from “self” and graft-host immune reactions, were only developed later in the 1960s (164). With the advent of HLA matching and a better understanding of HSCs, HSC transplantation became the gold-standard therapeutic intervention (albeit with its risks) to treat several conditions, such as blood-related cancers, bone marrow failure, and immunodeficiency syndromes.

There are two main types of HSC transplantation. Autologous transplants use patient-derived HSCs, whereas in allogeneic transplantation HSCs are collected from (matching) genetic-related or unrelated donors (165). Despite the fact that the best clinical outcomes are observed when the donor is an HLA-matching sibling, only 30% of the patients in need of an allogeneic transplantation will have that luck (166). Consequently, allogeneic HSC transplantation is usually associated with graft rejection by the host immune system, graft-versus-host disease (GVHD) caused by an immune response of contaminating T cells from transplanted tissues against the host, and an overall higher risk of transplant-related mortality (165,167). In autologous transplantation, even though there is no graft rejection or GVHD, there is a risk of graft contamination with cancer cells that can lead to relapse, and it has very little to no clinical applicability in the treatment of inherited hematopoietic disorders (165). The sources of HSCs also vary. These include bone marrow aspirations, peripheral blood (after HSC mobilization from the bone marrow with growth factors) (168), and umbilical cord blood (169), although the number of cells retrieved from the latter is still limited and insufficient to treat an adult (170). The modality of HSC transplantation and the cell source used to treat and eventually cure patients depend on the type of blood disorder. Nevertheless, limited donor matching, low cell number availability, and transplant-related complications still hinder the full-power application of this procedure (166).

### ***In vitro* approaches to generate definitive hematopoietic stem cells**

To surpass the constraints associated with HSC transplantation, efforts have been made towards the *ex vivo* expansion of definitive HSCs (171). In the bone marrow, the HSC microenvironment (or niche), cytokines and growth factors produced by endothelial, immune cells and other cell types at the niche, sustain HSC survival, self-renewal, and proliferation (172). Historically, attempts to expand and maintain HSCs *ex vivo* have met limited success, primarily due to the lack of suitable culture conditions. Experimental data implied that HSCs gradually lost their self-renewal ability through repeated cell divisions and long culture periods (173). Recently, optimization of culture conditions through the titration of naturally occurring cytokines and growth factors in serum-albumin free systems resulted in significant expansion of functional HSCs for over a month (174). Nevertheless, the population obtained was heterogeneous in terms of their self-renewal capacity. Additionally, high-throughput screenings identified several small molecules with the ability to expand HSCs *in vitro* (175,176). The small molecule UM171 (175), showed great promise in the expansion of umbilical cord blood for transplantation in a recently completed clinical trial (177).

Other approaches include the *de novo* generation of HSCs from embryonic or induced PSCs (iPSCs), and somatic cells (178). PSCs are stem cells that can divide indefinitely and differentiate into the three germ layers (endoderm, mesoderm and

ectoderm) that compose a whole organism, with the exception of the extra-embryonic tissues. These cells were originally found in the inner cell mass of embryos' blastocysts as embryonic stem cells (ESCs), in both mouse (179) and human (180), and later, to overcome tissue scarcity and/or ethical issues, were induced *in vitro* from somatic cells (181). PSCs are easily expanded and maintained in culture. However, initial differentiation protocols attempting to recapitulate definitive hematopoiesis, including EHT, have resulted in multi-lineage progenitors with no proven long-term engraftment. These progenitors resembled yolk sac progenitors more than definitive HSCs (178,182–185).

Additional strategies aimed to combine chemically defined culture conditions with the addition of TFs that play a role in HSC development and HSC self-renewal to forward the differentiation of PSCs towards the hematopoietic lineage (186–190). Ectopic expression of TFs for cell fate conversions will be further explored in the following chapter. In two examples from the early 2010s, overexpression of a RUNX1 isoform in human PSCs resulted in hematopoietic progenitors with short-term engraftment (186), and a combination of HOXA9, ERG, RORA, SOX4, and MYB induced multipotent progenitors that transiently engrafted mice and generated myeloid and adult-like erythroid cells (188). More recently, Sugimura *et al.* achieved multi-lineage reconstitution in primary and secondary recipients after transplantation, making it the first study to demonstrate robust iPSC-derived HSC self-renewal (190). The authors identified 7 TFs (ERG, HOXA5, HOXA9, HOXA10, LCOR, RUNX1 and PU.1) that were sufficient to convert cells undergoing *in vitro* EHT into HSPCs that contributed to erythroid and myeloid, as well as B and T cell output (190). Inducible expression of a single TF (MLL-AF4) in human iPSCs undergoing differentiation towards blood, was shown to promote multipotent long-term engraftment of induced HSPCs, however with the caveat that these cells became prone to leukemic transformation (cancer formation) with extended engraftment (189). Whether or not the latter attempts are feasible in clinical practice is yet to be addressed.

Direct cell conversion (or reprogramming) of blood-related and unrelated cell types has also been a line of research in the pursuit of on-demand *in vitro* generated transplantable HSCs.

# Cell fate reprogramming

During development, PSCs differentiate into the tissue-specific cell types of multicellular organisms. The maintenance and transmission of cell fate is controlled by complex transcriptional and epigenetic mechanisms (191,192). Epigenetics can be described as the study of heritable changes in gene expression without altering the underlying DNA sequence. Until the first half of the 20th century, lineage commitment and cell differentiation were seen as a unidirectional and irreversible process, as defined by Conrad Waddington's "epigenetic landscape" model (193,194). In his model, cells metaphorically behaved like marbles rolling down a hill, separating into different paths until they reached their final destination, in other words, a differentiated cell state. From this angle, one may consider cell differentiation an epigenetic process itself, since starting from one genotype, multicellular organisms develop various cell types with distinct gene expression patterns and functions (192). The idea of differentiation as a one-way process was challenged in the late 1950s by the pioneering work of John Gurdon on somatic cell nuclear transfer (SCNT) in frogs (195–197). In his most famous experiment, Gurdon transplanted nuclei from fully differentiated tadpole intestinal cells into enucleated eggs, resulting in adult frogs that were genetically identical to the respective somatic cell nucleus donor (196). His discoveries implied, for the first time, that adult cells could be reprogrammed back to a pluripotent state, challenging the central dogma in developmental biology at the time. For his achievements, Gurdon was awarded the Nobel Prize in Physiology or Medicine in 2012. Only later, in the 1990s, was SCNT used to clone the first mammals (198,199).

In the second half of the 20th century, another line of research came to light, this time focused on the fusion of two different cell types to evaluate changes in gene expression profiles. The fusion of mouse muscle cells with human amniotic cells produced non-dividing heterokaryons (cells with two or more non-fused nuclei) that expressed human muscle proteins (200), demonstrating for the first time that silent genes could be activated in cells where they were normally not expressed. It was not until the 21<sup>st</sup> century that scientists were able to reprogram somatic cells to pluripotency through fusion with ESCs (201,202). Somatic cell-ESC heterokaryons and hybrids (cell with two or more fused nuclei) differentiated into cells of the three germ layers and expressed pluripotent genes that define ESC identity (201–203).

Overall, studies on SCNT and cell fusion have shown that the differentiated state of somatic cells was not static or irreversible, indicating that enucleated eggs and ESCs

held factors that could rewrite the epigenetic networks controlling cell identity (204). Nonetheless, the underlying mechanisms responsible for the reprogramming of cell fates remained poorly understood. In 2006, Yamanaka and colleagues hypothesized that the factors that were involved in maintaining ESCs' stemness should be sufficient to induce pluripotency in somatic cells. By simply overexpressing four TFs, OCT4, SOX2, MYC, and KLF4, Yamanaka was able to reprogram fibroblasts into iPSCs (shortly mentioned in the previous chapter) (181,205). iPSCs formed colonies with ESC characteristics and gene signatures, as well as contributed to the three germ layers in subcutaneously transplanted mice (181). The groundbreaking work from Shinya Yamanaka earned him the Nobel Prize in Physiology or Medicine in 2012, together with John Gurdon, and paved the way for the establishment of a whole new scientific field: direct cell reprogramming.

## Direct cell reprogramming by transcription factors

The idea that defined factors could reshape the fate of a cell actually emerged before Yamanaka's work, in the late 1980s, when Lassar and colleagues reported that the ectopic expression of a coding sequence involved in skeletal muscle determination, MyoD1 was sufficient to induce myogenesis in mouse fibroblast (206). Even though the concepts of cell reprogramming and transdifferentiation were unknown or at least underappreciated at that time, this study contributed to the notion that genetic regulators such as TFs could specify and modulate cell identity. Essentially, direct cell reprogramming (or transdifferentiation) is the process by which differentiated cells are directly converted into a different specialized cell type without going through a pluripotent state (207). Both cell reprogramming and direct cell reprogramming fit under the umbrella of cell conversion, as they represent different routes to change cell identity. Nevertheless, direct cell reprogramming offers a few advantages over iPSC reprogramming. Firstly, it does not require further differentiation towards the desired cell type, resulting in a faster and more efficient procedure. Secondly, it can occur both *in vitro* and *in vivo*, making it more suitable for *in situ* tissue repair. Lastly, it poses a reduced risk of tumorigenesis, one of the major concerns in cell reprogramming (207).

Since Yamanaka defined a "cocktail" of TFs capable of reshaping cell lineages, similar direct reprogramming strategies have been employed to obtain clinically relevant differentiated cell types both *in vitro* and *in vivo*, such as cardiomyocytes (208–211), hepatocytes (212,213), pancreatic  $\beta$ -cells (214), several types of neurons, including glutamatergic (215,216), dopaminergic (217–220) and motor neurons (221), and neural stem cells (222–224). However, the overall efficiency of reprogramming in most studies is low, reprogrammed cells often need further maturation in culture and the safety of available methods for delivering gene, proteins or cells is continuously under debate (207).



Alternatively, small molecules have been explored as a safer and cheaper option. Small molecules are cell-permeable low molecular weight chemical compounds that can interact with cellular targets and modulate signaling pathways or alter DNA compaction, making it more accessible to other regulatory molecules. For those reasons, small molecules have been used alone or in conjugation with TFs to induce changes in transcriptional programs and enhance the reprogramming of different cell types (225). Successful examples include reprogramming into neurons (226–228) and cardiac cells (229,230). Nonetheless, small molecules are still unable to replace every TF combination and the duration of their active effect, plus the timing of their administration requires extensive investigation (207,225).

### **Direct cell reprogramming towards hematopoietic fates**

In the hematopoietic system, reprogramming strategies were also implemented to generate both mature and stem/progenitor cells (**Figure 5**) (231). The first report of hematopoietic lineage conversion came from the work of Thomas Graf in 1995 (232). By overexpressing GATA1, a key TF for the differentiation of the erythroid and megakaryocytic lineages, in avian myeloblasts, Graf induced the conversion of these cells into erythroid and megakaryocyte progenitors. Subsequent studies used the same TF to facilitate the conversion of several lympho-myeloid progenitors to erythroid and megakaryocytic cells (233,234). The common link among these studies was that GATA1, when used alone, was only able to induce reprogramming in immature cells, suggesting that GATA1 required additional factors to effectively drive reprogramming in more mature cell types. Indeed, the collective forced expression of GATA1, TAL1 and C/EBP $\alpha$  succeeded in reprogramming differentiated mature B cells into erythroid-like cells (237). Furthermore, GATA1, TAL1, LMO2, and c-MYC converted mouse and human fibroblasts into primitive-like erythroid progenitors (236). Addition of KLF1 or MYB to the previous TFs combination resulted in the expression of adult hemoglobin in reprogrammed cells. A study from the same group has shown that *bona fide* megakaryocyte progenitors were obtained after overexpressing the earlier four TFs (GATA1, TAL1, LMO2, and c-MYC) plus GATA2 and RUNX1, which biased the reprogramming process toward the megakaryocyte lineage (237).

Recently, a lot of efforts have been placed into reprogramming immune cell fates, especially macrophages/monocytes, dendritic cells, plus NK and T cells, to develop personalized cancer immunotherapies (**Figure 5**) (238). Macrophages were the first to be generated from committed lymphoid cells (pre-T and B cells) (239,240), and fibroblasts (241), using C/EBP $\alpha$  alone or C/EBP $\alpha$ / $\beta$  plus PU.1, respectively. The reprogrammed cells acquired macrophage-like phenotype, morphology, and function. Interestingly, PU.1 alone converted the same committed pre-T cells into myeloid dendritic cells, underscoring the importance of this TF for myeloid development (240). In fact, PU.1 was part of the TF cocktail that was recently used

to induce a conventional dendritic cell type 1 (cDC1) fate in mouse and human fibroblasts (242,243). The reprogrammed dendritic cells were able to process and present antigens at cell-surface, as well as secrete inflammatory cytokines and do cross-presentation of antigens. Of note, the same TF combination composed of PU.1, BATF3 and IRF8 reprogrammed mouse and human cancer cells into antigen-presenting cells (APCs), resembling cDC1s in morphology and function (244). Reprogramming restored the ability of cancer cells to present endogenous tumor-associated antigens and endorsed cytotoxic T cell-mediated killing. The same way reprogramming cancer cells to APCs is set to revolutionize the development of cancer immunotherapies, generating reprogrammed cells with hematopoietic progenitor/stem-like properties represents the ultimate goal of regenerative medicine for the treatment of blood disorders.

Pereira *et al.*, have taken advantage of the knowledge generated during reprogramming to mature cell types to induce a hemogenic program in mouse and human fibroblasts (245,246). Together, GATA2, GFI1B and FOS reprogrammed transgenic mouse embryonic fibroblasts harboring a human CD34 reporter (hCD34) into hemogenic endothelial-like precursor cells from which hematopoietic colonies emerged. Hemogenic precursors exhibited a Prominin1<sup>+</sup>Sca1<sup>+</sup>hCD34<sup>+</sup>CD45<sup>-</sup> cell-surface phenotype and endothelial-like transcriptional programs. Prominin1 is a somatic stem cell marker (247), Sca1 marks all HSCs and MPPs (130,248) and CD34 is a very well-characterized hemogenic/HSPC marker (47,55,130,137), whereas CD45 is found in nucleated blood cells (155). Notably, budding hematopoietic cells expressed markers and gene expression profiles characteristic of HSCs (245). The *in vivo* counterparts of the *in vitro* generated hemogenic precursors were later found in the mouse placenta (249). In the human system, reprogrammed cells could be separated from non-reprogrammed cells through the expression of CD49f, ACE, and CD34. Mechanistically, GATA2 binds first to its target genes and then recruits the other factors to both inhibit the expression of fibroblast genes and enable the expression of endothelial and hematopoietic genes (246). GATA2 targets include the CD34 gene, the murine HSC marker CD9 (150), the EHT facilitator G-coupled protein receptor GPR56 (250) and RUNX1. The transition between cell types reported *in vitro* resembled the EHT that occurs in the embryo and placenta, during specification of definitive hematopoiesis.

Several others have attempted to generate HSPCs from fibroblasts (251,252) and lineage committed blood cells (253), employing different culture conditions and combinations of TFs (**Figure 5**), with a range of hematopoietic reconstitution potentials. Nevertheless, starting with committed blood cells, rather than unrelated cell types such as fibroblasts, might be unviable from a therapeutic point-of-view when patients suffer from hematological disorders caused by mutations in progenitor or stem cell pools. Interestingly, GATA2 was either part of the TF cocktail or of the gene signature of reprogrammed cells, emphasizing its prominent role as a master regulator of hemogenic and hematopoietic stem cell specification.

Starting from endothelial cell sources resulted in reprogrammed HSPC-like cells with long-term engraftment ability (254,255), possibly due to developmental proximity of the cell types. As far as reprogramming to HSPCs goes, there is still no standardized cell source, culture conditions or TF combination to produce *bona fide* long-term progenitors for clinical use. Nonetheless, direct cell reprogramming strategies utilizing lineage-instructive TFs are powerful tools in the study of *in vivo* developmental processes that can be difficult to elucidate by other means.

A better understanding of HSC ontogeny is, therefore, crucial for the development of improved *ex vivo* expansion and manufacturing protocols for clinical applications. Genetic tools, such as Clustered Regularly Interspaced Short Palindromic Repeats (CRISPR)-based screenings, may prove useful in investigating the regulators of human hemogenic reprogramming and, ultimately, human EHT and HSC emergence.

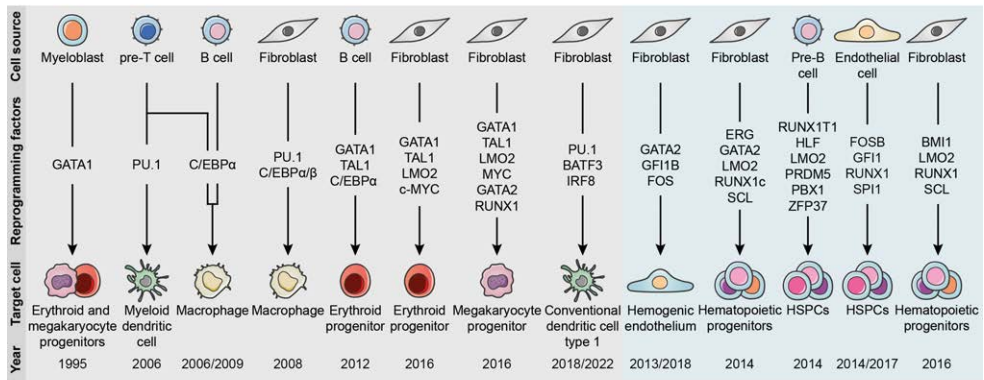


**Figure 5. Direct reprogramming strategies applied in the hematopoietic system.** Lineage-specific TFs reprogrammed hematopoietic and non-hematopoietic cells towards erythroid, megakaryocyte, dendritic cell, hemogenic endothelium, and hematopoietic stem and progenitor cell (HSPC) fates. Reprogramming approaches resulting in committed cell lineages are highlighted in grey, and immature fates are highlighted in blue. The year the studies were published is shown.

# The CRISPR/Cas9 system

## Discovery and mechanism of CRISPR/Cas complexes

Clustered regularly interspaced short palindromic repeat DNA sequences were initially discovered in 1987 in *Escherichia coli* and consisted of repeat elements separated by non-repeating DNA sequences, also known as spacers (256). Later, CRISPR elements were found in many bacteria and archaea (257), adjacent to various conserved genomic sequences called CRISPR-associated (Cas) genes (258). Cas genes encode proteins, i.e., enzymes, with both helicase and nuclease activities, capable of opening and cutting DNA (258). It was only after two decades following its initial discovery that scientists successfully attributed a function to the CRISPR/Cas system, identifying it as an adaptive immune system acting against bacteriophages and during plasmid transfer (259–261).

Mechanistically, upon infection, bacteria containing CRISPR sequences integrate a segment of phagic DNA in its genome as a new spacer region (261). CRISPR elements then undergo transcription and maturation into a single CRISPR RNA (crRNA), containing a protospacer sequence of 20 nucleotides that binds to the exogenous DNA through complementary base pairing (260). Besides the crRNA, the endogenous CRISPR system also requires another short RNA molecule, the trans-activating crRNA (tracrRNA) (262). While the mature crRNA serves as a guide for the CRISPR-associated protein 9 (Cas9), the tracrRNA forms a complex with the crRNA to facilitate the Cas9 protein-RNA complex formation. Recognition of the exogenous sequence by the dual-RNA structure prompts Cas9 to introduce double-strand cuts in the foreign DNA, resulting in its disruption and subsequent inactivation (262,263). Importantly, it was shown that the CRISPR system from one bacterium could be transferred to a different bacterium (264), and that Cas9 could be manipulated to target specific DNA sequences (262,263). In addition, the CRISPR-Cas9 system could be directed using a chimeric RNA formed by fusing the crRNA and the tracrRNA into a unified molecule - a single guide RNA (sgRNA) (262).

The successful recognition of the sgRNA requires the presence of short sequences rich in guanine, termed protospacer-adjacent motifs (PAMs) (265). Even though scientists have adapted various CRISPR/Cas systems for genome targeting, the most commonly used Cas9 is derived from *Streptococcus pyogenes* (SpCas9) (266). SpCas9 recognizes a common PAM sequence with the sequence NGG in the

genomes of most organisms, enabling the targeting of any DNA sequence located close to that PAM (267). This feature has opened avenues to use the CRISPR/Cas9 system as a promising genome-engineering tool.

The induced double-strand break can be repaired mainly through two different mechanisms: non-homologous end-joining (NHEJ) or homology-directed repair (HDR) (Figure 6) (268). NHEJ is the most frequently used mechanism by mammal cells in the absence of a complementary template sequence (269). This pathway is efficient, but prone to errors. During NHEJ, DNA is repaired by directly ligating the broken ends together with random nucleotides, normally leading to frameshift mutations, or base insertions and deletions at the break site that disrupt gene function (270). The HDR pathway requires the presence of an exogenous DNA template, either single-stranded or double-stranded, to fill in the gap created by Cas9. These template sequences contain homologous regions, known as homology arms, which are complementary to the 5' and 3' adjacent regions of the break. Moreover, DNA templates can be modified to accommodate engineered sequences placed between the homology arms (271). Consequently, DNA repair mechanisms have been harnessed and tailored to achieve numerous CRISPR/Cas9 applications in eukaryotes (272).

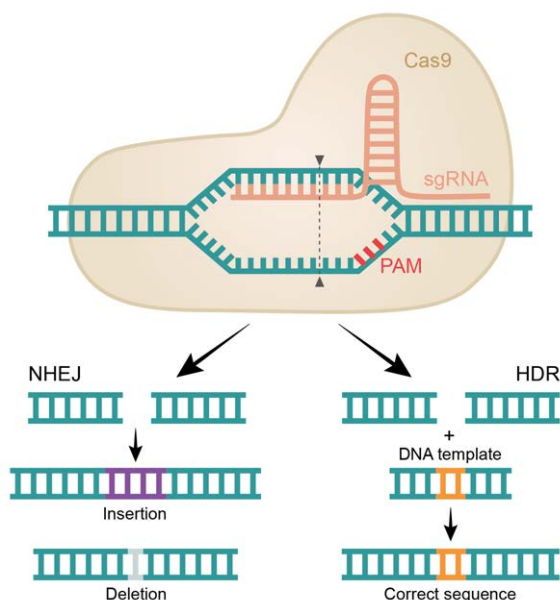


**Figure 6. Schematic representation of the CRISPR/Cas9 system and mechanisms of DNA repair.** The CRISPR/Cas9 complex is composed of a single guide (sg) RNA that directs Cas9 double-strand cuts at a target sequence, juxtaposed to a protospacer-adjacent motif (PAM). Double-strand breaks are repaired by the non-homologous end-joining (NHEJ) pathway leading to random mutations, including insertions and deletions, or by homology-directed repair (HDR) in the presence of a DNA template. The DNA template contains two homology arms and can be engineered to insert any desired sequence at the break site.

# Applications of CRISPR/Cas9

## Genetic models

Among many variations, one of its main applications is to allow targeted gene manipulation through the generation of KO or knock-in (KI) cell lines and animal models. KO mice can easily be generated by injecting Cas9 messenger RNA (mRNA) or protein, together with sgRNAs targeting one or multiple genes of interest to fertilized mouse zygotes and allowing the DNA breaks to be repaired by NHEJ (273). Errors caused during repair often result in gene disruption and loss of protein function. This type of model is very useful when studying the function of specific proteins *in vivo* or *in vitro*.

On the other hand, HDR is used when trying to achieve precise gene editing or create more complex KI mouse models by inserting reporter genes or protein tags, such as fluorescent proteins. One way to utilize precise gene editing is by generating specific mutations in mice responsible for human diseases (274). Disease modeling in transgenic organisms has the additional advantage of enabling drug testing in a controlled environment. Moreover, multiplex delivery of sgRNAs allows the investigation of polygenic diseases, i.e., affecting more than one gene, such as diabetes, cardiovascular diseases, neurodegenerative diseases, schizophrenia, and autism (275).

Interestingly, to overcome challenges in delivering the large Cas9 molecule to somatic cells, Platt and colleagues generated a *Cas9* gene KI mouse for efficient genome editing in multiple tissues *in vivo* using both viral and nonviral sgRNA delivery methods (276).

## Gene therapy

Gene therapy is the application of genetic materials and related techniques to cure human diseases caused by genetic mutations, involving the replacement of impaired genes with healthy, functional ones (277). The most commonly used carriers of engineered genomic components are viral vectors, such as adenoviruses, adeno-associated viruses and lentiviruses. Due to its flexibility and versatility of applications, the CRISPR/Cas9 system has been used in conjunction with well-established delivery methods to correct cancer and disease-inducing genes.

Examples in the hematopoietic system include Sickle Cell Disease (SCD) and  $\beta$ -Thalassemia, two monogenic disorders that affect hemoglobin production in RBCs. Both diseases are caused by mutations in the hemoglobin  $\beta$  subunit gene (*HBB*), resulting in impaired erythropoiesis. In this context, CRISPR KO of the TF BCL11A in CD34<sup>+</sup> HSCs from two patients with SCD and  $\beta$ -Thalassemia lifted the

suppression of fetal hemoglobin that compensated for the abnormal adult type and led to the attenuation of the diseases (278). Since SCD is caused by a defined single amino acid substitution, recent efforts were proven successful in correcting that mutation in patient's HSCs *ex vivo* (279). This approach used a combination of Cas9 protein with a chemical improved sgRNA and adeno-associated viral delivery of the correct DNA sequence to achieve homologous recombination at the *HBB* locus. A following study by the same group focused on the safety, efficacy, and toxicology of *HBB* gene correction in mobilized CD34<sup>+</sup> cells from healthy and SCD patient donors (280). Importantly, immunocompromised mice transplanted with edited human cells did not show abnormal hematopoiesis, genotoxicity, or tumorigenicity, setting the stage for clinical trials in patients with SCD.

Nevertheless, the limitations of CRISPR platforms need to be carefully addressed to ensure efficient and safe biomedical benefits. These include undesired off-target effects and NHEJ leaking in HDR systems, which can cause on-target effects, such as the formation of micronuclei with parts or whole chromosomes outside the main nucleus in cells, and chromosomal rearrangements (281).

## Genomic screenings

Delivery of sgRNA pools targeting virtually all genes can be used to disturb thousands of sites simultaneously, thereby enabling unbiased genome-wide functional screens to identify genes and proteins involved in different cellular processes. In this context, positive and negative selection screens have been performed in human cells by introducing loss- or gain-of-function mutations (282,283). Shalem *et al.*, delivered a genome-wide sgRNA library targeting more than 18,000 genes via lentivirus to human cells. The library was initially utilized in a negative selection screen to identify survival genes in both the melanoma A375 cell line and the stem cell line HUES62. Deep sequencing revealed important ribosomal genes, evident from the lack of sgRNAs targeting these genes in viable cells. Additionally, in the same study, researchers identified drug-resistant genes in the A375 cell line through a positive selection screen, resulting from the selective advantage caused by a gain-of-function mutation present in the surviving cells (282).

Similarly, genome-wide CRISPR/Cas9 screens have been used to identify positive and negative regulators of immune cell processes in human T cells (284) and mouse dendritic cells (285). Likewise, this tool could be useful in the discovery of regulators of HSPC self-renewal and differentiation, as well as in the identification of new therapeutic targets for the treatment of blood malignancies, such as AML (286). In fact, Yudovich and Bäckström have developed a combinatorial approach using lentiviral delivery of sgRNAs followed by transient expression of Cas9 mRNA introduced by electroporation in human cord blood-derived CD34<sup>+</sup> HSPCs (287,288). High editing efficiency was obtained for two surface markers and edited

cells were capable of engrafting and reconstituting the hematopoietic system of immunodeficient mice (287). This approach was later expanded to allow dual gene targeting and traceability of edited cells through the addition of fluorescent tags (288). Large screens are yet to be reported in HSCs. This might be due to difficulties in delivering the large Cas9 gene/protein or in acquiring enough homogeneous HSCs to maintain sgRNA representativity, wherein the utilization of a higher number of sgRNAs corresponds to an increased requirement for cells to achieve an identical representation of each sgRNA.

Knowledge from CRISPR/Cas9 KO screens in HSCs could then be applied to improve current methods for *ex vivo* HSC expansion and generation from iPSCs or alternative cell types. Moreover, the possibility of correcting defected genes using patient's somatic cells before iPSC or direct cell reprogramming is very enticing. Indeed, this technology has already been utilized in the context of cell reprogramming (289,290). A CRISPR/Cas9 KO screening identified the zinc finger protein *Zfp266* as the most robust barrier to the generation of iPSCs from mouse fibroblasts (290), and loss of the epigenetic regulator *Dmap1* kept cells in a progenitor state during cardiac reprogramming (289). Thus, CRISPR/Cas9 screening platforms could also prove useful in investigating the regulators of human hemogenic reprogramming and HSC specification.

Understanding the molecular drivers of hemogenic reprogramming will contribute to improving the efficiency and fidelity of the process. In this regard, TFs are major molecular players in the instruction of cell fates, as demonstrated by their use in cell reprogramming studies. Even though the role of many TFs for tissue-specific gene expression during interphase has been extensively studied, few reports have focused on their role in mitosis for the acquisition and maintenance of lineage identity (291,292).



# Transmission of cell fates through mitosis

During mitosis, cells undergo dramatic changes in nuclear organization and gene expression. The processes of chromatin condensation, nuclear envelope breakdown, detachment of RNA polymerase from chromosomes, and dispersion of TFs throughout the cytoplasm collectively result in the reduction of transcription to basal levels (293–296). Following mitosis and nuclear reassembly, transcriptional patterns of gene activation and repression must be reestablished in daughter cells, according to the cell lineage. These transitions between different states of gene expression impose a challenge for the preservation of cell identity. Therefore, several epigenetic mechanisms must be implemented to ensure proper lineage commitment. Classic mechanisms include the preservation of DNA methylation patterns in promoter regions for gene silencing, the propagation of post-translational histone modifications and small interfering RNA (siRNA)-mediated gene silencing (191,291).

DNA methylation is a well-characterized epigenetic mechanism that is inherited through cell division (297,298). Long-term gene silencing mediated by DNA methylation is crucial for the regulation of cell type-specific expression patterns, X chromosome inactivation and repression of repetitive elements. During each cell division, the patterns of DNA methylation, particularly at cytosine-guanine rich regions known as CpG islands located near promoter sites of genes, are reestablished after DNA replication (298). Restoration of DNA methylation states before the next S phase is critical for the maintenance of cell identity.

Nevertheless, there are indications that this mechanism may not be enough to successfully transmit transcription profiles through the cell cycle. For instance, it has been shown that the DNase I hypersensitive sites in the human *hsp70* locus remain open in mitotic chromatin, suggesting the presence of an “epigenetic mark” necessary to keep that region accessible (294). Years later, the TF HSF2 was reported to bind to the *hsp70i* promoter during mitosis to prevent condensation at that site and keep it open (299). This factor was compared to a “bookmark”, which marks the last page read from a book and allows the reader to resume from where they stopped (300). Since then, several general and lineage-specific TFs were found to bind to condensed chromosomes and mark specific chromatin sites during mitosis, a mechanism termed “mitotic bookmarking” (301,302).

This mechanism is not unique of TFs. Post-translational modifications in histone proteins have been recognized as another level of chromatin mitotic bookmarking (303,304). Histones are core protein components of chromatin responsible for organizing DNA in the nucleus into repetitive, compact units called nucleosomes (305,306). Each nucleosome is composed of DNA wrapped around a histone octamer formed by two copies of four histone proteins: H2A, H2B, H3, and H4. Post-translational modifications, such as acetylation and methylation at lysine (K) of H3 and H4 play a critical role in regulating gene expression and directing gene silencing or activation patterns in mother and daughter cells (307,308). For example, trimethylation of H3K9 and H3K27 are associated with a repressive chromatin state, while di- and trimethylation of H3K4, and acetylation of H3K27 and H4K16 are associated with active chromatin. Interestingly, histone methylation marks are highly retained in mitosis, whereas acetylation marks are overall decreased (303,307,308). Importantly, levels of H3K27 acetylation were comparable between asynchronous and mitotic ESCs (303). This “active enhancer” mark was found in promoters of housekeeping genes, as well as at enhancer regions of pluripotency-associated genes, suggesting a role for the transmission of stem cell identity after mitotic exit.

## Mitotic retention and bookmarking by transcription factors

Contrary to the initial belief that mitotic chromatin was silent and voided of TFs, numerous TFs have been reported to decorate condensed chromatin during cell division in recent years (301,302,309). Mitotic chromatin binding or retention can be defined as the broad association of proteins with mitotic chromatin, visualized by fluorescent imaging methods. In turn, bookmarking entails a direct physical interaction with specific genomic sites, normally detected with chromatin pull-down techniques (**Figure 7**) (310).

Mitotic bookmarking by TFs was proposed to facilitate the rapid reactivation of target genes in newborn cells entering interphase, thereby contributing to the propagation of transcriptional memory and the preservation of cell identity (301,310). Several studies revealed that the depletion of factors retained on mitotic chromatin delayed transcription reactivation of target genes upon mitotic exit (303,311–315). The hematopoietic TF GATA1, a major regulator of the erythroid lineage, remains bound to a subset of its target genes during mitosis (311). Mitotic degradation of GATA1 in erythroid cells led to the delayed restart of bookmarked genes’ expression, along with increased transcription of GATA1-repressed genes, such as *Gata2* and *Kit*, which are typically present in immature cells. The FOXA1 factor, which is necessary for hepatic differentiation, remains bound to mitotic

chromatin in live HUH7 adult human hepatoma cells and virtually all FOXA1-bound sites in mitotic cells are shared with asynchronous cells (312). Furthermore, FOXA1 knockdown during mitosis demonstrated that FOXA1 is essential for the initial activation of target genes following mitotic exit. Likewise, the pluripotency regulator ESRRB was shown to bind and control early G1 reactivation of bookmarked genes in ESCs (316). Additionally, Festuccia and colleagues showed that organized nucleosomal arrays remain intact during mitosis at sites bookmarked by ESRRB but are disrupted at non-bookmarked sites (317). The authors suggest that preservation of nucleosomal positioning during mitosis by ESRRB may facilitate the quick re-establishment of gene expression regulatory complexes at specific enhancers and promoters. However, these studies did not address the functional consequences of mitotic bookmarking at mitosis-to-G1 (M-G1) transition for cell fate commitment or maintenance.

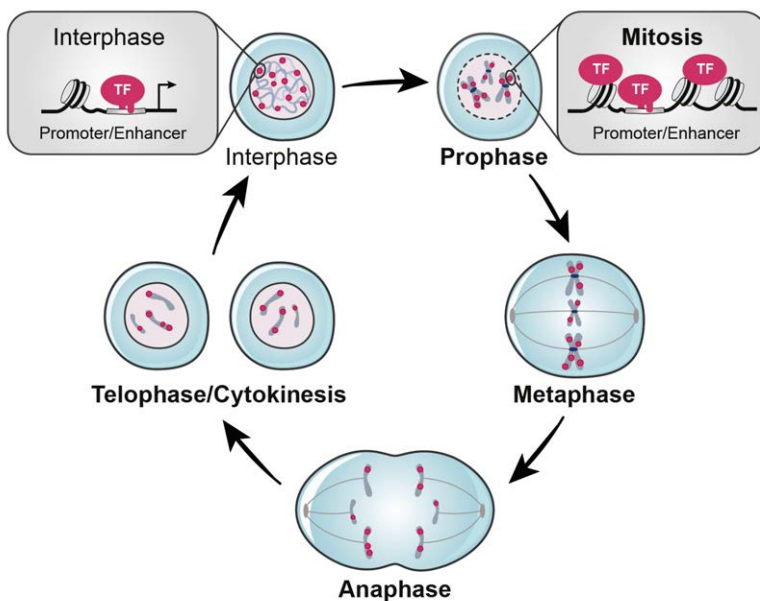


**Figure 7. Mitotic retention and bookmarking by transcription factors.** During interphase, transcription factors (TFs) bind to promoter and enhancer sites to allow gene transcription. In mitosis, several TFs remain bound to mitotic chromatin and some mark specific promoters/enhancers sites to prompt transcriptional activation of gene as cells re-enter interphase.

Timely destruction of pluripotency TFs SOX2 and OCT4 in mitotic ESCs compromised their ability to maintain pluripotency (303,315). The presence of SOX2 during the M-G1 transition was necessary not only to maintain the pluripotency lineage fate but also to induce neuroectodermal differentiation (315). Ectopic expression of a mitotic degradable OCT4 protein together with SOX2, KLF4 and cMYC, in mouse embryonic fibroblasts, resulted in decreased numbers of iPSC colonies, plus defects in upregulating the early pluripotency marker *Nanog* (303).

Of note, mitotic retention does not imply mitotic bookmarking, and the reactivation of gene expression in interphase can be governed by non-bookmarker factors. BRN2, a regulator of neural identity, was found to associate with mitotic chromosomes during the proliferation of neural stem cells but did not bookmark specific genomic regions (or at least DNA-specific interactions could not be detected). Nonetheless, when BRN2's ability to bind to chromosomes during mitosis was compromised, the expression of its target gene, *Nestin*, was reduced (309). These findings are in line with observations for FOXA1, in which target gene expression after mitotic exit occurred regardless of the bookmarked status of the genes, suggesting that TF accumulation on mitotic chromosomes by nonspecific binding might be enough to enable reactivation of all target genes (312).

### **Transcription factor binding (un)specificity during mitosis**

The association of TFs with DNA comprises both sequence-specific and non-sequence-specific interactions (292). Sequence-specific interactions involve the direct binding of residues within the DBD of TFs to specific DNA bases or recognition sequences, also known as motifs. These are stronger and last longer than nonspecific binding, which is mainly dependent on electrostatic interactions (318). Nonetheless, nonspecific interactions are thought to facilitate the search for sequence-specific regions (319) and are the predominant interaction responsible for the observable mitotic chromatin binding/retention (302,309,312). Importantly, mitotic chromatin binding/retention was correlated with electrostatic properties, particularly of TFs' DBDs (302). This observation suggests that this specific region is primarily responsible for DNA engagement, regardless of interaction type.

Fluorescence recovery after photobleaching (FRAP) is commonly used to assess the dynamic of protein movement between subcellular compartments. In FRAP, unbound and transiently bound TFs display a rapid recovery of the fluorescent signal after bleaching cells expressing fluorescent-tagged TFs with a laser beam. Conversely, a slow signal recovery indicates more stable interactions (320). Single molecule tracking is a complementary technique that focuses on following the behavior of an individual particle, allowing the quantification of the time spent by each tracked particle at a specific subcellular location (321). Overall, binding in mitosis is more dynamic than in interphase, with TF spending less time (reduced residence time) bound to chromatin in mitotic cells (312,315,316,322), suggesting that chromatin interactions are mostly transient and nonspecific.

FOXA1 was found to bind both specifically and unspecifically to mitotic DNA (312). ChIP-seq analysis revealed specific TF binding to a small subset of interphase genes. However, dissociation from the majority of interphase targets suggested the occurrence of nonspecific binding as well. This hypothesis was confirmed by faster FRAP half-times in mitotic cells compared to asynchronous cells. To further elucidate the role of specific versus nonspecific binding in the overall association of

FOXA1 with DNA, the researchers utilized two mutant GFP-tagged versions of the TF: one that disturbs specific DNA binding to DNA bases (GFP-FOXA1-NH), and one that disrupts nonspecific binding to phosphate groups of the DNA backbone (GFP-FOXA1-RR), affecting only slightly sequence-specific binding (323). When overexpressed in live mitotic cells, GFP-FOXA1-RR dispersed through the cytoplasm, while GFP-FOXA1-NH was mainly retained in mitotic chromatin, demonstrating that nonspecific binding, rather than specific binding, is responsible for mitotic chromatin binding. In a complementary approach, this time to determine the relevance of specific and nonspecific interactions to target known FOXA1 genomic sites in mitosis, they used both constructs in a ChIP experiment and showed that binding to FOXA motifs was only significantly impaired in GFP-FOXA-NH expressing mitotic cells. These results confirmed that bookmarking is most likely governed by sequence-specific DNA interactions, and broader chromatin retention is governed by nonspecific binding.

### **Methods to study mitotic retention and bookmarking**

The apparent misconception that mitotic chromatin was lacking many TFs was most likely related with the methodology used at that time to visualize proteins at the subcellular level. Mitotic retention was initially assessed with fluorescent-conjugated antibodies for the TF of interest, since it allowed probing the localization of endogenous proteins. However, the most widely used fixation method based on formaldehyde was shown to quickly disrupt the interactions of TFs with mitotic chromosomes (322). This disruption occurs through the rapid inward formation of cross-links between formaldehyde and the TFs, which depletes the cytoplasmic pool available to bind to chromatin. In turn, KI or overexpression of fluorescent proteins or tags fused to either N- or C-terminal positions of TFs have solved this, enabling the visualization of TFs by live-cell imaging, including many that were previously thought to be displaced (303,315,316,322). Additionally, this technique allows for quantitative assessments through the comparison of fluorescence intensities between chromatin and cytoplasm in mitotic cells.

Protein quantification of subcellular fractions by western blotting is also useful for interrogating the abundance and location of the TFs in mitotic cells, especially when it comes to detecting proteins in the cytoplasmic or chromatin-bound fractions. (303). More complex proteomic approaches, such as mass spectrometry of sorted mitotic chromosomes, are particularly valuable in the identification of new potential bookmarkers and TF protein complexes that might be established during mitosis (324). Fluorescent live-cell imaging and proteomic analysis of mitotic cells enable the assessment of chromatin decoration by TFs, but do not provide information about sequence-specific binding to genomic targets.

ChIP-seq is the most frequently used methodology to assess sequence-specific binding of TFs to mitotic DNA. Typically, TFs bind to tens of thousands of sites in

asynchronous cells. However, this number is reduced to a few thousand or even a few hundred in mitotic cells, even though global genomic accessibility remains unaltered (317,322,325). The reduction can be attributed to the transient binding nature of most TFs during mitosis or to the fact that ChIP-seq involves formaldehyde fixation, which can disrupt TF binding to mitotic DNA (303,311,312,315).

Double-fixation methods, involving an initial step of fixation with milder agents like disuccinimidyl glutarate (DSG), have been demonstrated to improve immunostaining and ChIP efficiency compared to formaldehyde fixation alone (317). However, this improvement was not consistent across all tested TFs, implying that intrinsic properties of the TFs or the binding sites might contribute to the low number of peaks observed. For these reasons, it is important to obtain pure population of mitotic cells to avoid signal contamination by interphase cells. Mitotic populations synchronized with cell cycle arresting drugs, such as nocodazole (that promotes cell arrest in prometaphase) can be FACS-purified using mitotic specific antibodies against either H3 serine 10 phosphorylation or phosphorylated serine/threonine residues followed by a proline, as these are common protein modifications occurring in mitosis (311,326,327). Another alternative, which is applicable only to adherent cells, involves performing a simple plate shake-off of arrested cells, referred to as "mitotic shake-off" (303,316,328). Cells undergoing mitosis or drug-induced mitotic arrest round up and can be easily collected at high purities by gently tapping the culture plate. In the future, alternatives to ChIP-seq that do not require the use of fixatives, such as CUT&RUN can be optimized for tissue-specific TFs to help overcome some of the current challenges in deciphering the true extend of TF-binding to DNA in mitosis (329,330).

#### *Methods to address the role of mitotic DNA binding*

To address the role of mitotic retention or bookmarking, several groups have adapted strategies to abrogate TF-DNA interaction during M-G1 transition by either degrading the TFs or impairing its binding to mitotic chromatin (303,309,311,312,315,316). Cell cycle transitions are possible due to the cyclic destruction and synthesis of cyclin proteins (331). Cyclin B1 forms a complex with cyclin-dependent kinase 1 to facilitate cell division. During cell cycle, cyclin B1 levels increase and reach their peak in metaphase. The degradation of cyclin B1 is necessary for cells to exit mitosis and enter the next interphase. This process is orchestrated by the anaphase-promoting complex, which marks cyclin B1 for destruction via ubiquitination at the onset of anaphase, thereby enabling the transition to the G1 phase (332). Using this knowledge, Kadauke and others generated fusion proteins containing the TF of interest, namely GATA1 (311), SOX2 (315) and OCT4 (303), and the mitosis-specific degradation (MD) domain of cyclin B1 (amino acids 13–91) to target TF for destruction at M-G1. Substitution of an arginine for an alanine (R42A) inactivated the domain and resulted in similar

protein levels throughout the cell cycle. Mitotic degradation of the TFs led to delayed expression of bookmarked genes, and in the case of SOX2 and OCT4, difficulties in inducing or maintaining pluripotency in culture (303,315). In a different study, FOXA1's role in the reactivation of its targets after mitosis was evaluated by siRNA-mediated gene knockdown (312). HUH7 cells were transfected with siRNA targeting *FOXA1*, arrested in mitosis and then released at different time points, and the impact for *de novo* RNA synthesis was measured by the incorporation of 5'-ethynyluridine (a modified detectable nucleotide). Nascent transcript quantification confirmed the requirement of FOXA1 for target gene expression (independently of bookmarking), while non-target genes did not require FOXA1 presence for their expression during mitotic exit. More recently, Soares *et al.*, developed a mitotic-specific dominant-negative approach to address the need of BRN2 for the reactivation of its target *Nestin* in early M-G1 (309). The negative-dominant construct comprised an inducible version of the DBD of BRN2 fused to an mCherry fluorescent protein, flanked by a nuclear export signal. The nuclear export signal would keep the construct outside the nucleus until mitosis, when nuclear envelop breakdown exposes mitotic chromatin to cytoplasmic content. During proliferation of neural stem cells, the negative-dominant construct could not prevent the association of endogenous GFP-tagged BRN2 proteins with metaphase chromatin. Nevertheless, reactivation of *Nestin* expression was impaired in the presence of the negative-dominant construct, as the number of *Nestin* transcripts were significantly reduced, supporting the importance of nonspecific DNA binding for chromatin engagement and gene reactivation at M-G1.

# Aims of the thesis

Hemogenic reprogramming holds promise in addressing challenges tied to HSC transplantation. However, novel findings regarding the markers and regulators of hemogenic reprogramming are needed to enhance the efficiency and fidelity of this system. These discoveries may also shed light on the corresponding *in vivo* developmental process, which are finely regulated by key TFs. The importance of TF-mediated mitotic bookmarking for *in vivo* lineage commitment during the development of a living organism remains to be addressed. This is particularly relevant in the context of developmental hematopoiesis, as cell division is intricately linked to HSC fate decisions.

Thus, the overarching aim of this thesis is to **elucidate the mechanisms controlling the specification of definitive HSPCs during hematopoietic development and reprogramming**. The main aim can be further divided into three specific aims, each one addressed in the individual studies included in this thesis:

1. Identify novel markers and genomic targets of GATA2 at the early stages of human hemogenic reprogramming (Study I);
2. Identify positive and negative regulators of hemogenic reprogramming through a CRISPR/Cas9-based screening (Study II);
3. Investigate the role of mitotic bookmarking by hemogenic reprogramming factors in HSC specification (Study III).



# Summary of results

## Study I – Hemogenic Reprogramming of Human Fibroblasts by Enforced Expression of Transcription Factors

Until now, no specific phenotype has been identified that differentiates human HSCs from their precursors, although certain molecules are expressed in developing HSCs. CD49f encoded by the integrin alpha 6 gene (*ITGA6*) is a marker of long-term repopulating HSCs (129) and of mesodermal hemato-endothelial precursors in human embryos (154). These cells are also positive for ACE (CD143) and may constitute the earliest precursors of human hemogenic endothelium before the appearance of CD34<sup>+</sup> IAHCs (152). Ectopic expression of GATA2, GFI1B and FOS is sufficient to induce hemogenic fate in mouse and human fibroblasts (245,246). Reprogrammed cells in the human system express CD49f, ACE, and a small percentage expresses CD34 (246). These cells upregulate several hematopoietic genes including the *CD9* gene, which is present in mouse HSCs (150) and plays a role in human HSPC homing (151). *CD9* has also been shown to be a direct target of GATA2 (246). Therefore, CD9 may constitute an additional marker human hemogenesis.

### **CD9 is a prospective marker of human hemogenic precursor cells**

In **paper I**, we describe the steps involved in hemogenic reprogramming of human dermal fibroblasts (HDFs) using a doxycycline inducible vector (pFUW-tetO), encoding GATA2, GFI1B and FOS individual factors. This paper also includes an alternative protocol to expand cell numbers for ChIP-seq analysis at day 2 of reprogramming. Importantly, we described the binding sites for GATA2 in *ITGA6* (CD49f) and *ACE* (CD143) loci when cells are co-transduced with the three factors or with GATA2 individually (**Figure 8A**). Flow cytometry analysis revealed 17% of CD49f<sup>+</sup>CD9<sup>+</sup> cells after 25 days of reprogramming induction. Inside the double positive population more than 80% of the cells expressed ACE/CD143 and a small percentage (~1%), CD34 (**Figure 8B**). Moreover, scRNA-seq of untransduced HDFs, day 2 unsorted cells, and purified reprogrammed cells at day 15 (CD49f<sup>+</sup>CD34<sup>-</sup>) and day 25 (CD49f<sup>+</sup>CD34<sup>+</sup>) demonstrated a gradual increase in the

expression levels of CD49f, CD9, CD143 and CD34 until day 25 (**Figure 8C**). *ITG6* and *CD9* were the first markers to be expressed, with high transcript levels already present at day 2, followed by *ACE* at day 15 and *CD34* at day 25. Since CD49f is co-expressed in ACE<sup>+</sup> cells in the mesoderm ventrally to the dorsal aorta (154), it is possible that CD9 may also represent an early marker of hemogenic precursors and hematopoietic specification.

Overall, our results identify CD9 as a prospective marker of human hemogenesis and illustrate the utility of *in vitro* hemogenic reprogramming as a platform to study a complex human developmental process otherwise difficult to assess *in vivo*.

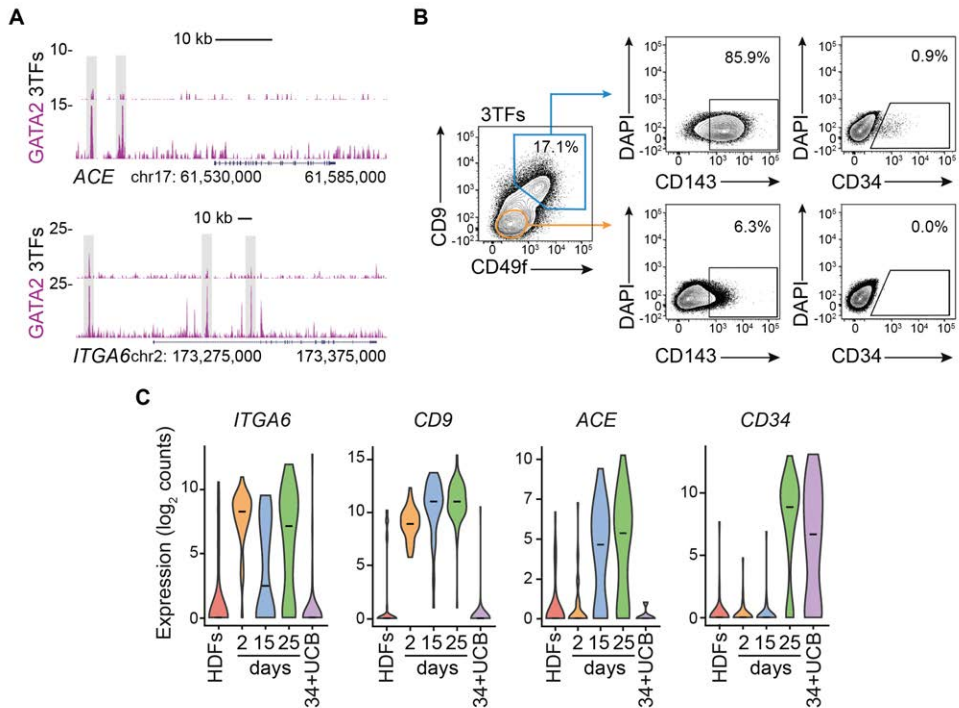


**Figure 8. CD9 and CD49f are early markers of human hemogenic reprogramming. A**, Genome browser profiles showing GATA2's binding sites (highlighted in grey) at *ITGA6* and *ACE* loci, 2 days after fibroblasts were transduced with the three individual transcription factors (3TFs) or with GATA2 alone. **B**, Gating strategy used to evaluate the expression of hemogenic markers by flow cytometry at day 25 of reprogramming. Cytometry plots depict percentage of double positive cells for CD49f and CD9 gated in the live-cell population (DAPI<sup>+</sup>). Expression of CD143 and CD34 inside either the double positive or double negative populations is shown. **C**, ScRNA-seq analysis of 253 cells undergoing reprogramming at different time points. Cells collected at days 2 (unsorted), 15 (CD49f<sup>+</sup>CD34<sup>-</sup>) and 25 (CD49f<sup>+</sup>CD34<sup>+</sup>) were assessed for the expression of *ITGA6*, *CD9*, *ACE* and *CD34* genes. HDFs and CD34<sup>+</sup> umbilical cord blood (34+UCB) cells were used as negative control and reference, respectively.

## Study II – Identifying Novel Regulators of Hemogenic Reprogramming with CRISPR/Cas9 Knockout Screening

CRISPR/Cas9 screens have been used for a wide range of applications including the creation of mouse models for disease modeling (274), the correction of human disorders caused by genetic mutations (279), and for the identification of positive and negative regulators of immune responses (284). In the context of cell reprogramming, CRISPR/Cas9 screening platforms have been used to identify barriers of pluripotency induction (290). Thus, similar approaches could be applied to uncover the regulators of human hemogenesis, through direct cell reprogramming towards hemogenic cells *in vitro*.

### **Optimization of a CRISPR/Cas9 lentiviral delivery system for gene knockout during human hemogenic reprogramming.**

In **paper II**, we outline a CRISPR/Cas9-based KO screening approach to identify barriers and facilitators of human hemogenic reprogramming (**Figure 9A**). We tested four different multiplicities of infection (MOI) using a constitutive Cas9 lentiviral vector with a blasticidin (BSD) selection marker in a well-established reprogramming system. In this system, the overexpression of three transcription factors (PU.1, IRF8, and BATF3 - collectively known as PIB) induces conventional dendritic cell fate in HDFs, and successful reprogramming can be measured through the expression of CD45, among other markers (333,334). Using CD45 expression as readout, we promoted gene KO by delivering a sgRNA targeting CD45 with a GFP marker before starting dendritic cell reprogramming (**Figure 9B**). Reprogramming efficiency was evaluated inside the GFP<sup>+</sup> populations and compared to a positive reprogramming control (HDFs selected for Cas9 and transduced with PIB, but not with sgRNA-CD45-GFP). Our results indicate that an MOI of 1 is sufficient to significantly decrease the expression of CD45 ( $p < 0.0001$ ) (**Figure 9B**). Consistent with other reports (335,336), we employed an MOI of 1 for subsequent experiments. Furthermore, no significant differences were observed in the GFP<sup>-</sup> population (data not shown), validating the specificity of sgRNA-induced KO.

Next, we employed a lentiviral delivery system that contained a GFP-tagged sgRNA library targeting 116 genes associated with HSC function, as well as (positive and negative) control targets (337,338). We tested two copy-number of lentiviral particles and assessed functional MOI by determining the percentage of GFP<sup>+</sup> cells. MOIs inferior to 0.5 have been used to ensure cell uptake of a single sgRNA (339). In our hands,  $2.34 \times 10^5$  copies of lentiviral particles resulted in a MOI of approximately 0.3 ( $29.1 \pm 4.3\%$ ) in three different HDF donors (**Figure 9C**).

Simultaneously, we adapted and optimized the protocol described in paper I to generate hemogenic cells by delivering constitutive versions of the hemogenic TFs GATA2, GFI1B, and FOS to HDFs, utilizing a single polycistronic lentiviral vector. From the six possible formulations, the order of GATA2 followed by FOS, and GFI1B (GFG<sup>B</sup>) translated to high levels of both GATA2 and GFI1B proteins (**Figure 9D**) and resulted in the highest reprogramming efficiency when compared to the individual TFs (3TFs), as measured by the expression of CD9 and CD49f ( $p=0.016$ ), and CD34 inside the double positive population ( $p<0.0001$ ) (**Figure 9E, F**).

To further enhance the delivery of the optimal polycistronic combination, we inserted the GFG<sup>B</sup> sequence onto an alternative lentiviral vector containing a puromycin (PURO) resistance gene (SFFV-GFG<sup>B</sup>-PURO). This modification allowed us to select transduced cells and obtain strong transcript expression, which led to the increase of the double positive population, with maintenance of the CD34 cell subset when compared to the original FUW vector (**Figure 9G**). Consequently, the proportion of fully reprogrammed viable cells (CD9<sup>+</sup>CD49f<sup>+</sup>CD34<sup>+</sup>) showed a significant increase ( $p=0.0002$ ) (**Figure 9H**), emphasizing that using the SFFV promoter in conjunction with antibiotic selection represents the optimal approach for hemogenic reprogramming.

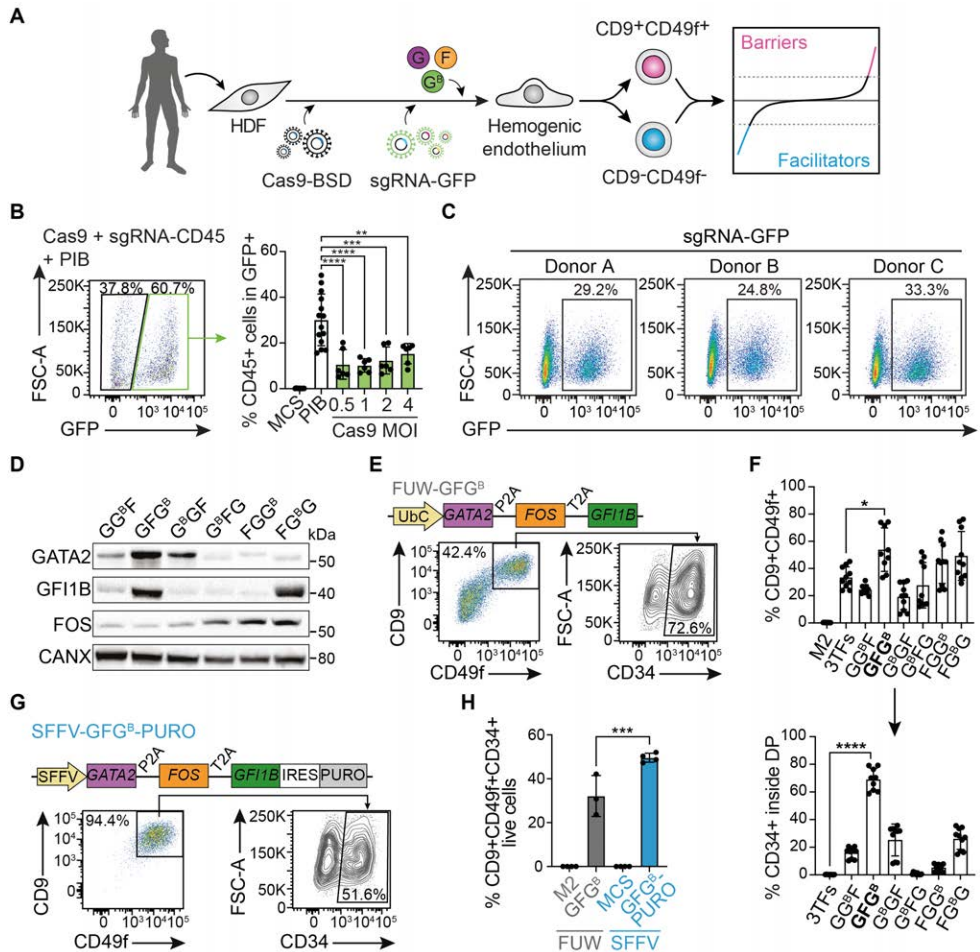


**Figure 9. Delivery of CRISPR/Cas9 components to primary human dermal fibroblasts and establishment of the optimal reprogramming vector for human hemogenic reprogramming.** **A**, Outline of the experimental approach to identify regulators of human hemogenic reprogramming. Human dermal fibroblasts (HDFs) were transduced with constitutive Cas9 and selected for blasticidin (BSD). Then, cells were transduced a second time with the GFP-tagged single guide (sg) RNA library and the GFP<sup>+</sup> population was purified. Lastly, GFP<sup>+</sup> cells were transduced a third time with lentiviral vectors containing the hemogenic reprogramming factors GATA2 (G), GF1B (G<sup>B</sup>) and FOS (F) in optimal order to induce hemogenic fate in fibroblasts. After 15 days, double positive and double negative populations for the hemogenic markers CD49f and CD9 were isolated for downstream analysis by next-generation sequencing to identify barriers and facilitators of hemogenic reprogramming. **B**, Gating strategy to determine CD45 expression inside GFP<sup>+</sup> live cells. Cas9 expressing cells were transduced with a sgRNA-GFP targeting CD45 and reprogrammed with SFFV polycistronic lentiviral vector comprising PU.1, IRF8 and BATF3 (PIB) sequences, to determine the optimal Cas9 multiplicity of infection (MOI) for efficient gene knockout. Percentage of CD45<sup>+</sup> cells after transduction with Cas9 at MOIs of 0.5, 1, 2, and 4, at day 9 of dendritic cell reprogramming is shown. Cells transduced with only the empty vector (MCS) or PIB, without sgRNA-CD45-GFP, were gated in the GFP<sup>-</sup> population to define the negative and positive controls, respectively. **C**, Flow cytometry plots used to visualize GFP expression in HDFs from three donors after transduction with lentiviral particles containing the optimized copy-number of the pooled sgRNA library to achieve an MOI of approximately 0.3-0.4. **D**, Western blot analysis showing the expression of the three TFs at day 5 of hemogenic reprogramming, after HDF transduction with each

polycistronic construct. Calnexin (CANX) was used as loading control. kDa, kilodaltons. **E**, Schematic representation of the GFG<sup>B</sup> construct under the control of the UbC promoter (FUW-GFG<sup>B</sup>). Each TF is separated by self-cleaving peptides, either P2A or T2A. Representative flow cytometry plots depicting the percentage of CD9<sup>+</sup>CD49f<sup>+</sup> and CD34<sup>+</sup> (inside the double positive gate) populations at day 15 of hemogenic reprogramming. **F**, Percentage of CD9<sup>+</sup>CD49f<sup>+</sup> cells and CD34<sup>+</sup> cells inside the double positive population for all polycistronic conditions and individual factors (3TFs) at day 15 of hemogenic reprogramming. FUW-M2rtTa (M2) was used as control. **G**, Schematic representation of the GFGB construct under the control of the SFFV promoter, followed by an internal ribosome entry (IRES) and puromycin (PURO) resistance sequence. Representative flow cytometry plots for the percentage of CD9<sup>+</sup>CD49f<sup>+</sup> cells and CD34<sup>+</sup> cells inside the double positive population are shown. **H**, Percentage of CD9<sup>+</sup>CD49f<sup>+</sup>CD34<sup>+</sup> cells in the FUW-GFG<sup>B</sup> or SFFV-GFG<sup>B</sup>-PURO conditions. M2 and SFFV-MCS (MCS) were used as negative controls. **F**, **H**, Statistical significance was analyzed by one-way ANOVA followed by Tukey's multiple comparisons test. \*p<0.05, \*\*\*p<0.001, \*\*\*\*p<0.0001. Mean ± SD is shown.

## CRISPR/Cas9 screening identifies regulators of human hemogenic reprogramming

After optimizing the conditions for Cas9 expression, sgRNA library expression, and hemogenic reprogramming, we conducted a CRISPR/Cas9 KO screening of HSC-related genes. Briefly, HDFs were selected for Cas9 expression, expanded, transduced with the sgRNA-GFP library using an MOI of 0.3-0.4, and reprogrammed with SFFV-GFG<sup>B</sup>-PURO. Fifteen days following transduction with the polycistronic vector, genomic DNA was collected from reprogrammed double positive (CD9<sup>+</sup>CD49f<sup>+</sup>) and non-reprogrammed double negative (CD9<sup>-</sup>CD49f<sup>-</sup>) sorted cells, as well day 0 (no reprogramming), and sgRNAs were amplified and sequenced (**Figure 10A, B**).

To determine the abundance of sgRNAs, we converted individual sgRNA signals into gene signals and normalized the data using non-targeting genes. Then, we calculated the signal fold-change (FC), which was log<sub>2</sub>-transformed, between reprogrammed samples and day 0 (baseline), and similarly between non-reprogrammed samples and day 0. Finally, we plotted the values for reprogrammed and non-reprogrammed conditions against each other (**Figure 10C**). From there, we identified top candidate genes by ranking them, according to the difference in log<sub>2</sub>FC values, and selected those enriched in reprogrammed and non-reprogrammed samples (**Figure 10D**). Genes that exhibited an elevated sgRNA count in the reprogrammed samples, leading to an increased fold-change, were identified as potential reprogramming barriers. Silencing these genes may contribute to enhancing reprogramming efficiency. Conversely, genes exhibiting increased fold-change in the non-reprogrammed population were defined as facilitators of hemogenic reprogramming (**Figure 10D**). Our analysis led to the identification of six barriers (in pink) and three facilitators (in blue).

From the barriers *CD44*, *CD34* and *ITG9* have been implicated in the hematopoietic system. CD34 and CD44 are two markers of intra-aortic hematopoietic clusters in the AGM region during early hematopoietic development (55,60,91), as well as of bone marrow HSPCs (137,340). However, our data suggests that initial silencing of

signal pathways controlled through these transmembrane proteins might be necessary for hemogenic specification. In fact, the later requirement of CD34 is consistent with its delayed expression during hemogenic reprogramming, occurring after CD9 and CD49f, as demonstrated in paper I. The Integrin Subunit Alpha 9 ( $\alpha 9$ , *ITGA9*) is a component of the integrin  $\alpha 9\beta 1$ , expressed in CD34<sup>+</sup> HSPCs (341). This integrin plays a role in facilitating the adhesion of HSPC to osteoblasts within the adult hematopoietic niche. Blocking  $\alpha 9\beta 1$  activity reduces HSPC proliferation (341), indicating that cells may enter a state of quiescence more characteristic of LT-HSCs in the absence of  $\alpha 9\beta 1$ . In the facilitator group, only STAG2 was described to play a role in hematopoiesis. STAG2, a member of the cohesin complex, has been reported to cooperate with STAG1 to control the generation of early endothelial-hematopoietic progenitors in zebrafish, suggesting a role in developmental hematopoiesis. Moreover, loss of STAG2 in HSPCs results in decreased HSC quiescence (342), and *Stag2* full KO mice die by E10.5 (343), reinforcing its role as a prospective facilitator of human hemogenesis. Additionally, we identified *DDX26B*, *SLC28A1*, and *SAXO2* as barriers, and *MTFR1* and *SCARAS* as facilitators, thus establishing these molecules as novel regulators of hemogenic reprogramming.

In summary, we have identified several barriers and facilitators that might function as regulators of the hemogenic reprogramming process and human EHT. Further validation of individual hits *in vitro* and in transplantation experiments *in vivo*, will offer a more comprehensive insight into their molecular mechanisms. Ultimately, this knowledge can be applied to improve the fidelity and efficiency of human hemogenic reprogramming for the generation of *bona fide* patient-specific HSCs and to increase our understanding regarding the specification of hemogenic cells.

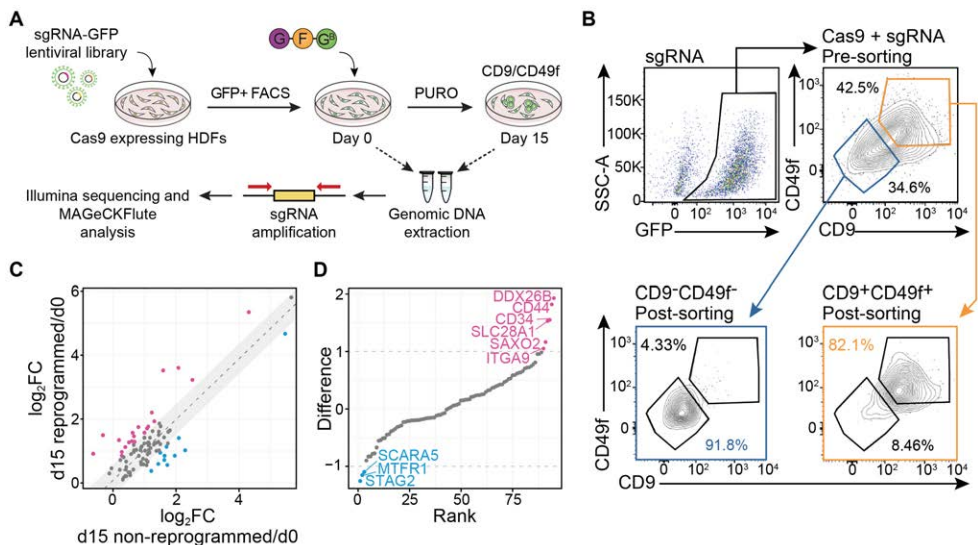


**Figure 10. CRISPR/Cas9 screening identified regulators of hemogenic reprogramming.** **A**, Outline of the KO screening strategy. Cas9 expressing human dermal fibroblasts (HDFs) were transduced with the GFP-tagged single guide (sg) RNA library at an MOI of approximately 0.3-0.4 and keeping a coverage of at least 300 cells per single guide. Following fluorescence-activated cell sorting (FACS) of the GFP<sup>+</sup> population, cells were transduced with the optimized SFFV polycistronic vector encoding GATA2 (G), GF11B (G<sup>B</sup>) and FOS (F) to allow induction of hemogenic program in fibroblasts. Puromycin (PURO) selection was performed during reprogramming. Genomic DNA samples were extracted from day 0 (no SFFV-GFG<sup>B</sup>) and from day 15 double positive (CD9<sup>+</sup>CD49f<sup>+</sup>) and double negative (CD9<sup>-</sup>CD49f<sup>-</sup>) populations. Prior to sequencing, guides were amplified with custom primers. After next-generation sequencing, computational data analysis was performed with MAGeCKFlute pipeline. **B**, Representative flow cytometry plots showing populations of interest isolated at day 15 of reprogramming, containing the sgRNA library, after antibiotic selection and staining for CD9 and CD49f. Double negative and double positive populations were obtained at a purity of approximately 90% and 80%, respectively, from a total of 3 replicates (one from one donor and two from a different donor). **C**, Median log<sub>2</sub> fold-change (FC) of sgRNA representation. Using day 0 (d0) as baseline for normalization, reprogrammed versus non-reprogrammed samples at day 15 (d15) were compared for enrichment analysis. The grey area delimits the cut-off corresponding to 1 standard deviation. Enriched genes in non-reprogrammed cells are defined as facilitators (blue dots) and enriched genes in reprogrammed cells identify barriers of reprogramming (pink dots). **D**, Rank distribution of candidate genes for hemogenic reprogramming barriers and facilitators according to log<sub>2</sub>FC difference between reprogrammed and non-reprogrammed cells.



## Study III – GATA2 Mitotic Bookmarking is Required for Definitive Hematopoiesis

As cells divide, previously established lineage-specific patterns of gene expression must be kept in daughter cells to preserve cell identity. Several TFs have been shown to facilitate the transmission of epigenetic memory during mitosis by remaining bound to condensed chromatin and by bookmarking specific genomic sites *in vitro* (301). However, the relevance of mitotic chromatin binding or bookmarking for lineage commitment or maintenance in living organisms has not been addressed before. We have shown that GATA2, GFI1B and FOS TFs are sufficient to induce hemogenic and hematopoietic fate in fibroblasts (245,246), thus in **paper III** we explore the hypothesis that specification of definitive hematopoiesis *in vivo* requires mitotic bookmarking activity by hemogenic factors.

### **GATA2 is retained in mitotic chromatin through C-terminal zinc finger-mediated DNA binding**

To address whether reprogramming factors would remain bound to chromatin in mitosis to facilitate hematopoietic specification *in vivo* (**Figure 11A**), we have analyzed the subcellular localization of each TF by both fluorescence microscopy and western blotting. HDFs overexpressing GATA2, GFI1B and FOS were initially blocked in mitosis and the presence of each TF was detected after subcellular protein fractionation (**Figure 11B**). GATA2 was mainly found in the chromatin-bound protein fraction, while GFI1B and FOS were found in the cytoplasmic protein fraction of prometaphase arrested cells. To confirm these results, we generated fusion constructs of the TFs with mCherry fluorescent proteins, allowing the visualization of the TFs using live-cell fluorescence microscopy. Interestingly, GATA2 co-localizes with chromatin during all phases of mitosis, while GFI1B gets enriched at later stages (anaphase) and FOS is completely excluded from chromatin (**Figure 11C**). Moreover, we have obtained similar results when using mouse embryonic fibroblasts, HEK 293T and the leukemic cell line K562 with endogenous TF expression (data not shown), suggesting that the mitotic retention function is an intrinsic mechanism of the TF and is independent of cell context.

Given that the ability to remain bound to mitotic chromatin is an intrinsic property of GATA2, we proceeded to dissect which protein domains were required for this mechanism. GATA2 comprises two transactivation domains, one negative regulatory domain, a nuclear localization signal (NLS) and a DBD (**Figure 11D**) (98). The DBD is divided into an N-terminal zinc-finger (N-ZF) and a C-terminal zinc finger (C-ZF) with homologous sequence, but different functions. The N-ZF has been implicated in stabilizing DNA-protein complexes and providing specificity to DNA binding, whereas the C-ZF recognizes and binds to GATA consensus

sequence (95,97). To define protein regions important for mitotic retention, we generated mCherry-GATA2 deletion constructs in which the N-terminal, the N-ZF, the C-ZF and the NLS were removed from the initial *Gata2* sequence. We observed that GATA2 was severely reduced from asynchronous and mitotic chromatin-bound fractions when the C-ZF, but not the N-ZF was deleted (**Figure 11E**). The removal of the NLS also resulted in a decrease in mitotic retention, as determined by live-cell imaging and western blotting analyses (**Figure 11E, F**). This observation could indicate the necessity of a functional nuclear import mechanism, as previously described for SOX2 (322). However, since we detected GATA2 in the nucleus during interphase in the absence of the NLS (**Figure 11F**), it is also possible that this deletion disturbs the adjacent C-ZF binding function and that other unrecognized regions might serve as NLS.

To confirm the requirement of C-ZF for mitotic retention, we selected GATA2 point mutations frequently found in leukemic and ES patients that influence DNA-binding affinity (**Figure 11D**) (344–346). C-ZF mutations associated with GATA2-deficiency syndrome manifestations, namely AML and/or ES, that were reported to reduce DNA-binding affinity, including R396Q, R398W, T354M, R361L, and C373R (344,346) led to a decrease in GATA2 mitotic retention (**Figure 11G**), suggesting that DNA-binding is necessary for GATA2 mitotic chromatin retention. In fact, the NLS deletion construct lacks residues R398 and R396, which supports the hypothesis that the disruption of GATA2's mitotic retention by this construct is linked to the need of C-ZF neighboring amino acids for DNA binding. A more refined deletion or single point mutations within the NLS might be necessary to properly investigate the role of the NLS for mitotic chromatin retention. Importantly L359V, which is described to increase GATA2's DNA-binding affinity (347) and R362Q, that has a modest impact in binding affinity (344), did not display impaired mitotic retention. Aligned with its relatively minor role in DNA binding, mutations within the N-ZF region did not influence the mitotic chromatin retention of GATA2 (data not shown).

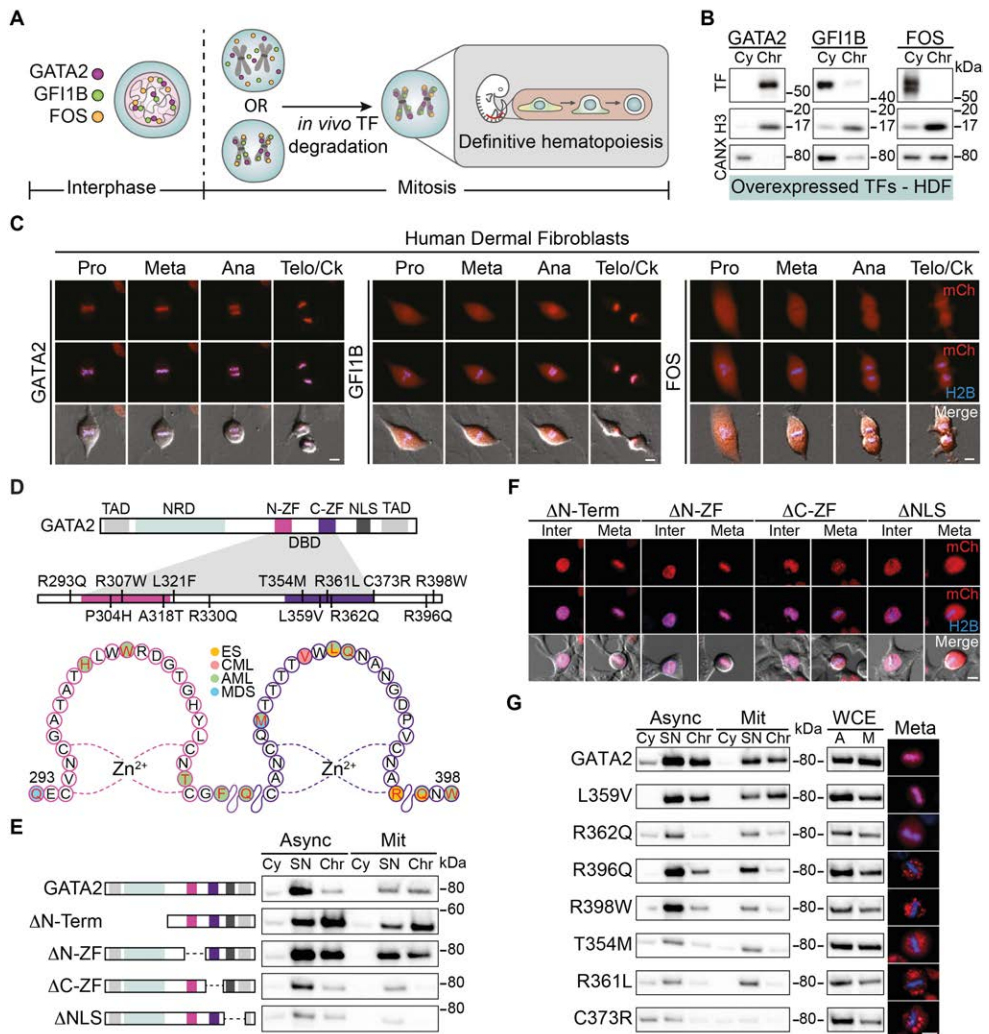


**Figure 11. Point mutations in the C-terminal zinc finger domain associated with GATA2-deficiency syndrome reduce mitotic chromatin retention of GATA2.** **A**, Experimental outline to address the role of mitotic retention and bookmarking by hemogenic reprogramming transcription factors (TFs) GATA2, GF1B and FOS for the specification of definitive hematopoiesis *in vivo*. **B**, TF expression in the cytoplasmic (Cy) and chromatin-bound (Chr) protein fractions of mitotic human dermal fibroblasts (HDFs) expressing the indicated TF. Histone 3 (H3) and calnexin (CANX) were used as loading controls. **C**, Representative live-cell micrographs of HDFs overexpressing mCherry (mCh)-TFs fusion proteins (red) during mitosis (Pro – prophase, Meta – metaphase, Telo/Ck – Telophase/Cytokinesis). **D**, Representation of GATA2 domains highlighting leukemia and Emberger syndrome (ES) point mutations in the N- and C- terminal zinc fingers (ZFs) of the DNA-binding domain (DBD). Germline mutations T354M, R361L, C373R, R396Q and R398W are associated with GATA2-deficiency syndrome. TAD – transactivation domain. NRD – negative regulatory domain. NLS – nuclear localization signal. CML – chronic myeloid leukaemia. AML – acute myeloid leukaemia. MDS – myelodysplastic syndrome. **E**, Protein expression in Cy, soluble nucleus (SN) and Chr fractions of both asynchronous (A, Async) and mitotic (M, Mit) 293T cells overexpressing deletion constructs. **F**, Live-cell micrographs of 293T cells overexpressing mCh-GATA2 deletion ( $\Delta$ ) constructs (red) excluding the N-terminal (amino acids 1-235),

N-ZF (287-342), C-ZF (243-379) or NLS (380-440) in interphase (Inter) and metaphase. **G**, Protein expression of mCherry-fused GATA2 mutants in the Cy, SN and Chr protein fractions of asynchronous and mitotic 293T cells, including whole-cell extracts (WCE). Representative cells in metaphase are shown (right). Histone 2B (H2B)-mTurquoise signal (blue) indicates DNA content. Scale bars, 10  $\mu$ m. kDA, kilodaltons.

## **GATA2 bookmarks regulators of hematopoietic stem and progenitor cell development and function**

To address whether GATA2 also possessed mitotic bookmarking activity, we examined the genome-wide occupancy of endogenous GATA2 in asynchronous and FACS-purified mitotic K562 cells through ChIP-seq. Our analysis revealed that GATA2 binds to a subset of its interphase targets during mitosis (1,598 peaks), which accounts for 15% of interphase genes. This finding thereby confirms that GATA2 is indeed a mitotic bookmarking factor. (**Figure 12A**). Next, to assess the differences in binding affinity of GATA2, we performed K-means clustering of asynchronous peaks, which resulted in three clusters (**Figure 12B**). Seventy-one percent of bookmarked peaks overlapped with cluster 1, which comprised a small fraction (9.5%) of GATA2 peaks in asynchronous cells exhibiting the highest peak intensities. This implies that GATA2 bookmarks sites with high TF affinity. Cluster 3 accounted for only 3% of the overlapped peaks and was consequently excluded from further analyses. With the previous observation in mind, we examined the density of binding sites by calculating the number of GATA2 binding motifs per peak within each group (**Figure 12C**). Notably, mitotic peaks contained significantly higher number of GATA2 motifs when compared to asynchronous peaks (KS test,  $p < 0.05$ ). This result suggests that GATA2 mitotic bookmarking is influenced by a pre-existing motif organization, where accumulation of GATA2 motifs translates to higher chromatin engagement during mitosis.

*De novo* motif enrichment analysis revealed that GATA2 binds preferentially to GATA, RUNX, and ETS motifs in mitosis (**Figure 12D**), suggesting TF cooperation with relevant hematopoietic factors. Building on this finding, we further explored the collaboration of GATA2 with other crucial factors for hematopoiesis and HSPC specification in both asynchronous and mitotic cells. These factors included the "heptad" TFs TAL1, LYL1, RUNX1, ERG, and FLI1, as well as PU.1 (ETS family), MYB, PBX, GFI1B, FOS, HES1, MEIS1, and HLF (61,73,87). We noticed a pronounced degree of motif co-occurrence within GATA2's mitotic peaks, particularly involving "heptad" TFs, PU.1 and FOS binding sites (**Figure 12E**). This observation points towards the retention of TF complexes and cooperative interactions with GATA2 during mitosis.

Regarding the overall distribution of the peaks in the genome, GATA2 binds to similar genomic regions in asynchronous and mitotic cells, with preference for promoters and active enhancers (**Figure 12F**). Interestingly, we observed a 1.8- and 2.2-fold binding decrease at "weak enhancer" (EnhWk, marked by H3K4me1) and

“bivalent enhancer” (EnhBiv, marked by H3K4me1 and H3K27me3) chromatin states respectively, attributed to lower mitotic retention at sites decorated with those marks (**Figure 12F-H**). Furthermore, upon integrating our data with histone mark databases from the ENCODE project for K562 cells (353), we observed that sites marked with H3K36me3 and H4K20me1 (transcription elongation marks) (354), were also depleted at mitotic peaks (**Figure 12G, H**). With respect to DNA accessibility, we did not identify significant differences between mitotic and asynchronous peaks, particularly within cluster 1 (**Figure 12G, H**). This indicates that chromatin accessibility does not pose a barrier for mitotic bookmarking, which aligns with previous reports (322).

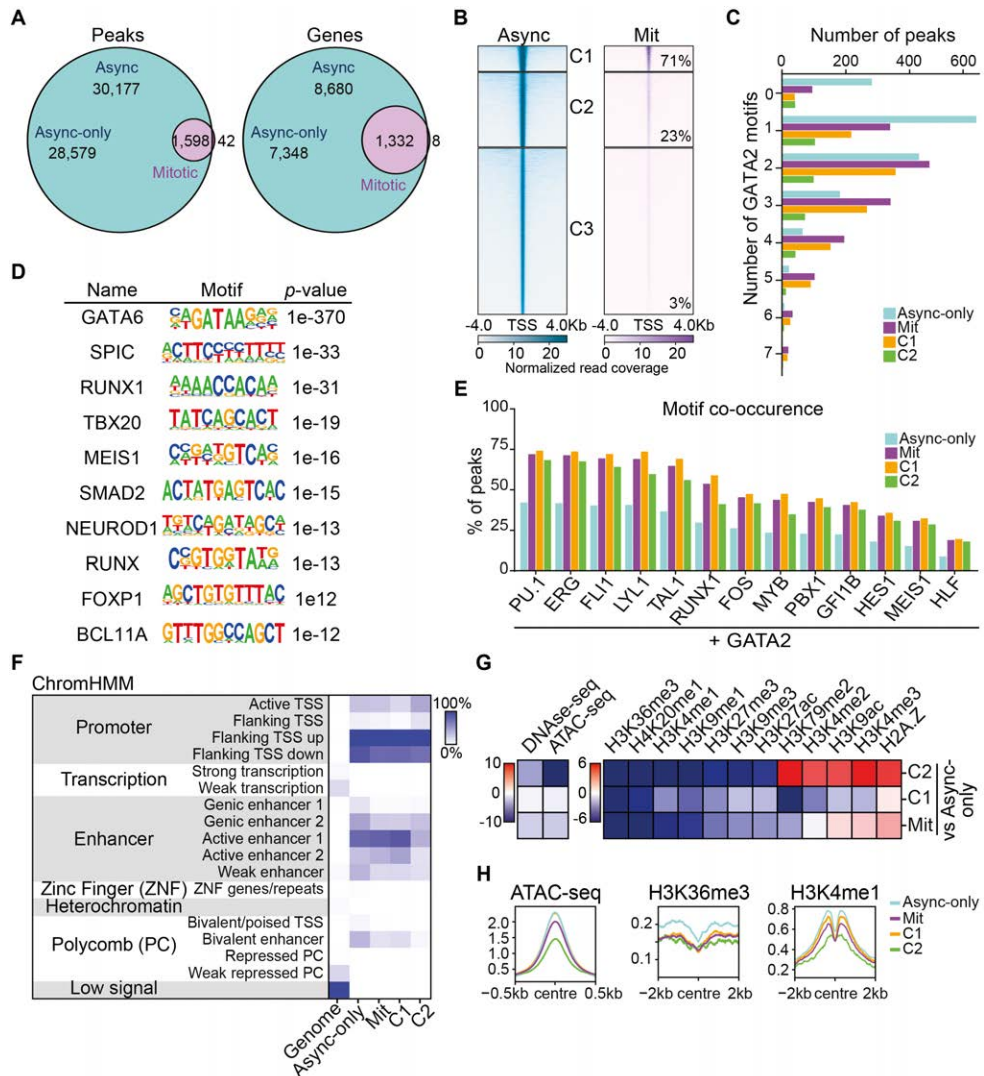


**Figure 12. GATA2 bookmarks a subset of its interphase genes and binds to regions depleted of specific histone marks in mitosis.** **A**, Venn diagram showing the number of ChIP-seq GATA2 peaks and genes shared between asynchronous (Async) and mitotic (Mit) K562 cells. Async-only refers to non-bookmarked peaks and genes in asynchronous cells. **B**, K-means clustering of Async (left) and Mit peaks (right). The percentage of mitotic (bookmarked) peaks overlapping with asynchronous peaks in each cluster (C) is shown. The 42 mitotic-unique peaks are not shown. **C**, Number of GATA2 motifs in Async-only peaks, mitotic peaks and mitotic clusters 1 (C1) and 2 (C2). **D**, *De novo* motif enrichment analysis for GATA2 mitotic bookmarked target sites. Top ten motifs are shown with respective *p*-values. **E**, Percentage of GATA2 peaks with motifs for relevant HSPC regulators. **F**, Enrichment heatmap of chromatin states representing the percentage of genome occupancy by GATA2 per group of peaks. Scale represents the percentage of peaks in each genomic segment. TSS – Transcription start site. **G**, Integration heatmap with histone marks, DNase-seq and ATAC-seq data for K562 cells (ENCODE). Scale represents the accumulated sum differences across bins between Async-only and Mit peaks and clusters. **H**, Histone marks and ATAC-seq profiles at peak summit (centre).

## **GATA2 is necessary at mitosis-to-G1 transition for definitive hematopoiesis *in vivo***

To address the role of mitotic retention and bookmarking *in vitro* and *in vivo*, we utilized the MD domain of cyclin B1 and a mutated non-functional version (MD<sub>mut</sub>) as an internal control. First, we induced hemogenic reprogramming in HDFs with MD-GATA2 or MD<sub>mut</sub>-GATA2, in combination with GFI1B and FOS, and followed the expression of the hemogenic marker CD9 for 12 days (**Figure 13A**). We noted a delay in CD9 expression when GATA2 was degraded during the M-G1 transition (**Figure 13B**), suggesting that GATA2 might have a role in hemogenic specification during this transition.

Based on the outcome obtained *in vitro*, we proceeded to create a mouse model in which the MD domain was inserted upstream of the *Gata2* gene using CRISPR-Cas9 technology (**Figure 13C**). The insertion of the MD sequence in both *Gata2* alleles resulted in mouse lethality, as homozygous pups could not be generated from two independent injections of edited ESCs (data not shown) or by crossing heterozygous mice (**Figure 13D**). Surprisingly, MD homozygous mice died at the onset of definitive hematopoiesis, between E10.5 and E11.5 (**Figure 13D, E**), phenocopying *Gata2* knock-out mice (76), as no heartbeat was detected past E11.5. Morphological analysis of E10.5 and E11.5 MD-*Gata2* embryos showed that MD/MD embryos were smaller and paler, particularly at E11.5, with evident lack of blood (**Figure 13E**). The insertion of the MD<sub>mut</sub> sequence, however, did not impair embryonic development (**Figure 13E**), confirming that the observed impact derived from the degradation of GATA2 at the M-G1 transition. Moreover, flow cytometry analysis of MD-*Gata2* embryonic erythroblasts revealed severe anemia at E11.5 (**Figure 13F**), likely serving as the primary factor contributing to embryo mortality.

To assess the impact of GATA2 degradation at M-G1 transition in definitive hematopoiesis we first analyzed embryos and IAHC formation by whole-embryo mounting followed by immunohistochemistry. At E10.5, we noted the depletion of

hematopoietic clusters in the ventral region of the dorsal aorta and a significant reduction in the dorsal region, among MD homozygous embryos (**Figure 13G, H**). As a complementary approach, we performed CFU assays at E9.5, E10.5 and E11.5 using cell suspensions from different hematopoietic tissues (**Figure 13I-K**). At E9.5 the number of colonies obtained from yolk sacs were comparable between genotypes (**Figure 13I**), suggesting that the formation of yolk sac progenitors is not affected by the loss of GATA2 at M-G1 transition. This comes in contrast with the classic *Gata2* null mouse model where the generation or function of both pro-definitive and definitive progenitors are impaired (79,81). When we looked at E10.5 embryos, we observed a decrease in the number of hematopoietic colonies derived from AGM, placenta and fetal liver by 2.9-, 4.6- and 3.2-fold, respectively, when compared to wild-type embryos (**Figure 13J**). This effect was even more prominent at E11.5, with colony numbers reduced 16- and 8- fold in AGM and placenta, respectively, when compared to MD<sub>mut</sub> homozygous mice (**Figure 13K**). These results reflect the lack of IAHCs at E10.5 and underscore the requirement of GATA2 at mitotic exit for definitive hematopoiesis.

Finally, we assessed the generation of HSPCs via transplantation of E11.5 placenta cells into sublethally irradiated recipient mice (**Figure 13L**). While wild-type and heterozygous mice engrafted irradiated recipients, placental HSPCs from MD homozygous mice did not contribute to long-term engraftment (6 months) in peripheral blood or in bone marrow (**Figure 13L**). As we did not observe significant differences in IAHC numbers or embryonic HSPC function between wild-type and heterozygous mice, we decided to evaluate the function of adult heterozygous HSCs instead. Therefore, we have performed competitive transplantations with bone marrow LSK-SLAM HSCs (LSK CD150<sup>+</sup>CD48<sup>-</sup>) from adult mice (**Figure 13M**). Interestingly, we observed reduced engraftment capacity of MD-*Gata2* heterozygous HSCs from adult bone marrow, suggesting a role for GATA2 mitotic bookmarking not only in HSC specification but also in HSC maintenance. Altogether, these results demonstrate that GATA2 is essential *in vivo* at M-G1 transition for definitive hematopoiesis.

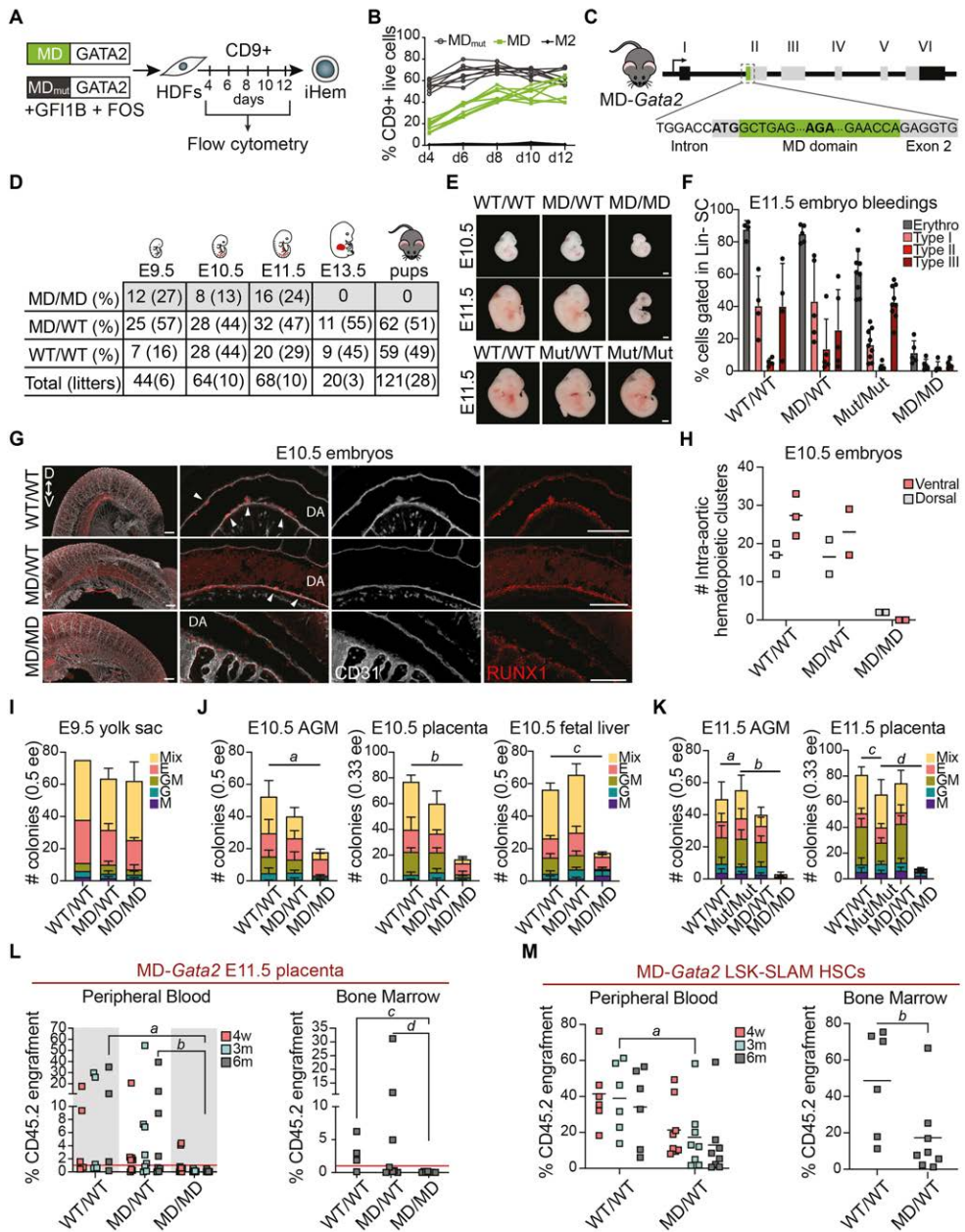


**Figure 13. Definitive hematopoiesis requires GATA2 at mitosis-to-G1 transition.** **A**, Direct reprogramming strategy to convert human dermal fibroblast (HDFs) into induced hemogenic cells (iHem). HDFs were transduced with lentivirus encoding MD- or MD<sub>mut</sub>-GATA2, plus GF11B and FOS factors, and the kinetics of CD9 activation was evaluated by flow cytometry. **B**, Quantification of CD9 expression from day (d) 4 to d12. M2rTA (M2) was used as control. **C**, Schematic representation of the mouse model developed to assess mitotic degradation of GATA2 *in vivo* by inserting the MD domain upstream the *Gata2* gene. **D**, Frequency of homozygous (MD/MD), heterozygous (MD/WT) and wild-type (WT/WT)



embryos at embryonic day (E) 9.5, E10.5, E11.5, E13.5 and pups, after crossing heterozygous mice. **E**, Representative images of MD-*Gata2* embryos at E10.5 and E11.5, and control MD<sub>mut</sub>-*Gata2* embryos at E11.5. Scale bars, 1 mm. **F**, Flow cytometry quantification of E11.5 erythroblasts after whole-embryo bleeding. Graphs show percentage of total erythroblasts (Erythro) or immature (type I) to mature (Type III) cells gated within lineage negative (Lin<sup>-</sup>) live single-cell (SC) population. Mean ± SD is shown. **G**, Immunohistochemistry images representing E10.5 WT/WT, MD/WT and MD/MD intra-aortic hematopoietic clusters expressing RUNX1 (red) and CD31 (white) in the ventral (V) or dorsal (D) sides of the dorsal aorta (DA). White arrowheads indicate clusters. Scale bars, 150 μm. **H**, Number (#) of intra-aortic hematopoietic clusters per genotype. Mean is shown. **I-K**, Colony-forming units for E9.5 yolk sac (I), for E10.5 aorta-gonad-mesonephros (AGM), placenta and fetal liver (J) and for E11.5 AGM and placenta (K) cell suspensions. Mean ± SD is represented. Macrophage (M), granulocyte (G), granulocyte/macrophage (GM), erythroid (E) and mixed colonies (Mix) are shown per embryo equivalent (ee). **J, K**, Statistical significance for the total number of colonies was calculated by one-way ANOVA followed by Bonferroni's multiple comparison test. **J**, a, *p*=0.01; b, *p*<0.001; c, *p*=0.002. **K**, a, *p*>0.99; c, *p*=0.61; b and d, *p*<0.001. Percentage of donor chimerism (CD45.2<sup>+</sup>) in peripheral blood 4 weeks (w), 3 and 6 months (m) after transplantation with E11.5 placenta cells, as well as bone marrow chimerism after 6 months. Red line indicates 1% chimerism. a, *p*=0.011; b, *p*=0.016; c, *p*=0.023; d, *p*=0.028. Statistical significance at 6 months was calculated with Kruskal-Wallis test followed by uncorrected Dunn's test. **M**, Percentage of donor chimerism 4 weeks, 3 months, and 6 months after competitive transplantation with 200 WT/MD or WT/WT LSK-SLAM HSCs (Lin<sup>-</sup>Sca1<sup>+</sup>cKit<sup>+</sup>CD150<sup>+</sup>CD48<sup>-</sup>). a, *p*=0,029. Bone marrow chimerism is also shown. b, *p*=0.020. Statistical significance was calculated with two-tailed Mann-Whitney test at 3 months (peripheral blood) or at 6 months (bone marrow).

Mechanistically, we believe that GATA2 remains bound to important endothelial and hematopoietic genes, through its C-ZF domain, in a cooperative environment with other HSPC regulators to ensure the faithful commitment of definitive HSPCs during embryonic development (**Figure 14**).

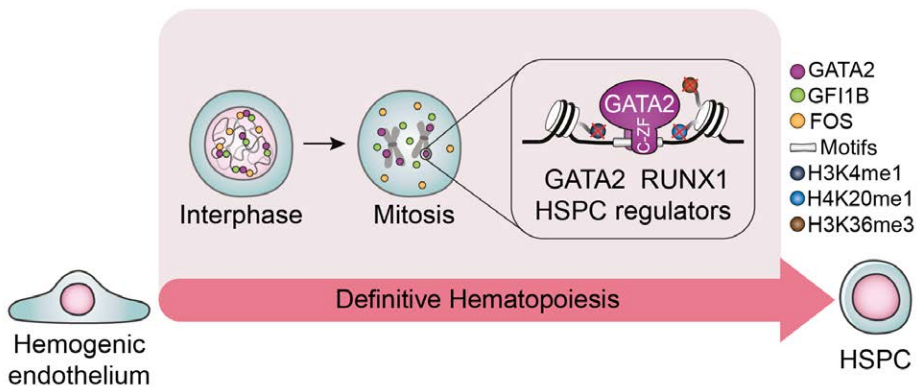


**Figure 14. Proposed model for the role of GATA2 bookmarking for definitive hematopoiesis.** GATA2 remains bound to key hematopoietic genes during mitosis through its C-terminal zinc finger (C-ZF) domain, cooperating with other regulators to allow faithful commitment of definitive HSPCs during embryonic development. Additionally, mitotic cells lose GATA2 binding at sites marked with H3K4me1, H3K36me3 and H4K20me1.

# Discussion and future directions

The precise characterization of human HSC precursors during ontogeny remains challenging, primarily due to the transient nature of EHT, coupled with the limited availability of human tissues throughout different stages of hematopoietic development. Hematopoietic differentiation protocols from human PSCs have allowed researchers to replicate HSC ontogeny, albeit with certain caveats. Extensive functional studies have reported an immunophenotype for PSC-derived hemogenic endothelium consisting of the co-expression of VE-cadherin, CD31, KDR (also known as VEGFR-2), CD117 (*KIT*) and CD34, and lack of the surface markers CD43, an early pan-hematopoietic marker, and CD73 that marks non-hemogenic endothelium (184,185,348). Nevertheless, no *in vivo* counterpart has been described in the human system.

Converting somatic cells, such as fibroblasts, directly into hemogenic progenitors constitutes an alternative approach for identifying novel markers of hemogenic/hematopoietic cells that are dynamically expressed during EHT. CD9, which was shown to be up-regulated in reprogrammed cells (246), is rapidly expressed at the cell-surface in the initial stages of hemogenic reprogramming, together with the LT-HSC marker CD49f. In study I, we also show that *ITGA6* (CD49f) and *ACE* are direct targets of GATA2 during the initial stages of hemogenic reprogramming, in addition to CD9 and CD34 (246), providing a link between human hemogenic precursor phenotype and GATA2. Our observations are in line with early histological and immunohistochemistry analysis of human embryos, where CD49f<sup>+</sup>ACE<sup>+</sup> mesodermal cells were found underneath the dorsal aorta in the AGM region (152). Hence, it is quite plausible that CD9 could serve as a novel marker for human HSC precursors. Detection of CD9 in human or mouse embryos will be crucial to confirming these results. Moreover, it will be interesting to determine the expression of the markers present in PSC-derived hemogenic cells in our reprogramming system and vice-versa. Perhaps, combined surface immunostaining could help us find a unified surface phenotype for *in vitro* generated hemogenic cells that could bring us closer to identifying an *in vivo* equivalent.

The feasibility of TF-mediated direct reprogramming to induce a hemogenic fate in fibroblasts prompted us to combine this technique with a CRISPR/Cas9-based approach to identify facilitators and barriers of this process through gene KO. In study II, we identified CD44 and CD34 as barriers of hemogenic reprogramming. CD44 has been recently found in mouse and human hemogenic endothelial cells,

cells undergoing EHT and in HSPCs (60,91,340). In mice, cells with low CD44 expression exhibited an endothelial-hematopoietic identity characterized by the expression of *Gata2*, *Runx1*, *Gfi1*, *Lmo2* and *Tall1* among other genes, and represented the precursors of CD44<sup>+</sup> hematopoietic cells in the AGM region (91,349). For these reasons, it is possible that CD44-mediated signaling is required in a stage-specific manner to allow definitive HSPC commitment.

CD34 is widely expressed in hematopoietic progenitors and precursors, being recognized as a key marker of hemogenic endothelium and HSPCs (47,55,137). Nevertheless, we identified it as a top hit for the barriers of reprogramming. This observation might be explained by the lack of CD34 expression in the earliest stages of human HSC ontogeny (152,350). Indeed, CD34<sup>-</sup> mesodermal cells underlying the developmental AGM region are believed to be the earliest precursors of CD34<sup>+</sup> intra-aortic hematopoietic clusters (152). CD34 expression is associated with the successful engraftment of donor HSCs (351) and the facilitation of erythroid and myeloid differentiation from yolk sac and fetal liver progenitors (352). However, KO mice progress through development with no significant differences in peripheral blood counts or bone marrow cellularity (352). This discovery could carry wider implications, given that CD34 is used as a positive marker for identifying HSPCs and hemogenic precursors derived from human PSCs protocols (183,184,186–188,190). On the other hand, loss of our top facilitator, STAG2, in zebrafish (*stag2b*) leads to the reduction of hematopoietic/vascular progenitors and the downregulation of primitive erythropoiesis (353). Furthermore, *Stag2* full KO mice die by E10.5 (343), highlighting STAG2's importance in the early specification of HSCs and reaffirming its role as a facilitator for the generation of hemogenic precursors.

The collective information acquired through the discovery of novel markers and regulators of human hemogenesis will advance the *ex vivo* generation and manipulation of patient-specific definitive HSCs for clinical applications.

As main regulators of tissue-specific gene expression, TFs are key players in guiding cell lineage instruction and, consequently, (direct) cell reprogramming strategies. In Study III, we explore a previously unappreciated role of TFs during the most challenging phase of cell cycle for maintaining cell identity – mitosis. The ability to remain bound to condensed mitotic chromatin is not the same for all TFs. GATA2 has the intrinsic ability to remain bound to chromatin of hematopoietic and non-hematopoietic cells during all phases of mitosis, contrary to GFI1B and FOS. A recent study divided TFs into three groups – depleted (chromatin signal lower than in the cytoplasm), intermediate (chromatin signal equal to cytoplasmic signal) and enriched (chromatin signal higher than the signal in cytoplasm) – depending on the visual inspection of metaphase chromatin (302). Interestingly, TFs with a C2H2 zinc-finger type, the same as GFI1B (354), fit mainly in the “depleted” or “intermediate” groups (302), which may be explained by protein phosphorylation that occurs in these family of TFs preventing their association with mitotic chromosomes (355). It is possible that GFI1B decorates chromatin at later stages of

mitosis due to dephosphorization events. FOS proteins create heterodimers with JUN proteins to form the AP-1 complex, which binds to regulatory regions of target genes. On its own, FOS cannot bind to DNA (356). Expressing FOS, either alone or together with GATA2/GFI1B, which are not part of the AP-1 complex, did not lead to its mitotic chromatin retention. It would be interesting to co-express FOS with JUN to assess the subcellular localization of the AP-1 complex during cell cycle.

GATA2 engages DNA through its ZF domains. The removal of the C-ZF but not the N-ZF resulted in reduced mitotic chromatin retention of GATA2. This difference in outcome might be explained by the distinct roles of the ZFs (95). Nevertheless, it indicates that DNA binding is required for mitotic chromatin retention, as previously shown (309,312,316,322). Moreover, single-point mutations in both ZFs, which are related to leukemia, provide additional support for the essential role of the C-ZF in mitotic retention. It has been shown that individuals with mutations in the N-ZF experience more favorable clinical outcomes compared to those with C-ZF mutations (115). Additionally, N-ZF mutants diminish chromatin occupancy and transcriptional activation by GATA2, though they do not completely abrogate these processes (345). Hence, disruption of mitotic retention might have unrecognized implications for certain diseases.

Similar to FOXA1 (312) and BRN2 (309), GATA2's interaction with mitotic chromatin is likely mediated by non-specific electrostatic interactions. For example, mutation in the positively charged R398 residue, that is not expected to bind directly to GATA consensus sites (357), disturbs critical electrostatic interactions with DNA minor groove (344). In contrast, R362 makes minor contacts with phosphate groups on DNA backbone, which seem irrelevant for mitotic retention of GATA2 (344). Whether or not these and other ZF mutations also affect sequence-specific DNA binding during mitosis remains to be addressed. This is particularly relevant since we show that GATA2 binds to a subset of its interphase sites, making it a *bona fide* bookmarking factor.

We showed that GATA2 peaks contain motifs of other important hematopoietic regulators including RUNX1, PU.1, ERG, FLY1, TAL1, FLI1, GFI1B and MYB, suggesting TF cooperation during mitosis. A crucial future experiment for examining the presence of these TFs during mitosis would involve the purification of mitotic chromosomes of K562 cells, followed by liquid-chromatography tandem mass spectrometry, a technique that combines the separation power of liquid chromatography with a series of mass analyzers (358). Staining of unfixed metaphasic chromosome preparations with Hoechst 33258 and chromomycin A3 enables FACS-purification on the basis of AT/GC content and forward scatter (359). Combination of enriched mitotic chromosomes with mass spectrometry has been used to identify hundreds of chromatin-bound proteins in ESCs (324). These included previously described pluripotent reprogramming factors, such as ESRRB and SOX2 (303,316). The identification of protein complexes could potentially be accomplished by employing affinity purification methods using tagged "bait"

proteins (such as GATA2) to identify the associated “prey” proteins, before performing mass spectrometry analysis. Frequently employed tags, such as the FLAG tag, can be integrated into the genome using CRISPR/Cas9, either before or after the “bait” protein, to establish cell lines with stable expression of affinity-tagged proteins (360). In the context of GATA2-deficiency syndrome, blast cells from patients carrying mutations in *GATA2* can theoretically be arrested in mitosis and submitted to chromosome sorting and mass spectrometry to assess TF retention or depletion compared to a healthy control. Alternatively, point-mutations can be added to FLAG-tagged hematopoietic cancer cell lines to analyze the disruption of TF complexes. It is plausible that distinct mutations could hinder GATA2’s chromatin association at different levels, potentially offering insight into the diverse disease phenotypes observed in pediatric and adult patients with GATA2 deficiencies.

A very important question in the mitotic bookmarking field remains: “What determines whether a transcription factor will remain bound to a particular site in mitosis?” (312). Caravaca *et al.* have shown that the intrinsic nucleosome occupancy score at FOXA1 sites is higher in mitotic cells when compared to asynchronous cells. This scoring system consists of a computational model that predicts the likelihood of a given DNA sequence to form a nucleosome. FOXA1 has been described as a pioneer factor as it possesses the ability to bind nucleosomal DNA (closed chromatin), making it accessible to other TFs and regulatory proteins for the activation of gene transcription (312,361). This result suggests that the nucleosomes in regions bookmarked by FOXA1 are more stably positioned compared to sites where FOXA1 binds only during interphase. However, since many TFs do not have pioneer factor activity, this measure might not apply to all bookmarking factors. GATA2, for example, binds mainly to open chromatin sites, with preference for active promoters and enhancers, as described in study III and during hemogenic reprogramming of HDFs (246). Hence, other TF or genome properties might predict mitotic bookmarking capacity.

Several studies have shown that H3 methylation marks are generally retained in mitosis, whereas H3 acetylation marks are decreased (303,307,308). In paper III, we showed that GATA2 binds less to sites decorated with transcription elongation marks (H3K36me3 and H4K20me1), consistent with the basal levels of gene expression reported in mitosis (296,307), and to sites with H3K4me1 and H3K27me3, which are associated with bivalent enhancers. Bivalent enhancers are regulatory DNA elements that carry both activating and repressive histone modifications, indicating their poised state for either gene activation or repression (362). Conversely, GATA2 mitotic binding is more frequent at transcriptionally active chromatin marked by H3K4me3 and H3K9ac, and at regions with H2A.Z. The histone 2 variant H2A.Z is associated with both transcription activation and repression, depending on the gene (363). Decreasing bookmarking at bivalent and weak enhancers, while increasing retention at active enhancers and promoters might

allow flexibility for gene expression upon G1 re-entrance, while maintaining important active genes marked. This supports the idea that M-G1 transition might serve as a time window for adjustments in gene expression profiles (364,365).

Importantly, we demonstrated that mitotic peaks contained more GATA2 motifs than asynchronous-only peaks, implying that a higher motif density is necessary for sequence-specific GATA2 binding during mitosis. This observation also suggests that the number of proximal motifs may serve as a predictive feature for determining whether a TF might be retained in a particular genomic site or not. If so, then is mitotic bookmarking an authentic epigenetic mechanism? Or is it determined by genomic elements? An experimental approach to tackle this question would involve inserting GATA2 motifs in non-bookmarked regions (asynchronous-only peaks) or, in turn, reducing the number of motifs in bookmarked sites and assessing bookmarking at those regions with CHIP-seq. Alternatively, it would also be plausible to increase the number of motif sites of non-bookmarker factors, such as BRN2 or NANOG, and assess whether or not these factors become bookmarkers. Nonetheless, it would be worthwhile to first analyze the number of TF motifs present per peak in asynchronous and mitotic cells using existing data from previously reported bookmarkers, to determine whether this feature applies to TFs other than GATA2.

Regarding the role of GATA2 at mitotic exit *in vivo*, our mouse model data show embryonic lethality comparable to the *Gata2* full KO mice, between E10.5 and E11.5. However, in contrast to the classical *Gata2*<sup>-/-</sup>, MD homozygous E9.5 embryos were indistinguishable from their wild-type or heterozygous counterparts, and yolk sac progenitors generated equivalent numbers of hematopoietic colonies and contained similar percentages of EMPs. Nevertheless, these progenitors were unable to contribute to blood between E10.5 and E11.5, consequently leading to anemia, indicating that GATA2 might not be necessary at M-G1 for the generation of pro-definitive progenitors in the yolk sac, but may still be required for their proliferation and/or function in other hematopoietic tissues, namely the fetal liver. The generation of pro-definitive progenitors may rely on mitotic bookmarking or retention by other TFs, such as TAL1 and LMO2 which regulate early hematopoiesis. The differential requirement of GATA2-mediated bookmarking might also be attributed to the distinct molecular signals governing EHT during the second and third waves of hematopoietic development (71–73). In fact, we found that GATA2 bookmarks the NOTCH-associated genes *HES1* and *JAG1*, which are expressed in the AGM region at E10.5 (73), establishing a connection between GATA2's bookmarking during mitosis and the regulation of the NOTCH pathway for HSC specification.

One limitation of our system is the acknowledged spillover of GATA2 degradation into the G1 phase. Therefore, we pose the question: could the observed effects potentially result from an overall reduction in GATA2 levels during development? In GATA2 haploinsufficient mice (*Gata2*<sup>+/-</sup>) there is a significant decrease in the

number of hematopoietic colonies in CFU assays derived from E10 AGM and yolk sac (78). However, our heterozygous MD-*Gata2* HSPCs generated a similar number of hematopoietic colonies compared to wild-type HSPCs, and embryos exhibited comparable numbers of IAHCs. More importantly, *Gata2*<sup>+/-</sup> mice that have a 50% reduction of GATA2 are viable, meaning that cutting down GATA2 levels by half does not result in the abolition of definitive hematopoiesis, whereas the deletion of GATA2 during the M-G1 transition is critical. Moreover, MD homozygous mice have functional yolk sac progenitors, contrary to the double/heterozygous KOs. These observations suggest that there is a specific impact in removing GATA2 at M-G1 for definitive hematopoiesis that is not present during earlier stages of hematopoietic development. Therefore, reduction of GATA2 levels by itself is not enough to explain our results. To better address this question, it will be relevant to check the allelic expression and protein analysis of hematopoietic tissues with the three genotypes (MD/MD, MD/WT and WT/WT) at different embryonic days, to complement our current data. Additionally, transcriptional profiling at the single-cell level of HSPC populations during embryonic development (yolk sac, AGM, placenta and fetal liver) would allow us to molecularly characterize the impact of GATA2 degradation in mitosis in both homozygous and heterozygous mice. Furthermore, the development of a double transgenic MD-*Gata2* mouse crossed with a well-established model expressing a fluorescent tagged version of GATA2, like the *Gata2Venus* mouse (83), will allow the assessment of protein degradation kinetics throughout the cell cycle *in vivo*. In parallel, improving mitotic-specific degron mouse models for GATA2 (and other factors) by fine-tuning the time window for mitotic degradation could help shed light into the effective requirement of TF-mediated mitotic bookmarking for the specification of cell lineages. Nonetheless, we provide, for the first time, evidence supporting a requirement for mitotic retention or bookmarking for lineage commitment and blood specification.

We also demonstrate that heterozygous MD-*Gata2* HSCs underperformed compared to wild-type cells in competitive transplantation assays, suggesting that GATA2 plays a role during M-G1 in the proper maintenance of HSC function in adult mice. Similarly to the examination of HSPC expression profiles during development, performing scRNA-seq on adult hematopoietic tissues (bone marrow, spleen, and peripheral blood) will provide information about the critical regulators of HSPC maintenance. The next logical step will be to further characterize the impact of heterozygosity in our mouse model by evaluating the numbers and lineages of hematopoietic cells in the peripheral blood, spleen, and bone marrow. This is particularly relevant in the context of GATA-deficiency syndrome since there is a discrepancy between GATA2 haploinsufficiency phenotypes in mouse and human. Using our model, we can evaluate the percentage of myeloid progenitors, as well as NK cells, dendritic cells and monocytes through immunostaining, and compare the results to our MD<sub>mut</sub>-*Gata2* control. Individuals with hereditary *GATA2* mutations show predisposition to myelodysplastic syndrome (MDS) and acute myeloid leukemia (AML). It would be interesting to address the potential role of

GATA2 mitotic bookmarking in leukemic transformation. For the study of leukemia initiation, it would be important to follow MD-*Gata2* heterozygous mice for a long time after periods of stress-induced hematopoiesis (5FU, PolyI:C, etc.) to assess whether those mice would be a better model for the human predisposition to leukemia in GATA2-deficiency syndrome. Moreover, to investigate the impact of GATA2 bookmarking on leukemia progression, the introduction of the MD degraon into human leukemic cell lines, such as K562 or HL-60, which express GATA2 would be informative. Subsequently, we could assess whether they undergo lineage-specific differentiation or remain in a leukemic state upon induction of differentiation. Alternatively, we could resort to inducible mouse models that allow the control of leukemia initiation upon addition of doxycycline, such as the MLL-ENL system. This model is based on a translocation leading to the expression of an MLL-ENL fusion protein which results in acute mixed-lineage leukemia, that maintains GATA2 expression (366). To evaluate whether mitotic bookmarking by GATA2 promotes or abrogates the progression of leukemia, the MD-*Gata2* model could be crossed with MLL-ENL model and leukemia initiated.

Altogether, the studies encompassed in my thesis make a substantial contribution to the current understanding of the regulatory mechanisms that govern definitive hematopoiesis. I have identified a novel marker of human hemogenesis, CD9, described molecular barriers and facilitators in human hemogenic reprogramming – highlighting CD34 and CD44 as barriers and STAG2 as a facilitator – and ultimately characterized the pivotal role of the GATA2 bookmark during M-G1 transition in the specification of definitive hematopoiesis *in vivo* (Figure 15).

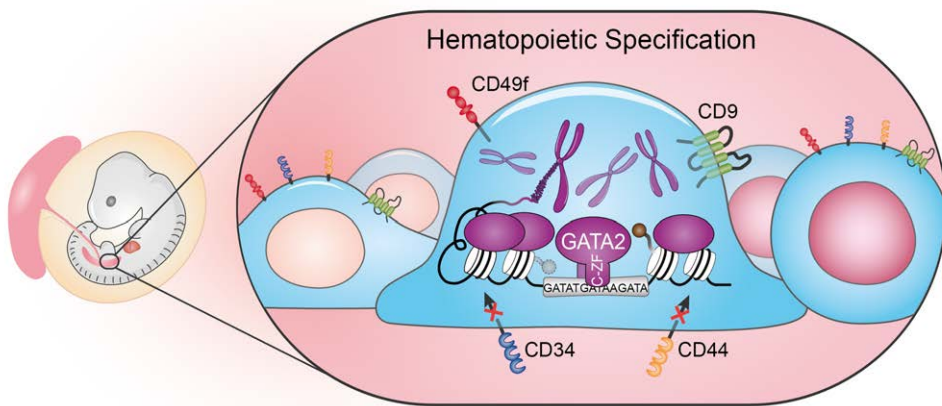


**Figure 15. Mechanisms underlying the specification of human definitive hematopoiesis.** Overview diagram highlighting the outcomes of the thesis in the context of definitive hematopoietic specification. It shows GATA2 bookmarking sites enriched with GATA2 motifs in a representative hemogenic cell undergoing mitosis, during the specification of definitive hematopoiesis in the aorta-gonad-mesonephros of the developing embryo. The hemogenic precursor, which ultimately becomes a hematopoietic stem cell, expresses CD49f and CD9, while signaling pathways controlled by CD34 and CD44 are suppressed.



# References

1. Weiss Ch, Jelkmann W. Functions of the Blood. In: Schmidt RF, Thews G, editors. *Human Physiology*. Berlin, Heidelberg: Springer Berlin Heidelberg; 1989. p. 402–38.
2. Metcalf D. The molecular control of cell division, differentiation commitment and maturation in haemopoietic cells. *Nature*. 1989 May;339(6219):27–30.
3. Akashi K, Traver D, Miyamoto T, Weissman IL. A clonogenic common myeloid progenitor that gives rise to all myeloid lineages. *Nature*. 2000 Mar;404(6774):193–7.
4. Zhang Y, Gao S, Xia J, Liu F. Hematopoietic Hierarchy – An Updated Roadmap. *Trends Cell Biol*. 2018;28(12):976–86.
5. Wu L, D’Amico A, Hochrein H, O’Keeffe M, Shortman K, Lucas K. Development of thymic and splenic dendritic cell populations from different hemopoietic precursors. *Blood*. 2001;98(12):3376–82.
6. Laurenti E, Göttgens B. From haematopoietic stem cells to complex differentiation landscapes. *Nature*. 2018 Jan 25;553(7689):418–26.
7. Brown G, Ceredig R. Modeling the hematopoietic landscape. Vol. 7, *Frontiers in Cell and Developmental Biology*. 2019.
8. Buenrostro JD, Corces MR, Lareau CA, Wu B, Schep AN, Aryee MJ, et al. Integrated Single-Cell Analysis Maps the Continuous Regulatory Landscape of Human Hematopoietic Differentiation. *Cell*. 2018;173(6).
9. Karamitros D, Stoilova B, Aboukhalil Z, Hamey F, Reinisch A, Samitsch M, et al. Single-cell analysis reveals the continuum of human lympho-myeloid progenitor cells article. *Nat Immunol*. 2018;19(1).
10. Macaulay IC, Svensson V, Labalette C, Ferreira L, Hamey F, Voet T, et al. Single-Cell RNA-Sequencing Reveals a Continuous Spectrum of Differentiation in Hematopoietic Cells. *Cell Rep*. 2016;14(4).
11. Velten L, Haas SF, Raffel S, Blaszkiewicz S, Islam S, Hennig BP, et al. Human haematopoietic stem cell lineage commitment is a continuous process. *Nat Cell Biol*. 2017;19(4).
12. Dzierzak E, Bigas A. Blood Development: Hematopoietic Stem Cell Dependence and Independence. *Cell Stem Cell*. 2018;22(5):639–51.
13. Palis J, Robertson S, Kennedy M, Wall C, Keller G. Development of erythroid and myeloid progenitors in the yolk sac and embryo proper of the mouse. *Development*. 1999;126(22).

14. Tober J, Koniski A, McGrath KE, Vemishetti R, Emerson R, De Mesy-Bentley KKL, et al. The megakaryocyte lineage originates from hemangioblast precursors and is an integral component both of primitive and of definitive hematopoiesis. *Blood*. 2007;109(4).
15. Sankaran VG, Orkin SH. The switch from fetal to adult hemoglobin. *Cold Spring Harb Perspect Med*. 2013;3(1).
16. McGrath KE, Frame JM, Palis J. Early hematopoiesis and macrophage development. Vol. 27, *Seminars in Immunology*. 2015.
17. McGrath KE, Koniski AD, Malik J, Palis J. Circulation is established in a stepwise pattern in the mammalian embryo. *Blood*. 2003;101(5).
18. Ginhoux F, Lim S, Hoeffel G, Low D, Huber T. Origin and differentiation of microglia. *Frontiers in Cellular Neuroscience*. 2013.
19. Ginhoux F, Greter M, Leboeuf M, Nandi S, See P, Gokhan S, et al. Fate Mapping Analysis Reveals That Adult Microglia Derive from Primitive Macrophages. *Science* (1979). 2010 Nov 5;330(6005):841–5.
20. Luckett WP. Origin and differentiation of the yolk sac and extraembryonic mesoderm in presomite human and rhesus monkey embryos. *American Journal of Anatomy*. 1978;152(1).
21. Fukuda T. Fetal hemopoiesis - I. Electron microscopic studies on human yolk sac hemopoiesis. *Virchows Archiv B Cell Pathology Zell-pathologie*. 1973;14(1).
22. Bian Z, Gong Y, Huang T, Lee CZW, Bian L, Bai Z, et al. Deciphering human macrophage development at single-cell resolution. *Nature*. 2020;582(7813).
23. North T, Gu TL, Stacy T, Wang Q, Howard L, Binder M, et al. *Cbfa2* is required for the formation of intra-aortic hematopoietic clusters. *Development*. 1999;126(11).
24. Gao L, Tober J, Gao P, Chen C, Tan K, Speck NA. *RUNX1* and the endothelial origin of blood. *Exp Hematol*. 2018;68:2–9.
25. Yzaguirre AD, de Bruijn MFTR, Speck NA. The role of *Runx1* in embryonic blood cell formation. In: *Advances in Experimental Medicine and Biology*. 2017.
26. Frame JM, McGrath KE, Palis J. Erythro-myeloid progenitors: “definitive” hematopoiesis in the conceptus prior to the emergence of hematopoietic stem cells. *Blood Cells Mol Dis*. 2013 Dec;51(4):220–5.
27. Ulloa BA, Habbsa SS, Potts KS, Lewis A, McKinstry M, Payne SG, et al. Definitive hematopoietic stem cells minimally contribute to embryonic hematopoiesis. *Cell Rep*. 2021 Sep;36(11):1–17.
28. Soares-Da-Silva F, Freyer L, Elsaid R, Burlen-Defranoux O, Iturri L, Sismeiro O, et al. Yolk sac, but not hematopoietic stem cell-derived progenitors, sustain erythropoiesis throughout murine embryonic life. *Journal of Experimental Medicine*. 2021;218(4).
29. McGrath KE, Frame JM, Fegan KH, Bowen JR, Conway SJ, Catherman SC, et al. Distinct Sources of Hematopoietic Progenitors Emerge before HSCs and Provide Functional Blood Cells in the Mammalian Embryo. *Cell Rep*. 2015;11(12):1892–904.

30. Hoeffel G, Ginhoux F. Fetal monocytes and the origins of tissue-resident macrophages. *Cell Immunol.* 2018;330.
31. Gomez Perdiguero E, Klapproth K, Schulz C, Busch K, Azzoni E, Crozet L, et al. Tissue-resident macrophages originate from yolk-sac-derived erythro-myeloid progenitors. *Nature.* 2015;518(7540).
32. Hoeffel G, Chen J, Lavin Y, Low D, Almeida FF, See P, et al. C-Myb<sup>+</sup> Erythro-Myeloid Progenitor-Derived Fetal Monocytes Give Rise to Adult Tissue-Resident Macrophages. *Immunity.* 2015;42(4).
33. Neo WH, Lie-A-Ling M, Fadlullah MZH, Lacaud G. Contributions of Embryonic HSC-Independent Hematopoiesis to Organogenesis and the Adult Hematopoietic System. *Front Cell Dev Biol.* 2021;9(February).
34. Cumano A, Furlonger C, Paige CJ. Differentiation and characterization of B-cell precursors detected in the yolk sac and embryo body of embryos beginning at the 10- to 12-somite stage. *Proc Natl Acad Sci U S A.* 1993;90(14).
35. Yokota T, Huang J, Tavian M, Nagai Y, Hirose J, Zúñiga-Pflücker JC, et al. Tracing the first waves of lymphopoiesis in mice. *Development.* 2006;133(10).
36. Böiers C, Carrelha J, Lutteropp M, Luc S, Green JCA, Azzoni E, et al. Lymphomyeloid contribution of an immune-restricted progenitor emerging prior to definitive hematopoietic stem cells. *Cell Stem Cell.* 2013;13(5).
37. Yoshimoto M, Porayette P, Glosson NL, Conway SJ, Carlesso N, Cardoso AA, et al. Autonomous murine T-cell progenitor production in the extra-embryonic yolk sac before HSC emergence. *Blood.* 2012;119(24).
38. Hadland B, Yoshimoto M. Many layers of embryonic hematopoiesis: new insights into B-cell ontogeny and the origin of hematopoietic stem cells. *Exp Hematol.* 2018 Apr 1;60:1–9.
39. Ivanovs A, Rybtsov S, Ng ES, Stanley EG, Elefanty AG, Medvinsky A. Human haematopoietic stem cell development: From the embryo to the dish. *Development (Cambridge).* 2017;144(13):2323–37.
40. Mikkola HKA, Gekas C, Orkin SH, Dieterlen-Lievre F. Placenta as a site for hematopoietic stem cell development. *Exp Hematol.* 2005;33(9 SPEC. ISS.).
41. De Bruijn MFTR, Speck NA, Peeters MCE, Dzierzak E. Definitive hematopoietic stem cells first develop within the major arterial regions of the mouse embryo. *EMBO Journal.* 2000;19(11).
42. Ottersbach K, Dzierzak E. The murine placenta contains hematopoietic stem cells within the vascular labyrinth region. *Dev Cell.* 2005;8(3):377–87.
43. Yokomizo T, Dzierzak E. Three-dimensional cartography of hematopoietic clusters in the vasculature of whole mouse embryos. *Development.* 2010;137(21).
44. Zovein AC, Hofmann JJ, Lynch M, French WJ, Turlo KA, Yang Y, et al. Fate Tracing Reveals the Endothelial Origin of Hematopoietic Stem Cells. *Cell Stem Cell.* 2008;3(6):625–36.
45. Boisset JC, van Cappellen W, Andrieu-Soler C, Galjart N, Dzierzak E, Robin C. In vivo imaging of haematopoietic cells emerging from the mouse aortic endothelium. *Nature.* 2010;464(7285):116–20.

46. Kissa K, Herbomel P. Blood stem cells emerge from aortic endothelium by a novel type of cell transition. *Nature*. 2010;464(7285):112–5.
47. Mizuochi C, Fraser ST, Biasch K, Horio Y, Kikushige Y, Tani K, et al. Intra-aortic clusters undergo endothelial to hematopoietic phenotypic transition during early embryogenesis. *PLoS One*. 2012;7(4).
48. Taoudi S, Gonneau C, Moore K, Sheridan JM, Blackburn CC, Taylor E, et al. Extensive hematopoietic stem cell generation in the AGM region via maturation of VE-Cadherin+CD45+ pre-definitive HSCs. *Cell Stem Cell*. 2008;3(1).
49. Rybtsov S, Sobiesiak M, Taoudi S, Souilhol C, Senserrich J, Liakhovitskaia A, et al. Hierarchical organization and early hematopoietic specification of the developing HSC lineage in the AGM region. *Journal of Experimental Medicine*. 2011;208(6).
50. Rybtsov S, Batsivari A, Bilotkach K, Paruzina D, Senserrich J, Nerushev O, et al. Tracing the origin of the HSC hierarchy reveals an SCF-dependent, IL-3-independent CD43- embryonic precursor. *Stem Cell Reports*. 2014;3(3):489–501.
51. Kieusseian A, de la Grange PB, Burlen-Defranoux O, Godin I, Cumano A. Immature hematopoietic stem cells undergo maturation in the fetal liver. *Development (Cambridge)*. 2012;139(19).
52. Rybtsov S, Ivanovs A, Zhao S, Medvinsky A. Concealed expansion of immature precursors underpins acute burst of adult HSC activity in foetal liver. *Development (Cambridge)*. 2016;143(8).
53. Costa G, Kouskoff V, Lacaud G. Origin of blood cells and HSC production in the embryo. *Trends Immunol*. 2012;33(5):215–23.
54. Tavian M, Hallais MF, Péault B. Emergence of intraembryonic hematopoietic precursors in the pre-liver human embryo. *Development*. 1999;126(4).
55. Tavian M, Coulombel L, Luton D, Clemente HS, Dieterlen-Lièvre F, Péault B. Aorta-associated CD34+ hematopoietic cells in the early human embryo. *Blood*. 1996;87(1).
56. Ivanovs A, Rybtsov S, Welch L, Anderson RA, Turner ML, Medvinsky A. Highly potent human hematopoietic stem cells first emerge in the intraembryonic aorta-gonad-mesonephros region. *J Exp Med*. 2011;208(12):2417–27.
57. Easterbrook J, Rybtsov S, Gordon-Keylock S, Ivanovs A, Taoudi S, Anderson RA, et al. Analysis of the Spatiotemporal Development of Hematopoietic Stem and Progenitor Cells in the Early Human Embryo. *Stem Cell Reports*. 2019;12(5).
58. Péault B, Oberlin E, Tavian M. Emergence of hematopoietic stem cells in the human embryo. *C R Biol*. 2002;325(10).
59. Hou S, Li Z, Zheng X, Gao Y, Dong J, Ni Y, et al. Embryonic endothelial evolution towards first hematopoietic stem cells revealed by single-cell transcriptomic and functional analyses. *Cell Res*. 2020;30(5):376–92.
60. Zeng Y, He J, Bai Z, Li Z, Gong Y, Liu C, et al. Tracing the first hematopoietic stem cell generation in human embryo by single-cell RNA sequencing. *Cell Res*. 2019 Nov;29(11):881–94.

61. Calvanese V, Capellera-Garcia S, Ma F, Fares I, Liebscher S, Ng ES, et al. Mapping human haematopoietic stem cells from haemogenic endothelium to birth. *Nature*. 2022;604(7906):534–40.
62. Guibentif C, Rönn RE, Böiers C, Lang S, Saxena S, Soneji S, et al. Single-Cell Analysis Identifies Distinct Stages of Human Endothelial-to-Hematopoietic Transition. *Cell Rep*. 2017;19(1):10–9.
63. Warren AJ, Colledge WH, Carlton MBL, Evans MJ, Smith AJH, Rabbitts TH. The Oncogenic Cysteine-rich LIM domain protein Rbtn2 is essential for erythroid development. *Cell*. 1994;78(1).
64. Shivdasani RA, Mayer EL, Orkin SH. Absence of blood formation in mice lacking the T-cell leukaemia oncoprotein tal-1/SCL. *Nature*. 1995;373(6513).
65. Tober J, Yzaguirre AD, Piwarzyk E, Speck NA. Distinct temporal requirements for Runx1 in hematopoietic progenitors and stem cells. *Development (Cambridge)*. 2013;140(18).
66. Wang Q, Stacy T, Binder M, Marín-Padilla M, Sharpe AH, Speck NA. Disruption of the Cbfa2 gene causes necrosis and hemorrhaging in the central nervous system and blocks definitive hematopoiesis. *Proc Natl Acad Sci U S A*. 1996;93(8).
67. Cai Z, De Bruijn M, Ma X, Dortland B, Luteijn T, Downing JR, et al. Haploinsufficiency of AML1 affects the temporal and spatial generation of hematopoietic stem cells in the mouse embryo. *Immunity*. 2000;13(4).
68. Lancrin C, Mazan M, Stefanska M, Patel R, Lichtinger M, Costa G, et al. GFI1 and GFI1B control the loss of endothelial identity of hemogenic endothelium during hematopoietic commitment. *Blood*. 2012;120(2):314–22.
69. Bruveris FF, Ng ES, Leitoguinho AR, Motazedian A, Vlahos K, Sourris K, et al. Human yolk sac-like haematopoiesis generates RUNX1-, GFI1- and/or GFI1B-dependent blood and SOX17-positive endothelium. *Development*. 2020 Oct 29;147(20).
70. Hadland BK, Huppert SS, Kanungo J, Xue Y, Jiang R, Gridley T, et al. A requirement for Notch1 distinguishes 2 phases of definitive hematopoiesis during development. *Blood*. 2004;104(10):3097–105.
71. Chen MJ, Li Y, De Obaldia ME, Yang Q, Yzaguirre AD, Yamada-Inagawa T, et al. Erythroid/Myeloid Progenitors and Hematopoietic Stem Cells Originate from Distinct Populations of Endothelial Cells. *Cell Stem Cell*. 2011 Dec;9(6):541–52.
72. Hadland BK, Huppert SS, Kanungo J, Xue Y, Jiang R, Gridley T, et al. A requirement for Notch1 distinguishes 2 phases of definitive hematopoiesis during development. *Blood*. 2004 Nov 15;104(10):3097–105.
73. Robert-Moreno À, Espinosa L, de la Pompa JL, Bigas A. RBPjk-dependent Notch function regulates Gata2 and is essential for the formation of intra-embryonic hematopoietic cells. *Development*. 2005;132(5):1117–26.
74. Burns CE, Traver D, Mayhall E, Shepard JL, Zon LI. Hematopoietic stem cell fate is established by the Notch-Runx pathway. *Genes Dev*. 2005;19(19).
75. Bray SJ. Notch signalling: A simple pathway becomes complex. Vol. 7, *Nature Reviews Molecular Cell Biology*. 2006.

76. Tsai FY, Keller G, Kuo FC, Weiss M, Chen J, Rosenblatt M, et al. An early haematopoietic defect in mice lacking the transcription factor GATA-2. *Nature*. 1994;371(6494):221–6.
77. Chen MJ, Yokomizo T, Zeigler BM, Dzierzak E, Speck NA. Runx1 is required for the endothelial to haematopoietic cell transition but not thereafter. *Nature*. 2009;457(7231).
78. Pater E De, Kaimakis P, Vink CS, Yokomizo T, Yamada-inagawa T, Linden R Van Der, et al. Gata2 is required for HSC generation and survival. *J Exp Med*. 2013;210(13):2843–50.
79. Ling KW, Ottersbach K, van Hamburg JP, Oziemlak A, Tsai FY, Orkin SH, et al. GATA-2 Plays Two Functionally Distinct Roles during the Ontogeny of Hematopoietic Stem Cells. *Journal of Experimental Medicine*. 2004 Oct 4;200(7):871–82.
80. Tsai FY, Orkin SH. Transcription Factor GATA-2 Is Required for Proliferation/Survival of Early Hematopoietic Cells and Mast Cell Formation, But Not for Erythroid and Myeloid Terminal Differentiation. *Blood*. 1997;89(10):3636–43.
81. Minegishi N, Ohta J, Yamagiwa H, Suzuki N, Kawauchi S, Zhou Y, et al. The mouse GATA-2 gene is expressed in the para-aortic splanchnopleura and aortagonsads and mesonephros region. *Blood*. 1999;93(12):4196–207.
82. Kaimakis P, De Pater E, Eich C, Kartalaei PS, Kauts ML, Vink CS, et al. Functional and molecular characterization of mouse Gata2-independent hematopoietic progenitors. *Blood*. 2016;127(11).
83. Eich C, Arlt J, Vink CS, Solaimani Kartalaei P, Kaimakis P, Mariani SA, et al. In vivo single cell analysis reveals Gata2 dynamics in cells transitioning to hematopoietic fate. *Journal of Experimental Medicine*. 2018 Jan;215(1):233–48.
84. Tipping AJ, Pina C, Castor A, Hong D, Rodrigues NP, Lazzari L, et al. High GATA-2 expression inhibits human hematopoietic stem and progenitor cell function by effects on cell cycle. *Blood*. 2009;113(12).
85. Rodrigues NP, Janzen V, Forkert R, Dombkowski DM, Boyd AS, Orkin SH, et al. Haploinsufficiency of GATA-2 perturbs adult hematopoietic stem-cell homeostasis. *Blood*. 2005;106(2):477–85.
86. Sun W, Downing JR. Haploinsufficiency of AML1 results in a decrease in the number of LTR-HSCs while simultaneously inducing an increase in more mature progenitors. *Blood*. 2004;104(12).
87. Wilson NK, Foster SD, Wang X, Knezevic K, Schütte J, Kaimakis P, et al. Combinatorial transcriptional control in blood stem/progenitor cells: Genome-wide analysis of ten major transcriptional regulators. *Cell Stem Cell*. 2010;7(4):532–44.
88. Moignard V, Macaulay IC, Swiers G, Buettner F, Schütte J, Calero-Nieto FJ, et al. Characterization of transcriptional networks in blood stem and progenitor cells using high-throughput single-cell gene expression analysis. *Nat Cell Biol*. 2013;15(4):363–72.

89. Ranzoni AM, Tangherloni A, Berest I, Riva SG, Myers B, Strzelecka PM, et al. Integrative Single-Cell RNA-Seq and ATAC-Seq Analysis of Human Developmental Hematopoiesis. *Cell Stem Cell*. 2021;28(3).
90. Vink CS, Calero-Nieto FJ, Wang X, Maglitto A, Mariani SA, Jawaid W, et al. Iterative Single-Cell Analyses Define the Transcriptome of the First Functional Hematopoietic Stem Cells. *Cell Rep*. 2020;31(6).
91. Oatley M, Bölükbaşı ÖV, Svensson V, Shvartsman M, Ganter K, Zirngibl K, et al. Single-cell transcriptomics identifies CD44 as a marker and regulator of endothelial to haematopoietic transition. *Nat Commun*. 2020;11(1).
92. Pinto do O P. Expression of the LIM-homeobox gene LH2 generates immortalized Steel factor-dependent multipotent hematopoietic precursors. *EMBO J*. 1998 Oct 1;17(19):5744–56.
93. Orkin SH. GATA-Binding Transcription Factors in Hematopoietic Cells. *Blood*. 1992;80(3):575–81.
94. Ko LJ, Engel JD. DNA-Binding Specificities of the GATA Transcription Factor Family. *Mol Cell Biol*. 1993;13(7):4011–22.
95. Yang HY, Evans T. Distinct roles for the two cGATA-1 finger domains. *Mol Cell Biol*. 1992;12(10):4562–70.
96. Trainor CD, Ghirlando R, Simpson MA. GATA Zinc Finger Interactions Modulate DNA Binding and Transactivation. *Journal of Biological Chemistry*. 2000;275(36):28157–66.
97. Whyatt DJ, DeBoer E, Grosveld F. The two zinc finger-like domains of GATA-1 have different DNA binding specificities. *EMBO Journal*. 1993;12(13):4993–5005.
98. Vicente C, Conchillo A, García-Sánchez MA, Otero MD. The role of the GATA2 transcription factor in normal and malignant hematopoiesis. *Crit Rev Oncol Hematol*. 2012;82(1):1–17.
99. Minegishi N, Suzuki N, Yokomizo T, Pan X, Fujimoto T, Takahashi S, et al. Expression and domain-specific function of GATA-2 during differentiation of the hematopoietic precursor cells in midgestation mouse embryos. *Blood*. 2003;102(3):896–905.
100. Rodrigues NP, Boyd AS, Fugazza C, May GE, Guo Y, Tipping AJ, et al. GATA-2 regulates granulocyte-macrophage progenitor cell function. *Blood*. 2008 Dec 15;112(13):4862–73.
101. Grass JA, Boyer ME, Pal S, Wu J, Weiss MJ, Bresnick EH. GATA-1-dependent transcriptional repression of GATA-2 via disruption of positive autoregulation and domain-wide chromatin remodeling. *Proceedings of the National Academy of Sciences*. 2003 Jul 22;100(15):8811–6.
102. Huang Z, Dore LC, Li Z, Orkin SH, Feng G, Lin S, et al. GATA-2 Reinforces Megakaryocyte Development in the Absence of GATA-1. *Mol Cell Biol*. 2009 Sep 1;29(18):5168–80.
103. Zhang P, Zhang X, Iwama A, Yu C, Smith KA, Mueller BU, et al. PU.1 inhibits GATA-1 function and erythroid differentiation by blocking GATA-1 DNA binding. *Blood*. 2000 Oct 15;96(8):2641–8.

104. Walsh JC, DeKoter RP, Lee HJ, Smith ED, Lancki DW, Gurish MF, et al. Cooperative and Antagonistic Interplay between PU.1 and GATA-2 in the Specification of Myeloid Cell Fates. *Immunity*. 2002 Nov;17(5):665–76.
105. Rodrigues NP, Tipping AJ, Wang Z, Enver T. GATA-2 mediated regulation of normal hematopoietic stem/progenitor cell function, myelodysplasia and myeloid leukemia. *International Journal of Biochemistry and Cell Biology*. 2012;44(3):457–60.
106. Calvo KR, Hickstein DD. The spectrum of GATA2 deficiency syndrome. *Blood*. 2023 Mar 30;141(13):1524–32.
107. Hahn CN, Chong CE, Carmichael CL, Wilkins EJ, Brautigam PJ, Li XC, et al. Heritable GATA2 mutations associated with familial myelodysplastic syndrome and acute myeloid leukemia. *Nat Genet*. 2011 Oct 4;43(10):1012–7.
108. Ostergaard P, Simpson MA, Connell FC, Steward CG, Brice G, Woollard WJ, et al. Mutations in GATA2 cause primary lymphedema associated with a predisposition to acute myeloid leukemia (Emberger syndrome). *Nat Genet*. 2011 Oct 4;43(10):929–31.
109. Hsu AP, Sampaio EP, Khan J, Calvo KR, Lemieux JE, Patel SY, et al. Mutations in GATA2 are associated with the autosomal dominant and sporadic monocytopenia and mycobacterial infection (MonoMAC) syndrome. *Blood*. 2011 Sep 8;118(10):2653–5.
110. Vinh DC, Patel SY, Uzel G, Anderson VL, Freeman AF, Olivier KN, et al. Autosomal dominant and sporadic monocytopenia with susceptibility to mycobacteria, fungi, papillomaviruses, and myelodysplasia. *Blood*. 2010 Feb 25;115(8):1519–29.
111. Bigley V, Collin M. Dendritic cell, monocyte, B and NK lymphoid deficiency defines the lost lineages of a new GATA-2 dependent myelodysplastic syndrome. *Haematologica*. 2011 Aug 1;96(8):1081–3.
112. Dickinson RE, Griffin H, Bigley V, Reynard LN, Hussain R, Haniffa M, et al. Exome sequencing identifies GATA-2 mutation as the cause of dendritic cell, monocyte, B and NK lymphoid deficiency. *Blood*. 2011 Sep 8;118(10):2656–8.
113. Collin M, Dickinson R, Bigley V. Haematopoietic and immune defects associated with GATA2 mutation. *Br J Haematol*. 2015;169(2):173–87.
114. Hou HA, Lin YC, Kuo YY, Chou WC, Lin CC, Liu CY, et al. GATA2 mutations in patients with acute myeloid leukemia-paired samples analyses show that the mutation is unstable during disease evolution. *Ann Hematol*. 2015 Feb 21;94(2):211–21.
115. Tien F ming, Hou H an, Tsai C hong, Tang J luh, Chiu Y chiao, Chen C yuan, et al. GATA2 zinc finger 1 mutations are associated with distinct clinico-biological features and outcomes different from GATA2 zinc finger 2 mutations in adult acute myeloid leukemia. *Blood Cancer J*. 2018 Sep;8(9):1–13.
116. Onodera K, Fujiwara T, Onishi Y, Itoh-Nakadai A, Okitsu Y, Fukuhara N, et al. GATA2 regulates dendritic cell differentiation. *Blood*. 2016 Jul 28;128(4):508–18.



117. Lim KC, Hosoya T, Brandt W, Ku CJ, Hosoya-Ohmura S, Camper SA, et al. Conditional Gata2 inactivation results in HSC loss and lymphatic mispatterning. *Journal of Clinical Investigation*. 2012 Oct 1;122(10):3705–17.
118. McCulloch EA, Till JE. The sensitivity of cells from normal mouse bone marrow to gamma radiation in vitro and in vivo. *Radiat Res*. 1962;16(6):822–32.
119. Till JE, McCulloch EA. A direct measurement of the radiation sensitivity of normal mouse bone marrow cells. *Radiat Res*. 1961;14(2):213–22.
120. Becker AJ, McCulloch EA, Till JE. Cytological demonstration of the clonal nature of spleen colonies derived from transplanted mouse marrow cells. *Nature*. 1963;197:452–4.
121. Magli MC, Iscove NN, Odartchenko N. Transient nature of early haematopoietic spleen colonies. *Nature*. 1982;295(5849):527–9.
122. Osawa M, Hanada KI, Hamada H, Nakauchi H. Long-term lymphohematopoietic reconstitution by a single CD34<sup>-</sup> low/negative hematopoietic stem cell. *Science* (1979). 1996;273(5272):242–5.
123. Walter D, Lier A, Geiselhart A, Thalheimer FB, Huntscha S, Sobotta MC, et al. Exit from dormancy provokes DNA-damage-induced attrition in haematopoietic stem cells. *Nature*. 2015;520(7548).
124. Pietras EM, Warr MR, Passegué E. Cell cycle regulation in hematopoietic stem cells. *Journal of Cell Biology*. 2011;195(5):709–20.
125. Pietras EM, Warr MR, Passegué E. Cell cycle regulation in hematopoietic stem cells. *Journal of Cell Biology*. 2011;195(5):709–20.
126. Yang L, Bryder D, Adolfsson J, Nygren J, Månsson R, Sigvardsson M, et al. Identification of Lin-Sca1<sup>+</sup>kit<sup>+</sup>CD34<sup>+</sup>Flt3<sup>-</sup> short-term hematopoietic stem cells capable of rapidly reconstituting and rescuing myeloablated transplant recipients. *Blood*. 2005;105(7).
127. Oguro H, Ding L, Morrison SJ. SLAM family markers resolve functionally distinct subpopulations of hematopoietic stem cells and multipotent progenitors. *Cell Stem Cell*. 2013;13(1).
128. Laurenti E, Frelin C, Xie S, Ferrari R, Dunant CF, Zandi S, et al. CDK6 levels regulate quiescence exit in human hematopoietic stem cells. *Cell Stem Cell*. 2015;16(3).
129. Notta F, Doulatov S, Laurenti E, Poepl A, Jurisica I, Dick JE. Isolation of Single Human Hematopoietic Stem Cells Capable of Long-Term Multilineage Engraftment. *Science* (1979). 2011 Jul 8;333(6039):218–21.
130. Laurenti E, Göttgens B. From haematopoietic stem cells to complex differentiation landscapes. *Nature*. 2018 Jan;553(7689):418–26.
131. Divisions S renewal, Bernitz JM, Kim HS, Macarthur B, Sieburg H, Bernitz JM, et al. Hematopoietic Stem Cells Count and Remember Article Hematopoietic Stem Cells Count and Remember Self-Renewal Divisions. 2016;1296–309.
132. Brown M, Wittwer C. Flow Cytometry: Principles and Clinical Applications in Hematology. *Clin Chem*. 2000 Aug 1;46(8):1221–9.

133. Cimato TR, Furlage RL, Conway A, Wallace PK. Simultaneous measurement of human hematopoietic stem and progenitor cells in blood using multicolor flow cytometry. *Cytometry B Clin Cytom.* 2016 Sep;90(5):415–23.
134. Mayle A, Luo M, Jeong M, Goodell MA. Flow cytometry analysis of murine hematopoietic stem cells. *Cytometry Part A.* 2013 Jan;83A(1):27–37.
135. Tindle RW, Nichols RAB, Chan L, Campana D, Catovsky D, Birnie GD. A novel monoclonal antibody BI-3C5 recognises myeloblasts and non-B non-T lymphoblasts in acute leukaemias and CGL blast crises, and reacts with immature cells in normal bone marrow. *Leuk Res.* 1985 Jan;9(1):1–9.
136. Civin CI, Strauss LC, Brovall C, Fackler MJ, Schwartz JF, Shaper JH. Antigenic analysis of hematopoiesis. III. A hematopoietic progenitor cell surface antigen defined by a monoclonal antibody raised against KG-1a cells. *The Journal of Immunology.* 1984 Jul 1;133(1):157–65.
137. Stella CC, Cazzola M, Fabritiis P De, Vincentiis A De, Gianni M, Lanza F, et al. CD34-Positive Cells: Biology and Clinical Relevance. *Haematologica.* 1995;80(4):367–87.
138. Majeti R, Park CY, Weissman IL. Identification of a Hierarchy of Multipotent Hematopoietic Progenitors in Human Cord Blood. *Cell Stem Cell.* 2007 Dec;1(6):635–45.
139. Murray L, Chen B, Galy A, Chen S, Tushinski R, Uchida N, et al. Enrichment of human hematopoietic stem cell activity in the CD34+Thy- 1+Lin- subpopulation from mobilized peripheral blood. *Blood.* 1995 Jan 15;85(2):368–78.
140. LaSalle JM, Hafler DA. The coexpression of CD45RA and CD45RO isoforms on T cells during the S/G2/M stages of cell cycle. *Cell Immunol.* 1991;138(1).
141. Lansdorp PM, Sutherland HJ, Eaves CJ. Selective expression of CD45 isoforms on functional subpopulations of CD34+ hemopoietic cells from human bone marrow. *J Exp Med.* 1990 Jul 1;172(1):363–6.
142. van Ranst PCF, Snoeck HW, Lardon F, Lenjou M, Nijs G, Weekx SFA, et al. TGF- $\beta$  and MIP-1 $\alpha$  exert their main inhibitory activity on very primitive CD3++CD38- cells but show opposite effects on more mature CD34+CD38+ human hematopoietic progenitors. *Exp Hematol.* 1996;24(13):1509–15.
143. Larochelle A, Vormoor J, Hanenberg H, Wang JCY, Bhatia M, Lapidot T, et al. Identification of primitive human hematopoietic cells capable of repopulating NOD/SCID mouse bone marrow: Implications for gene therapy. *Nat Med.* 1996 Dec;2(12):1329–37.
144. Anjos-Afonso F, Currie E, Palmer HG, Foster KE, Taussig DC, Bonnet D. CD34- Cells at the Apex of the Human Hematopoietic Stem Cell Hierarchy Have Distinctive Cellular and Molecular Signatures. *Cell Stem Cell.* 2013 Aug;13(2):161–74.
145. Ikuta K, Weissman IL. Evidence that hematopoietic stem cells express mouse c-kit but do not depend on steel factor for their generation. *Proceedings of the National Academy of Sciences.* 1992 Feb 15;89(4):1502–6.
146. Spangrude GJ, Heimfeld S, Weissman IL. Purification and Characterization of Mouse Hematopoietic Stem Cells. *Science* (1979). 1988 Jul;241(4861):58–62.

147. Kiel MJ, Yilmaz ÖH, Iwashita T, Yilmaz OH, Terhorst C, Morrison SJ. SLAM Family Receptors Distinguish Hematopoietic Stem and Progenitor Cells and Reveal Endothelial Niches for Stem Cells. *Cell*. 2005 Jul;121(7):1109–21.
148. Adolfsson J, Borge OJ, Bryder D, Theilgaard-Mönch K, Åstrand-Grundström I, Sitnicka E, et al. Upregulation of Flt3 Expression within the Bone Marrow Lin–Sca1+c-kit+ Stem Cell Compartment Is Accompanied by Loss of Self-Renewal Capacity. *Immunity*. 2001 Oct;15(4):659–69.
149. Kent DG, Copley MR, Benz C, Wöhrer S, Dykstra BJ, Ma E, et al. Prospective isolation and molecular characterization of hematopoietic stem cells with durable self-renewal potential. *Blood*. 2009;113(25).
150. Karlsson G, Rörby E, Pina C, Soneji S, Reckzeh K, Miharada K, et al. The Tetraspanin CD9 Affords High-Purity Capture of All Murine Hematopoietic Stem Cells. *Cell Rep*. 2013;4(4):642–8.
151. Leung KT, Yuen K, Chan Y, Ng PC, Lau TK, Chiu WM, et al. The tetraspanin CD9 regulates migration, adhesion, and homing of human cord blood CD34+ hematopoietic stem and progenitor cells. *Blood*. 2011;117(6):1840–51.
152. Sinka L, Biasch K, Khazaal I, Péault B, Tavian M. Angiotensin-converting enzyme (CD143) specifies emerging lympho-hematopoietic progenitors in the human embryo. *Blood*. 2012 Apr 19;119(16):3712–23.
153. Jokubaitis VJ, Sinka L, Driessen R, Whitty G, Haylock DN, Bertocello I, et al. Angiotensin-converting enzyme (CD143) marks hematopoietic stem cells in human embryonic, fetal, and adult hematopoietic tissues. *Blood*. 2008 Apr 15;111(8):4055–63.
154. Julien E, El R, Tavian M. Origin of the hematopoietic system in the human embryo. *FEBS Lett*. 2016;590(22):3987–4001.
155. Tsuji T, Sakata T, Hamaguchi Y, Wang, F sheng, Houwen B. New rapid flow cytometric method for the enumeration of nucleated red blood cells. *Cytometry*. 1999 Dec 1;37(4):291–301.
156. Sutherland HJ, Lansdorp PM, Henkelman DH, Eaves AC, Eaves CJ. Functional characterization of individual human hematopoietic stem cells cultured at limiting dilution on supportive marrow stromal layers. *Proceedings of the National Academy of Sciences*. 1990 May;87(9):3584–8.
157. Cooper SH, Capitano ML, Broxmeyer HE. Experimental Models of Mouse and Human Hematopoietic Stem Cell Transplantation. In: *Methods in Molecular Biology*. 2023. p. 205–32.
158. Maryanovich M, Gross A. Competitive Bone-marrow Transplantations. *Bio Protoc*. 2014;4(11).
159. Greiner DL, Hesselton RA, Shultz LD. SCID Mouse Models of Human Stem Cell Engraftment. *Stem Cells*. 1998 May;16(3):166–77.
160. Ito M, Hiramatsu H, Kobayashi K, Suzue K, Kawahata M, Hioki K, et al. NOD/SCID/ $\gamma$ cnul mouse: an excellent recipient mouse model for engraftment of human cells. *Blood*. 2002 Nov 1;100(9):3175–82.
161. Congdon CC. Experimental Treatment of Total-body Irradiation Injury: A Brief Review. *Blood*. 1957 Aug 1;12(8):746–54.

162. Thomas ED, Lochte HL, Lu WC, Ferrebee JW. Intravenous Infusion of Bone Marrow in Patients Receiving Radiation and Chemotherapy. *New England Journal of Medicine*. 1957;257(11):491–6.
163. Thomas ED, Lochte HL, Cannon JH, Sahler OD, Ferrebee JW. Supralethal whole body irradiation and isologous marrow transplantation in man. *Journal of Clinical Investigation*. 1959 Oct 1;38(10 Pt 1-2):1709–16.
164. van Rood JJ, Eernisse JG. The Detection of Transplantation Antigens in Leukocytes. In: *Progress in surgery*. 1969. p. 217–52.
165. Maedler-Kron C, Marcus VA, Michel RP. Hematopoietic Stem Cell Transplantation. In: *Pathology of Transplantation*. Cham: Springer International Publishing; 2016. p. 401–49.
166. Ballen KK, Koreth J, Chen YB, Dey BR, Spitzer TR. Selection of optimal alternative graft source: mismatched unrelated donor, umbilical cord blood, or haploidentical transplant. *Blood*. 2012 Mar 1;119(9):1972–80.
167. Penack O, Peczynski C, Mohty M, Yakoub-Agha I, Styczynski J, Montoto S, et al. How much has allogeneic stem cell transplant-related mortality improved since the 1980s? A retrospective analysis from the EBMT. *Blood Adv*. 2020;4(24).
168. Hoggatt J, Pelus LM. Mobilization of hematopoietic stem cells from the bone marrow niche to the blood compartment. *Stem Cell Res Ther*. 2011 Apr 14;2(2):13.
169. Broxmeyer HE, Douglas GW, Hangoc G, Cooper S, Bard J, English D, et al. Human umbilical cord blood as a potential source of transplantable hematopoietic stem/progenitor cells. *Proceedings of the National Academy of Sciences*. 1989 May;86(10):3828–32.
170. Smith AR, Wagner JE. Alternative haematopoietic stem cell sources for transplantation: place of umbilical cord blood. *Br J Haematol*. 2009 Oct;147(2):246–61.
171. Tajer P, Pike-Overzet K, Arias S, Havenga M, Staal F. Ex Vivo Expansion of Hematopoietic Stem Cells for Therapeutic Purposes: Lessons from Development and the Niche. *Cells*. 2019 Feb 18;8(2):169.
172. Mendelson A, Frenette PS. Hematopoietic stem cell niche maintenance during homeostasis and regeneration. Vol. 20, *Nature Medicine*. 2014.
173. Ema BH, Takano H, Sudo K, Nakauchi H. In Vitro Self-Renewal Division of Hematopoietic Stem Cells. 2000;192(9):0–7.
174. Wilkinson AC, Ishida R, Kikuchi M, Sudo K, Morita M, Crisostomo RV, et al. Long-term ex vivo haematopoietic-stem-cell expansion allows nonconditioned transplantation. *Nature*. 2019;571(7763).
175. Fares I, Chagraoui J, Gareau Y, Gingras S, Ruel R, Mayotte N, et al. Pyrimidoindole derivatives are agonists of human hematopoietic stem cell self-renewal. *Science (1979)*. 2014 Sep 19;345(6203):1509–12.
176. Boitano AE, Wang J, Romeo R, Bouchez LC, Parker AE, Sutton SE, et al. Aryl Hydrocarbon Receptor Antagonists Promote the Expansion of Human Hematopoietic Stem Cells. *Science (1979)*. 2010 Sep 10;329(5997):1345–8.

177. Cohen S, Roy J, Lachance S, Delisle JS, Marinier A, Busque L, et al. Hematopoietic stem cell transplantation using single UM171-expanded cord blood: a single-arm, phase 1–2 safety and feasibility study. *Lancet Haematol*. 2020 Feb;7(2):e134–45.
178. Vo L, Daley G. De novo generation of HSCs from somatic and pluripotent stem cell sources. *Blood*. 2015;125(17):2641–8.
179. Evans MJ, Kaufman MH. Establishment in culture of pluripotential cells from mouse embryos. *Nature*. 1981 Jul;292(5819):154–6.
180. Thomson JA, Itskovitz-Eldor J, Shapiro SS, Waknitz MA, Swiergiel JJ, Marshall VS, et al. Embryonic Stem Cell Lines Derived from Human Blastocysts. *Science* (1979). 1998 Nov 6;282(5391):1145–7.
181. Takahashi K, Yamanaka S. Induction of Pluripotent Stem Cells from Mouse Embryonic and Adult Fibroblast Cultures by Defined Factors. *Cell*. 2006;126(4):663–76.
182. Sturgeon CM, Ditadi A, Awong G, Kennedy M, Keller G. Wnt signaling controls the specification of definitive and primitive hematopoiesis from human pluripotent stem cells. *Nat Biotechnol*. 2014 Jun 18;32(6):554–61.
183. Kennedy M, Awong G, Sturgeon CM, Ditadi A, LaMotte-Mohs R, Zúñiga-Pflücker JC, et al. T Lymphocyte Potential Marks the Emergence of Definitive Hematopoietic Progenitors in Human Pluripotent Stem Cell Differentiation Cultures. *Cell Rep*. 2012 Dec;2(6):1722–35.
184. Choi KD, Vodyanik MA, Togarrati PP, Suknuntha K, Kumar A, Samarjeet F, et al. Identification of the Hemogenic Endothelial Progenitor and Its Direct Precursor in Human Pluripotent Stem Cell Differentiation Cultures. *Cell Rep*. 2012 Sep;2(3):553–67.
185. Rafii S, Kloss CC, Butler JM, Ginsberg M, Gars E, Lis R, et al. Human ESC-derived hemogenic endothelial cells undergo distinct waves of endothelial to hematopoietic transition. *Blood*. 2013;121(5):770–81.
186. Ran D, Shia WJ, Lo MC, Fan JB, Knorr DA, Ferrell PI, et al. RUNX1a enhances hematopoietic lineage commitment from human embryonic stem cells and inducible pluripotent stem cells. *Blood*. 2013 Apr 11;121(15):2882–90.
187. Elcheva I, Brok-Volchanskaya V, Kumar A, Liu P, Lee JH, Tong L, et al. Direct induction of haematoendothelial programs in human pluripotent stem cells by transcriptional regulators. *Nat Commun*. 2014 Jul 14;5(1):4372.
188. Doulatov S, Vo LT, Chou SS, Kim PG, Arora N, Li H, et al. Induction of Multipotential Hematopoietic Progenitors from Human Pluripotent Stem Cells via Respecification of Lineage-Restricted Precursors. *Cell Stem Cell*. 2013 Oct;13(4):459–70.
189. Tan YT, Ye L, Xie F, Beyer AI, Muench MO, Wang J, et al. Respecifying human iPSC-derived blood cells into highly engraftable hematopoietic stem and progenitor cells with a single factor. *Proceedings of the National Academy of Sciences*. 2018 Feb 27;115(9):2180–5.

190. Sugimura R, Jha DK, Han A, Soria-Valles C, da Rocha EL, Lu YF, et al. Haematopoietic stem and progenitor cells from human pluripotent stem cells. *Nature*. 2017 May 25;545(7655):432–8.
191. Allis CD, Jenuwein T. The molecular hallmarks of epigenetic control. *Nat Rev Genet*. 2016;17(8):487–500.
192. Goldberg AD, Allis CD, Bernstein E. Epigenetics: A Landscape Takes Shape. *Cell*. 2007;128(4):635–8.
193. Ladewig J, Koch P, Brüstle O. Leveling Waddington: The emergence of direct programming and the loss of cell fate hierarchies. *Nat Rev Mol Cell Biol*. 2013;14(4):225–36.
194. Waddington CH. *The Strategy of genes*. Allen G, Unwin LTD, editors. The strategy of genes. 1957.
195. Gurdon JB. Adult frogs derived from the nuclei of single somatic cells. *Dev Biol*. 1962;4(2):256–73.
196. Gurdon JB. The Developmental Capacity of Nuclei taken from Intestinal Epithelium Cells of Feeding Tadpoles. *Development*. 1962 Dec 1;10(4):622–40.
197. Gurdon JB, Elsdale TR, Fischberg M. Sexually mature individuals of *Xenopus laevis* from the transplantation of single somatic nuclei. *Nature*. 1958;182:64–5.
198. Wakayama T, Perry ACF, Zuccotti M, Johnson KR, Yanagimachi R. Full-term development of mice from enucleated oocytes injected with cumulus cell nuclei. *Nature*. 1998;394(6691):369–74.
199. Wilmut I, Schnieke AE, McWhir J, Kind AJ, Campbell KH. Viable offspring derived from fetal and adult mammalian cells. Vol. 385, *Nature*. 1997. p. 810–3.
200. Blau HM, Chiu CP, Webster C. Cytoplasmic activation of human nuclear genes in stable heterocaryons. *Cell*. 1983;32(4):1171–80.
201. Tada M, Takahama Y, Abe K, Nakatsuji N, Tada T. Nuclear reprogramming of somatic cells by in vitro hybridization with ES cells. *Current Biology*. 2001;11(19):1553–8.
202. Cowan CA, Atienza J, Melton DA, Eggan K. Nuclear Reprogramming of Somatic Cells after Fusion with Human Embryonic Stem Cells. *Science* (1979). 2005;309(5739):1369–73.
203. Pereira CF, Terranova R, Ryan NK, Santos J, Morris KJ, Cui W, et al. Heterokaryon-based reprogramming of human B lymphocytes for pluripotency requires Oct4 but not Sox2. *PLoS Genet*. 2008;4(9).
204. Egli D, Birkhoff G, Eggan K. Mediators of reprogramming: Transcription factors and transitions through mitosis. *Nat Rev Mol Cell Biol*. 2008;9(7):505–16.
205. Takahashi K, Tanabe K, Ohnuki M, Narita M, Ichisaka T, Tomoda K. Induction of Pluripotent Stem Cells from Adult Human Fibroblasts by Defined Factors. *Cell*. 2007;131(5):861–72.
206. Davis RL, Weintraub H, Lassar AB. Expression of a single transfected cDNA converts fibroblasts to myoblasts. *Cell*. 1987 Dec 24;51(6):987–1000.
207. Wang H, Yang Y, Liu J, Qian L. Direct cell reprogramming: approaches, mechanisms and progress. *Nat Rev Mol Cell Biol*. 2021 Jun;22(6):410–24.

208. Ieda M, Fu J dong, Delgado-Olguin P, Vedantham V, Hayashi Y, Bruneau BG, et al. Direct Reprogramming of Fibroblasts into Functional Cardiomyocytes by Defined Factors. *Cell*. 2010;142(3):375–86.
209. Inagawa K, Miyamoto K, Yamakawa H, Muraoka N, Sadahiro T, Umei T, et al. Induction of cardiomyocyte-like cells in infarct hearts by gene transfer of Gata4, Mef2c, and Tbx5. *Circ Res*. 2012;111(9):1147–56.
210. Qian L, Huang Y, Spencer CI, Foley A, Vedantham V, Liu L, et al. In vivo reprogramming of murine cardiac fibroblasts into induced cardiomyocytes. *Nature*. 2012;485:593–8.
211. Song K, Nam YJ, Luo X, Qi X, Tan W, Huang GN, et al. Heart repair by reprogramming non-myocytes with cardiac transcription factors. *Nature*. 2012;485(7400):599–604.
212. Sekiya S, Suzuki A. Direct conversion of mouse fibroblasts to hepatocyte-like cells by defined factors. *Nature*. 2011;475(7356):390–5.
213. Huang P, He Z, Ji S, Sun H, Xiang D, Liu C, et al. Induction of functional hepatocyte-like cells from mouse fibroblasts by defined factors. *Nature*. 2011;475(7356):386–9.
214. Zhou Q, Brown J, Kanarek A, Rajagopal J, Melton DA. In vivo reprogramming of adult pancreatic exocrine cells to  $\beta$ -cells. *Nature*. 2008;455(7213).
215. Guo Z, Zhang L, Wu Z, Chen Y, Wang F, Chen G. In vivo direct reprogramming of reactive glial cells into functional neurons after brain injury and in an Alzheimer's disease model. *Cell Stem Cell*. 2014;14(2).
216. Vierbuchen T, Ostermeier A, Pang ZP, Kokubu Y, Südhof TC, Wernig M. Direct conversion of fibroblasts to functional neurons by defined factors. *Nature*. 2010 Feb 25;463(7284):1035–41.
217. Pfisterer U, Kirkeby A, Torper O, Wood J, Nelander J, Dufour A, et al. Direct conversion of human fibroblasts to dopaminergic neurons. *Proc Natl Acad Sci U S A*. 2011;108(25).
218. Torper O, Pfisterer U, Wolf DA, Pereira M, Lau S, Jakobsson J, et al. Generation of induced neurons via direct conversion in vivo. *Proceedings of the National Academy of Sciences*. 2013 Apr 23;110(17):7038–43.
219. Caiazzo M, Dell'Anno MT, Dvoretzkova E, Lazarevic D, Taverna S, Leo D, et al. Direct generation of functional dopaminergic neurons from mouse and human fibroblasts. *Vol. 476, Nature*. 2011.
220. Liu X, Li F, Stubblefield EA, Blanchard B, Richards TL, Larson GA, et al. Direct reprogramming of human fibroblasts into dopaminergic neuron-like cells. *Cell Res*. 2012;22(2):321–32.
221. Son EY, Ichida JK, Wainger BJ, Toma JS, Rafuse VF, Woolf CJ, et al. Conversion of mouse and human fibroblasts into functional spinal motor neurons. *Cell Stem Cell*. 2011;9(3):205–18.
222. Ring KL, Tong LM, Balestra ME, Javier R, Andrews-Zwilling Y, Li G, et al. Direct reprogramming of mouse and human fibroblasts into multipotent neural stem cells with a single factor. *Cell Stem Cell*. 2012;11(1):100–9.

223. Niu W, Zang T, Zou Y, Fang S, Smith DK, Bachoo R, et al. In vivo reprogramming of astrocytes to neuroblasts in the adult brain. *Nat Cell Biol.* 2013;15(9).
224. Corti S, Nizzardo M, Simone C, Falcone M, Donadoni C, Salani S, et al. Direct reprogramming of human astrocytes into neural stem cells and neurons. *Exp Cell Res.* 2012;318(13).
225. Kim Y, Jeong J, Choi D. Small-molecule-mediated reprogramming: a silver lining for regenerative medicine. *Exp Mol Med.* 2020 Feb 20;52(2):213–26.
226. Li X, Zuo X, Jing J, Ma Y, Wang J, Liu D, et al. Small-Molecule-Driven Direct Reprogramming of Mouse Fibroblasts into Functional Neurons. *Cell Stem Cell.* 2015 Aug;17(2):195–203.
227. Dai P, Harada Y, Takamatsu T. Highly efficient direct conversion of human fibroblasts to neuronal cells by chemical compounds. *J Clin Biochem Nutr.* 2015;56(3):166–70.
228. Wang Y, Yang H, Yang Q, Yang J, Wang H, Xu H, et al. Chemical conversion of mouse fibroblasts into functional dopaminergic neurons. *Exp Cell Res.* 2016 Oct;347(2):283–92.
229. Cao N, Huang Y, Zheng J, Spencer CI, Zhang Y, Fu JD, et al. Conversion of human fibroblasts into functional cardiomyocytes by small molecules. *Science (1979).* 2016 Jun 3;352(6290):1216–20.
230. Park G, Yoon BS, Kim YS, Choi SC, Moon JH, Kwon S, et al. Conversion of mouse fibroblasts into cardiomyocyte-like cells using small molecule treatments. *Biomaterials.* 2015 Jun;54:201–12.
231. Wei C, Yu P, Cheng L. Hematopoietic Reprogramming Entangles with Hematopoiesis. *Trends Cell Biol.* 2020 Oct;30(10):752–63.
232. Kulesa H, Frampton J, Graf T. GATA-1 reprograms avian myelomonocytic cell lines into eosinophils, thromboblats, and erythroblasts. *Genes Dev.* 1995;9(10).
233. Heyworth C, Pearson S, May G, Enver T. Transcription factor-mediated lineage switching reveals plasticity in primary committed progenitor cells. *EMBO Journal.* 2002;21(14).
234. Iwasaki H, Mizuno SI, Wells RA, Cantor AB, Watanabe S, Akashi K. GATA-1 converts lymphoid and myelomonocytic progenitors into the megakaryocyte/erythrocyte lineages. *Immunity.* 2003;19(3).
235. Sadahira K, Fukuchi Y, Kunimono H, Sakurai M, Ikeda Y, Okamoto S, et al. Direct reprogramming of terminally differentiated B cells into erythroid lineage. *FEBS Lett.* 2012;586(20):3645–52.
236. Capellera-Garcia S, Pulecio J, Dhulipala K, Siva K, Rayon-Estrada V, Singbrant S, et al. Defining the Minimal Factors Required for Erythropoiesis through Direct Lineage Conversion. *Cell Rep.* 2016;15(11):2550–62.
237. Pulecio J, Alejo-Valle O, Capellera-Garcia S, Vitaloni M, Rio P, Mejía-Ramírez E, et al. Direct Conversion of Fibroblasts to Megakaryocyte Progenitors. *Cell Rep.* 2016;17(3):671–83.



238. Pires CF, Rosa FF, Kurochkin I, Pereira CF. Understanding and Modulating Immunity With Cell Reprogramming. *Front Immunol.* 2019;10(December):1–24.
239. Bussmann LH, Schubert A, Phong T, Manh V, Andres L De, Desbordes SC, et al. A Robust and Highly Efficient Immune Cell Reprogramming System. *Cell Stem Cell.* 2009;5(5):554–66.
240. Laiosa C V., Stadtfeld M, Xie H, de Andres-Aguayo L, Graf T. Reprogramming of Committed T Cell Progenitors to Macrophages and Dendritic Cells by C/EBP $\alpha$  and PU.1 Transcription Factors. *Immunity.* 2006;25(5).
241. Feng R, Desbordes SC, Xie H, Tillo ES, Pixley F, Stanley ER, et al. PU.1 and C/EBP $\alpha$  /beta convert fibroblasts into macrophage-like cells. *PNAS.* 2008;105(16).
242. Rosa FF, Pires CF, Kurochkin I, Halitzki E, Zahan T, Arh N, et al. Single-cell transcriptional profiling informs efficient reprogramming of human somatic cells to cross-presenting dendritic cells. *Sci Immunol.* 2022 Mar;7(69):1–18.
243. Rosa FF, Pires CF, Kurochkin I, Ferreira AG, Gomes AM, Palma LG, et al. Direct reprogramming of fibroblasts into antigen-presenting dendritic cells. *Sci Immunol.* 2018;3(30):eaau4292.
244. Zimmermannova O, Ferreira AG, Ascic E, Velasco Santiago M, Kurochkin I, Hansen M, et al. Restoring tumor immunogenicity with dendritic cell reprogramming. *Sci Immunol.* 2023 Jul 14;8(85).
245. Pereira CF, Chang B, Qiu J, Niu X, Papatsenko D, Hendry CE, et al. Induction of a Hemogenic Program in Mouse Fibroblasts. *Cell Stem Cell.* 2013;13(2):205–18.
246. Gomes AM, Kurochkin I, Chang B, Daniel M, Law K, Satija N, et al. Cooperative Transcription Factor Induction Mediates Hemogenic Reprogramming. *Cell Rep.* 2018;25(10):2821–35.
247. Kania G, Corbeil D, Fuchs J, Tarasov K V., Blyszczuk P, Huttner WB, et al. Somatic Stem Cell Marker Prominin-1/CD133 Is Expressed in Embryonic Stem Cell–Derived Progenitors. *Stem Cells.* 2005 Jun 2;23(6):791–804.
248. Holmes C, Stanford WL. Concise Review: Stem Cell Antigen-1: Expression, Function, and Enigma. *Stem Cells.* 2007 Jun 1;25(6):1339–47.
249. Pereira CF, Chang B, Gomes A, Bernitz J, Papatsenko D, Niu X, et al. Hematopoietic Reprogramming In Vitro Informs In Vivo Identification of Hemogenic Precursors to Definitive Hematopoietic Stem Cells. *Dev Cell.* 2016;36(5):525–39.
250. Solaimani Kartalaei P, Yamada-Inagawa T, Vink CS, de Pater E, van der Linden R, Marks-Bluth J, et al. Whole-transcriptome analysis of endothelial to hematopoietic stem cell transition reveals a requirement for Gpr56 in HSC generation. *Journal of Experimental Medicine.* 2015 Jan 12;212(1):93–106.
251. Batta K, Florkowska M, Kouskoff V, Lacaud G. Direct Reprogramming of Murine Fibroblasts to Hematopoietic Progenitor Cells. *Cell Rep.* 2014;9(5):1871–84.
252. Cheng H, Ang HYK, A. EL Farran C, Li P, Fang HT, Liu TM, et al. Reprogramming mouse fibroblasts into engraftable myeloerythroid and lymphoid progenitors. *Nat Commun.* 2016;7(13396):1–15.

253. Riddell J, Gazit R, Garrison BS, Guo G, Saadatpour A, Mandal PK, et al. Reprogramming committed murine blood cells to induced hematopoietic stem cells with defined factors. *Cell*. 2014;157(3):549–64.
254. Sandler V, Lis R, Liu Y, Kedem A, James D, Elemento O, et al. Reprogramming human endothelial cells to haematopoietic cells requires vascular induction. *Nature*. 2014;511(7509):312–8.
255. Lis R, Karrasch CC, Poulos MG, Kunar B, Redmond D, Duran JGB, et al. Conversion of adult endothelium to immunocompetent haematopoietic stem cells. *Nature*. 2017;545(7655):439–45.
256. Ishino Y, Shinagawa H, Makino K, Amemura M, Nakata A. Nucleotide sequence of the *iap* gene, responsible for alkaline phosphatase isozyme conversion in *Escherichia coli*, and identification of the gene product. *J Bacteriol*. 1987 Dec;169(12):5429–33.
257. Mojica FJM, Díez-Villasenor C, Soria E, Juez G. Biological significance of a family of regularly spaced repeats in the genomes of Archaea, Bacteria and mitochondria. *Mol Microbiol*. 2000 Apr;36(1):244–6.
258. Jansen Ruud, Embden JanDA van, Gaastra Wim, Schouls LeoM. Identification of genes that are associated with DNA repeats in prokaryotes. *Mol Microbiol*. 2002 Mar;43(6):1565–75.
259. Garneau JE, Dupuis MÈ, Villion M, Romero DA, Barrangou R, Boyaval P, et al. The CRISPR/Cas bacterial immune system cleaves bacteriophage and plasmid DNA. *Nature*. 2010 Nov 4;468(7320):67–71.
260. Brouns SJJ, Jore MM, Lundgren M, Westra ER, Slijkhuis RJH, Snijders APL, et al. Small CRISPR RNAs guide antiviral defense in prokaryotes. *Science* (1979). 2008;321(5891).
261. Barrangou R, Fremaux C, Deveau H, Richards M, Boyaval P, Moineau S, et al. CRISPR Provides Acquired Resistance Against Viruses in Prokaryotes. *Science* (1979). 2007 Mar 23;315(5819):1709–12.
262. Jinek M, Chylinski K, Fonfara I, Hauer M, Doudna JA, Charpentier E. A Programmable Dual-RNA–Guided DNA Endonuclease in Adaptive Bacterial Immunity. *Science* (1979). 2012 Aug 17;337(6096):816–21.
263. Gasiunas G, Barrangou R, Horvath P, Siksnyš V. Cas9–crRNA ribonucleoprotein complex mediates specific DNA cleavage for adaptive immunity in bacteria. *Proceedings of the National Academy of Sciences*. 2012 Sep 25;109(39).
264. Sapranauškas R, Gasiunas G, Fremaux C, Barrangou R, Horvath P, Siksnyš V. The *Streptococcus thermophilus* CRISPR/Cas system provides immunity in *Escherichia coli*. *Nucleic Acids Res*. 2011 Nov;39(21):9275–82.
265. Mojica FJM, Díez-Villaseñor C, García-Martínez J, Almendros C. Short motif sequences determine the targets of the prokaryotic CRISPR defence system. *Microbiology (N Y)*. 2009 Mar 1;155(3):733–40.
266. Le Rhun A, Escalera-Maurer A, Bratovič M, Charpentier E. CRISPR-Cas in *Streptococcus pyogenes*. *RNA Biol*. 2019 Apr 3;16(4):380–9.

267. Anders C, Niewoehner O, Duerst A, Jinek M. Structural basis of PAM-dependent target DNA recognition by the Cas9 endonuclease. *Nature*. 2014 Sep 27;513(7519):569–73.
268. Xue C, Greene EC. DNA Repair Pathway Choices in CRISPR-Cas9-Mediated Genome Editing. *Trends in Genetics*. 2021 Jul;37(7):639–56.
269. Chang HHY, Pannunzio NR, Adachi N, Lieber MR. Non-homologous DNA end joining and alternative pathways to double-strand break repair. *Nat Rev Mol Cell Biol*. 2017 Aug 17;18(8):495–506.
270. Jeggo PA. DNA Breakage and Repair. In: *Advances in Genetics*. 1998. p. 185–218.
271. Sung P, Klein H. Mechanism of homologous recombination: mediators and helicases take on regulatory functions. *Nat Rev Mol Cell Biol*. 2006 Oct 1;7(10):739–50.
272. Hsu PD, Lander ES, Zhang F. Development and Applications of CRISPR-Cas9 for Genome Engineering. *Cell*. 2014 Jun;157(6):1262–78.
273. Wang H, Yang H, Shivalila CS, Dawlaty MM, Cheng AW, Zhang F, et al. One-Step Generation of Mice Carrying Mutations in Multiple Genes by CRISPR/Cas-Mediated Genome Engineering. *Cell*. 2013 May;153(4):910–8.
274. Yang W, Tu Z, Sun Q, Li XJ. CRISPR/Cas9: Implications for Modeling and Therapy of Neurodegenerative Diseases. *Front Mol Neurosci*. 2016 Apr 28;9(APR).
275. Cong L, Ran FA, Cox D, Lin S, Barretto R, Habib N, et al. Multiplex Genome Engineering Using CRISPR/Cas Systems. *Science (1979)*. 2013 Feb 15;339(6121):819–23.
276. Platt RJ, Chen S, Zhou Y, Yim MJ, Swiech L, Kempton HR, et al. CRISPR-Cas9 Knockin Mice for Genome Editing and Cancer Modeling. *Cell*. 2014 Oct;159(2):440–55.
277. Mulligan RC. The basic science of gene therapy. *Science (1979)*. 1993;260(5110).
278. Frangoul H, Altshuler D, Cappellini MD, Chen YS, Domm J, Eustace BK, et al. CRISPR-Cas9 Gene Editing for Sickle Cell Disease and  $\beta$ -Thalassemia. *Obstet Gynecol Surv*. 2021 Jun;76(6):327–9.
279. Dever DP, Bak RO, Reinisch A, Camarena J, Washington G, Nicolas CE, et al. CRISPR/Cas9  $\beta$ -globin gene targeting in human haematopoietic stem cells. *Nature*. 2016 Nov 17;539(7629):384–9.
280. Lattanzi A, Camarena J, Lahiri P, Segal H, Srifa W, Vakulskas CA, et al. Development of  $\beta$ -globin gene correction in human hematopoietic stem cells as a potential durable treatment for sickle cell disease. *Sci Transl Med*. 2021 Jun 16;13(598).
281. Leibowitz ML, Papatnasiou S, Doerfler PA, Blaine LJ, Sun L, Yao Y, et al. Chromothripsis as an on-target consequence of CRISPR–Cas9 genome editing. *Nat Genet*. 2021 Jun 12;53(6):895–905.

282. Shalem O, Sanjana NE, Hartenian E, Shi X, Scott DA, Mikkelsen TS, et al. Genome-Scale CRISPR-Cas9 Knockout Screening in Human Cells. *Science* (1979). 2014 Jan 3;343(6166):84–7.
283. Wang T, Wei JJ, Sabatini DM, Lander ES. Genetic Screens in Human Cells Using the CRISPR-Cas9 System. *Science* (1979). 2014 Jan 3;343(6166):80–4.
284. Shifrut E, Carnevale J, Tobin V, Roth TL, Woo JM, Bui CT, et al. Genome-wide CRISPR Screens in Primary Human T Cells Reveal Key Regulators of Immune Function. *Cell*. 2018 Dec;175(7):1958-1971.e15.
285. Parnas O, Jovanovic M, Eisenhaure TM, Herbst RH, Dixit A, Ye CJ, et al. A Genome-wide CRISPR Screen in Primary Immune Cells to Dissect Regulatory Networks. *Cell*. 2015 Jul;162(3):675–86.
286. Lin S, Larrue C, Scheidegger NK, Seong BKA, Dharia N V, Kuljanin M, et al. An In Vivo CRISPR Screening Platform for Prioritizing Therapeutic Targets in AML. *Cancer Discov*. 2022 Feb;12(2):432–49.
287. Yudovich D, Bäckström A, Schmiderer L, Žemaitis K, Subramaniam A, Larsson J. Combined lentiviral- and RNA-mediated CRISPR/Cas9 delivery for efficient and traceable gene editing in human hematopoietic stem and progenitor cells. *Sci Rep*. 2020 Dec;10(1):1–11.
288. Bäckström A, Yudovich D, Žemaitis K, Nilsén Falek L, Subramaniam A, Larsson J. Combinatorial gene targeting in primary human hematopoietic stem and progenitor cells. *Sci Rep*. 2022 Oct 28;12(1):18169.
289. Yu JSL, Palano G, Lim C, Moggio A, Drowley L, Plowright AT, et al. CRISPR-Knockout Screen Identifies Dmap1 as a Regulator of Chemically Induced Reprogramming and Differentiation of Cardiac Progenitors. *Stem Cells*. 2019 Jul 1;37(7):958–72.
290. Kaemena DF, Yoshihara M, Beniazza M, Ashmore J, Zhao S, Bertenstam M, et al. B1 SINE-binding ZFP266 impedes mouse iPSC generation through suppression of chromatin opening mediated by reprogramming factors. *Nat Commun*. 2023;14(1).
291. Ito K, Zaret KS. Maintaining Transcriptional Specificity Through Mitosis. *Annu Rev Genomics Hum Genet*. 2022 Aug 31;23(1):53–71.
292. Soares MAF, Oliveira RA, Castro DS. Function and regulation of transcription factors during mitosis-to-G1 transition. *Open Biol*. 2022 Jun;12(6):1–11.
293. Prescott DM, Bender MA. Synthesis of RNA and protein during mitosis in mammalian tissue culture cells. *Exp Cell Res*. 1962;26(2):260–8.
294. Martínez-Balbás MA, Dey A, Rabindran SK, Ozato K, Wu C. Displacement of sequence-specific transcription factors from mitotic chromatin. *Cell*. 1995;83(1):29–38.
295. Terasaki M, Campagnola P, Rolls MM, Stein PA, Ellenberg J, Hinkle B, et al. A new model for nuclear envelope breakdown. *Mol Biol Cell*. 2001;12(2):503–10.
296. Palozola KC, Donahue G, Liu H, Grant GR, Becker JS, Cote A, et al. Mitotic transcription and waves of gene reactivation during mitotic exit. *Science* (1979). 2017;358(6359):119–22.
297. Wigler M. The somatic replication of DNA methylation. *Cell*. 1981;24(1):33–40.

298. Bird A. DNA methylation patterns and epigenetic memory. *Genes Dev.* 2002 Jan 1;16(1):6–21.
299. Xing H, Wilkerson D, Mayhew C, Lubert E, Skaggs H, Goodson M, et al. Mechanism of hsp70i Gene Bookmarking. *Science* (1979). 2005;307(5708):421–3.
300. Sarge KD, Park-Sarge OK. Gene bookmarking: keeping the pages open. *Trends Biochem Sci.* 2005;30(11):9–14.
301. Festuccia N, Gonzalez I, Owens N, Navarro P. Mitotic bookmarking in development and stem cells. *Development.* 2017;144(20):3633–45.
302. Raccaud M, Friman ET, Alber AB, Agarwal H, Deluz C, Kuhn T, et al. Mitotic chromosome binding predicts transcription factor properties in interphase. *Nat Commun.* 2019;10(1):1–16.
303. Liu Y, Pelham-Webb B, Di Giammartino DC, Li J, Kim D, Kita K, et al. Widespread Mitotic Bookmarking by Histone Marks and Transcription Factors in Pluripotent Stem Cells. *Cell Rep.* 2017;19(7):1283–93.
304. Javasky E, Shamir I, Gandhi S, Egri S, Sandler O, Rothbart SB, et al. Study of mitotic chromatin supports a model of bookmarking by histone modifications and reveals nucleosome deposition patterns. *Genome Res.* 2018 Oct;28(10):1455–66.
305. Davey CA, Sargent DF, Luger K, Maeder AW, Richmond TJ. Solvent Mediated Interactions in the Structure of the Nucleosome Core Particle at 1.9Å Resolution. *J Mol Biol.* 2002 Jun;319(5):1097–113.
306. Luger K, Mäder AW, Richmond RK, Sargent DF, Richmond TJ. Crystal structure of the nucleosome core particle at 2.8 Å resolution. *Nature.* 1997 Sep;389(6648):251–60.
307. Valis E, Sánchez-Molina S, Martínez-Balbás MA. Role of histone modifications in marking and activating genes through mitosis. *Journal of Biological Chemistry.* 2005;280(52):42592–600.
308. Wang F, Higgins JMG. Histone modifications and mitosis: countermarks, landmarks, and bookmarks. *Trends Cell Biol.* 2013 Apr;23(4):175–84.
309. Soares MAF, Soares DS, Teixeira V, Heskol A, Bressan RB, Pollard SM, et al. Hierarchical reactivation of transcription during mitosis-to-G1 transition by Brn2 and Ascl1 in neural stem cells. *Genes Dev.* 2021;35(13):1020–34.
310. Raccaud M, Suter DM. Transcription factor retention on mitotic chromosomes: regulatory mechanisms and impact on cell fate decisions. *FEBS Lett.* 2017;592(6):878–87.
311. Kadauke S, Udugama MI, Pawlicki JM, Achtman JC, Jain DP, Cheng Y, et al. Tissue-specific mitotic bookmarking by hematopoietic transcription factor GATA1. *Cell.* 2012;150(4):725–37.
312. Caravaca JM, Donahue G, Becker JS, He X, Vinson C, Zaret KS. Bookmarking by specific and nonspecific binding of FoxA1 pioneer factor to mitotic chromosomes. *Genes Dev.* 2013;27(3):251–60.
313. Yang Z, He N, Zhou Q. Brd4 Recruits P-TEFb to Chromosomes at Late Mitosis To Promote G1 Gene Expression and Cell Cycle Progression. *Mol Cell Biol.* 2008;28(3):967–76.

314. Young DW, Hassan MQ, Yang XQ, Galindo M, Javed A, Zaidi SK, et al. Mitotic retention of gene expression patterns by the cell fate-determining transcription factor Runx2. *PNAS*. 2007;104(9):3189–94.
315. Deluz C, Friman ET, Strebinger D, Benke A, Raccaud M, Callegari A, et al. A role for mitotic bookmarking of SOX2 in pluripotency and differentiation. *Genes Dev*. 2016;30(22):2538–50.
316. Festuccia N, Dubois A, Vandormael-Pourmin S, Tejada EG, Mouren A, Bessonnard S, et al. Mitotic binding of Esrrb marks key regulatory regions of the pluripotency network. *Nat Cell Biol*. 2016;18(11):1139–48.
317. Festuccia N, Owens N, Papadopoulou T, Gonzalez I, Tachtsidi A, Vandoermelpourin S, et al. Transcription factor activity and nucleosome organization in mitosis. *Genome Res*. 2019;29(2):250–60.
318. Privalov PL, Dragan AI, Crane-Robinson C. Interpreting protein/DNA interactions: distinguishing specific from non-specific and electrostatic from non-electrostatic components. *Nucleic Acids Res*. 2011 Apr 1;39(7):2483–91.
319. Suter DM. Transcription Factors and DNA Play Hide and Seek. *Trends Cell Biol*. 2020 Jun;30(6):491–500.
320. Phair RD, Misteli T. Kinetic modelling approaches to in vivo imaging. *Nat Rev Mol Cell Biol*. 2001 Dec;2(12):898–907.
321. Gebhardt JCM, Suter DM, Roy R, Zhao ZW, Chapman AR, Basu S, et al. Single-molecule imaging of transcription factor binding to DNA in live mammalian cells. *Nat Methods*. 2013 May 24;10(5):421–6.
322. Teves SS, An L, Hansen AS, Xie L, Darzacq X, Tjian R. A dynamic mode of mitotic bookmarking by transcription factors. *Elife*. 2016;5(22280):1–24.
323. Sekiya T, Muthurajan UM, Luger K, Tulin A V., Zaret KS. Nucleosome-binding affinity as a primary determinant of the nuclear mobility of the pioneer transcription factor FoxA. *Genes Dev*. 2009 Apr 1;23(7):804–9.
324. Djeghloul D, Patel B, Kramer H, Dimond A, Whilding C, Brown K, et al. Identifying proteins bound to native mitotic ESC chromosomes reveals chromatin repressors are important for compaction. *Nat Commun*. 2020 Dec;11(1):1–15.
325. Hsiung CCS, Morrissey CS, Udugama M, Frank CL, Keller CA, Baek S, et al. Genome accessibility is widely preserved and locally modulated during mitosis. *Genome Res*. 2015 Feb;25(2):213–25.
326. Loomis RJ, Naoe Y, Parker JB, Savic V, Bozovsky MR, Macfarlan T, et al. Chromatin Binding of SRp20 and ASF/SF2 and Dissociation from Mitotic Chromosomes Is Modulated by Histone H3 Serine 10 Phosphorylation. *Mol Cell*. 2009 Feb;33(4):450–61.
327. Campbell AE, Hsiung CCS, Blobel GA. Comparative analysis of mitosis-specific antibodies for bulk purification of mitotic populations by fluorescence-activated cell sorting. *Biotechniques*. 2014;56(2):90–4.
328. Fox MH, Read RA, Bedford JS. Comparison of synchronized Chinese hamster ovary cells obtained by mitotic shake-off, hydroxyurea, aphidicolin, or methotrexate. *Cytometry*. 1987 May;8(3):315–20.

329. Skene PJ, Henikoff S. An efficient targeted nuclease strategy for high-resolution mapping of DNA binding sites. *Elife*. 2017 Jan 16;6.
330. Oomen ME, Hansen AS, Liu Y, Darzacq X, Dekker J. CTCF sites display cell cycle-dependent dynamics in factor binding and nucleosome positioning. *Genome Res*. 2019 Feb;29(2):236–49.
331. Lim S, Kaldis P. Cdks, cyclins and CKIs: roles beyond cell cycle regulation. *Development*. 2013 Aug 1;140(15):3079–93.
332. King RW, Peters JM, Tugendreich S, Rolfe M, Hieter P, Kirschner MW. A 20s complex containing CDC27 and CDC16 catalyzes the mitosis-specific conjugation of ubiquitin to cyclin B. *Cell*. 1995 Apr;81(2):279–88.
333. Rosa FF, Pires CF, Kurochkin I, Ferreira AG, Gomes AM, Palma LG, et al. Direct reprogramming of fibroblasts into antigen-presenting dendritic cells. *Sci Immunol*. 2018;3(30):eaau4292.
334. Rosa FF, Pires CF, Kurochkin I, Halitzki E, Zahan T, Arh N, et al. Single-cell transcriptional profiling informs efficient reprogramming of human somatic cells to cross-presenting dendritic cells. *Sci Immunol*. 2022 Mar 4;7(69):1–18.
335. Lewis M, Prouzet-Mauléon V, Lichou F, Richard E, Iggo R, Turcq B, et al. A genome-scale CRISPR knock-out screen in chronic myeloid leukemia identifies novel drug resistance mechanisms along with intrinsic apoptosis and MAPK signaling. *Cancer Med*. 2020;9(18).
336. Doench JG, Hartenian E, Graham DB, Tothova Z, Hegde M, Smith I, et al. Rational design of highly active sgRNAs for CRISPR-Cas9-mediated gene inactivation. *Nat Biotechnol*. 2014;32(12).
337. Galeev R, Baudet A, Kumar P, Rundberg Nilsson A, Nilsson B, Soneji S, et al. Genome-wide RNAi Screen Identifies Cohesin Genes as Modifiers of Renewal and Differentiation in Human HSCs. *Cell Rep*. 2016 Mar;14(12):2988–3000.
338. Žemaitis K, Subramaniam A, Galeev R, Prosz A, Jassinskaja M, Hansson J, et al. RNAi Screen Identifies MTA1 as an Epigenetic Modifier of Differentiation Commitment in Human HSPCs. *Exp Hematol*. 2022 Nov;115:20–9.
339. Joung J, Konermann S, Gootenberg JS, Abudayyeh OO, Platt RJ, Brigham MD, et al. Genome-scale CRISPR-Cas9 knockout and transcriptional activation screening. *Nat Protoc*. 2017 Apr 23;12(4):828–63.
340. Cao H, Heazlewood SY, Williams B, Cardozo D, Nigro J, Oteiza A, et al. The role of CD44 in fetal and adult hematopoietic stem cell regulation. *Haematologica*. 2016 Jan 1;101(1):26–37.
341. Schreiber TD, Steinl C, Essl M, Abele H, Geiger K, Muller CA, et al. The integrin  $\alpha 9\beta 1$  on hematopoietic stem and progenitor cells: involvement in cell adhesion, proliferation and differentiation. *Haematologica*. 2009 Nov 1;94(11):1493–501.
342. Viny AD, Bowman RL, Liu Y, Lavallée VP, Eisman SE, Xiao W, et al. Cohesin Members Stag1 and Stag2 Display Distinct Roles in Chromatin Accessibility and Topological Control of HSC Self-Renewal and Differentiation. *Cell Stem Cell*. 2019;25(5).

343. De Koninck M, Lapi E, Badía-Careaga C, Cossío I, Giménez-Llorente D, Rodríguez-Corsino M, et al. Essential Roles of Cohesin STAG2 in Mouse Embryonic Development and Adult Tissue Homeostasis. *Cell Rep.* 2020;32(6).
344. Kazenwadel J, Betterman KL, Chong C eng, Stokes PH, Lee YK, Secker GA, et al. GATA2 is required for lymphatic vessel valve development and maintenance. *J Clin Invest.* 2015;125(8):2979–94.
345. Katsumura KR, Mehta C, Hewitt KJ, Soukup AA, Fraga de Andrade I, Ranheim EA, et al. Human leukemia mutations corrupt but do not abrogate GATA-2 function. *Proceedings of the National Academy of Sciences.* 2018 Oct;115(43):10109–18.
346. Chong CE, Venugopal P, Stokes PH, Lee YK, Brautigan PJ, Yeung DTO, et al. Differential effects on gene transcription and hematopoietic differentiation correlate with GATA2 mutant disease phenotypes. *Leukemia.* 2018;32(1):194–202.
347. Zhang S jiang, Ma L yuan, Huang Q hua, Li G, Gu B wei, Gao X dong, et al. Gain-of-function mutation of GATA-2 in acute myeloid transformation of chronic myeloid leukemia. *PNAS.* 2008;105(6):2076–81.
348. Vodyanik MA, Thomson JA, Slukvin II. Leukosialin (CD43) defines hematopoietic progenitors in human embryonic stem cell differentiation cultures. *Blood.* 2006 Sep 15;108(6):2095–105.
349. Bergiers I, Andrews T, Bölükbaşı ÖV, Buness A, Janosz E, Lopez-Anguina N, et al. Single-cell transcriptomics reveals a new dynamical function of transcription factors during embryonic hematopoiesis. *Elife.* 2018;7.
350. Cortés F, Debacker C, Péault B, Labastie MC. Differential expression of KDR/VEGFR-2 and CD34 during mesoderm development of the early human embryo. *Mech Dev.* 1999;83(1–2).
351. Hughes MR, Canals Hernaez D, Cait J, Refaeli I, Lo BC, Roskelley CD, et al. A sticky wicket: Defining molecular functions for CD34 in hematopoietic cells. *Exp Hematol.* 2020 Jun;86:1–14.
352. Cheng J, Baumhueter S, Cacalano G, Carver-Moore K, Thibodeaux H, Thomas R, et al. Hematopoietic defects in mice lacking the sialomucin CD34. *Blood.* 1996 Jan 15;87(2):479–90.
353. Ketharnathan S, Labudina A, Horsfield JA. Cohesin Components Stag1 and Stag2 Differentially Influence Haematopoietic Mesoderm Development in Zebrafish Embryos. *Front Cell Dev Biol.* 2020;8.
354. Möröy T, Vassen L, Wilkes B, Khandanpour C. From cytopenia to leukemia: The role of Gfi1 and Gfi1b in blood formation. *Blood.* 2015;126(24):2561–9.
355. Dovat S, Ronni T, Russell D, Ferrini R, Cobb BS, Smale ST. A common mechanism for mitotic inactivation of C2H2 zinc finger DNA-binding domains. *Genes Dev.* 2002;16(23):2985–90.
356. Angel P, Karin M. The role of Jun, Fos and the AP-1 complex in cell-proliferation and transformation. *Biochim Biophys Acta.* 1991;1072(2–3):129–57.



357. Chen Y, Bates DL, Dey R, Chen PH, Machado ACD, Laird-Offringa IA, et al. DNA Binding by GATA Transcription Factor Suggests Mechanisms of DNA Looping and Long-Range Gene Regulation. *Cell Rep.* 2012 Nov;2(5):1197–206.
358. Thomas SN, French D, Jannetto PJ, Rappold BA, Clarke WA. Liquid chromatography–tandem mass spectrometry for clinical diagnostics. *Nature Reviews Methods Primers.* 2022 Dec 8;2(1):96.
359. Gribble SM, Ng BL, Prigmore E, Fitzgerald T, Carter NP. Array painting: a protocol for the rapid analysis of aberrant chromosomes using DNA microarrays. *Nat Protoc.* 2009 Dec 5;4(12):1722–36.
360. Morris JH, Knudsen GM, Verschueren E, Johnson JR, Cimermancic P, Greninger AL, et al. Affinity purification–mass spectrometry and network analysis to understand protein-protein interactions. *Nat Protoc.* 2014 Nov 2;9(11):2539–54.
361. Soufi A, Donahue G, Zaret KS. Facilitators and impediments of the pluripotency reprogramming factors’ initial engagement with the genome. *Cell.* 2012;151(5):994–1004.
362. Kumar D, Cinghu S, Oldfield AJ, Yang P, Jothi R. Decoding the function of bivalent chromatin in development and cancer. *Genome Res.* 2021 Dec;31(12):2170–84.
363. Lamaa A, Humbert J, Aguirrebengoa M, Cheng X, Nicolas E, Côté J, et al. Integrated analysis of H2A.Z isoforms function reveals a complex interplay in gene regulation. *Elife.* 2020 Feb 28;9.
364. Hsiung CCS, Bartman CR, Huang P, Ginart P, Stonestrom AJ, Keller CA, et al. A hyperactive transcriptional state marks genome reactivation at the mitosis–G1 transition. *Genes Dev.* 2016 Jun 15;30(12):1423–39.
365. Soufi A, Dalton S. Cycling through developmental decisions: how cell cycle dynamics control pluripotency, differentiation and reprogramming. *Development.* 2016;143(23):4301–11.
366. Stavropoulou V, Almosailekh M, Royo H, Spetz JF, Juge S, Brault L, et al. A Novel Inducible Mouse Model of MLL-ENL-driven Mixed-lineage Acute Leukemia. *Hemasphere.* 2018 Aug;2(4):e51.



Paper I





Video Article

# Hemogenic Reprogramming of Human Fibroblasts by Enforced Expression of Transcription Factors

Rita Silvério-Alves<sup>1,2,3</sup>, Andreia M. Gomes<sup>3</sup>, Ilia Kurochkin<sup>4</sup>, Kateri A. Moore<sup>5,6</sup>, Carlos-Filipe Pereira<sup>1,2,3</sup>

<sup>1</sup>Molecular Medicine and Gene Therapy, Lund Stem Cell Center, Lund University

<sup>2</sup>Wallenberg Center for Molecular, Lund University

<sup>3</sup>Center for Neuroscience and Cell Biology, University of Coimbra

<sup>4</sup>Skolkovo Institute of Science and Technology

<sup>5</sup>Department of Cell, Developmental and Regenerative Biology, Icahn School of Medicine at Mount Sinai

<sup>6</sup>Black Family Stem Cell Institute, Icahn School of Medicine at Mount Sinai

Correspondence to: Carlos-Filipe Pereira at [filipe.pereira@med.lu.se](mailto:filipe.pereira@med.lu.se)

URL: <https://www.jove.com/video/60112>

DOI: [doi:10.3791/60112](https://doi.org/10.3791/60112)

Keywords: Developmental Biology, Issue 153, hemogenic reprogramming, fibroblast, transcription factors, hematopoiesis, hematopoietic stem and progenitor cells, endothelial-to-hematopoietic transition

Date Published: 11/4/2019

Citation: Silvério-Alves, R., Gomes, A.M., Kurochkin, I., Moore, K.A., Pereira, C.F. Hemogenic Reprogramming of Human Fibroblasts by Enforced Expression of Transcription Factors. *J. Vis. Exp.* (153), e60112, doi:10.3791/60112 (2019).

## Abstract

The cellular and molecular mechanisms underlying specification of human hematopoietic stem cells (HSCs) remain elusive. Strategies to recapitulate human HSC emergence *in vitro* are required to overcome limitations in studying this complex developmental process. Here, we describe a protocol to generate hematopoietic stem and progenitor-like cells from human dermal fibroblasts employing a direct cell reprogramming approach. These cells transit through a hemogenic intermediate cell-type, resembling the endothelial-to-hematopoietic transition (EHT) characteristic of HSC specification. Fibroblasts were reprogrammed to hemogenic cells via transduction with GATA2, GF11B and FOS transcription factors. This combination of three factors induced morphological changes, expression of hemogenic and hematopoietic markers and dynamic EHT transcriptional programs. Reprogrammed cells generate hematopoietic progeny and repopulate immunodeficient mice for three months. This protocol can be adapted towards the mechanistic dissection of the human EHT process as exemplified here by defining GATA2 targets during the early phases of reprogramming. Thus, human hemogenic reprogramming provides a simple and tractable approach to identify novel markers and regulators of human HSC emergence. In the future, faithful induction of hemogenic fate in fibroblasts may lead to the generation of patient-specific HSCs for transplantation.

## Video Link

The video component of this article can be found at <https://www.jove.com/video/60112/>

## Introduction

Definitive hematopoietic stem and progenitor cells (HSPCs) emerge in the aorta-gonad-mesonephros (AGM) region and placenta from endothelial precursors with hemogenic capacity, through an endothelial-to-hematopoietic transition (EHT)<sup>1,2</sup>. Hemogenic precursors (HPs) express both endothelial and hematopoietic markers, but their precise identification remains elusive, particularly in the human system. Despite being a relatively conserved process in mammals, hematopoietic stem cell (HSC) development still differs significantly between humans and mouse models<sup>3,4</sup>. Therefore, *in vitro* approaches to recapitulate human HSC development are needed.

Differentiation of pluripotent stem cells (PSCs) to HSCs, although promising, has met limited success over the past 20 years, mostly due to the available differentiation protocols, which result in primitive hematopoietic progenitors with poor engraftment ability<sup>5,6,7</sup>. Alternatively, direct cell reprogramming methodologies have been applied to generate HSPC-like cells from multiple cell types, using transcription factors (TFs)<sup>8,9</sup>. In particular, the overexpression of three TFs, Gata2, Gfi1b and cFos, converted mouse embryonic fibroblasts into HSPCs through an HP intermediate with a defined phenotype (Prom1+Sca-1+CD34+CD45-)<sup>10</sup>. This process resembled the EHT that occurs in the embryo and placenta, during specification of definitive hematopoiesis. This phenotype enabled the identification and isolation of a population of HPs in the mouse placenta that after short-term culture and Notch activation generated serially transplantable HSCs<sup>11</sup>.

So far, no phenotype has been established that distinguishes human HSCs from their precursors, but some molecules are known to be expressed in emerging HSCs. Integrin alpha 6 (ITGA6 or CD49f) is highly expressed in long-term repopulating HSCs, the most immature cells in the HSC compartment<sup>12</sup>, and angiotensin-converting enzyme (ACE or CD143) is present in CD34 negative hematopoietic precursors in embryonic blood-forming tissues<sup>13</sup>.

Recently, we have demonstrated that human versions of the three TFs, GATA2, FOS and GF11B reprogram human dermal fibroblasts (HDFs) into HPs with short-term engraftment capacity<sup>14</sup>. In the initial phases of reprogramming, GATA2 engages open chromatin and recruits GF11B

and FOS to repress fibroblast genes and activate endothelial and hematopoietic genes. Induced cells highly expressed CD49f and ACE, and contained a small percentage of cells expressing the HSPC marker CD34. The CD9 gene, which is expressed in HSCs<sup>15</sup> and is important for HSC homing<sup>16</sup>, was shown to be a direct target of GATA2 and among the most up-regulated genes in reprogrammed cells<sup>14</sup>. CD9 may therefore constitute an additional marker for HPs of human definitive hematopoiesis.

In this protocol, we describe the generation of HSPC-like cells from human fibroblasts through enforced expression of GATA2, GF11B and FOS, as well as an adapted method for chromatin immunoprecipitation (ChIP)-sequencing (seq) analysis at the onset of reprogramming. TFs were encoded in a doxycycline (DOX)-inducible lentiviral vector (pFUW-tetO) that contains a tetracycline response element (TRE) and a minimal CMV promoter, and were transduced together with a constitutive vector containing the reverse tetracycline transactivator protein (pFUW-M2rtTA). When DOX (analog of tetracycline) is added after transduction, it binds to the rtTA protein which interacts with the TRE allowing TF transcription (Tet-On system). The procedure requires 25 days to complete. For ChIP-seq experiments, HDFs were transduced with tagged versions of GATA2 (pFUW-tetO-3xFLAG-GATA2) and GF11B (pLV-tetO-HA-GF11B), plus pFUW-tetO-FOS and TF binding sites were analyzed two days after DOX supplementation.

Ultimately, homogenic reprogramming of human fibroblasts provides an *in vitro* tractable system to study the mechanisms underlying human developmental hematopoiesis and a potential source of patient-specific HSPCs for future clinical application.

## Protocol

This protocol was performed according to Lund University's human research ethics committee guidelines and should be done in accordance with individual institutional guidelines.

### 1. Reagent Preparation

1. For Dulbecco's modified Eagle's medium (DMEM)/20% fetal bovine serum (FBS), mix high glucose DMEM containing sodium pyruvate with 20% FBS, 1% penicillin-streptomycin (pen/strep), 1% L-glutamine, 1% non-essential amino acids and  $10^{-4}$ -M 2-mercaptoethanol.
2. For complete DMEM, mix high glucose DMEM containing sodium pyruvate with 10% FBS, 1% Pen/strep and 1% L-glutamine.
3. For hematopoietic medium, mix hematopoietic medium (**Table of Materials**) with  $10^{-6}$  M hydrocortisone and 1% pen/strep.
4. Use phosphate-buffered saline (PBS) without calcium or magnesium.

### 2. Human Dermal Fibroblast Isolation

**NOTE:** HDFs can be purchased from certified suppliers (**Table of Materials**). In that case, expand fibroblasts and use them directly in reprogramming experiments (section 4). Alternatively, HDFs can be isolated from donors. If fibroblasts are isolated from different donors, keep the samples separated from each other at all steps of the protocol. Label plates/wells and collection tubes with the identification number of each donor.

1. Obtain HDFs from 3 mm round skin punch biopsies performed by qualified physicians.
2. Coat three wells of a tissue culture-treated 6-well plate with 500  $\mu$ L of 0.1% gelatin and incubate for 20 min at 37  $^{\circ}$ C.
3. Aspirate the remaining gelatin solution and add 750  $\mu$ L of DMEM/20% FBS to each well. The entire surface of the well should be covered with medium.
4. Add 1.5 mL of DMEM/20% FBS to the inside surface of a sterile 100 mm petri dish lid and spread the drop with the aid of a 5 mL serological pipette.
5. Place the skin biopsy in the medium on the lid with sterilized forceps.
6. Dissect the skin biopsy into nine identical sections, using one sterilized scalpel to hold the biopsy in place and a second scalpel to cut.
7. Place three biopsy pieces per well using pointed forceps. Make sure the pieces attach to the bottom of the well.
8. Lay a 22 mm coverslip on top of the pieces and apply some pressure.
9. Incubate the plate at 37  $^{\circ}$ C, 5% CO<sub>2</sub>, for a week. Check cells daily and add 200  $\mu$ L of DMEM/20% FBS every 2 days to replace evaporated medium.
10. After one week, add up to 2 mL of DMEM/20% FBS and replace medium every 2–3 days.
11. **Passage cells at 1:4 ratio when wells are confluent (about 4–8 weeks).**
  1. Prepare 0.1% gelatin coated tissue culture-treated 6-well plates.
  2. Aspirate medium from wells at 80% confluency and wash once with 1 mL of PBS.
  3. Remove coverslip with sterile forceps and place the coverslip into a new well of a 6-well plate, with the tissue side up.
 

**NOTE:** Cells that remained attached to the coverslip will also be harvested.
  4. Add 500  $\mu$ L of dissociation solution (**Table of Materials**) per well (including wells with the coverslips) and incubate at 37  $^{\circ}$ C, 5% CO<sub>2</sub> for 5–10 min. Check when cells start to rise from the bottom of the well and inactivate the dissociation solution by adding 500  $\mu$ L of DMEM/20% FBS to each well.
  5. Collect fibroblasts from all the wells into a 15 mL conical tube. Add extra medium to the wells to collect the remaining cells. Centrifuge the tube at 350  $\times$  g for 5 min.
  6. In the meantime, add 500  $\mu$ L of DMEM/20% FBS to each well of previously gelatin coated plates.
  7. Aspirate medium and resuspend fibroblasts in 6 mL of DMEM/20% FBS.
  8. Add 500  $\mu$ L of fibroblast suspension to each well (two 6-well plates per sample/donor in total). Incubate cells overnight at 37  $^{\circ}$ C, 5% CO<sub>2</sub>.
12. On the next day, add 1 mL of DMEM/20% FBS to each well. Replace medium with 2 mL of DMEM/20% FBS every 2–3 days until wells are 80% confluent.
13. Repeat section 2.11 for three confluent wells until third passage is reached.

14. Freeze fibroblasts from confluent wells (passages 1 and 3).

1. Aspirate medium from the wells and wash once with 1 mL of PBS.
2. Dissociate and collect fibroblasts as described in steps 2.11.4 and 2.11.5.
3. Count cells with a hemocytometer and centrifuge the tube at 350 x g for 5 min.
4. After centrifugation, aspirate medium and resuspend fibroblasts in FBS with 10% DMSO at a density of 5 x 10<sup>5</sup> cells/mL.
5. Add 1 mL of the cell suspension per cryovial and freeze cells overnight at -80 °C using a freezing container. Move vials to -150 °C (liquid nitrogen) for long-term storage.

### 3. Lentiviral Production

1. Grow HEK293T cells in a 100 mm tissue culture-treated dish with 10 mL of complete DMEM, at 37 °C, 5% CO<sub>2</sub>, until confluency is reached.
2. On the day prior to transfection, aspirate medium and wash the dish carefully with 5 mL of PBS.
3. After removing PBS, add 1.5 mL of dissociation solution and incubate at 37 °C, 5% CO<sub>2</sub> for 5–10 min to dissociate cells from the dish.  
**NOTE:** It is recommended to warm both PBS and dissociation solution before using, so that cells do not suffer a thermal shock.
4. Inactivate dissociation solution with 3 mL of complete DMEM and transfer the cell suspension to a 15 mL conical tube. Wash the dish with 5 mL of complete DMEM to remove remaining attached cells and transfer this volume to the 15 mL conical tube.
5. Centrifuge cell suspension at 350 x g for 5 min.
6. Aspirate supernatant and split the cell pellet evenly between six 100 mm tissue culture-treated dishes in a final volume of 10 mL of complete DMEM per dish. Cells should be approximately 60% confluent by the time of transfection.
7. **On the next day, transfect cells with the plasmid mixes as follows:**  
**NOTE:** This part of the protocol describes the production of lentiviruses in one 100 mm tissue culture-treated dish per plasmid mix. To obtain higher volumes of lentiviral supernatant for concentration, use at least four 100 mm HEK293T cell culture dishes per mix.
  1. In a 15 mL conical tube, add 10 µg of the three transfer plasmids together: 3.33 µg of pFUW-tetO-GATA2 (Addgene #125028)<sup>14</sup>, 3.33 µg of pFUW-tetO-GF1B (Addgene #125597)<sup>14</sup> and 3.33 µg of pFUW-tetO-FOS (Addgene #125598)<sup>14</sup>, plus 10 µg of the 2<sup>nd</sup> generation psPAX2 packaging vector encoding the *Gag*, *Pol*, *Tat* and *Rev* genes (Addgene #12260) and 5 µg of pMD2.G envelope vector encoding the VSV-G gene (Addgene #12259). Add water up to 500 µL.
  2. In two new 15 mL conical tubes add 10 µg of FUW-M2rTA plasmid (Addgene #20342)<sup>17</sup>, 10 µg of psPAX2 packaging vector and 5 µg of pMD2.G envelope vector to each tube. Add water up to 500 µL. One tube is going to be used as a control.
  3. To each tube add 62.5 µL of 2 M CaCl<sub>2</sub>. Next, release bubbles into each mixture using a Pasteur pipet inserted into a pipet controller. While bubbles are forming, pipette 500 µL of *N,N*-bis(2-hydroxyethyl)-2-aminoethanesulfonic acid (BES) buffered saline (pH 7.1, 25 °C), with a P1000 pipette, drop-wise against the Pasteur pipet and onto the mixture.
  4. Incubate tubes at room temperature for at least 15 min. The mixtures will appear slightly cloudy after some time.
8. Meanwhile, aspirate medium from HEK293T cell dishes (passed the day before) and add 10 mL of complete DMEM without antibiotics. Be careful and add medium slowly as HEK293T cells are semi-adherent.
9. Distribute each individual mixture (approximately 1 mL) evenly and drop-wise into separate dishes and incubate overnight at 37 °C, 5% CO<sub>2</sub>.
10. Replace medium with 4 mL of complete DMEM, 24 h after incubation. Incubate overnight at 37 °C, 5% CO<sub>2</sub>. If available, incubate instead at 32 °C, 5% CO<sub>2</sub>, as the reduced temperature will increase the half-life of the lentiviral particles.
11. **Collect supernatant with lentiviral particles three times to a 50 mL conical tube. Do not mix different lentiviral particles at this point. Each dish will result in 12 mL of lentiviral supernatant. Four dishes of the same viral preparation fit into one 50 mL conical tube.**  
**CAUTION:** Perform lentiviral collection in a biosafety level-2 laboratory in a laminar flow hood dedicated for lentiviral work and place viral contaminated waste (tubes, tips, dishes) in an appropriate container for biohazardous materials.
  1. Do the first collection 16 h after the last incubation and add 4 mL of complete DMEM. Incubate at 37 °C, 5% CO<sub>2</sub>.
  2. Do the second collection 8 h after the first to the same tube, add 4 mL of complete DMEM and incubate at 37 °C, 5% CO<sub>2</sub>.
  3. Do the third collection 16 h after the second to the same tube and discard the dishes.  
**NOTE:** Store lentiviral supernatants at 4 °C after each collection.
12. Filter each lentiviral supernatant using a 0.45 µm low-protein binding filter with a cellulose acetate membrane (**Table of Materials**) to a clean tube.
13. Add a maximum of 15 mL of filtered supernatant to a centrifugal filter unit with a regenerated cellulose membrane (**Table of Materials**) and spin at 4,000 x g for 25 min, at 4 °C. Discard flow-through. A viscous liquid containing lentiviruses will remain in the filter unit.
14. Repeat step 3.13 by adding 15 mL of supernatant on top of the filter unit, until there is no more lentiviral supernatant left.  
**NOTE:** When there are only a few milliliters of supernatant to concentrate, decrease the spinning time to 10 min. If there is still extra liquid (non-viscous) on the filter, centrifuge for an additional 10 min.
15. Make aliquots (50–200 µL depending on the initial supernatant volume) of each type of concentrated lentiviruses and store at -80 °C for long-term storage (1–2 years) or at 4 °C for short-term storage (1–2 weeks).  
**NOTE:** Concentrated or non-concentrated lentiviruses can also be used fresh. Do not re-freeze and thaw as this results in reduced titer.

### 4. Hemogenic Reprogramming

**NOTE:** Use HDFs with a passage number of three (P3) or higher (until P10) to perform reprogramming experiments.

1. Coat a 100 mm tissue culture-treated dish with 5 mL of 0.1% gelatin and incubate at 37 °C for 20 min. Aspirate the remaining gelatin solution.
2. Thaw a fibroblast vial and plate cells in the 0.1% gelatin-coated dish. Incubate overnight at 37 °C, 5% CO<sub>2</sub>. If necessary, expand fibroblasts for a longer period of time until the desired passage and confluency are reached.
3. Coat a 6-well tissue culture-treated plate with 500 µL of 0.1% gelatin solution and incubate at 37 °C for 20 min. Remove extra gelatin.
4. Plate HDFs at a density of 150,000 cells per plate (25,000 cells per well) in 2 mL of complete DMEM per well. Incubate overnight at 37 °C, 5% CO<sub>2</sub>, to allow cell attachment.

5. Replace medium with 2 mL of complete DMEM plus 8 µg/mL polybrene. Prepare a 1:1 ratio mix of pool-produced TF lentiviruses and M2rtTA in a new microcentrifuge tube.  
**NOTE:** In this protocol, pool-production of lentiviruses for the three TFs is performed, which, in authors' hands, results in higher reprogramming efficiency. Alternatively, it is suggested to perform a titration of the individual lentiviral particles by qPCR<sup>18</sup>, on a standard cell line. This will be used to define the volume of individual viruses necessary to meet a multiplicity of infection (MOI) optimal for co-transduction and hemogenic reprogramming.
6. Distribute 10 to 100 µL of lentiviral mixture per well, to transduce HDFs. This is day -2 of reprogramming.  
**NOTE:** Defining the optimal volume of lentiviral mix for efficient reprogramming, without compromising cell viability, requires optimization (see **Supplementary Figure 1** for more details). HDFs with more than 7 passages may require higher volumes of viruses than cells with lower passages.
7. After 16 h of incubation, remove viruses and add complete DMEM. Allow cells to recover for 6–8 h.
8. After recovery, aspirate medium and add 2 mL of complete DMEM with 8 µg/mL polybrene.
9. Do a second transduction as described in step 4.6 and incubate at 37 °C, 5% CO<sub>2</sub> for 16 h. This is day -1 of reprogramming. The lentiviral mix can be prepared on day -2 for both transductions and kept at 4 °C.
10. On the next day, remove the viruses and add complete DMEM supplemented with 1 µg/mL DOX. This is day 0 of reprogramming. Incubate at 37 °C, 5% CO<sub>2</sub> for 48 h.
11. **At day 2 of reprogramming, split each well at 1:2 ratio.**
  1. Aspirate medium and wash cells with 1 mL of PBS.
  2. Aspirate PBS and dissociate cells with 500 µL of dissociation solution. Incubate 5–10 min at 37 °C, 5% CO<sub>2</sub>.
  3. Inactivate the dissociation solution with 1 mL of complete DMEM and collect cells into a conical tube. Centrifuge at 350 × g for 5 min.
  4. Resuspend the pellet in hematopoietic medium (see step 1.3), supplemented with 1 µg/mL DOX, and plate cells into new tissue culture-treated 6-well plates coated with 0.1% gelatin to a final volume of 2 mL per well.
12. Change medium (hematopoietic medium plus DOX) twice a week for the duration of the reprogramming cultures (25 days).
13. Analyze resulting reprogrammed cells at different time points by brightfield or fluorescence microscopy (see **Supplementary Figure 2**), flow cytometry, bulk and single-cell RNA sequencing, and transplantation assays for the acquisition of hematopoietic morphology, presence of endothelial and hematopoietic markers, acquisition of endothelial/hematopoietic gene expression profile and regeneration capacity<sup>14</sup>.

## 5. Optimization of Fibroblast Expansion for ChIP-seq Analysis at the Onset of Hemogenic Reprogramming

1. Plate 300,000 HDFs (<P8) in 0.1% gelatin coated tissue culture-treated 6-well plates with complete DMEM to a final volume of 2 mL per well. Incubate overnight at 37 °C, 5% CO<sub>2</sub>.
2. On the following day, replace medium with complete DMEM supplemented with 8 µg/mL polybrene.
3. Transduce cells with individual factors: pFUW-tetO-FOS<sup>14</sup>, pLV-tetO-HA-GFI1B (Addgene #125599)<sup>14</sup> and pFUW-tetO-3xFLAG-GATA2 (Addgene #125600)<sup>14</sup> or with a pool of the three factors, plus FUW-M2rtTA at 1:1 ratio. Use 10–20 µL total virus (individual TF + M2rtTA or three TFs + M2rtTA). Incubate cells overnight at 37 °C, 5% CO<sub>2</sub>.  
**NOTE:** It is recommended to use twelve 6-well plates per condition (for each individual TF and the three TFs combined).
4. Remove lentiviruses and add complete DMEM 16 h after the first transduction. Let cells recover for 6–8 h.
5. Transduce cells a second time with the same amount of virus per condition and incubate at 37 °C, 5% CO<sub>2</sub>.
6. On the next day remove viruses and add complete DMEM. Incubate at 37 °C, 5% CO<sub>2</sub> for 24 h.
7. Re-plate each well into a 0.1% gelatin coated tissue culture-treated 100 mm dish with complete DMEM to a final volume of 10 mL per dish. This represents approximately a 1:6 passage.
8. Allow cells to grow for 6 days at 37 °C, 5% CO<sub>2</sub>.
9. On day 6 after re-plating, aspirate medium and add complete DMEM with 1 µg/mL DOX. Incubate cells at 37 °C, 5% CO<sub>2</sub> for 2 days.
10. Collect fibroblasts and analyze genomic binding sites of the three TFs transduced individually or in combination, by ChIP-seq 2 days after DOX supplementation<sup>14</sup>.  
**NOTE:** The final seventy-two 100 mm dishes will contain between 20–50 × 10<sup>6</sup> cells, sufficient to perform ChIP-seq experiments and replicates.

## Representative Results

A schematic representation of the reprogramming approach using HDFs is illustrated in **Figure 1A**. Fibroblasts are acquired from commercial sources or collected from human donors and expanded *in vitro* previous to reprogramming. After plating, cells are transduced twice with GATA2, GFI1B and FOS (and M2rtTA) lentiviruses, and doxycycline is added at day 0 of reprogramming. On day 2, cells are split and plated in hematopoietic medium until day 25 of culture. Reprogrammed cells may be generated at different time points for multiple applications including transplantation in immunocompromised mice, single-cell RNA-sequencing (scRNA-seq) of purified cell populations (day 2 unsorted, day 15 CD49f<sup>+</sup> CD34<sup>+</sup> and day 25 CD49f<sup>+</sup> CD34<sup>+</sup> cells), as well as microscopy and flow cytometry analysis for the cell surface markers CD49f, CD34, CD9 and CD143. Representative cytometry plots show ~17% of reprogrammed cells expressing both CD49f and CD9 (**Figure 1B, left panel**), after 25 days of reprogramming. The majority of double positive cells express CD143 (~86%), and a small population express CD34 (0.9%), suggesting a dynamic hemogenic fate induction. These markers are not activated in M2rtTA transduced HDFs cultured for 25 days (**Figure 1B, right panel**). Immunofluorescence images confirm expression of CD9 and CD143 in adherent and round cells, morphologically distinct from fibroblasts that are negative for these markers (**Figure 1C**). Human hemogenic colonies also express CD49f and CD34<sup>+</sup>. scRNA-seq analysis of HDFs, day 2 unsorted cells, and purified reprogrammed cells at day 15 (CD49f<sup>+</sup> CD34<sup>+</sup>) and day 25 (CD49f<sup>+</sup> CD34<sup>+</sup>) show a stepwise increase in CD49f, CD9 and CD143 expression from day 2 to day 25. CD49f and CD9 positive cells appear first during the reprogramming process, between day 2 and 15, indicating that these molecules may represent markers of early human hemogenesis. CD143 expression starts to be



detected at day 15 and CD34 expressing cells are detected only at later time points (day 25). CD34<sup>+</sup> umbilical cord blood (UCB) cells were used as reference (**Figure 1D**).

**Figure 2A** describes a modified protocol to generate sufficient number of cells for ChIP-seq analysis at the initial stages of hemogenic reprogramming (day 2). First, HDFs are plated at a density two times higher than in the standard protocol (300,000 cells versus 150,000 cells per plate). After transduction, each well is re-plated into a 100 mm dish allowing cells to expand for 6 days before supplementing medium with DOX. Cells are analyzed 2 days after adding DOX and consequent TF expression. **Figure 2B** shows genome browser profiles of GATA2 binding to genomic regulatory regions of *ITGA6* and *ACE* when cells are co-transduced with the three factors (3TFs) or GATA2 individually. GATA2 also binds to open chromatin regions of *CD9* and *CD34* genes<sup>14</sup>.

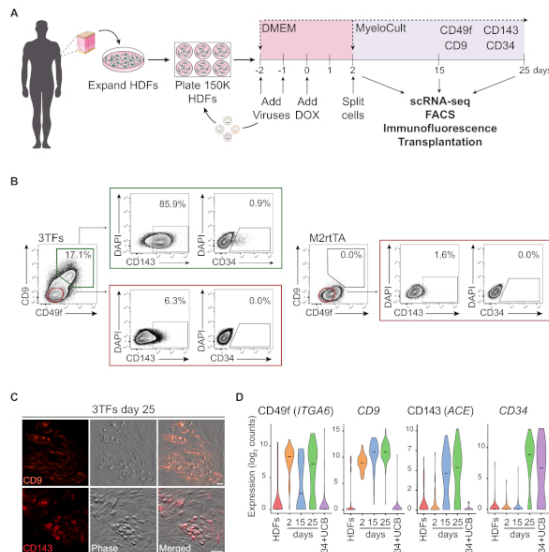


**Figure 1: Induction of hemogenic fate in human dermal fibroblasts. (A)** Experimental strategy for hemogenic reprogramming of human dermal fibroblasts (HDFs). Fibroblasts from skin punch biopsies are collected from donors, expanded and transduced with GATA2, GF1B, FOS and M2rTA lentiviruses. Doxycycline (DOX) is added to the culture at day 0 of reprogramming and cells are analyzed at several time points until day 25. scRNA-seq, single cell RNA-sequencing. FACS, Fluorescence-Activated Cell Sorting. **(B)** Gating strategy used to evaluate the expression of hemogenic/hematopoietic markers by flow cytometry at day 25 after transduction with the three transcription factors (3TFs). Cytometry plots show percentage of double positive cells for CD49f and CD9, gated in the live-cell population (DAPI-negative). Within the double positive population, the expression of CD143 and CD34 is shown. HDFs transduced only with M2rTA virus under the same culture conditions are used as control. **(C)** Immunofluorescence images of day 25 reprogrammed colonies confirming the expression of CD9 (upper panel) and CD143 (lower panel). Cells were stained with antibodies (**Table of Materials**) diluted 1:100 in PBS/2% FBS with mouse serum, incubated 20 min at 37 °C, 5% CO<sub>2</sub>, washed three times and imaged in PBS/2% FBS. Phase, phase-gradient contrast. Scale bars = 50 μm. **(D)** ScRNA-seq analysis of 253 cells at different time points. Expression of *ITGA6*, *CD9*, *ACE* and *CD34* is activated during reprogramming. Cells are collected at day 2 (unsorted), day 15 (CD49f<sup>+</sup>CD34<sup>-</sup>) and day 25 (CD49f<sup>+</sup>CD34<sup>+</sup>), HDFs and CD34<sup>+</sup> umbilical cord blood (34+UCB) cells are used as references. [Please click here to view a larger version of this figure.](#)

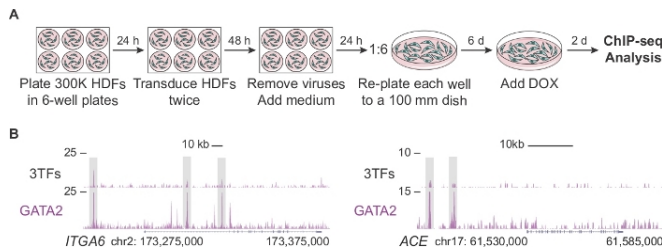
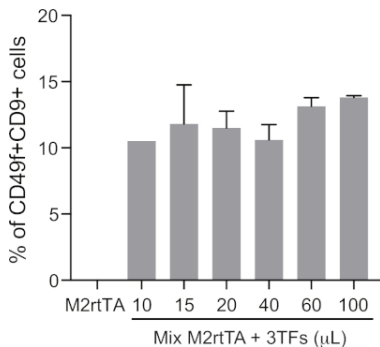
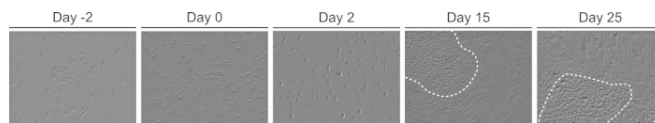


**Figure 2: Expansion of human dermal fibroblasts for ChIP-seq analysis.** (A) Experimental strategy depicting a modified protocol to generate high numbers of transduced human dermal fibroblasts (HDFs) for ChIP-seq at day 2 of reprogramming. 300,000 cells are plated in 6-well plates and transduced twice with individual factors (pFUW-tetO-FOS, pLV-tetO-HA-GFI1B or pFUW-tetO-3xFLAG-GATA2) or a combination of the three factors (plus M2rtTA). After removing viruses, fibroblasts are expanded for six days in 100 mm dishes. Doxycycline (DOX) is added at day 0 and cells are collected two days after DOX addition. (B) Genome browser profiles highlighting GATA2-binding sites (grey boxes) at *ITGA6* and *ACE* loci two days after transduction with the three transcription factors (3TFs) or with GATA2 alone. The total number of mapped reads is represented on the y-axis. [Please click here to view a larger version of this figure.](#)



**Supplementary Figure 1: Defining an optimized lentiviral volume for efficient hemogenic reprogramming.** Increasing volumes of concentrated (10 to 100  $\mu$ L) pool-produced lentiviral particles (3TFs: GATA2, GFI1B and FOS) are used to transduce human dermal fibroblasts (HDFs), together with M2rtTA at a ratio of 1:1, following steps 4.5–4.12 of the protocol. Reprogrammed cells are analyzed at day 25 to define an optimal volume of transduction for hemogenic reprogramming, given by the percentage of CD49f<sup>+</sup>CD9<sup>+</sup> cells gated in live-cells (DAPI-negative). Cell viability can be assessed by quantifying the absolute number of live cells at day 25. HDFs transduced with M2rtTA (100  $\mu$ L) are used as negative control. [Please click here to view a larger version of this figure.](#)



**Supplementary Figure 2: Morphology changes during hemogenic reprogramming of human dermal fibroblasts.** Human Dermal Fibroblast (HDF) cultures are imaged at the day of the first transduction (day -2), when DOX is added to the cultures (day 0), two days (day 2) and fifteen days (day 15) after DOX supplementation, and at the end-point of the experiment (day 25). Hemogenic colonies at days 15 and 25 are highlighted. Scale bars = 100  $\mu$ m. [Please click here to view a larger version of this figure.](#)

## Discussion

In this article, a method is described to generate hematopoietic progenitor cells directly from human fibroblasts, which go through an HP cell intermediate, similarly to definitive HSCs<sup>14</sup>.

Pool-production of lentiviral particles encoding GATA2, GFI1B and FOS was preferred over individual production, since in our hands it results in higher reprogramming efficiencies (unpublished data). Lentiviruses, as members of the *Retroviridae* family, normally contain two copies of positive single-stranded RNA<sup>19</sup>. The increased reprogramming efficiency may be due to packaging of two different transgenes in the same lentiviral particle, resulting in increased number of cells co-transduced with the three transcription factors. To ensure the success of this protocol, it is necessary to transduce HDFs with adequate amount of virus depending on the cell passage to obtain an optimal balance between reprogramming efficiency and cell viability, as recommended in step 4.6. Moreover, fresh non-concentrated viruses can be used. It is recommended to transduce cells with 0.5-3 mL of 3TFs pool and M2rtTA. Also, cell density should be adjusted according to the application.

150 000 HDFs per 6-well plate (step 4.4) provided the optimal density to perform FACS, transplantation and flow cytometry analysis of reprogrammed cells. For ChIP-seq experiments, more cells were required from the beginning (step 5.1). It is important to check cells regularly for morphological changes and replace hematopoietic medium twice a week to support the emergence of induced hematopoietic cells. Addition of hematopoietic cytokines or co-culture in feeder layers may increase reprogramming efficiency.

With this method, we can identify new hematopoietic markers that are dynamically expressed during hemogenic reprogramming. CD9, which was shown to be up-regulated in reprogrammed cells at the transcriptional level<sup>14</sup>, is rapidly expressed at the cell surface in the initial phases of reprogramming together with CD49f and CD143, serving as a novel marker of human HSC precursors. We also show that *ITGA6* and *ACE* are direct targets of GATA2 during the initial stages of hemogenic reprogramming, in addition to *CD9* and *CD34*<sup>14</sup>, providing a direct mechanistic link between human hemogenic precursor phenotype and GATA2.

One advantage of this system resides in the use of relatively homogeneous fibroblast cultures. While PSCs are easily expanded and maintained *in vitro*, differentiation protocols generate heterogeneous populations that include hematopoietic progenitors, which engraft poorly<sup>5,6,7</sup>. Moreover, there is a risk of tumorigenesis when transplanting PSC-derived HSPCs, since undifferentiated PSCs may still remain in culture even after employing differentiation protocols. Alternatively to fibroblasts, direct reprogramming to HSCs has been applied to blood-committed progenitors<sup>20</sup> and endothelial cells<sup>21</sup>. However, starting with blood-restricted progenitor cells hinders therapeutic application of the resulting HSCs if the patient carries mutations that affect the stem/progenitor hematopoietic population<sup>22</sup>. In the case of endothelial cells, these are more difficult to obtain compared to fibroblasts, and constitute a very heterogeneous cell population in terms of phenotype, function and structure, which are organ-dependent<sup>23</sup>. Other studies have succeeded in reprogramming mouse fibroblasts into engraftable hematopoietic progenitors<sup>24,25</sup> yet, so far, no other protocol describes the generation of HSPC-like cells from human fibroblasts.

This approach, coupled with pharmacological inhibition, gene knock-out, or knock-down permits to define individual or combination of factors that are required to directly induce human HSCs. Employing high efficiency screening methodologies based on recent CRISPR-Cas9 technologies in HDFs prior to reprogramming, represents an exciting endeavor for defining novel regulators of human definitive hematopoiesis. In the future, reprogramming non-blood related human cell types such as fibroblasts will serve as a platform to generate healthy patient-tailored hematopoietic progenitor cells for clinical applications.

## Disclosures

The authors have nothing to disclose.

## Acknowledgments

The Knut and Alice Wallenberg foundation, the Medical Faculty at Lund University and Region Skåne are acknowledged for generous financial support. This work was supported by a grant from Olle Engkvists Stiftelse (194-0694 to Filipe Pereira) and PhD scholarships from Fundação para a Ciência e Tecnologia (PTDC/BIM-MED/0075/2014 to Filipe Pereira, and SFRH/BD/135725/2018 and SFRH/BD/51968/2012 to Rita Alves and Andreia Gomes). This study was also supported by funds from NIH and NYSTEM (1R01HL119404 and C32597GG to Kateri A. Moore).

## References

- Ivanovs, A. et al. Highly potent human hematopoietic stem cells first emerge in the intraembryonic aorta-gonad-mesonephros region. *Journal of Experimental Medicine*. **208**, 2417–2427 (2011).
- Tavian, M., Biasch, K., Sinka, L., Vallet, J., Péault, B. Embryonic origin of human hematopoiesis. *International Journal of Developmental Biology*. **1065**, 1061–1065 (2010).
- Medvinsky, A., Rybtsov, S., Taoudi, S. Embryonic origin of the adult hematopoietic system: advances and questions. *Development*. **138**, 1017–1031 (2011).
- Ivanovs, A. et al. Human haematopoietic stem cell development: from the embryo to the dish. *Development*. **144**, 2323–2337 (2017).
- Daniel, M. G., Pereira, C.-F., Lemischka, I. R., Moore, K. A. Making a Hematopoietic Stem Cell. *Trends in Cell Biology*. **26**, 202–214 (2016).
- Vo, L., Daley, G. De novo generation of HSCs from somatic and pluripotent stem cell sources. *Blood*. **125**, 2641–2648 (2015).
- Rafii, S. et al. Human ESC-derived hemogenic endothelial cells undergo distinct waves of endothelial to hematopoietic transition. *Blood*. **121**, 770–781 (2013).
- Ebina, W., Rossi, D. J. Transcription factor-mediated reprogramming toward hematopoietic stem cells. *EMBO Journal*. **34**, 694–709 (2015).
- Sugimura, R. et al. Haematopoietic stem and progenitor cells from human pluripotent stem cells. *Nature*. **545**, 432–438 (2017).
- Pereira, C. F. et al. Induction of a Hemogenic Program in Mouse Fibroblasts. *Cell Stem Cell*. **13**, 205–218 (2013).
- Pereira, C. F. et al. Hematopoietic Reprogramming *In vitro* Informs *In Vivo* Identification of Hemogenic Precursors to Definitive Hematopoietic Stem Cells. *Developmental Cell*. **36**, 525–539 (2016).
- Notta, F. et al. Isolation of Single Human Hematopoietic Stem Cells Capable of Long-Term Multilineage Engraftment. *Science*. **333**, 218–221 (2011).
- Sinka, L., Biasch, K., Khazaal, I., Péault, B., Tavian, M. Angiotensin-converting enzyme (CD143) specifies emerging lympho-hematopoietic progenitors in the human embryo. *Blood*. **119**, 3712–3724 (2012).
- Gomes, A. M. et al. Cooperative Transcription Factor Induction Mediates Hemogenic Reprogramming. *Cell Reports*. **25**, 2821–2835 (2018).
- Karlsson, G. et al. Report The Tetraspanin CD9 Affords High-Purity Capture of All Murine Hematopoietic Stem Cells. *Cell Reports*. **4**, 642–8 (2013).
- Leung, K. T. et al. The tetraspanin CD9 regulates migration, adhesion, and homing of human cord blood CD34+ hematopoietic stem and progenitor cells. *Blood*. **117**, 1840–1851 (2011).
- Hockemeyer, D. et al. A drug-inducible system for direct reprogramming of human somatic cells to pluripotency. *Cell Stem Cell*. **3**, 346–353 (2008).

18. Kutner, R. H., Zhang, X., Reiser, J. Production, concentration and titration of pseudotyped HIV-1-based lentiviral vectors. *Nature Protocols*. **4**, 495–505 (2009).
19. Suzuki, Y. S., Suzuki, Y. Gene Regulatable Lentiviral Vector System. In *Viral Gene Therapy*. Edited by Ke, X., 286–308, IntechOpen. (2011).
20. Riddell, J. et al. Reprogramming committed murine blood cells to induced hematopoietic stem cells with defined factors. *Cell*. **157**, 549–564 (2014).
21. Lis, R. et al. Conversion of adult endothelium to immunocompetent haematopoietic stem cells. *Nature*. **545**, 439–445 (2017).
22. Pereira, C., Lemischka, I. R., Moore, K. 'From blood to blood': de-differentiation of hematopoietic progenitors to stem cells. *EMBO Journal*. **33**, 1511–1513 (2014).
23. Noian, D. J. et al. Molecular Signatures of Tissue-Specific Microvascular Endothelial Cell Heterogeneity in Organ Maintenance and Regeneration. *Developmental Cell*. **26**, 204–219 (2013).
24. Batta, K., Florkowska, M., Kouskoff, V., Lacaud, G. Direct Reprogramming of Murine Fibroblasts to Hematopoietic Progenitor Cells. *Cell Reports*. **9**, 1871–1884 (2014).
25. Cheng, H. et al. Reprogramming mouse fibroblasts into engraftable myeloerythroid and lymphoid progenitors. *Nature Communications*. **7**, 1–15 (2016).

Paper II





# Identifying Novel Regulators of Hemogenic Reprogramming with CRISPR/Cas9 Knockout Screening

Camila Vazquez Echegaray<sup>1,2</sup>, Rita Silvério-Alves<sup>1,2,3,4</sup>, Ilia Kurochkin<sup>1,2</sup>, Nina Lipjankic<sup>1,2</sup>, Alexandra Bäckström<sup>1</sup>, Kristijonas Žemaitis<sup>1</sup>, Jonas Larsson<sup>1,2</sup> and Carlos-Filipe Pereira<sup>1,2,3\*</sup>

## Affiliations

<sup>1</sup>Molecular Medicine and Gene Therapy, Lund Stem Cell Centre, Lund University, BMC A12, 221 84, Lund, Sweden.

<sup>2</sup>Wallenberg Centre for Molecular Medicine, Lund University, BMC A12, 221 84, Lund, Sweden.

<sup>3</sup>CNC - Centre for Neuroscience and Cell Biology, University of Coimbra, Largo Marquês do Pombal 3004-517, Coimbra, Portugal.

<sup>4</sup>Doctoral Programme in Experimental Biology and Biomedicine, University of Coimbra, Largo Marquês do Pombal 3004-517, Coimbra, Portugal.

\*Corresponding author. E-mail: filipe.pereira@med.lu.se

## Abstract

Hematopoietic stem cells (HSCs) self-renew and continuously produce mature blood cells. For these reasons, HSC transplantation is the only curative treatment for a variety of hematologic malignancies, although it remains challenging to produce HSCs *in vitro*. The generation of HSCs by direct cell reprogramming has the potential to overcome these limitations. We have previously shown that the ectopic expression of the transcription factors (TFs) GATA2, GFI1B and FOS in fibroblasts generates hematopoietic stem and progenitor cells through a dynamic endothelial to hematopoietic transition. However, a comprehensive understanding of the molecular regulators underlying this complex process in humans is needed to improve the efficiency and fidelity of the process. Here, we optimized a CRISPR/Cas9 knockout screening toolbox to map genes encoding for positive and negative regulators of hemogenic reprogramming. We show efficient editing in human dermal fibroblasts with a single guide RNA library targeting genes implicated in HSC self-renewal and expansion. Moreover, we improved the reprogramming process by using a single polycistronic lentiviral vector to deliver the three hemogenic TFs. A TF order generating high levels of GATA2 and GFI1B resulted in the highest reprogramming efficiency, measured by the activation of the early hemogenic markers CD9 and CD49f. After reprogramming and purification of successfully and unsuccessfully reprogrammed populations, we identified novel regulators that may function as barriers or facilitators of hemogenic reprogramming. Overall, our findings provide the foundation for CRISPR/Cas9 screening to define regulators of human hemogenic reprogramming, which ultimately may provide an efficient source of patient-specific HSCs.

## Introduction

Hematopoietic stem cells (HSCs) continuously replenish blood through a balance between self-renewal and differentiation, being widely used in curative medicine to treat hematological disorders<sup>1</sup>. However, HSC numbers are often insufficient to meet transplantation demands, and expansion of HSCs *in vitro* is still a challenging process<sup>2</sup>. HSCs are generated during embryonic development at the aorta-gonad-mesonephros (AGM) region and placenta from hemogenic endothelium, through an endothelial-to-hematopoietic transition (EHT)<sup>3,4</sup>. Even though this process is conserved in vertebrates<sup>5-7</sup>, human EHT has a unique site-dependent gene signature<sup>8</sup>. Moreover, the study of human HSC ontogeny is hampered by limited sample availability at different developmental stages<sup>8,9</sup> or complex pluripotent stem cell (PSC) differentiation protocols<sup>10,11</sup>.

Direct cell reprogramming has been used as a tool not only to generate cell types of interest but also to mimic developmental programs *in vitro*, otherwise difficult to study *in vivo*<sup>12,13</sup>. As we have previously shown, ectopic expression of GATA2, GFI1B and FOS transcription factors (TFs) was enough to induce an hemogenic fate in fibroblasts with the subsequent appearance of hematopoietic colonies, recapitulating HSC ontogeny *in vitro*<sup>12,14,15</sup>. Importantly, hemogenic precursors with similar phenotypes and global gene expression were identified in mouse placenta<sup>16</sup>. Therefore, dissecting this direct reprogramming system may shed light on the molecular regulators driving hemogenic reprogramming and consequently human EHT.

CRISPR/Cas9 screens have been used as a powerful approach to identify positive and negative regulators of immune cell processes<sup>17,18</sup>, as well as to uncover potential target genes for treating blood malignancies, such as acute myeloid leukemia (AML)<sup>19</sup>. Recently, this technology has also been utilized in the context of cell reprogramming to pluripotency<sup>20</sup> or alternative cell fates<sup>21</sup>. Genome-wide CRISPR/Cas9 knockout (KO) screenings have identified the zinc finger protein *Zfp266* as the most robust barrier to the generation of induced PSCs (iPSCs) from mouse embryonic fibroblasts<sup>20</sup>, and loss of the epigenetic regulator *Dmap1* sustained cells in a progenitor state in cardiac reprogramming<sup>21</sup>. Thus, we reasoned that CRISPR/Cas9 screening platforms could also prove useful in investigating the regulators of human hemogenic reprogramming.

Here, we developed a CRISPR/Cas9 KO screening approach to identify positive and negative molecular regulators that facilitate or inhibit the emergence of hemogenic cells. We utilized a constitutive Cas9 and a single guide (sg) RNA library targeting 116 genes implicated in HSC self-renewal and expansion. In parallel, we established the delivery of the hemogenic TFs GATA2, GFI1B and FOS to human dermal fibroblasts (HDFs) using a single lentiviral vector that also allowed antibiotic-mediated selection of transduced cells. We tested six polycistronic constructions and demonstrated that the order of GATA2, FOS, and GFI1B translated to high levels of GATA2 and GFI1B, resulting in the highest reprogramming efficiency. This efficiency was measured by the activation of the early hemogenic markers CD9 and CD49f<sup>14,15</sup>. Fifteen days after inducing reprogramming of edited fibroblasts, we purified reprogrammed (CD9<sup>+</sup>CD49f<sup>+</sup>) and non-reprogrammed (CD9<sup>-</sup>CD49f<sup>-</sup>)



populations and screened them by deep sequencing to quantify sgRNA abundance. Through guide enrichment analysis, we obtained candidate genes that may function as facilitators and barriers of homogenic reprogramming, including signaling interactors and TFs. These candidates will be further investigated in future studies to elucidate their molecular mechanisms. Defining the drivers of homogenic reprogramming will contribute to improving the efficiency and fidelity of the process, potentially leading to the successful generation of patient-derived hematopoietic stem and progenitor cells (HSPCs) *in vitro*, in sufficient numbers for the treatment of blood malignancies.

## Results

### Optimization of a CRISPR/Cas9 lentiviral delivery system for gene knockout

To identify barriers and facilitators of homogenic cell fate acquisition in fibroblasts undergoing reprogramming, we started by determining the optimal levels of Cas9 for gene KO (**Fig. 1A, B**). We conducted a functional assessment of a constitutive Cas9 lentiviral vector with a blasticidin (BSD) selection cassette using four different multiplicities of infection (MOI). This assessment was carried out in a fast, well-established reprogramming setting, where we induced dendritic cell type 1 (DC1) fate in human dermal fibroblasts (HDFs) within 9 days of transduction by ectopically expressing PU.1, IRF8, and BATEF3 (PIB) TFs<sup>22-24</sup>. Successful reprogramming towards DC1s is accompanied by the expression of CD45 among other surface markers. Using CD45 expression as readout, we promoted gene KO by delivering a sgRNA targeting CD45 with a GFP marker before starting cDC1 reprogramming (**Fig. 1B**). Reprogramming efficiency was later evaluated inside the GFP<sup>+</sup> and GFP<sup>-</sup> populations against a reprogramming control (HDFs selected for Cas9 and transduced with PIB, but not with sgRNA-CD45-GFP) (**Fig. 1C**). Our data show that an MOI of 1 is sufficient to significantly decrease the expression of CD45 ( $p < 0.0001$ ) (**Fig. 1D**). Interestingly, an increase in Cas9 MOI did not result in enhanced CD45 KO during reprogramming ( $p(\text{MOI } 1) < 0.0001$ ,  $p(\text{MOI } 2) = 0.0001$ ,  $p(\text{MOI } 4) = 0.0015$ ). This might be due to intracellular saturation of Cas9 molecules and, in agreement with previous reports<sup>25,26</sup>, an MOI of 1 was established for future experiments. To confirm that the impact in CD45 was indeed induced by Cas9, we checked the percentage of reprogrammed cells (CD45<sup>+</sup>) gated in the GFP<sup>-</sup> cell population, as these cells contained Cas9, but not the sgRNA for CD45 (**Fig. 1E**). We did not observe differences in the percentage of reprogrammed cells inside GFP<sup>-</sup> population, validating the specificity of sgRNA-induced KO. In addition to the functional assays, we assessed Cas9 expression by western blot from samples of three HDF donors (Supplementary Table 1), transduced with Cas9 at an MOI of 1 and following selection with blasticidin (**Fig. 1F**). These cells were further expanded for following experiments.

Next, we determined the conditions for the addition of the CRISPR/Cas9 sgRNA library targeting HSC-related genes. We utilized a lentiviral delivery system encoding a sgRNA with a chimeric guide RNA backbone that has been previously modified to enhance gene editing efficiency<sup>27</sup>, as well as

a GFP reporter (**Fig. 1G**). Each sgRNA cassette contains a single guide targeting a specific gene, covering a total of approximately 10 guides per gene. The 116 genes targeted by the library were derived from functional shRNA screens on human cord blood HSPCs or have been previously implicated in HSPC function or leukemia<sup>28,29</sup>. The selected genes play central roles in HSPC proliferation and maintenance. To ensure that each cell receives only one sgRNA construction, we tittered the lentivirus particles to achieve a functional MOI of approximately 0.3-0.4, translated into approximately 30-40% GFP<sup>+</sup> transduced cells, as previously reported<sup>30</sup> (**Fig. 1H**). We tested two copy-number of lentiviral particles and assessed functional MOI by determining the percentage of GFP<sup>+</sup> cells. While  $1.17 \times 10^5$  copies of lentiviral particles encoding the sgRNA library resulted in an MOI minor or equal to 0.2 across all three replicates (data not shown), doubling the viral copies resulted in an MOI of approx. 0.3 ( $29.1 \pm 4.3\%$ ). Following transduction with  $2.34 \times 10^5$  lentiviral copies, GFP<sup>+</sup> cells were sorted to a purity higher than 90% and expanded before undergoing hemogenic reprogramming (**Fig. 1I**).

### **Polycistronic vector encoding GATA2, GFI1B and FOS in a defined stoichiometry increases hemogenic reprogramming efficiency**

Polycistronic vectors can efficiently reprogram cells to pluripotency<sup>31,32</sup> or towards differentiated cell types<sup>22,33</sup> by combining several TFs into a single viral vector. The order of the TFs in the polycistronic vector matters as this impacts the stoichiometry of the factors. Ensuring the expression of GATA2, GFI1B and FOS in all transduced cells and at optimal relative levels may be critical for hemogenic reprogramming. For that, we have generated six polycistronic vectors where GATA2 (G), GFI1B (G<sup>B</sup>) and FOS (F) are positioned in different orders and separated by 2A “self-cleaving” peptides (**Fig. 2A**). Expression of each protein was confirmed five days after reprogramming (**Fig. 2B**). Reprogramming efficiency was assessed by the percentage of double positive cells for CD9 and CD49f hemogenic markers, 15 days after transduction of HDFs with three individual vectors (3TFs) or with each of the polycistronic vectors (**Fig. 2C, D**). Only GFG<sup>B</sup> condition resulted in a significantly higher percentage of CD9<sup>+</sup>CD49f<sup>+</sup> cells ( $p=0.016$ ) when compared to the 3TFs. We then checked the expression of the HSPC marker CD34 gated in the double positive population (**Fig. 2E, F**). Remarkably, the expression of CD34 in GFG<sup>B</sup> transduced cells was prominently higher than in the 3TFs condition ( $p<0.0001$ ). This might be explained by the increased levels of both GATA2 and GFI1B proteins obtained with this construct (**Fig. 2B**), which results in efficient hemogenic reprogramming.

To further optimize the delivery of the best polycistronic combination, we subcloned the GFG<sup>B</sup> sequence onto a different lentiviral vector with a puromycin (PURO) resistance gene (SFFV- GFG<sup>B</sup>-PURO) to enable selection of transduced cells, and the SFFV promoter for stronger expression in hematopoietic cells (**Fig. 2G, H**). This construct combined with antibiotic selection led to the increase of the double positive population, with maintenance of the CD34 cell subset, when compared to the original FUW vector (**Fig. 2G, H**). Therefore, the percentage of fully reprogrammed live cells (CD9<sup>+</sup>CD49f<sup>+</sup>CD34<sup>+</sup>) was significantly higher ( $p=0.0002$ ) (**Fig. 2I**), suggesting that expression of the

factors using an SFFV promoter combined with antibiotic selection is optimal for hemogenic reprogramming.

### **CRISPR/Cas9-mediated KO screening identified barriers and facilitators of hemogenic reprogramming**

We then performed KO screening using the optimized conditions for Cas9 expression, sgRNA library expression, and hemogenic reprogramming. Using the 1,056 guides in the library, we kept an average coverage of 300 HDFs/sgRNA/replicate. Genomic DNA was collected from double positive and double negative ( $CD9^+CD49f^+$ ,  $CD9^-CD49f^-$ ) sorted cells, as well day 0 (non-transduced with TFs), and sgRNAs were amplified and sequenced (**Fig. 3A**). Fluorescence-activated cell sorting (FACS) isolation at day 15 yielded purity percentages higher than 90% and 80% for the non-reprogrammed and reprogrammed populations, respectively (**Fig. 3B**).

To determine the abundance of sgRNAs, we converted individual sgRNA signals into gene signals and normalized the data using non-targeting genes. Then, we calculated the signal fold-change, which was  $\log_2$ -transformed, between reprogrammed ( $CD9^+CD49f^+$ ) samples and day 0 (baseline), and similarly between non-reprogrammed ( $CD9^-CD49f^-$ ) samples and day 0. Finally, we plotted the values for reprogrammed and non-reprogrammed conditions against each other (**Fig. 3C**). Using the MAGeCKFlute pipeline, we identified top candidate genes by ranking them and selecting those enriched in reprogrammed and non-reprogrammed samples (**Fig. 3D**, Supplementary Table 2). Genes with an increased sgRNA count in the reprogrammed samples, which equates to an increase in the fold-change, were defined as reprogramming barriers, since its silencing may lead to better reprogramming efficiency. On the other hand, genes that showed increased fold-change in the non-reprogrammed population were defined as facilitators of hemogenic reprogramming. Here, we report six barriers – *DDX26B*, *CD44*, *CD34*, *SLC28A1*, *SAXO2* and *ITGA9* – and 3 facilitators – *STAG2*, *MTFR1* and *SCAR5* (**Table 1**). *DDX26B* encodes a subunit of the Integrator protein complex. This complex interacts with RNA polymerase II to mediate 3' end processing of small nuclear RNAs including spliceosome components that catalyze pre-mRNA splicing<sup>34</sup>. Several Integrator complex subunits have been implicated in normal HSPC development and homeostasis<sup>35,36</sup>, yet no specific role for *DDX26B* has been described. *CD34* and *CD44* are two markers of intra-aortic hematopoietic clusters in the AGM region during early hematopoietic development<sup>37,38</sup>, as well as of bone marrow HSPCs<sup>39,40</sup>, where *CD44* is involved in HSC homing<sup>41</sup>. The presence of *CD44* and *CD34* as top hits suggests that the signaling pathways activated by these transmembrane proteins might need to be silenced during the earliest stages of hemogenic reprogramming to ensure accurate lineage specification. From the remaining barriers, only *ITGA9* has been described in the hematopoietic system. Integrin Subunit Alpha 9 ( $\alpha 9$ ) is part of the integrin  $\alpha 9\beta 1$  which is expressed in  $CD34^+$  HSPCs<sup>42</sup>. This integrin is important for HSPC adhesion to osteoblasts in the niche. Blocking  $\alpha 9\beta 1$  activity reduces HSPC proliferation and differentiation<sup>42</sup>, suggesting that cells might maintain a state of quiescence in the absence of  $\alpha 9\beta 1$ . In the facilitator group,

only STAG2 plays a role in hematopoiesis. STAG2, a member of the cohesin complex, has been reported to cooperate with STAG1 to control the production of mesoderm-derived primitive hemato-vascular progenitors<sup>43</sup>, indicating a necessity for early hematopoietic specification.

Overall, the screening results for hemogenic barriers and facilitators demonstrated significant enrichment in specific genes that could play a role as modulators of the reprogramming process and human EHT. Further individual validation both *in vitro* and *in vivo* will provide detailed information regarding their molecular mechanism.

**Table 1.** List of the top discovered genes and their overall function according to GeneCards.

	Gene	Function
Barriers	<i>DDX26B</i>	Processing of small nuclear RNAs.
	<i>CD44</i>	Receptor for hyaluronan. Mediates cell-cell and cell-matrix interactions.
	<i>CD34</i>	Mediates the attachment of stem cells to the bone marrow matrix.
	<i>SLC28A1</i>	Sodium-coupled nucleoside transporter protein.
	<i>SAXO2</i>	Involved in microtubule anchoring and stabilization.
	<i>ITGA9</i>	Alpha integrin. When bound to the $\beta 1$ chain forms the receptor for VCAM1.
Facilitators	<i>STAG2</i>	Cohesion of sister chromatids after DNA replication.
	<i>MTRF1</i>	Mitochondrial protein. Might play a role in protection against oxidative stress.
	<i>SCARA5</i>	Scavenger receptor implicated in iron ion transmembrane transport.

## Conclusions and discussion

HSCs play a crucial role in replenishing blood cells and serve as the basis for curative treatments of hematologic malignancies. However, the limited availability of HSCs and challenges in their *in vitro* production have motivated researchers to explore alternative approaches, such as direct cell reprogramming. In addition, CRISPR/Cas9-based genetic screens have been previously reported in the investigation of HSC biology<sup>44</sup>, as well as the impact of genetic variants and mutations on HSC function and behavior<sup>45,46</sup>. However, none of the approaches has been attempted during direct cell reprogramming towards the hemogenic or hematopoietic lineages.

In this study, we aimed to identify novel regulators of hemogenic reprogramming using a high-content CRISPR/Cas9-based KO screening approach. First, we successfully optimized the CRISPR/Cas9 KO toolbox to efficiently target genes implicated in HSC self-renewal and expansion in human fibroblasts. This is a crucial checkpoint to proceed with systematic screening, especially considering that Cas9 toxicity related to on-target effects, such as micronuclei formation and chromosome reengagement, were found in human HSPCs<sup>47</sup>. Additionally, we identified an optimal stoichiometry of hemogenic TFs (GATA2, GFI1B, and FOS) using a polycistronic lentiviral vector, leading to enhanced reprogramming efficiency. Our screening revealed a set of candidate genes that may function as barriers or facilitators of human hemogenic reprogramming. Notably, we identified

*DDX26B*, *CD44*, *CD34*, *SLC28A1*, *SAXO2* and *ITGA9* as barriers, while *STAG2*, *MTFR1* and *SCARA5* were identified as facilitators. Modulating the barriers of hemogenic reprogramming may be key to improving the generation of HSPC from patient-derived somatic cell sources *in vitro*. CD44 is a cell-surface protein receptor that has a role in HSPC homing<sup>41</sup> and has been recently identified as a marker of cells undergoing EHT in the mouse AGM region<sup>38</sup>. Cells with low levels of CD44 exhibited an endothelial-hematopoietic identity characterized by the expression of *Gata2*, *Runx1*, *Gfi1*, *Itgb3*, *Lyl1*, *Erg*, *Fli1*, *Lmo2* and *Tall1*, and represented the precursors of CD44<sup>+</sup> cells, which were restricted to the hematopoietic lineage<sup>38,48</sup>. In agreement, our approach has identified CD44 as a barrier of the first stages of human hemogenic reprogramming (identified by the early markers CD9 and CD49f), suggesting a conserved role for CD44 in regulating EHT and a possible stage-specific requirement for its signaling to allow definitive HSPC commitment.

Interestingly, the surface glycoprotein CD34, a very well-established marker of hemogenic endothelium and HSPCs<sup>37,40,49</sup>, shows a similar enrichment to CD44, being a top hit in the barriers group. This might be explained by the lack of CD34 expression in the earliest stages of human HSC ontogeny<sup>50,51</sup>. In fact, CD34 negative mesodermal cells at the para-aortic splanchnopleure region (pre-AGM), marked by angiotensin-converting enzyme (ACE) expression are thought to be the earliest precursors of CD34<sup>+</sup> intra-aortic hematopoietic clusters<sup>51</sup>. KO studies in mice showed that lack of CD34 impaired erythroid and myeloid differentiation from the yolk sac and fetal liver tissues due to a reduced number of hematopoietic progenitors<sup>52</sup>. However, null embryos progress through development and give rise to viable adult mice with no significant differences in the number or type of hematopoietic cells, either in peripheral blood or bone marrow<sup>52</sup>. Our data suggests a function for CD34 in hemogenic reprogramming and the specification of early human hemogenic endothelium, where CD34-mediated signaling may be detrimental in the first steps of definitive EHT. Later requirement of CD34 is in agreement with its delayed expression during hemogenic reprogramming, being expressed after CD9 and CD49f<sup>4,15</sup>. This finding may have broader implications as CD34 is used as a positive marker to identify HSPCs and EHT precursors obtained from human iPSCs<sup>53-58</sup>.

The strongest hit in the facilitators group was *STAG2*. Loss of *STAG2* in HSPCs results in commitment bias towards the myeloid lineage and decreased quiescence in HSCs<sup>59</sup>. Importantly, *STAG1/2* proteins have been implicated in primitive hematopoiesis in zebrafish<sup>43</sup>, and *Stag2* full KO mice die by E10.5<sup>60</sup>, reflecting a requirement for developmental hematopoiesis. These studies support the facilitator role of *STAG2* in hemogenic reprogramming.

In conclusion, our study presents an informative *in vitro* platform to identify novel regulators involved in hemogenic reprogramming and specification. Additionally, it provides critical insights into the molecular regulation of hemogenic reprogramming and human EHT and highlights potential molecular cornerstones for the generation of patient-specific HSCs.

## **Methods**

### **Cell culture**

Human embryonic kidney (HEK) 293T cells and HDFs were maintained in DMEM (Dulbecco's modified Eagle's medium) complete media supplemented with 10% (v/v) FBS, 2 mM L-glutamine and antibiotics (penicillin and streptomycin, 10 µg/ml). Cells were maintained at 37°C and 5% (v/v) CO<sub>2</sub>. HDFs undergoing cDC1 reprogramming were cultured in DMEM complete media and HDFs undergoing hemogenic reprogramming were cultured in MyeloCult H5100 (StemCell Technologies) supplemented with 1mM of hydrocortisone (StemCell Technologies) and antibiotic-antimycotic (1X).

### **Molecular cloning**

For reprogramming experiments, human GATA2, GFI1B and FOS TF sequences were cloned separately into the constitutive FUW vector under the control of a human ubiquitin C (UbC) promoter, using In-Fusion HD Cloning Kit (Takara), according to manufacturer's instructions. Polycistronic cassettes containing codon-optimized human sequences for GATA2, FOS and GFI1B in six different orders and interspaced by 2A self-cleaving peptide sequences were synthesized into a pAMP plasmid backbone (Twist) and later cloned into a FUW-UbC vector by enzymatic restriction. The first two coding sequences lacked the stop codon. Briefly, pAMP and FUW-UbC plasmids were digested with BamHI (Thermo Fisher Scientific), separated in a 1% agarose gel (NuSieve GTG Agarose, Lonza) and purified using the NucleoSpin Gel and PCR clean-up kit (Sigma). Then, restricted sequences were ligated to the FUW-UbC vector (T4 ligation, New England Biolabs) and transformed into Stellar Competent Cells (Takara). Overnight liquid cultures were used for plasmid isolation (GenElute HP Plasmid Maxiprep Kit, Sigma). GFG<sup>B</sup> sequence was later cloned into a SFFV-IRES-PURO (splenic focus forming virus (SFFV) promoter) as before, with the exception that for insertion of the cassette in the SFFV vector, the pAMP backbone and SFFV plasmid were digested with Sall and NheI. See Supplementary Table 3 for more information regarding cloning primers.

### **Lentiviral production**

Eighty percent-confluent 150 mm plates (Thermo Fisher Scientific) with HEK293T cells were transfected with a mixture of 10 µg transfer plasmid, 7.5 µg packaging construct expressing the viral packaging proteins and 2.5 µg envelope plasmid encoding the VSV-G protein, together with 30 µg/mL polyethylenimine. Viral supernatants were harvested 36, 48, and 72 hours after transfection, filtered (0.45 µm) and concentrated 100-fold with Lenti-X Virus Concentrator (Takara) and stored at -80 °C. GATA2, GFI1B and FOS (3TFs) were pool-produced.

## Quantification of viral titers

Lentiviral RNA was purified from 50  $\mu\text{L}$  viral aliquots using the NucleoSpin RNA Virus Kit (Takara), according to the manufacturer's instructions. RNA was eluted in 50  $\mu\text{L}$  RNase-free water. Viral titers were determined following the Lenti-X qRT-PCR Titration Kit (Takara) protocol using MicroAmp Optical 96-Well Reaction Plates (Thermo Fisher Scientific) and the QuantStudio 1 Real-Time PCR System (Thermo Fisher Scientific). Average Ct values from the control dilution replicates were plotted versus the copy number to generate a standard curve. The standard curve and non-template control Ct values were used to determine average Ct values for each duplicate sample dilution and calculate sample RNA genome content. Final copy numbers were determined according to the instructions available in the Lenti-X qRT-PCR Titration Kit User Manual (Takara).

## Lentiviral transduction and reprogramming

For the Cas9 multiplicity of infection (MOI) optimization experiment, *Streptococcus pyogenes* Cas9 was introduced into cells via lentiviral delivery with the vector LentiCas9-Blast (Addgene #52962), with Cas9 under the control of the EF-1 $\alpha$  promoter and a blasticidin resistance cassette. HDFs were plated at the density of 800,000 cells per 100 mm gelatin-coated plate. The following day, HDFs were transduced once with Cas9 to establish a MOI of 0.5, 1, 2 and 4. The relation between functional MOI and percentage of cells obtained after selection can be approximated by the Poisson distribution,  $p_{\text{survival}} = 1 - e^{-m}$ , where  $m = \text{MOI}^{61}$ . The culture media was supplemented with 10  $\mu\text{g}/\text{mL}$  blasticidin 48 hours post-transduction, for 8 days for selection of Cas9-transduced cells. Next, selected cells were transduced with sgRNA for CD45 ( $7.6 \times 10^8$  TU/mL) and reprogrammed to induce cDC1 fate. For next-generation sequencing (NGS) experiments, Cas9 transduced HDFs (MOI=1) were transduced with the sgRNA library. The cells were plated at the density of 800,000 cells per 100 mm plate and 24 hours later transduced with the sgRNA library lentiviral vector to achieve a MOI of approximately 0.3. HDFs FACS purified for GFP expression 48 hours following sgRNA library transduction. Later, GFP<sup>+</sup> expanded cells were transduced to promote hemogenic reprogramming. For CD reprogramming in fibroblast, a SFFV lentiviral vector containing a polycistronic cassette with PU.1, IRF8 and BATF3 (PIB) was delivered in two subsequential transductions, as described<sup>25,32</sup>. Before each transduction, 8  $\mu\text{g}/\text{mL}$  polybrene was added to the media. Cells were kept in complete DMEM and the percentage of CD45<sup>+</sup> cells was determined by flow cytometry at the experiment endpoint of 9 days. Hemogenic reprogramming of HDF was done as previously described<sup>14</sup> with some modifications: cells were incubated overnight with FUW-3TFs or polycistronic lentiviral particles in media supplemented with polybrene (8  $\mu\text{g}/\text{ml}$ ). Cells were transduced twice in consecutive days. Day 0 was considered the day of the first transduction. Cells were split 1:2 at day 4 and cultured in MyeloCult H5100 (StemCell Technologies) supplemented with 1mM of hydrocortisone (StemCell Technologies) and antibiotic-antimycotic (1X), until the end of the experiment at day 15. Hemogenic markers were assessed by flow cytometry at the experiment endpoint.

Media was changed twice a week. When appropriate, puromycin was added to plates from day 5 of reprogramming until the end of the experiment.

### **Western blot**

Whole-cell lysates were obtained from 1 million HDFs after incubation with 200  $\mu$ L ice-cold RIPA buffer (Thermo Fisher Scientific), supplemented with 1X Halt Protease Inhibitor Cocktail (Thermo Fisher Scientific), 1 mM phenylmethylsulfonyl fluoride (PMSF) (Sigma) and 5 mM sodium fluoride (NaF) (Sigma). Cells were vortexed and placed on ice 5 for min. This was repeated 4 times. Lysates were span at 4000 g at 4°C for 5 min and the supernatant was transferred to a new tube. Protein lysates were diluted 1:2 in Laemmli buffer (Bio-Rad) with 5% 2-Mercaptoethanol (Sigma) and boiled at 98 °C for 10 min. Samples were run in a Bolt 4-12%, Bis-Tris (Invitrogen) SDS-PAGE gel, using a Mini Gel Tank (Thermo Fisher Scientific) and Blot MOPS SDS running buffer (Invitrogen). Transfer was performed in an iBlot 2 (Thermo Fisher Scientific) dry system for 7 min. Membranes were incubated overnight at 4 °C with unconjugated primary antibodies against Cas9, GATA2, GFI1B, FOS, and Calnexin (all 1:1000), and with anti-rabbit horseradish peroxidase-conjugated secondary antibodies. Membranes were incubated with ECL prime (Amersham) for 5 min and revealed in a ChemiDoc instrument (Bio-Rad). Similar cell number were used between conditions. Additional information regarding antibodies can be found in Supplementary Table 4.

### **Flow cytometry and FACS**

For Cas9 optimization, CD45 knockout efficiency was evaluated 9 days after transduction with the reprogramming viral vectors expressing PIB factors. Hemogenic reprogramming efficiency was evaluated 15 days after transduction with polycistronic transgenes or pooled-produced TFs. Cells undergoing cDC1 reprogramming were dissociated, pelleted, and incubated with APC-CD45 antibody diluted (1:100) in PBS with 2% FBS at 4 °C for 20 min. Cells undergoing hemogenic reprogramming were incubated with 1:100 dilutions of PE-CD9, PE/Cy7-CD49f and AF488-CD34. Single live (DAPI<sup>-</sup>) cells were analyzed. Cells were analyzed in LSR FORTESSA, LSR FORTESSA x20, or LSR II (BD Biosciences). For isolation of cells containing the sgRNA library, HDFs were dissociated, pelleted and resuspended in PBS with 2% FBS for GFP purification. Reprogrammed HDFs expressing Cas9 and sgRNA library (GFP<sup>+</sup>), that were used for NGS, were incubated with PE-CD9 and PE-Cy7-CD49f antibodies and double positive and double negative populations were isolated. Cells were sorted with either FACSFACS Aria II Melody or FACSFACS Aria III (BD Biosciences). All flow cytometry data was analyzed using the FlowJo software (FlowJo version 10.8.1). Additional information regarding antibodies can be found in Supplementary Table 4.



## CRISPR/Cas9 screening

Cas9-expressing fibroblasts were generated by transducing the cells with LentiCas9-Blast lentivirus at MOI=1. Briefly, cells were plated at the density of 800,000 cells per 100 mm plate and were selected with blasticidin for 9 days and maintained in blasticidin-containing media prior to library transduction. SgRNA for CD45 and the sgRNA library used in this study were cloned into the lentiCRISPR v2 backbone (Addgene #52961) which has been modified to enhance knockout efficiency, as previously described<sup>28</sup>. Genes targeted by the sgRNA library were derived from various databases including functional shRNA screens on human HSPCs and literature on both normal and malignant HSPC function, namely acute myeloid leukemia (AML) and myelodysplastic syndrome (MDS). Selected genes are mainly regulators of HSPC proliferation and maintenance. The sequences for the gRNAs targeting the 116 selected genes were derived from the GeCKOv2 library<sup>62</sup> and the Broad GPP genome-wide Brunello library<sup>63</sup>, and for genes not present in these libraries, the sgRNA design tool CRISPick (Broad Institute) was used. sgRNA sequences and target genes are listed in the Source Data file. For library transduction, cells were plated at the density of 800,000 cells per 100 mm plate and 24 hours later transduced with the sgRNA library lentiviral vector to achieve a MOI of ~0.3-0.4, with >300x coverage. HDFs were FACS-purified for GFP expression 48 hours following sgRNA library transduction. Later, GFP<sup>+</sup> expanded cells were transduced to promote hemogenic reprogramming. One million cells were collected before reprogramming to serve as reference point for baseline sgRNA distribution (day 0 – HDFs expressing Cas9 and the sgRNA library, but no TFs). At day 15, puromycin resistant, GFP<sup>+</sup> and CD9/CD49f stained cells were sorted using FACS AriaIII (BD Biosciences) and collected pellets were stored at -20 °C. Genomic DNA was extracted using the QIAmp Blood Mini Kit (Qiagen). Amplification of sgRNA regions from the extracted genome was performed by a 2-step PCR reaction protocol, first using custom-made primers harboring the sgRNA region (Supplementary Table 5), followed by a second PCR for indexing Illumina Nextera XT adapters (Illumina). Libraries were thoroughly checked for quality control using Qubit (Thermo Fisher) and Bioanalyzer (Agilent). The resulting libraries from 3 independent replicates – one sample from one donor (Lonza) and two replicates from a second donor (ScienCell) – were sequenced using the Illumina NextSeq 500/550 High Output 150 cycles kit in a NextSeq 500 platform (Illumina) to determine sgRNA representation. After demultiplexing, sgRNA read count data was input to the CRISPR screen analysis pipeline MAGeCKFlute<sup>64</sup>. MAGeCK was used to identify gene hits and downstream analysis was performed using FluteMLE, with loess normalization.

## Statistical analysis

Comparisons between groups were performed by one-way ANOVA followed by Tukey's multiple comparison test with GraphPad Prism 9 software. See figure legends for more detail. *P* values are shown when relevant (\**p*<0.05; \*\**p*<0.01; \*\*\**p*<0.001; \*\*\*\**p*<0.0001).

## References

1. Skulimowska, I. *et al.* The biology of hematopoietic stem cells and its clinical implications. *FEBS J* **289**, 7740–7759 (2022).
2. Che, J. L. C. *et al.* Identification and characterization of in vitro expanded hematopoietic stem cells. *EMBO Rep* **23**, 1–19 (2022).
3. Medvinsky, A., Rybtsov, S. & Taoudi, S. Embryonic origin of the adult hematopoietic system: Advances and questions. *Development* **138**, 1017–1031 (2011).
4. Zovein, A. C. *et al.* Fate Tracing Reveals the Endothelial Origin of Hematopoietic Stem Cells. *Cell Stem Cell* **3**, 625–636 (2008).
5. Boisset, J.-C. *et al.* In vivo imaging of haematopoietic cells emerging from the mouse aortic endothelium. *Nature* **464**, 116–120 (2010).
6. Kissa, K. & Herbomel, P. Blood stem cells emerge from aortic endothelium by a novel type of cell transition. *Nature* **464**, 112–115 (2010).
7. Dzierzak, E. & Bigas, A. Blood Development: Hematopoietic Stem Cell Dependence and Independence. *Cell Stem Cell* **22**, 639–651 (2018).
8. Calvanese, V. *et al.* Mapping human haematopoietic stem cells from haemogenic endothelium to birth. *Nature* **604**, 534–540 (2022).
9. Zeng, Y. *et al.* Tracing the first hematopoietic stem cell generation in human embryo by single-cell RNA sequencing. *Cell Res* **29**, 881–894 (2019).
10. Guibentif, C. *et al.* Single-Cell Analysis Identifies Distinct Stages of Human Endothelial-to-Hematopoietic Transition. *Cell Rep* **19**, 10–19 (2017).
11. Canu, G. *et al.* Analysis of endothelial-to-haematopoietic transition at the single cell level identifies cell cycle regulation as a driver of differentiation. *Genome Biol* **21**, 157 (2020).
12. Pereira, C. F. *et al.* Induction of a Hemogenic Program in Mouse Fibroblasts. *Cell Stem Cell* **13**, 205–218 (2013).
13. Wang, H., Yang, Y., Liu, J. & Qian, L. Direct cell reprogramming: approaches, mechanisms and progress. *Nat Rev Mol Cell Biol* **22**, 410–424 (2021).
14. Silvério-Alves, R., Gomes, A. M., Kurochkin, I., Moore, K. A. & Pereira, C.-F. Hemogenic Reprogramming of Human Fibroblasts by Enforced Expression of Transcription Factors. *Journal of Visualized Experiments* **153**, 1–8 (2019).
15. Gomes, A. M. *et al.* Cooperative Transcription Factor Induction Mediates Hemogenic Reprogramming. *Cell Rep* **25**, 2821–2835 (2018).
16. Pereira, C. F. *et al.* Hematopoietic Reprogramming In Vitro Informs In Vivo Identification of Hemogenic Precursors to Definitive Hematopoietic Stem Cells. *Dev Cell* **36**, 525–539 (2016).
17. Shifrut, E. *et al.* Genome-wide CRISPR Screens in Primary Human T Cells Reveal Key Regulators of Immune Function. *Cell* **175**, 1958–1971.e15 (2018).
18. Parnas, O. *et al.* A Genome-wide CRISPR Screen in Primary Immune Cells to Dissect Regulatory Networks. *Cell* **162**, 675–686 (2015).
19. Lin, S. *et al.* An In Vivo CRISPR Screening Platform for Prioritizing Therapeutic Targets in AML. *Cancer Discov* **12**, 432–449 (2022).
20. Kaemena, D. F. *et al.* B1 SINE-binding ZFP266 impedes mouse iPSC generation through suppression of chromatin opening mediated by reprogramming factors. *Nat Commun* **14**, (2023).
21. Yu, J. S. L. *et al.* CRISPR-Knockout Screen Identifies Dmap1 as a Regulator of Chemically Induced Reprogramming and Differentiation of Cardiac Progenitors. *Stem Cells* **37**, 958–972 (2019).
22. Rosa, F. F. *et al.* Direct reprogramming of fibroblasts into antigen-presenting dendritic cells. *Sci Immunol* **3**, eaau4292 (2018).

23. Rosa, F. F. *et al.* Single-cell transcriptional profiling informs efficient reprogramming of human somatic cells to cross-presenting dendritic cells. *Sci Immunol* **7**, 1–18 (2022).
24. Rosa, F., Pires, C., Zimmermannova, O. & Pereira, C.-F. Direct Reprogramming of Mouse Embryonic Fibroblasts to Conventional Type 1 Dendritic Cells by Enforced Expression of Transcription Factors. *Bio Protoc* **10**, (2020).
25. Lewis, M. *et al.* A genome-scale CRISPR knock-out screen in chronic myeloid leukemia identifies novel drug resistance mechanisms along with intrinsic apoptosis and MAPK signaling. *Cancer Med* **9**, (2020).
26. Doench, J. G. *et al.* Rational design of highly active sgRNAs for CRISPR-Cas9-mediated gene inactivation. *Nat Biotechnol* **32**, (2014).
27. Yudovich, D. *et al.* Combined lentiviral- and RNA-mediated CRISPR/Cas9 delivery for efficient and traceable gene editing in human hematopoietic stem and progenitor cells. *Sci Rep* **10**, 1–11 (2020).
28. Galeev, R. *et al.* Genome-wide RNAi Screen Identifies Cohesin Genes as Modifiers of Renewal and Differentiation in Human HSCs. *Cell Rep* **14**, 2988–3000 (2016).
29. Žemaitis, K. *et al.* RNAi Screen Identifies MTA1 as an Epigenetic Modifier of Differentiation Commitment in Human HSPCs. *Exp Hematol* **115**, 20–29 (2022).
30. Joung, J. *et al.* Genome-scale CRISPR-Cas9 knockout and transcriptional activation screening. *Nat Protoc* **12**, 828–863 (2017).
31. Carey, B. W. *et al.* Reprogramming of murine and human somatic cells using a single polycistronic vector. *PNAS* **106**, 2–7 (2009).
32. Sommer, C. A. *et al.* Induced Pluripotent Stem Cell Generation Using a Single Lentiviral Stem Cell Cassette. *Stem Cells* **27**, 543–549 (2009).
33. Wang, L. *et al.* Stoichiometry of Gata4, Mef2c, and Tbx5 Influences the Efficiency and Quality of Induced Cardiac Myocyte Reprogramming. *Circ Res* **116**, 237–244 (2015).
34. Baillat, D. *et al.* Integrator, a Multiprotein Mediator of Small Nuclear RNA Processing, Associates with the C-Terminal Repeat of RNA Polymerase II. *Cell* **123**, 265–276 (2005).
35. Tao, S., Cai, Y. & Sampath, K. The Integrator subunits function in hematopoiesis by modulating Smad/BMP signaling. *Development* **136**, 2757–2765 (2009).
36. Zhang, P. *et al.* INTS11 regulates hematopoiesis by promoting PRC2 function. *Sci Adv* **7**, (2021).
37. Tavian, M. *et al.* Aorta-associated CD34<sup>+</sup> hematopoietic cells in the early human embryo. *Blood* **87**, (1996).
38. Oatley, M. *et al.* Single-cell transcriptomics identifies CD44 as a marker and regulator of endothelial to haematopoietic transition. *Nat Commun* **11**, (2020).
39. Cao, H. *et al.* The role of CD44 in fetal and adult hematopoietic stem cell regulation. *Haematologica* **101**, 26–37 (2016).
40. Stella, C. C. *et al.* CD34-Positive Cells: Biology and Clinical Relevance. *Haematologica* **80**, 367–387 (1995).
41. Avigdor, A. *et al.* CD44 and hyaluronic acid cooperate with SDF-1 in the trafficking of human CD34<sup>+</sup> stem/progenitor cells to bone marrow. *Blood* **103**, (2004).
42. Schreiber, T. D. *et al.* The integrin  $\alpha 9\beta 1$  on hematopoietic stem and progenitor cells: involvement in cell adhesion, proliferation and differentiation. *Haematologica* **94**, 1493–1501 (2009).
43. Ketharnathan, S., Labudina, A. & Horsfield, J. A. Cohesin Components Stag1 and Stag2 Differentially Influence Haematopoietic Mesoderm Development in Zebrafish Embryos. *Front Cell Dev Biol* **8**, (2020).
44. Wagenblast, E. *et al.* Functional profiling of single CRISPR/Cas9-edited human long-term hematopoietic stem cells. *Nat Commun* **10**, 4730 (2019).

45. Mercier, F. E. *et al.* In vivo genome-wide CRISPR screening in murine acute myeloid leukemia uncovers microenvironmental dependencies. *Blood Adv* **6**, 5072–5084 (2022).
46. Secker, K.-A. *et al.* Inhibition of DOT1L and PRMT5 promote synergistic anti-tumor activity in a human MLL leukemia model induced by CRISPR/Cas9. *Oncogene* **38**, 7181–7195 (2019).
47. Leibowitz, M. L. *et al.* Chromothripsis as an on-target consequence of CRISPR–Cas9 genome editing. *Nat Genet* **53**, 895–905 (2021).
48. Bergiers, I. *et al.* Single-cell transcriptomics reveals a new dynamical function of transcription factors during embryonic hematopoiesis. *Elife* **7**, (2018).
49. Mizuochi, C. *et al.* Intra-aortic clusters undergo endothelial to hematopoietic phenotypic transition during early embryogenesis. *PLoS One* **7**, (2012).
50. Cortés, F., Debacker, C., Péault, B. & Labastie, M. C. Differential expression of KDR/VEGFR-2 and CD34 during mesoderm development of the early human embryo. *Mech Dev* **83**, (1999).
51. Sinka, L., Biasch, K., Khazaal, I., Péault, B. & Tavian, M. Angiotensin-converting enzyme (CD143) specifies emerging lympho-hematopoietic progenitors in the human embryo. *Blood* **119**, 3712–3723 (2012).
52. Cheng, J. *et al.* Hematopoietic defects in mice lacking the sialomucin CD34. *Blood* **87**, 479–490 (1996).
53. Kennedy, M. *et al.* T Lymphocyte Potential Marks the Emergence of Definitive Hematopoietic Progenitors in Human Pluripotent Stem Cell Differentiation Cultures. *Cell Rep* **2**, 1722–1735 (2012).
54. Ran, D. *et al.* RUNX1a enhances hematopoietic lineage commitment from human embryonic stem cells and inducible pluripotent stem cells. *Blood* **121**, 2882–2890 (2013).
55. Choi, K.-D. *et al.* Identification of the Hemogenic Endothelial Progenitor and Its Direct Precursor in Human Pluripotent Stem Cell Differentiation Cultures. *Cell Rep* **2**, 553–567 (2012).
56. Elcheva, I. *et al.* Direct induction of haematoendothelial programs in human pluripotent stem cells by transcriptional regulators. *Nat Commun* **5**, 4372 (2014).
57. Sugimura, R. *et al.* Haematopoietic stem and progenitor cells from human pluripotent stem cells. *Nature* **545**, 432–438 (2017).
58. Doulatov, S. *et al.* Induction of Multipotential Hematopoietic Progenitors from Human Pluripotent Stem Cells via Respecification of Lineage-Restricted Precursors. *Cell Stem Cell* **13**, 459–470 (2013).
59. Viny, A. D. *et al.* Cohesin Members Stag1 and Stag2 Display Distinct Roles in Chromatin Accessibility and Topological Control of HSC Self-Renewal and Differentiation. *Cell Stem Cell* **25**, (2019).
60. De Koninck, M. *et al.* Essential Roles of Cohesin STAG2 in Mouse Embryonic Development and Adult Tissue Homeostasis. *Cell Rep* **32**, (2020).
61. Chen, Y.-H. *et al.* Phosphatidylserine Vesicles Enable Efficient En Bloc Transmission of Enteroviruses. *Cell* **160**, 619–630 (2015).
62. Sanjana, N. E., Shalem, O. & Zhang, F. Improved vectors and genome-wide libraries for CRISPR screening. *Nat Methods* **11**, 783–784 (2014).
63. Doench, J. G. *et al.* Optimized sgRNA design to maximize activity and minimize off-target effects of CRISPR-Cas9. *Nat Biotechnol* **34**, 184–191 (2016).
64. Wang, B. *et al.* Integrative analysis of pooled CRISPR genetic screens using MAGeCKFlute. *Nat Protoc* **14**, 756–780 (2019).

## Figures

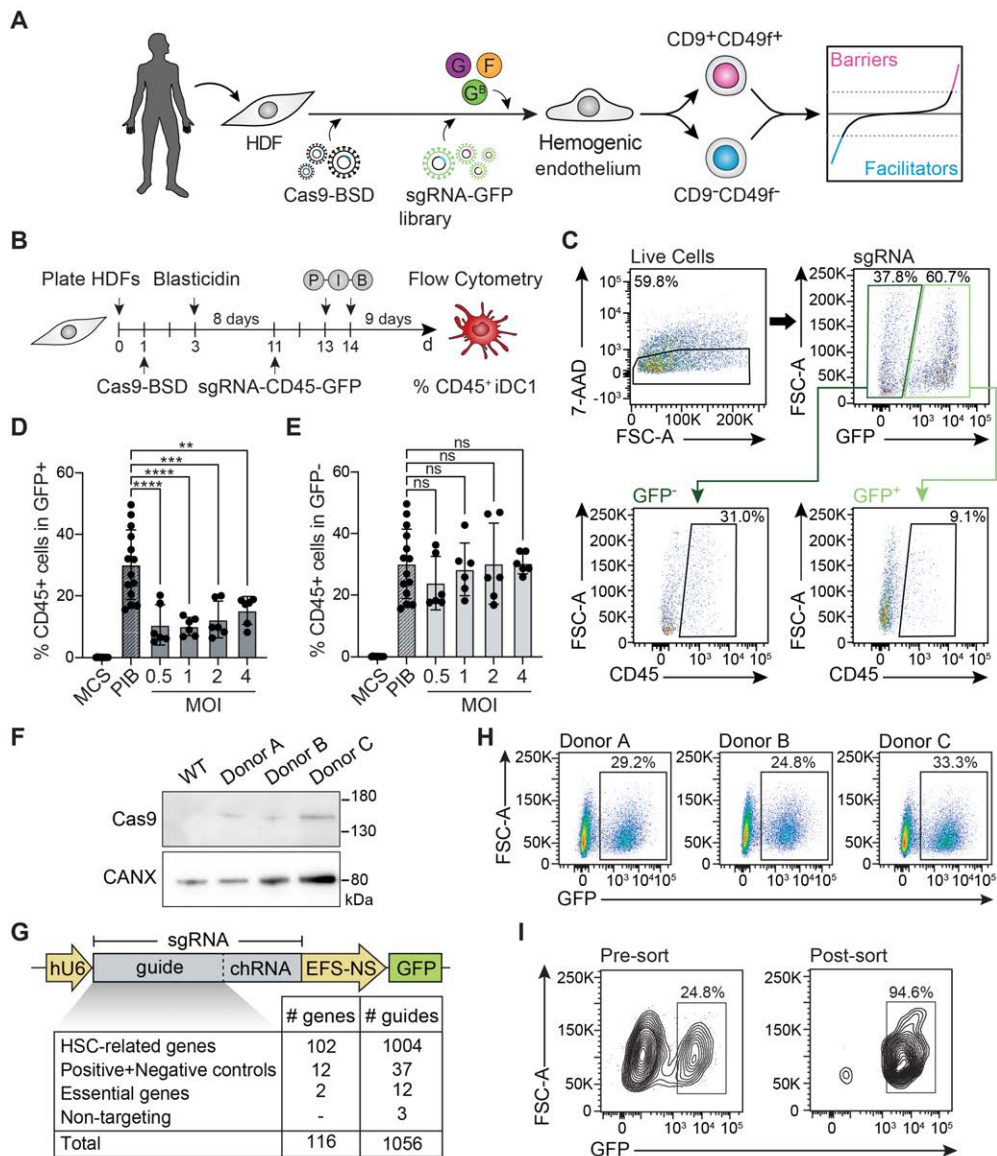


**Figure 1. Optimization of a CRISPR/Cas9 screening system in primary human dermal fibroblasts.** **A**, Outline of the experimental approach to identify regulators of human hemogenic endothelium specification. Human dermal fibroblasts (HDFs) were transduced with constitutive Cas9 with resistance to blasticidin (BSD), selected and transduced with single guide (sg) RNA library with a GFP marker targeting hematopoietic stem cell (HSC)-related genes. Following purification of the GFP<sup>+</sup> population, cells were transduced a third time with viral vectors containing the hemogenic reprogramming factors GATA2 (G), GFI1B (G<sup>B</sup>) and FOS (F) to allow induction of hemogenic program in fibroblasts. At the experimental endpoint (day 15), double positive and double negative populations for the hemogenic markers CD49f and CD9 were isolated for downstream analysis by next-generation sequencing to identify barriers and facilitators of hemogenic reprogramming. **B**, Strategy to determine the optimal

Cas9 multiplicity of infection (MOI) for efficient knockout in a well-characterized direct cell reprogramming system. HDFs of three donors were transduced with Cas9 lentiviral particles and selected with blasticidin for 8 days. Then, cells were transduced with a sgRNA co-expressing GFP targeting CD45, an early marker of dendritic cell type I (DC1) reprogramming, and later with SFFV polycistronic lentiviral vector comprising PU.1, IRF8 and BATF3 (PIB) sequences. On day 9 of reprogramming, induced DC1 (iDC1) cells were analyzed by flow cytometry to assess the surface expression of CD45. **C**, Representative flow cytometry plots showing the gating strategy for CD45 expression inside either GFP<sup>-</sup> (no guide) or GFP<sup>+</sup> (with guide) live cells (7-AAD<sup>-</sup>). **D**, Percentage of CD45<sup>+</sup> cells at Cas9 MOIs 0.5, 1, 2, and 4 from each donor, gated in GFP<sup>+</sup> populations (n=3 biological replicates). Cells transduced with only the empty vector (MCS) or PIB, without sgRNA-CD45-GFP, were gated in the GFP<sup>-</sup> population to define the negative and positive controls, respectively. **E**, Quantification of CD45 expression in the GFP<sup>-</sup> population of Cas9 transduced cells (n=3 biological replicates). **F**, Cas9 protein expression (MOI=1) in three HDF donors. An untransduced wild-type (WT) sample was included as negative control. Calnexin (CANX) was used as loading control. **G**, Schematic representation of the sgRNA library plasmid. SgRNAs contain a chimeric scaffold (chrRNA) to optimize Cas9 binding and knockout. The guide and scaffold sequences are expressed under the human U6 promoter and GFP reporter is expressed under the EFS-NS promoter. Guides include hematopoietic stem cell (HSC)-related genes, controls, and non-targeting sequences. **H**, Flow cytometry plots of GFP expression in HDFs from three donors transduced with the optimized copy-number of the pooled sgRNA library lentiviral particles to achieve an MOI between 0.3-0.4. **I**, Flow cytometry plots representing the percentage of GFP<sup>+</sup> cells (with no Cas9) before (pre-sort) and after (post-sort) fluorescence-activated cell sorting. **D**, **E**, Statistical significance was analyzed by one-way ANOVA followed by Tukey's multiple comparisons test. \*\*p<0.01, \*\*\*p<0.001, \*\*\*\*p<0.0001, ns - non-significant. Mean ± SD is shown.

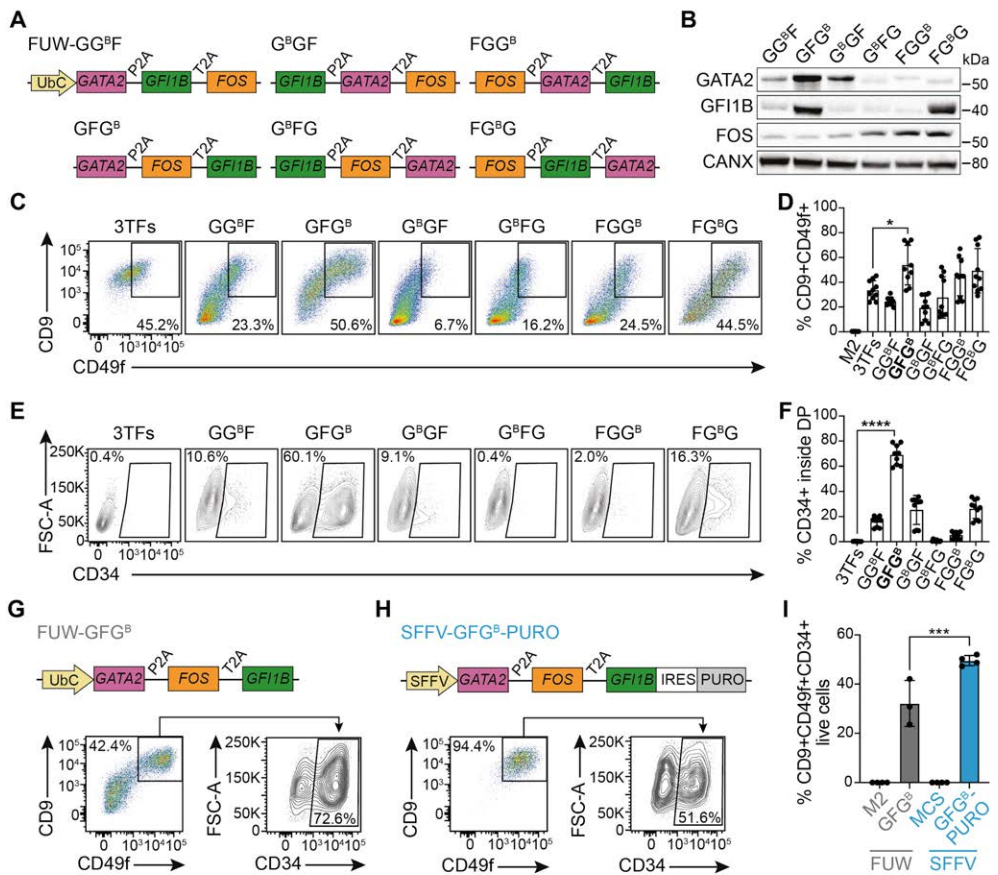


**Figure 2. High levels of GATA2 and GFI1B are necessary for efficient hemogenic reprogramming.** **A**, Schematic representation of the six constitutive polycistronic lentiviral plasmids encoding GATA2 (G), GFI1B (G<sup>B</sup>) and FOS (F) transcription factors (TFs) in different orders, separated by P2A and T2A self-cleaving peptides, under the control of the human ubiquitin C promoter (UbC). **B**, Western blot bands showing the expression of the three TFs at day 5 of hemogenic reprogramming, after transducing human dermal fibroblasts with each individual construct. Calnexin (CANX) was used as loading control. kDa, kilodaltons. **C**, Representative flow cytometry plots for the percentage of CD9<sup>+</sup>CD49f<sup>+</sup> cells inside the live cell population (7-AAD<sup>-</sup>) transduced with either the individual factors (FUW-3TFs) or the polycistronic vectors, at day 15 days of reprogramming. FUW-M2rtTa (M2) was used as control. **D**, Quantification of CD9<sup>+</sup>CD49f<sup>+</sup> cells (n=9-10 technical replicates). **E**, Representative flow cytometry plots of CD34<sup>+</sup> cells inside the double positive population. **F**, Quantification of CD34<sup>+</sup> cells inside the double positive population (n=9-10 technical replicates). **G**, **H**, Schematic representation of the GFG<sup>B</sup> construct under the control of the UbC (**G**) or the SFFV promoter, followed by an internal ribosome entry (IRES) and puromycin (PURO) resistance sequence (**H**). Representative plots for the percentage of CD9<sup>+</sup>CD49f<sup>+</sup> live cells, as well as CD34<sup>+</sup> cells inside the double positive population, at day 15 of the same reprogramming experiment is shown. Cells transduced with the SFFV vector were selected with puromycin starting from day 5. **I**, Quantification of the percentage of CD9<sup>+</sup>CD49f<sup>+</sup>CD34<sup>+</sup> cells when comparing FUW-GFG<sup>B</sup> with SFFV-GFG<sup>B</sup>-PURO. M2 and SFFV-MCS (MCS) were used as negative controls. **D**, **F**, **I**, Statistical significance was analyzed by one-way ANOVA followed by Tukey's multiple comparisons test. \**p*<0.05, \*\*\**p*<0.001, \*\*\*\**p*<0.0001. Mean ± SD is shown.

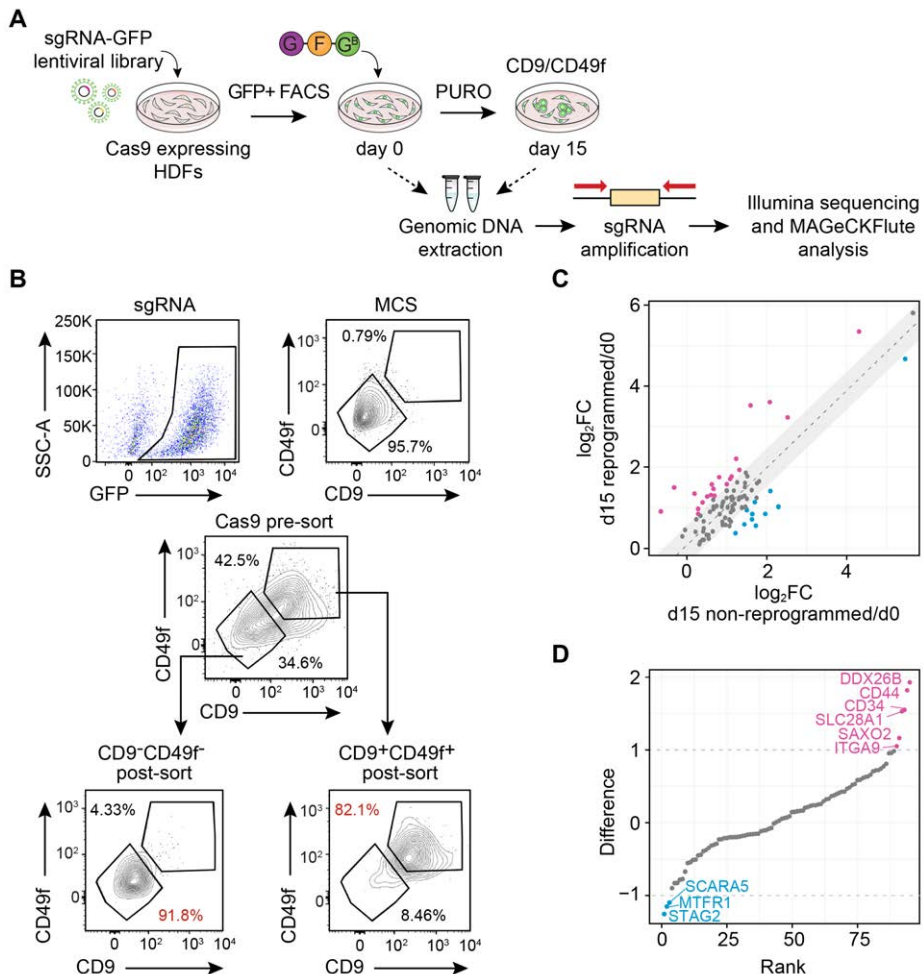


**Figure 3. CRISPR/Cas9 screening identified regulators of hemogenic reprogramming.** **A**, Schematic diagram of the screening strategy. Cas9 expressing human dermal fibroblasts (HDFs) were transduced with the GFP-tagged single guide (sg) RNA library at an MOI of approximately 0.3-0.4, keeping a coverage of at least 300 cells per single guide. Following purification of the GFP<sup>+</sup> population by fluorescence-activated cell sorting (FACS), cells were transduced with the optimized polycystronic vector encoding for GATA2 (G), GFI1B (G<sup>B</sup>) and FOS (F) to allow induction of hemogenic program in fibroblasts. Puromycin (PURO) selection was performed during reprogramming. Genomic DNA samples were extracted from day 0 (no transduction with the SFFV vector) and from day 15 double positive and double negative populations for the hemogenic markers CD49f and CD9. Sequencing library was prepared with a 2-step PCR, starting with the specific amplification of the guides with custom primers. After next-generation sequencing, computational data analysis was performed with MAGeCKFlute pipeline. **B**, Flow cytometry plots showing FACS-isolated populations at day 15 of reprogramming containing the sgRNA library, after antibiotic selection and staining for CD9 and CD49f. MCS serves as negative control. **C**, Median log<sub>2</sub> fold-change (FC) of sgRNA representation. Using day 0 (d0) as baseline for normalization, reprogrammed versus non-reprogrammed samples at day 15 (d15) were compared for enrichment analysis. The grey area delimits the cut-off corresponding to 1 standard deviation. Enriched genes in non-reprogrammed cells are defined as facilitators (blue dots) and enriched genes in reprogrammed cells identify barriers of reprogramming (pink dots). **D**, Rank distribution of candidate genes for hemogenic reprogramming barriers and facilitators according to FC difference between reprogrammed and non-reprogrammed cells.



## Supplementary Information

**Supplementary Table 1.** Information regarding the human dermal fibroblast donors.

ID	Cell type	Provider	Catalog #	Age	Sex
Donor A	Human Dermal Fibroblasts-adult	ScienCell	2320	22	Female
Donor B	NHDF-Ad – Human Dermal Fibroblasts, Adult	Lonza	CC-2511	55	Male
Donor C	Human Dermal Fibroblasts, adult (HDFa)	Gibco	C0135C	40	Female

**Supplementary Table 2.** Candidate genes obtained from the single guide RNA screening. DP – double positive (CD9<sup>+</sup>CD49f<sup>+</sup>) population; DN – double negative (CD9<sup>-</sup>CD49f<sup>-</sup>) population; FC – fold-change.

Gene	EntrezID	DP/day 0 (log <sub>2</sub> FC)	DN/day 0 (log <sub>2</sub> FC)	Difference
SDPR	8436	1.234	1.744	-0.511
MTA1	9112	1.228	0.994	0.234
IGHMBP2	3508	1.409	1.002	0.407
HDAC1	3065	1.596	1.754	-0.158
PRAF2	11230	5.814	5.660	0.154
TMEM141	85014	1.575	0.623	0.952
PLAT	5327	1.317	0.600	0.717
TERT	7015	1.208	1.297	-0.089
MTA3	57504	0.236	0.546	-0.309
CAPRN1	4076	1.186	0.660	0.527
ZNF573	126231	1.423	1.622	-0.199
KDM1A	23028	0.419	0.216	0.202
MRC1	4360	1.499	1.450	0.049
CXXC1	30827	0.366	0.444	-0.078
PDLIM1	9124	1.713	1.081	0.631
SCARA5	286133	0.859	1.961	-1.101
RGR	5995	1.409	1.174	0.235
DDX26B	203522	3.527	1.593	1.934
PPM1H	57460	1.936	1.313	0.623
HMGB3P30	203510	1.278	0.507	0.770
STAG2	10735	1.031	2.290	-1.259
SMC3	9126	0.262	-0.460	0.722
GRK1	6011	1.011	1.466	-0.455
SLC28A1	9154	3.611	2.075	1.536
JARID2	3720	1.298	0.689	0.609
CHEK2	11200	1.272	1.131	0.141
HMHA1	23526	1.238	1.314	-0.077
KCNK9	51305	1.864	1.474	0.390
IGF2BP2	10644	0.898	0.575	0.323
ZNF34	80778	0.605	1.438	-0.833
SMC4	10051	0.096	0.322	-0.227

UBR7	55148	3.234	2.520	0.714
NCAPD2	9918	0.318	0.762	-0.444
ACSM5	54988	1.614	1.455	0.158
TRPV1	7442	1.583	0.999	0.583
TRAPPC13	80006	0.505	0.421	0.084
SMAD2	4087	0.980	0.279	0.701
LTC4S	4056	0.415	0.646	-0.231
TMBIM1	64114	1.005	1.020	-0.014
MED13	9969	0.944	1.160	-0.216
PIK3CA	5290	2.211	1.233	0.978
ITGA9	3680	5.354	4.309	1.045
FMR1	2332	1.086	1.194	-0.107
NCAPH	23397	0.790	1.002	-0.212
FLT3	2322	0.326	0.541	-0.215
SPG11	80208	1.032	0.743	0.289
CD45	5788	0.550	1.067	-0.516
HDAC2	3066	0.574	0.970	-0.395
CEBPA	1050	1.209	1.503	-0.294
RRNAD1	51093	1.654	1.808	-0.155
SH2B3	10019	1.629	1.257	0.372
RNF213	57674	0.708	1.060	-0.352
AMZ1	155185	0.998	1.377	-0.380
CXCR4	7852	1.131	0.392	0.739
USP21	27005	1.022	0.876	0.146
MTFR1	9650	0.569	1.726	-1.156
IL17RA	23765	1.103	0.892	0.211
EREG	2069	1.140	1.698	-0.558
UBA2	10054	0.029	0.771	-0.742
DYSF	8291	1.773	1.119	0.654
RERE	473	0.305	-0.115	0.419
LUC7L2	51631	1.765	1.514	0.252
KRT24	192666	4.677	5.464	-0.787
TOR3A	64222	0.659	1.104	-0.445
TEX14	56155	1.138	0.911	0.227
ENO1	2023	0.109	0.400	-0.291
STAG1	10274	0.950	1.136	-0.186
SAXO2	283726	1.349	0.190	1.159
RP1L1	94137	0.861	0.281	0.581
CLPTM1	1209	0.208	0.388	-0.180
IL17RC	84818	1.413	2.089	-0.676
CDX2	1045	0.328	0.492	-0.164
PRKAR2A	5576	0.652	0.886	-0.234
UROS	7390	0.843	0.821	0.023

TBC1D10C	374403	1.263	1.103	0.161
IL17RB	55540	0.663	0.417	0.246
C14orf119	55017	0.800	0.338	0.462
TXK	7294	0.904	1.098	-0.194
C10orf113	10529	1.414	0.993	0.421
CCDC26	137196	1.469	0.665	0.804
PRPSAP2	5636	0.165	0.333	-0.168
PCDHA4	56144	0.953	1.500	-0.547
OCIAD2	132299	0.857	1.635	-0.778
MKRN2	23609	0.725	1.629	-0.903
SMC1A	8243	0.050	0.252	-0.202
FBXO42	54455	1.757	0.808	0.949
RPL9	6133	-0.071	1.521	-1.592
PTH1R	5745	1.281	1.443	-0.161
PTOV1	53635	1.027	1.138	-0.110
SLC4A3	6508	1.213	1.154	0.059
PSKH1	5681	0.220	0.424	-0.204
MTA2	9219	0.713	0.233	0.480
SMC2	10592	-0.020	0.245	-0.265
APBB2	323	1.194	1.124	0.069
TOM1L1	10040	0.574	0.893	-0.319
BAIAP2L1	55971	1.026	0.667	0.358
DDX6	1656	0.657	0.900	-0.243
BEND4	389206	0.384	1.216	-0.832
RAD21	5885	0.378	0.740	-0.362
FH	2271	0.414	0.407	0.006
RUNX1	861	1.251	1.373	-0.122
PDZD8	118987	0.752	0.955	-0.203
C5	727	0.112	0.313	-0.201
CD44	960	1.501	-0.323	1.824
NCAPG	64151	0.511	0.197	0.314
CHD4	1108	1.165	0.668	0.497
VEZT	55591	0.595	1.022	-0.427
RCOR1	23186	0.327	0.436	-0.109
CD34	947	0.921	-0.635	1.556
CD29	3688	0.466	-0.048	0.515
ACTR6	64431	0.377	0.970	-0.593
RPL23A	6147	0.543	0.617	-0.074
AHR	196	0.980	0.664	0.317

**Supplementary Table 3.** Primer sequences used for cloning.

Plasmid name	Primer name	Sequences
FUW-GATA2	FUW-GATA2_F	GAAGCTTGGGCCCGGGATCCATGGAGGTGGCGCCCGAG
	FUW-GATA2_R	GCTTGATATCGAATGGATCCCTAGCCCATGGCGGTCACCA
FUW-GFI1B	FUW-GFI1B_F	GAAGCTTGGGCCCGGGATCCATGCCACGCTCCTTCCTG
	FUW-GFI1B_R	GCTTGATATCGAATGGATCCTCACTTGAGATTGTGCTGGCTC
FUW-FOS	FUW-FOS_F	GAAGCTTGGGCCCGGGATCCATGATGTTCTCGGGCTTCAACGCA
	FUW-FOS_R	GCTTGATATCGAATGGATCCTCACAGGGCCAGCAGCGT

**Supplementary Table 4.** List of antibodies and dyes used in the study.

Antibody/dye	Application	Supplier	Cat. number
Rabbit anti-GATA2	Western blot	Abcam	ab173817
Rabbit anti-GFI1B	Western blot	CST	5849
Rabbit anti-FOS	Western blot	Sigma	SAB4500995
Rabbit anti-cas9 ( <i>S. pyogenes</i> ) (E7M1H)	Western blot	CST	19526
Rabbit IgG, HRP-linked F(ab') <sub>2</sub> fragment	Western blot	GE Healthcare	NA9340
Rabbit anti-Calnexin	Western blot	Abcam	ab22595
PECy7 anti-human/mouse CD49f (GoH3)	Flow cytometry/FACS	BioLegend	313622
PE anti-human CD9 (HI9a)	Flow cytometry/FACS	BioLegend	312106
APC anti human CD45 (HI30)	Flow cytometry	BioLegend	304037
FITC anti-human CD34 (581)	Flow cytometry	BioLegend	343504
7-Actinomycin D (7-AAD)	Flow cytometry	Becton Dickinson	559525
4', 6-Diamidino-2-Phenylindole (DAPI)	Flow cytometry/FACS	Invitrogen	D3571

**Supplementary Table 5.** Primers used to amplify sgRNAs.

Primer name	Sequences
F_i5_sgLib_NGS_PCR1	TCGTCGGCAGCGTCAGATGTGTATAAGAGACAGATATCTTGTTG AAAGGACGAAACAC
R_i7_sgLib_NGS_PCR1	GTCTCGTGGGCTCGGAGATGTGTATAAGAGACAGTTTCAAGTTG ATAACGGACTAGCC

Paper III






# GATA2 mitotic bookmarking is required for definitive haematopoiesis

Received: 8 August 2022

Accepted: 26 July 2023

Published online: 14 August 2023

 Check for updates

Rita Silvério-Alves<sup>1,2,3,4</sup>, Iliá Kurochkin<sup>1,2</sup>, Anna Rydström<sup>1</sup>,  
Camila Vazquez Echegaray<sup>1,2</sup>, Jakob Haider<sup>1,2</sup>, Matthew Nicholls<sup>5</sup>,  
Christina Rode<sup>5</sup>, Louise Thelaus<sup>1,2</sup>, Aida Yifter Lindgren<sup>1,2</sup>,  
Alexandra Gabriela Ferreira<sup>1,2,3,4</sup>, Rafael Brandão<sup>6</sup>, Jonas Larsson<sup>1,2</sup>,  
Marella F. T. R. de Bruijn<sup>5</sup>, Javier Martin-Gonzalez<sup>6</sup> &  
Carlos-Filipe Pereira<sup>1,2,3</sup> ✉

In mitosis, most transcription factors detach from chromatin, but some are retained and bookmark genomic sites. Mitotic bookmarking has been implicated in lineage inheritance, pluripotency and reprogramming. However, the biological significance of this mechanism *in vivo* remains unclear. Here, we address mitotic retention of the hemogenic factors GATA2, GF1B and FOS during haematopoietic specification. We show that GATA2 remains bound to chromatin throughout mitosis, in contrast to GF1B and FOS, via C-terminal zinc finger-mediated DNA binding. GATA2 bookmarks a subset of its interphase targets that are co-enriched for RUNX1 and other regulators of definitive haematopoiesis. Remarkably, homozygous mice harbouring the cyclin B1 mitosis degradation domain upstream *Gata2* partially phenocopy knockout mice. Degradation of GATA2 at mitotic exit abolishes definitive haematopoiesis at aorta-gonad-mesonephros, placenta and foetal liver, but does not impair yolk sac haematopoiesis. Our findings implicate GATA2-mediated mitotic bookmarking as critical for definitive haematopoiesis and highlight a dependency on bookmarkers for lineage commitment.

Mitosis entails nuclear envelope breakdown and chromatin condensation, leading to RNA polymerase and transcription factor (TF) detachment from chromosomes, bringing transcription down to residual levels<sup>1–3</sup>. Nevertheless, lineage-specific transcriptional patterns must be re-established to preserve cell identity after each cell division. Recently, retention of TFs at mitotic chromatin has emerged as a novel mechanism to convey transcriptional memory from mother to daughter cells<sup>4,5</sup>. In addition to the ability to decorate mitotic chromatin, several TFs were shown to mark specific genomic

sites, a mechanism termed “mitotic bookmarking”<sup>6–8</sup>. Mitotic retention and bookmarking have been investigated in differentiated cell-types<sup>9–12</sup>, embryonic stem cells (ESCs)<sup>13–16</sup>, and more recently in adult stem cells<sup>17</sup>. Depleting TFs at mitosis-to-G1 (M-G1) transition in cell cultures retarded the reactivation of bookmarked genes’ transcription and impaired cell fate acquisition<sup>9,11,12,14,16,18</sup>. However, the importance of the mitotic bookmarking mechanism for *in vivo* lineage commitment during the development of a living organism remains to be addressed.

<sup>1</sup>Molecular Medicine and Gene Therapy, Lund Stem Cell Center, Lund University, BMC A12, 221 84 Lund, Sweden. <sup>2</sup>Wallenberg Centre for Molecular Medicine, Lund University, BMC A12, 221 84 Lund, Sweden. <sup>3</sup>CNC - Centre for Neuroscience and Cell Biology, University of Coimbra, Largo Marquês do Pombal, 3004-517 Coimbra, Portugal. <sup>4</sup>Doctoral Programme in Experimental Biology and Biomedicine, University of Coimbra, Largo Marquês do Pombal, 3004-517 Coimbra, Portugal. <sup>5</sup>MRC Molecular Haematology Unit, MRC Weatherall Institute of Molecular Medicine, Radcliffe Department of Medicine, University of Oxford, OX3 9DS Oxford, UK. <sup>6</sup>Core Facility for Transgenic Mice, Department of Experimental Medicine, University of Copenhagen, Blegdamsvej 3B, 2200 Copenhagen, Denmark. ✉ e-mail: [filipe.pereira@med.lu.se](mailto:filipe.pereira@med.lu.se)

Developmental haematopoiesis is a stepwise process, starting with a first wave in the yolk sac at E7.5, which generates primitive erythrocytes, macrophages and megakaryocytes, followed by a pro-definitive (second) wave of progenitors, including definitive erythromyeloid progenitors (EMPs) and a third wave resulting in the specification of hematopoietic stem cells (HSCs)<sup>19</sup>. Definitive HSCs emerge in the dorsal aorta of the aorta–gonad–mesonephros (AGM) region and placenta at embryonic day (E) 10.5<sup>20</sup>, through an endothelial-to-hematopoietic transition (EHT)<sup>21,22</sup>. Emergent HSCs migrate to the foetal liver and proliferate before colonising the bone marrow, where they remain mainly quiescent<sup>20</sup>. As cell cycle is tightly connected with the specification and maintenance of haematopoietic stem and progenitor cell (HSPC) fate, haematopoiesis provides an attractive biological system to address the role of TF-mediated mitotic bookmarking *in vivo*.

We have previously demonstrated direct reprogramming of mouse<sup>23,24</sup> and human fibroblasts<sup>25,26</sup> to HSPCs by overexpressing the TFs GATA2, GFI1B and FOS. These TFs induced a dynamic hemogenic process, recapitulating EHT and HSC ontogeny<sup>24</sup>. Here, we used fluorescence live-cell imaging combined with chromatin immunoprecipitation sequencing (ChIP-seq) to identify hemogenic factors with bookmarking ability. We then generated a mouse model to assess the role of GATA2-mediated bookmarking *in vivo* during hematopoietic commitment.

## Results

### Mitotic retention of hemogenic factors

To address whether hemogenic TFs display mitotic retention with the potential impact on the specification of definitive haematopoiesis *in vivo* (Fig. 1a), we analysed the subcellular localisation of GATA2, GFI1B and FOS after nocodazole arrest in transduced human dermal fibroblasts (HDFs) and HEK 293T cells (Fig. 1b, Supplementary Fig. 1a–c). GATA2 protein was detected in the nuclear fractions (soluble nucleus and chromatin-bound), in contrast to GFI1B, which was mainly present in the cytoplasmic and soluble nucleus fractions. FOS was almost exclusively present in the cytoplasmic fraction in both mitotic and asynchronous cells, indicating an overall weak binding to chromatin throughout the cell cycle<sup>25</sup>. These results suggest that mitotic retention is determined by the intrinsic DNA binding ability of each transcription factor. In addition, we overexpressed each TF fused to an mCherry fluorescent protein and addressed mitotic retention by live-cell imaging. GATA2 colocalised with chromatin during all phases of mitosis, while GFI1B was enriched at later stages (starting at anaphase) and FOS was completely excluded from chromatin in human fibroblasts (Fig. 1c, Supplementary Movies 1–3), mouse fibroblasts (Supplementary Fig. 1d) and K562 cells (Supplementary Fig. 1e). Positioning mCherry at the N- or C-terminal regions resulted in similar mitotic retention patterns (Supplementary Fig. 1f). Mitotic chromatin enrichment was significantly higher for GATA2 (Fig. 1d). Nevertheless, the stage-specific retention of GFI1B at anaphase highlights differential retention kinetics of mitotic bookmarking factors (Fig. 1c, Supplementary Fig. 1d, e). To exclude bias derived from overexpression, we verified mitotic retention of endogenous TFs in K562 cells (Fig. 1e, Supplementary Fig. 1g). As expected, the three TFs showed similar retention profiles, confirming robust GATA2 mitotic retention. Importantly, TF mitotic retention ability did not correlate with absolute mRNA or protein levels of endogenous or overexpressed TFs (Fig. 1f–h). Since GATA2, GFI1B and FOS cooperate during hemogenic reprogramming<sup>25</sup>, we reasoned that co-expression could increase the retention of excluded factors. However, neither GFI1B nor FOS showed increased chromatin enrichment when co-expressed with GATA2 or with the two additional factors (Fig. 1i, j, Supplementary Fig. 1h). These results suggest that mitotic retention is an intrinsic feature of GATA2 that is not dependent on TF cooperation, protein abundance or cellular context.

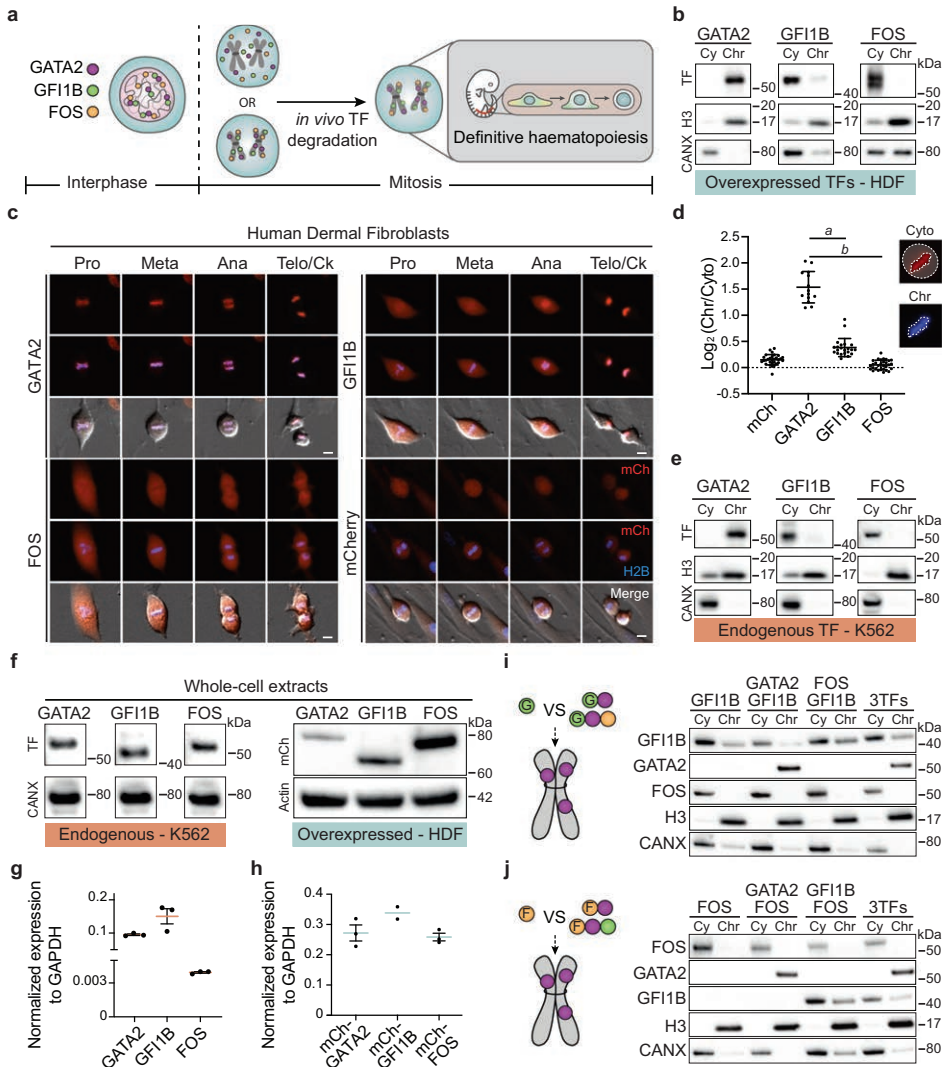
### GATA2 mitotic retention requires DNA binding

We proceeded to dissect the protein domains required for GATA2 mitotic retention. The DNA-binding domain of GATA2 comprises an N-terminal zinc finger (N-ZF) and a C-terminal zinc finger (C-ZF) with homologous sequences, but different functions (Fig. 2a). The N-ZF has been implicated in stabilising DNA-protein complexes, whereas the C-ZF recognises and binds GATA consensus sequences<sup>27</sup>. To define domains required for mitotic retention, we generated mCherry-GATA2 deletion constructs lacking N-terminal, N-ZF, C-ZF and nuclear localisation signal (NLS). Interestingly, GATA2 was reduced from chromatin-bound protein fraction when the C-ZF, but not the N-ZF was deleted (Fig. 2b–d Supplementary Fig. 2a). The deletion of the NLS also led to the reduction of mitotic retention as assessed by imaging and subcellular fractionation followed by western blotting. This may reflect the requirement of active nuclear import, as previously described for SOX2<sup>23</sup>. However, since we detected GATA2 in the interphasic nucleus in the absence of the NLS (Fig. 2b), it is also possible that this deletion disturbs adjacent C-ZF functions. To confirm the requirement of C-ZF for mitotic retention, we selected GATA2 point mutations commonly found in leukemic and Emberger syndrome (ES) patients that influence DNA-binding affinity (Fig. 2a)<sup>28–30</sup>. C-ZF mutations associated with Acute Myeloid Leukaemia (AML) and/or ES that reduce DNA-binding affinity<sup>28,30</sup>, including R396Q, R398W, T354M, R361L, and C373R, showed reduced GATA2 mitotic retention by fluorescent microscopy (Fig. 2e, Supplementary Fig. 2c–j, Supplementary Movie 4), suggesting that DNA-binding is necessary for GATA2 mitotic chromatin retention. L359V, which is described to increase the DNA-binding affinity of GATA2<sup>31</sup> and R362Q, which has a modest impact in binding affinity<sup>28</sup>, did not display impaired mitotic retention (Fig. 2e, Supplementary Fig. 2e, g, Supplementary Movie 5). Quantification of chromatin-associated GATA2 by western blotting revealed decreased GATA2 chromatin binding in both mitotic and asynchronous cells for GATA2 mutations that have reduced DNA-binding affinity, particularly T354M, R361L and C373R (Fig. 2e, f, Supplementary Fig. 2b). In addition to DNA-binding perturbations, mutations in GATA2 may introduce complex conformational changes and modifications in protein stability, making it difficult to reveal mitosis-specific effects with this approach. Interestingly, both L359V and C373R mutants failed to efficiently reprogram HDFs to hemogenic cells (Fig. 2g), indicating that an intact C-ZF is critical for GATA2's reprogramming function and a different approach is necessary to uncover the role of GATA2 in mitosis. In agreement with its less important function for DNA binding, N-ZF mutations did not impact GATA2 mitotic retention (Supplementary Fig. 3). Taken together, these data suggest that GATA2 mitotic retention requires DNA-binding mediated by the C-ZF domain.

### GATA2 bookmarks key HSPC regulators

Next, we examined the genome-wide occupancy of endogenous GATA2 in asynchronous and fluorescence-activated cell sorting (FACS)-purified mitotic K562 cells using ChIP-seq. K562 cells were double-fixed (Supplementary Fig. 4a–d) prior to sorting to reduce potential artefacts caused by formaldehyde-only fixation<sup>13,32</sup>. Our analysis showed that GATA2 binds to a subset (1,598 peaks) of interphase target sites during mitosis, confirming bookmarking activity (Fig. 3a). The overall number of mitotic peaks was comparable to the pluripotency regulator ESRRB (1980 peaks)<sup>15</sup>. Bookmarked sites accounted for 15.3% of interphase genes including *GATA2* auto-regulation, the key regulator of definitive haematopoiesis *RUNX1*<sup>33</sup> and the HSC marker *CD9*<sup>34</sup> (Fig. 3b, Supplementary Fig. 4e, Supplementary Data 2). Since mitotic-unique peaks were scarce (42), had low read coverage, and were not located at genes with a known function in haematopoiesis, these were not included in further analyses. To investigate the differences in binding affinity of GATA2, we performed K-means clustering of asynchronous peaks, which resulted in three clusters (Fig. 3c). Most mitotic (bookmarked) peaks (71%) were assigned to





cluster 1, which contained a small fraction (9.5%) of GATA2 peaks in asynchronous cells with the highest peak intensities, suggesting that GATA2 bookmarks sites with high TF affinity. Cluster 3 accounted for only 3% of overlapped peaks (44 peaks) and, therefore, was excluded in further analyses. Next, we looked at the density of binding sites, by calculating the number of GATA2 binding motifs per peak in each group (Fig. 3d). Interestingly, mitotic peaks contained a significantly higher number of GATA2 motifs when compared to asynchronous peaks (KS test,  $p$ -value  $< 0.05$ ). This observation implies that GATA2 mitotic bookmarking is influenced by a pre-existing motif structure, where increased number of binding sites translates into higher chromatin engagement in mitosis. We then performed

peak enrichment analysis based on asynchronous, mitotic, and mitotic clusters (Supplementary Fig. 4f, Supplementary Data 2). Gene Ontology Biological Processes showed co-enriched terms including “immune system development” ( $p$ -value =  $2.4 \times 10^{-7}$ ,  $1.2 \times 10^{-3}$  and  $8 \times 10^{-4}$  in asynchronous, mitotic and cluster 1, respectively), “hematopoietic or lymphoid organ development” ( $p$ -value =  $1.2 \times 10^{-6}$ ,  $4.8 \times 10^{-3}$  and  $3.4 \times 10^{-3}$ ) and “hemopoiesis” ( $p$ -value =  $1.0 \times 10^{-5}$ ,  $2.7 \times 10^{-2}$  and  $2.7 \times 10^{-2}$ ). Moreover, motif enrichment analysis revealed that mitotic peaks were enriched for GATA, RUNX, and ETS motifs (Fig. 3e, Supplementary Fig. 4g), suggesting that GATA2 cooperates in mitosis with hematopoietic regulators. Therefore, we investigated TF cooperation in asynchronous and mitotic cells with other important

**Fig. 1 | GATA2 is retained at mitotic chromatin independently of cell context.**

**a** Experimental approach to address mitotic bookmarking function of the hemogenic reprogramming transcription factors (TFs) GATA2, GFII1B and FOS, and their role in vivo for definitive haematopoiesis. **b** TF expression in the cytoplasmic (Cy) and chromatin-bound (Chr) protein fractions of mitotic human dermal fibroblasts (HDFs) expressing the indicated TF. Histone 3 (H3) and calnexin (CANX) were used as loading controls. kDa, kilodaltons. **c** Live-cell images of HDFs overexpressing mCherry (mCh)-TFs fusion proteins (red) during mitosis (Pro – prophase, Meta – metaphase, Telo/Ck – Telophase/Cytokinesis). Histone 2B (H2B)-mTurquoise (blue) signal shows DNA content. Mitotic events: n(GATA2) = 48, n(GFII1B) = 24, n(FOS) = 30, n(mCherry) = 137. Scale bars, 10  $\mu$ m. **d** Quantification of the ratio between signal intensity of chromatin-retained and cytoplasm-localised TFs in metaphasic HDFs. n(mCherry) = 30, n(GATA2) = 14, n(GFII1B) = 22, n(FOS) = 30. Mean  $\pm$  SD is represented. Statistical significance was analysed by one-way ANOVA followed by Bonferroni's multiple comparison test. *a* and *b*,  $p < 0.001$ .

**e** Endogenous expression of GATA2, GFII1B and FOS in cytoplasmic and chromatin-bound fractions of mitotic K562 cells. H3 and CANX were used as loading controls. **f** Protein expression from asynchronous HDFs (overexpressed TFs, right panel) and K562 (endogenous TFs, left panel) whole-cell extracts. HDFs were transfected with mCh-TFs and the same number of mCh<sup>+</sup> cells were FACS-purified for western blotting. CANX and Actin were used as loading controls. **g** Transcript levels of each endogenous TF in K562 cells.  $n = 3$  biological independent samples per condition. Expression was normalised to GAPDH. **h** Transcript levels for overexpressed mCh-TFs in mCh<sup>+</sup> FACS-purified HDFs. n(mCh-GATA2) = 3 technical replicates, n(mCh-GFII1B) = 2 technical replicates. (mCh-FOS) = 3 technical replicates. **g, h** Mean  $\pm$  SD is represented. Expression was normalised to GAPDH. **i, j** Protein levels of GATA2, GFII1B and FOS in Cy and Chr fractions of mitotic HEK 293T cells when GFII1B (**i**) or FOS (**j**), were transfected individually or in combination with one or two additional TFs. Western blots were performed twice. Source data are provided as a Source Data file.

factors for haematopoiesis and HSPC specification, including the “heptad” TFs TAL1, LYL1, RUNX1, ERG, and FLII<sup>35</sup>, plus PU.1 (SPI1), MYB<sup>35</sup>, PBX<sup>36</sup>, GFII1B, FOS, HES1<sup>37</sup>, MEIS1<sup>35</sup> and HLF<sup>36</sup> (Fig. 3f). We observed a high degree of motif co-occurrence at GATA2 mitotic peaks particularly for PU.1, “heptad” TFs, RUNX1 and FOS, implying that TF complexes and cooperativity with GATA2 is maintained during mitosis. This was confirmed by integration with available ChIP-seq data<sup>38,39</sup>, which demonstrated a high degree of overlap between GATA2 mitotic peaks and the binding sites for RUNX1, PU.1, FOS, and TAL1 (Fig. 3g). We then inspected the genomic distribution of asynchronous and mitotic GATA2 peaks. Overall, GATA2 genomic distribution was retained in mitosis, with preference for promoters and active enhancers (Fig. 3h, Supplementary Fig. 4h). Interestingly, we observed a 1.8- and 2.2-fold binding decrease at “weak enhancer” (EnhWk, marked by H3K4me1) and “bivalent enhancer” (EnhBiv, marked by H3K4me1 and H3K27me3) chromatin states respectively, attributed to lower mitotic retention at sites decorated with H3K4me1 (Fig. 3i, j, Supplementary Data 2). Besides the potential biological role, the reduction of H3K4me1 also confirms that bookmarked sites are not derived from contamination with asynchronous cells. Furthermore, we integrated our data with histone marks and chromatin accessibility data (DNase-seq and ATAC-seq) available for K562 cells from ENCODE project<sup>38</sup> (Fig. 3i, j, Supplementary Data 2). In addition to H3K4me1, H3K36me3 and H4K20me1, which are associated with transcriptional elongation, also showed lower abundance at mitotic peaks<sup>40</sup>. Regarding accessibility to nucleases, we did not find major differences between mitotic and asynchronous peaks, especially when looking at cluster 1 mitotic peaks, suggesting that chromatin accessibility does not represent a barrier for mitotic bookmarking<sup>41</sup>. Altogether, our results show that GATA2 bookmarks critical regulators of HSPC specification and function.

**Bookmarking is critical in vivo**

Next, we utilised the mitotic degradation (MD) domain of cyclin B1<sup>41,46</sup> to assess the role of GATA2-mediated mitotic bookmarking. Substitution of arginine for an alanine (R42A) inactivates the domain (MD<sub>mut</sub>)<sup>41</sup> and results in similar protein levels throughout the cell cycle. We assessed protein levels of MD- or MD<sub>mut</sub>-GATA2 constructs before and after release from nocodazole arrest, using degradation of cyclin B1 as a control for mitotic degradation. While cyclin B1 was quickly degraded after nocodazole release, we observed induced GATA2 protein degradation over time, with the highest impact on MD-GATA2 degradation at 4 hours, increased protein levels after 6 hours and returning to MD<sub>mut</sub>-GATA2 levels in asynchronous cells (Fig. 4a, Supplementary Fig. 5a). For better resolution of protein degradation during specific phases of cell cycle, we fused the MD or MD<sub>mut</sub> domains to an mTurquoise fluorescent protein and observed mTurquoise signal reduction by flow cytometry at both mitosis and G1 phases (Supplementary Fig. 5b–d).

To gain initial insight regarding the role of GATA2 at M-G1 transition for HSPC generation, we induced hemogenic reprogramming in HDFs with MD-GATA2 or MD<sub>mut</sub>-GATA2, in combination with GFII1B and FOS<sup>25,26</sup> (Fig. 4b). We observed that expression of the surface marker CD9, an early marker of hemogenic reprogramming<sup>25,26</sup> which is also bookmarked by GATA2 (Supplementary Fig. 4e), was delayed when GATA2 was degraded at M-G1 transition (Fig. 4c), highlighting the importance of GATA2 mitotic bookmarking for hemogenesis. To uncover the transcriptional impact of degrading GATA2 at M-G1 transition, we employed single-cell RNA-sequencing (scRNA-seq) at early stages of hemogenic reprogramming. We profiled 32,773 cells derived from untransduced HDFs (two independent donors), and 4 and 6 days after induction of hemogenic reprogramming. We first confirmed that cells derived from the two donors undergo similar transcriptional changes using Uniform Manifold Approximation and Projection (UMAP) (Supplementary Fig. 5e–g) and in agreement with flow cytometry data, CD9 expression was delayed when reprogramming was induced with MD-GATA2 (Supplementary Fig. 5h). To investigate the differences between the transcriptional program in MD-GATA2 and MD<sub>mut</sub>-GATA2 reprogrammed cells, we performed differential gene expression analysis (Supplementary Data 3) focusing on GATA2 bookmarked targets (Fig. 4d). This analysis revealed that 28 and 75 genes were downregulated, and 18 and 37 genes were upregulated at day 4 and 6 respectively, when GATA2 was degraded at mitotic exit, pointing to a role of GATA2 at M-G1 in the activation of the hematopoietic program during reprogramming. Downregulated genes with MD-GATA2 included *ZBTB16*, an epigenetic regulator of HSC fate<sup>41</sup> and *TEAD1* which helps driving hematopoietic specification<sup>42</sup>. Reassuringly, genes that require GATA2 at mitotic exit during reprogramming were predicted to be regulated by GATA2 with ChIP Enrichment Analysis (ChEA, Supplementary Data 3), and contained GATA2 motifs, as well as motifs of other hematopoietic TFs (Fig. 4e). We observed high enrichment with the “heptad” TFs members, especially at day 6, suggesting their cooperative action also in mitosis to impose hemogenic fate.

To address the role of GATA2 bookmarking in vivo, we generated a mouse model where the MD domain was inserted upstream the *Gata2* gene via CRISPR-Cas9 (Fig. 4f, Supplementary Fig. 6a). The insertion of MD in both *Gata2* alleles resulted in lethality, as homozygous pups could not be generated from two independent injections of edited ESCs (Supplementary Fig. 6b) or by crossing heterozygous mice (Fig. 4g). Remarkably, MD homozygous mice died at the onset of definitive haematopoiesis, between E10.5 and E11.5 (Fig. 4g, h, Supplementary Fig. 6c), phenocopying *Gata2* knockout mice<sup>43</sup>. When we compared the expected Mendelian ratios, we found higher frequencies of wild-type (WT) mice at the expense of heterozygous mice, particularly at E10.5 (observed 44% vs expected 25%), E13.5 (observed 45%) and postnatally (observed 49%) (Fig. 4g), suggesting a more profound impact in MD-*Gata2* mice when compared to *Gata2* full

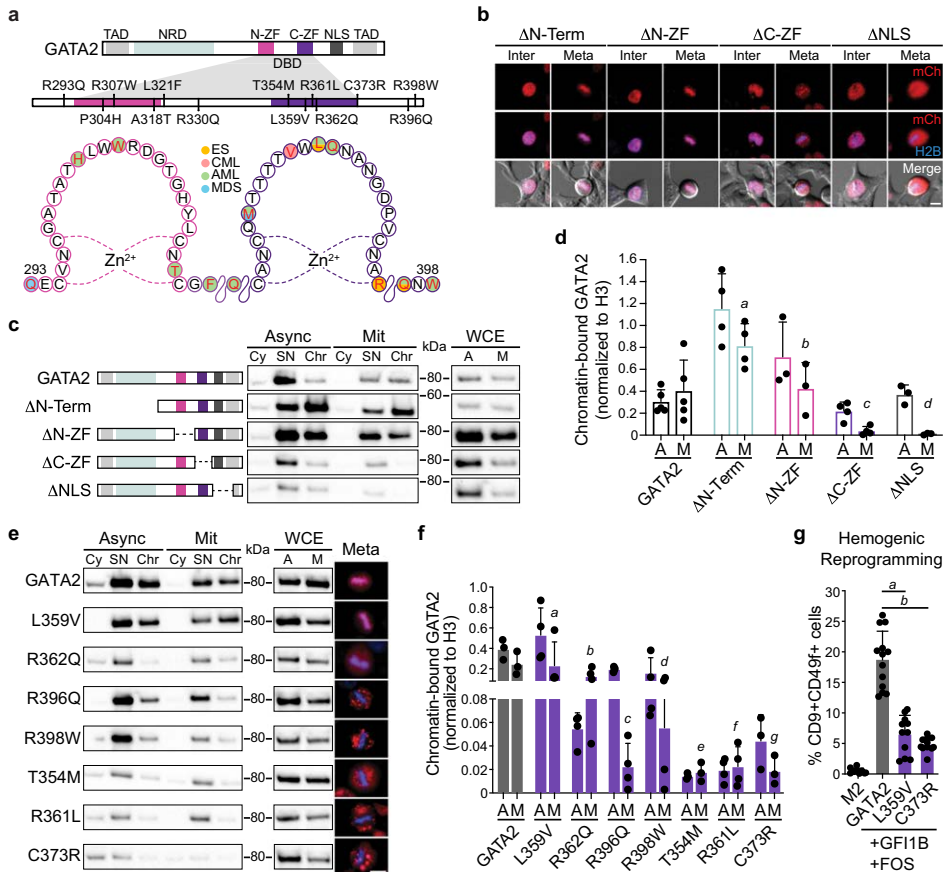
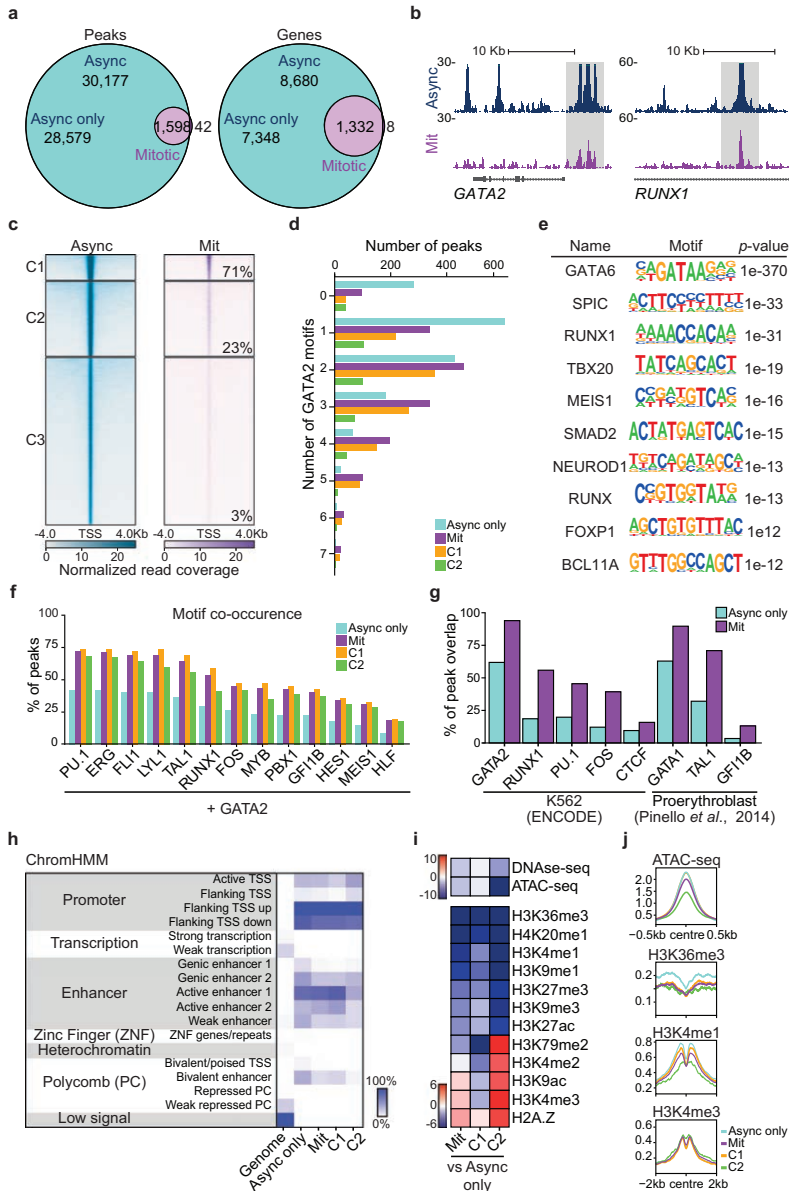


**Fig. 2 | Point mutations in GATA2 C-terminal zinc finger associated with leukaemia and Emberger syndrome reduce mitotic retention.** **a** Representation of GATA2 domains highlighting leukaemia and Emberger syndrome (ES)-associated point mutations in the N- and C-terminal zinc fingers (ZF) of DNA-binding domain (DBD). TAD – transactivation domain. NRD – negative regulatory domain. NLS – nuclear localisation signal. CML – chronic myeloid leukaemia. AML – acute myeloid leukaemia. MDS – myelodysplastic syndrome. **b** Live-cell images of 293T cells overexpressing mCherry (mCh)-GATA2 deletion ( $\Delta$ ) constructs (red) excluding the N-terminal (amino acids 1–235), N-ZF (287–342), C-ZF (243–379) or NLS (380–440) in interphase (Inter) and metaphase (Meta). Mitotic events: n( $\Delta$ N-Terminal) = 395, n( $\Delta$ N-ZF) = 375, n( $\Delta$ C-ZF) = 100, n( $\Delta$ NLS) = 52. Scale bar, 10  $\mu$ m. **c**, Protein expression in whole-cell extracts (WCE), cytoplasmic (Cy), soluble nucleus (SN) and chromatin-bound (Chr) fractions of both asynchronous (A, Async) and mitotic (M, Mit) 293T cells overexpressing deletion constructs. Representative blots were acquired with the same exposure time for asynchronous and mitotic cells. kDa, kilodaltons. **d**, Western blot quantifications of GATA2 deletions at Chr fraction in asynchronous and mitotic cells after normalising to H3. n(GATA2) = 5, n( $\Delta$ N-Term)

= 4, n( $\Delta$ N-ZF) = 3, n( $\Delta$ C-ZF) = 4, n( $\Delta$ NLS) = 3. Statistical analysis performed by two-way ANOVA followed by Fisher's LSD test and comparisons of mitotic retention of each deletion to GATA2 are shown. *a*,  $p = 0.005$ ; *b*,  $p = 0.89$ , *c* and *d*,  $p = 0.01$ . **e** Protein expression of mCherry-fused GATA2 mutants in the Cy, SN and Chr protein fractions of asynchronous and mitotic 293T. Representative cells in metaphase are shown (right). Histone 2B (H2B)-mTurquoise signal (blue) indicates DNA content. Scale bar, 10  $\mu$ m. **f** Quantification of GATA2 mutants at Chr fraction. n(GATA2) = 3, n(L359V) = 4, n(R362Q) = 4, n(R396Q) = 4, n(R398W) = 4, n(T354M) = 3, n(R361L) = 4, n(C373R) = 3. Statistical analysis performed by two-way ANOVA followed by Fisher's LSD test and comparisons of mitotic retention of each mutant to GATA2 are shown. *a*,  $p = 0.86$ ; *b*,  $p = 0.17$ , *c* and *f*,  $p = 0.01$ ; *d*,  $p = 0.03$ ; *e* and *g*,  $p = 0.02$ . **g** Hemogenic reprogramming efficiency (% CD9<sup>+</sup>CD49<sup>+</sup> cells) with GATA2, L359V or C373R, plus GF1B and FOS. M2rtTA (M2) was used as control. n(M2) = 10, n(GATA2) = 13, n(L359V) = 11, n(C373R) = 11. Mean  $\pm$  SD is represented. Statistical significance was analysed by one-way ANOVA followed by Bonferroni's test. *a* and *b*,  $p < 0.001$ . Source data are provided as Source Data file.

knockout model which showed near-Mendelian ratios (29%)<sup>43</sup>. This might be explained by an allelic bias in MD-*Gata2* heterozygous mice resulting in preferential expression of MD over the WT allele (Supplementary Fig. 6d). Morphological analysis of E10.5 and E11.5 MD-*Gata2* embryos showed that MD/MD embryos were smaller and paler,

particularly at E11.5, with evident lack of blood (Fig. 4h, Supplementary Fig. 6e). This contrasted with insertion of MD<sub>int</sub> upstream the *Gata2* gene, which did not hamper embryonic development (Fig. 4h, Supplementary Fig. 6f, g). As an additional control, we have confirmed that the MD-GATA2 protein was expressed in vivo by western blotting on



heterozygous E9.5 yolk sac-derived hematopoietic colonies (Supplementary Fig. 6h). Flow cytometry analysis of MD-*Gata2* embryonic erythroblasts showed premature erythroid maturation at E10.5 (Fig. 4i, Supplementary Fig. 6i), resulting in severe anaemia at E11.5 (Fig. 4j). Our results illustrate the critical importance of GATA2 at M-G1 transition for embryonic development.

### Definitive haematopoiesis requires bookmarking

Definitive HSPCs emerge in intra-aortic hematopoietic clusters (IAHCs) positive for RUNX1 and the endothelial marker CD31<sup>33,44</sup>. To assess the impact of GATA2 degradation at M-G1 transition in definitive haematopoiesis, we first analysed embryos and cluster formation by whole-embryo mounting followed by immunohistochemistry. We observed

**Fig. 3 | GATA2 bookmarks a subset of interphasic target genes with roles in definitive haematopoiesis.** **a** Venn diagram showing the number of ChIP-seq GATA2 peaks and genes shared between asynchronous (Async) and mitotic K562 cells. Async only refers to non-bookmarked peaks and genes in asynchronous cells. **b** Gene tracks for GATA2 binding sites at *GATA2* and *RUNX1* loci showing both mitotic (Mit) bookmarked (grey) and asynchronous unique peaks. Kb – kilobase. **c** K-means clustering of Async (left) and Mit peaks (right). The percentage of mitotic (bookmarked) peaks overlapping with asynchronous peaks in each cluster is shown. The 42 mitotic-unique peaks are not shown. **d** Number of GATA2 motifs in Async only peaks, mitotic peaks and mitotic clusters 1 (C1) and 2 (C2). **e** De Novo motif enrichment analysis for GATA2 mitotic bookmarked target sites. Top ten

motifs are shown with respective p-values. **f** Percentage of GATA2 peaks where motifs for relevant HSPCs regulators are also present. **g** Percentage of overlap between GATA2 peaks and peaks for HSPC regulators from available ChIP-seq datasets. **h** Chromatin-state enrichment heatmap representing the percentage of genome occupancy of GATA2 per group of peaks. Scale represents the percentage of peaks at each genomic segment. TSS – Transcription start site. **i** Integration heatmap with histones marks, DNase-seq and ATAC-seq data for K562 cells (ENCODE). Scale represents the accumulated sum differences across bins between Async only and mitotic peaks and clusters. **j** Histone marks and ATAC-seq profiles at peak summit (centre). Source data are provided as Source Data file.

an abolishment of hematopoietic clusters in the ventral region of the dorsal aorta and severe reduction at the dorsal region in MD homozygous embryos at E10.5 (Fig. 5a, b). Also, although the number of wild-type and heterozygous clusters was similar, heterozygous clusters were overall smaller. Interestingly, at E9.5, RUNX1 was unchanged, particularly in the vitelline artery where expression is stronger at this developmental stage<sup>33</sup> (Supplementary Fig. 7a). To assess HSPC function, we performed colony-forming unit (CFU) assays. At E9.5 the number of colonies obtained from yolk sacs were comparable between genotypes (Fig. 5c), suggesting that yolk sac progenitors are not affected by the loss of GATA2 at M-G1 transition. Indeed, the percentage of CD41<sup>+</sup>c-kit<sup>+</sup>Ter119<sup>+</sup> s in the yolk sac was similar between groups (WT/WT, 5.40 ± 1.43%; MD/WT, 3.88 ± 1.00%; MD/MD, 4.08 ± 0.45%) (Supplementary Fig. 7b). This result comes in contrast to *Gata2* full or conditional knockout models where both AGM and yolk sac haematopoiesis were shown to be impaired<sup>43,45</sup>. When we investigated E10.5 embryos, we observed a decrease in the number of hematopoietic colonies derived from AGM, placenta and foetal liver by 2.9-, 4.6- and 3.2-fold, respectively, when compared to WT (Fig. 5d). This effect was even more striking at E11.5, with colony numbers reduced by 16- and 8-fold in AGM and placenta, respectively, when compared to MD<sub>mit</sub> homozygous mice (Fig. 5e). These results reflect the lack of RUNX1<sup>+</sup>CD31<sup>+</sup> hematopoietic clusters at E10.5 and illustrate the requirement of GATA2 at mitotic exit for definitive haematopoiesis. We then investigated the generation of HSPCs by transplantation of E11.5 placenta cells into sublethal irradiated CD45.1 or CD45.1/2 recipient mice (Supplementary Fig. 8a). While wild-type and heterozygous mice engrafted irradiated recipients, placental HSPCs from MD homozygous mice did not show long-term engraftment (6 months) in peripheral blood or bone marrow (Fig. 5f–h, Supplementary Fig. 8b). Short-term engraftment (4 weeks) was observed in 2 out of 8 mice (4.1% and 4.4% CD45.2<sup>+</sup> cells), but these cells did not contribute to either myeloid or lymphoid lineages (Supplementary Fig. 8c). Since we could not observe significant differences in IAHC numbers or in embryonic HSPC function between wild-type and heterozygous mice, we evaluated adult heterozygous HSC function. Therefore, we performed competitive transplantation with bone marrow LSK-SLAM HSCs (Lineage Kit<sup>+</sup>Sca-1<sup>+</sup>CD150<sup>+</sup>CD48<sup>+</sup>) from adult mice (Supplementary Fig. 8d, e). GATA2 haploinsufficiency (heterozygous from full *Gata2* knockout) translates into reduced engraftment of bone marrow HSCs<sup>46</sup>. Likewise, we observed reduced engraftment capacity of MD-*Gata2* heterozygous HSCs from adult bone marrow (Fig. 5i–k), suggesting a role for GATA2 mitotic bookmarking not only in HSC specification but also in HSC maintenance. Altogether, these results demonstrate that GATA2 is essential in vivo at M-G1 transition for definitive haematopoiesis. We propose that GATA2 remains bound to key hematopoietic genes during mitosis through its C-ZF domain, cooperating with HSPC regulators to allow faithful commitment of definitive HSPCs during embryonic development (Fig. 5l).

## Discussion

We show the hemogenic TF GATA2 remains bound to chromatin throughout mitosis, independently of cellular context or absolute

protein levels, and bookmarks important HSPC regulators. Abolishing GATA2 during M-G1 transition arrests embryonic development at the onset of definitive haematopoiesis. Unexpectedly, we also found that GFI1B was retained in a mitotic phase-specific manner starting from anaphase. The ability to bind to mitotic chromatin has been mainly associated with non-specific binding mediated by electrostatic interactions between TFs and DNA<sup>42,47</sup>, where amino acid polarity and absolute charge per DNA-binding domain were predicted to play a major role<sup>42</sup>. While differences in electrostatic forces might explain the differences in enrichment capabilities of TFs, the kinetics of this process requires further exploration. The pro-neural TF ASCL1 was shown to decorate mitotic chromatin in late telophase<sup>47</sup>, due to nuclear import at the time of nuclear envelope reassembling. The association of TFs at anaphase, as we report for GFI1B, illustrates stage-specific mitotic chromatin retention and may be controlled by independent mechanisms.

GATA2 binds DNA through its zinc finger domains. Removal of the C-terminal zinc finger (C-ZF) of the DNA-binding domain reduced mitotic retention of GATA2, while deletion of the N-terminal region or the N-terminal zinc finger (N-ZF) of the DNA binding domain did not. This may be due to the different functions of the zinc fingers<sup>27</sup>, but nonetheless suggests that mitotic retention requires DNA binding, in agreement with previous studies<sup>13,15,17</sup>. We used mutations commonly found in patients with leukaemia, myelodysplastic syndrome (MDS) and ES, that were reported to interfere with DNA-binding affinity of GATA2, to implicate the requirement for the C-ZF, but not the N-ZF for mitotic retention. Patients with N-ZF mutations have better clinical outcomes, than patients with C-ZF mutations<sup>48</sup> and N-ZF mutants reduce, but do not abolish, chromatin occupation and transcriptional activation by GATA2<sup>29</sup>. C-ZF mutations impact GATA2 DNA-binding affinity at different levels: L359V (CML) shows increased affinity<sup>31</sup>, R362Q (AML) has modest to no impact in binding affinity, T354M and R398W (AML/MDS) show moderate reduction in affinity to DNA and the ES mutations R361L, C373R and R396Q result in little to no DNA binding, as evaluated by EMSA<sup>28,30</sup>. However, the nature of these interactions is not completely clear (specific versus non-specific binding), as C-ZF and contiguous residues of GATA proteins form both direct hydrogen bonds and Van der Waals contacts with DNA bases<sup>49</sup>. Of note, NLS deletion (amino acids 380-440) includes the R396 and R398 residues, which may explain the impact observed in mitotic retention. Although GATA2 mitotic retention mediated by DNA binding is probably regulated by electrostatic forces, as described for many TFs<sup>42,47</sup>, sequence-specific interaction cannot be discarded, particularly since we show that GATA2 binds to a subset of its interphase targets in mitosis, making it a bona fide mitotic bookmarking factor. Our findings underscore a potential unappreciated role of disruption of mitotic retention in human disease.

Among GATA2 bookmarked genes, we found several members of the “heptad” TFs (*ERG*, *GATA2*, *LMO2*, *LYL1*, *RUNX1*) that regulate gene expression and function in HSPCs<sup>35</sup>. Indeed, GATA2-bound sites are enriched for GATA, PU.1 and RUNX1 motifs, suggesting cooperation in mitosis between GATA2 and other key hematopoietic regulators. Bookmarked sites showed biologically

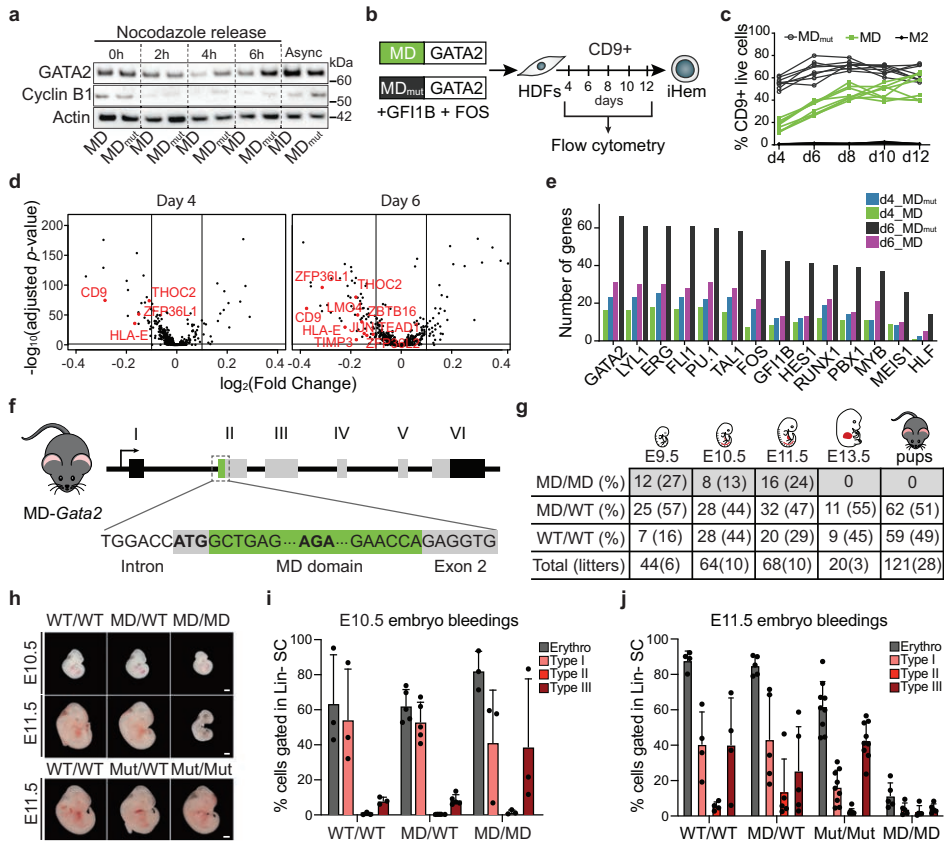


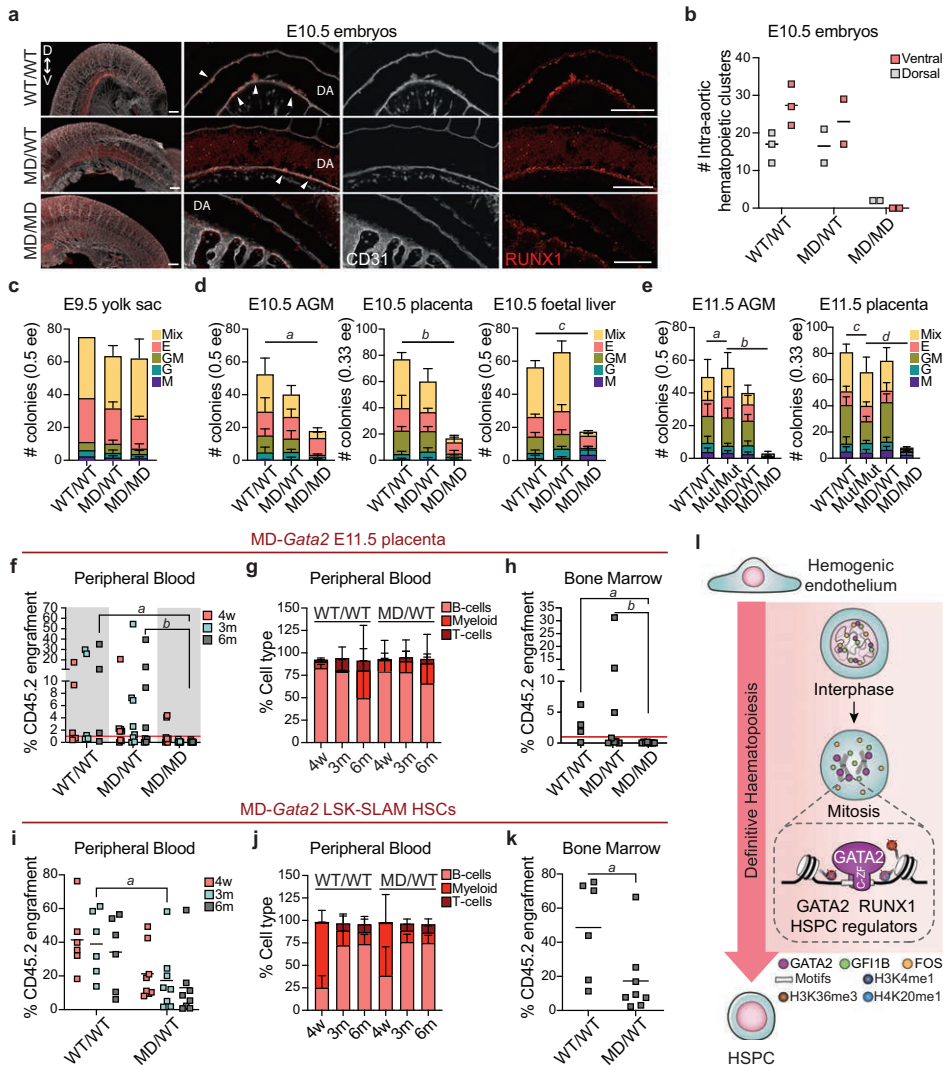
**Fig. 4 | GATA2 is required at the mitosis-to-G1 transition in vivo for embryonic development.** **a** Western blot analysis of GATA2 and cyclin B1 proteins in HEK 293T expressing GATA2 fused to the mitotic degradation (MD) domain of cyclin B1 or an inactive form (MD<sub>mut</sub>) before (0h) and 2, 4 and 6 hours (h) after release from nocodazole arrest. Actin shown as loading control. Async – Asynchronous cells. Western blots were performed twice. kDa, kilodaltons. **b** Direct reprogramming strategy to convert human dermal fibroblast (HDFs) into induced homogenic cells (iHem). HDFs were transduced with lentivirus encoding MD- or MD<sub>mut</sub>-GATA2, plus GF1B and FOS factors, and the kinetics of CD9 activation was evaluated by flow cytometry. CD9 expression from day (d) 4 to d12. M2rTA (M2) was used as control. **c** Quantification of CD9 expression from day (d) 4 to d12. M2rTA (M2) was used as control. **d** Volcano plots showing differential gene expression of GATA2 bookmarked genes at day 4 and 6 of reprogramming with MD-GATA2 and MD<sub>mut</sub>-GATA2. Relevant genes downregulated in MD-GATA2 condition (left) are highlighted in red. **e** Number of bookmarked differentially expressed genes between MD-GATA2 and MD<sub>mut</sub>-GATA2 conditions at d4 and d6, with binding sites

for HSPC regulators. Upregulated genes in MD<sub>mut</sub>-GATA2 condition at d4 and d6 (d4\_MD<sub>mut</sub> and d6\_MD<sub>mut</sub>, respectively), and upregulated genes in MD-GATA2 at d4 and d6 (d4\_MD and d6\_MD, respectively) are shown. **f** Schematic representation of the mouse model developed to assess mitotic degradation of GATA2 in vivo by inserting the MD domain upstream *Gata2* gene. **g** Frequency of homozygous (MD/MD), heterozygous (MD/WT) and wild-type (WT/WT) embryos at embryonic day (E) 9.5, E10.5, E11.5, E13.5 and pups, after crossing heterozygous mice. **h** Representative images of MD-*Gata2* embryos at E10.5 and E11.5, and control MD<sub>mut</sub>-*Gata2* embryos at E11.5. Scale bars, 1mm. **i, j** Flow cytometry quantification of E10.5 (i) and E11.5 (j) erythroblasts after whole-embryo bleeding. Graphs show percentage of total erythroblasts (Erythro) or immature (type I) to mature (Type III) erythroblasts gated within lineage negative (Lin-) live single cell (SC) population. n(E10.5 WT/WT) = 3, n(E10.5 MD/WT) = 5, n(E10.5 MD/MD) = 3 n(E11.5 WT/WT) = 4, n(E11.5 MD/WT) = 5, n(E11.5 Mut/Mut) = 9, n(E11.5 MD/MD) = 5. Mean ± SD is shown. Source data are provided as Source Data file.

relevant Gene Ontology terms for hematopoietic lineage development. Accordingly, TF co-occupancy analysis shows motifs with high co-occurrence at GATA2 peaks, including PU.1 and RUNX1 among other “heptad” TFs, pointing towards the maintenance of cooperative events in mitosis. Importantly, a gradual increase in RUNX1 and PU.1 expression together with a down-regulation of endothelial genes was observed in homogenic endothelial cells of the AGM, suggesting a role for PU.1 in

hematopoietic fate specification, in addition to the well-described role in controlling myeloid/erythroid lineage differentiation<sup>50</sup>. Moreover, the cooperative action between GATA2 and RUNX1 is of fundamental importance for the specification of HSCs, as supported by the phenotype of *Gata2*<sup>-/-</sup>:*Runx1*<sup>-/-</sup> double heterozygous mice<sup>35</sup>.

In mitosis, we observed a reduction of GATA2 at sites marked with H3K4me1 associated with enhancers, as well as H3K36me3 and



H4K20me1, associated with transcriptional elongation. The reduction in histone marks associated with elongation may reflect an overall reduction in transcription in mitosis. As for H3K4me1, decreased binding at bivalent and weak enhancers, while increasing retention at active enhancer and promoter sites might allow gene expression flexibility upon G1 re-entrance, while maintaining important active genes marked. This supports the idea that M-G1 transition might serve as a time-window for adjustments in future gene expression profiles<sup>51,52</sup>. Moreover, we showed that mitotic bookmarking is correlated with binding affinity to peaks with higher density of GATA2 motifs. Whether this pre-existing motif structure represents a transversal feature of other TF bookmarkers needs to be addressed in future studies.

*Gata2*-null mice die between E10.5 and E11.5, before the emergence of definitive HSCs, from severe anaemia<sup>43</sup>. E9.5 *GATA2*<sup>-/-</sup> embryos had primitive erythroid cells in circulation, but impaired yolk sac haematopoiesis. Definitive EMPs arise in the yolk sac from hemogenic endothelium between E8.25 and E10, before homing the foetal liver at E10.5, from where they sustain embryonic haematopoiesis, including definitive erythropoiesis<sup>53</sup>. Our data show embryo lethality similarly to the *Gata2* knockout model, however, MD-*Gata2* homozygous E9.5 embryos were indistinguishable from their wild-type counterparts, and yolk sac progenitors generated hematopoietic colonies in numbers comparable to those of wild-type and heterozygous yolk sacs. Moreover, yolk sac suspensions expressed similar

**Fig. 5 | GATA2 bookmarking is required for definitive haematopoiesis.**

**a** Immunohistochemistry images representing E10.5 wild-type (WT/WT), heterozygous (MD/WT) and homozygous (MD/MD) intra-aortic hematopoietic clusters expressing RUNX1 (red) and CD31 (white) in the ventral (V) or dorsal (D) sides of the dorsal aorta (DA). White arrowheads indicate clusters. Scale bars, 150  $\mu$ m. **b** Number (#) of intra-aortic hematopoietic clusters per genotype. n(WT/WT) = 3, n(MD/WT) = 2, n(MD/MD) = 2 embryos. Mean is shown. **c–e** Colony-forming units for E9.5 yolk sac (**c**), for E10.5 aorta-gonad-mesonephros (AGM), placenta and foetal liver (**d**) and for E11.5 AGM and placenta (**e**) cell suspensions. n(WT/WT) = 2–5, n(MD/WT) = 3–4, n(MD/MD) = 3–5, n(Mut/Mut) = 5 embryos. Mean  $\pm$  SD is represented. Macrophage (M), granulocyte (G), granulocyte/macrophage (GM), erythroid (E) and mixed colonies (Mix) are shown per embryo equivalent (ee). **d, e** Statistical significance for the total number of colonies was calculated by one-way ANOVA followed by Bonferroni's multiple comparison test. **d, a**,  $p = 0.01$ ; **b**,  $p < 0.001$ , **c**,  $p = 0.002$ . **e, a, b, c** and **d**,  $p < 0.001$ . **f**, Percentage of donor chimerism (CD45.2<sup>+</sup>) 4 weeks (w), and 3 and 6 months (m) after transplantation with E11.5 placenta cells. Red line indicates 1% chimerism. n(WT/WT, 4w, 3m) = 5, n(WT/WT,

**6m**) = 4, n(MD/WT, 4w, 3m, 6m) = 8, n(MD/MD, 4w, 3m, 6m) = 8. **a**,  $p = 0.01$ ; **b**,  $p = 0.016$ . **g**, Quantification of donor contribution to myeloid and lymphoid lineages. Only mice with donor chimerism above 1% were considered. n(WT/WT, 4w, 3m, 6m) = 3, n(WT/WT, 6m) = 4, n(MD/WT, 4w, 3m) = 5, n(MD/WT, 6m) = 4. **h**, Percentage of donor chimerism in bone marrow 6 months after transplantation. n(WT/WT) = 4, n(MD/WT) = 8, n(MD/MD) = 8. **a**,  $p = 0.023$ ; **b**,  $p = 0.028$ . **f, h**, Statistical significance at 6 months was calculated with Kruskal-Wallis test followed by uncorrected Dunn's test. **i**, Percentage of donor chimerism 4 weeks, 3 months and 6 months after competitive transplantation (see Supplementary Fig. 7, Methods). n(WT/WT) = 6, n(MD/WT) = 8. **a**,  $p = 0.029$ . **j**, Quantification of donor contribution to blood lineages. n(WT/WT, 4w, 3m, 6m) = 6, n(MD/WT, 4w, 3m, 6m) = 8. **k**, Percentage of donor chimerism in bone marrow 6 m after transplantation. n(WT/WT) = 6, n(MD/WT) = 8. **a**,  $p = 0.020$ . **i, k**, Statistical significance was calculated with two-tailed Mann-Whitney test at 3 months (**i**) or at 6 months (**k**). **l**, Proposed model for the role of GATA2 bookmarking for definitive haematopoiesis. HSPC, hematopoietic stem and progenitor cell. Source data are provided as Source Data file.

levels of EMP markers. Nevertheless, these progenitors did not contribute to blood output between E10.5 and E11.5, consequently leading to anaemia. This suggests that GATA2 might not be necessary at M-G1 transition for the generation of yolk sac progenitors, but an impact in their maintenance or function cannot be disregarded. Additionally, HSPC generation was severely reduced in the embryo proper at E10.5 and E11.5, suggesting a requirement of GATA2-mediated bookmarking during this developmental stage. Even though definitive EMPs and HSPCs arise through an EHT, hemogenic endothelia in the yolk sac and in the AGM region (and major arteries) are molecularly distinct and governed by different pathways<sup>54</sup>. For example, Notch control of *Gata2* expression is required for the generation of hematopoietic clusters in the AGM, but not for definitive yolk sac haematopoiesis<sup>37,55</sup>. In agreement, we found the Notch1 target *HES1* and the Notch ligand *JAG1*, both expressed in the AGM region at E10.5<sup>37</sup> to be bookmarked by GATA2, providing a direct link between GATA2 mitotic bookmarking and HSC specification via Notch pathway regulation. GATA2 haploinsufficient mice (*Gata2*<sup>+/−</sup>) show a 2.7- and 1.6-fold decrease in the number of CFU colonies derived from E10 AGM and YS, respectively<sup>36</sup>. Moreover, *Gata2*<sup>+/−</sup> bone marrow HSPCs showed reduced engraftment capacity<sup>36</sup>. In contrast, embryonic MD-GATA2<sup>+/−</sup> HSPCs generated similar numbers of CFUs when compared to wild-type HSPCs, and had similar numbers of IAHCs. These could be explained by either a differential requirement for mitotic bookmarking of blood progenitors throughout development or different cell cycle dependencies. Nevertheless, engraftment of irradiated recipients by bone marrow heterozygous LSK-SLAM HSCs was reduced, reinforcing the requirement of GATA2 mitotic bookmarking for proper function of definitive HSCs.

It has been previously reported that GATA2 levels are higher at S-phase and lower at G1/S and G2/M<sup>37</sup>. Using a *Gata2Venus* mouse model, GATA2 protein levels were shown to oscillate in cells undergoing EHT<sup>38</sup>. A limitation of our study is that MD-GATA2 protein degradation remains to be characterised in detail throughout the cell cycle in vivo. This characterisation is important given that GATA2 degradation persists for several hours beyond mitotic exit, potentially interfering with GATA2 function in G1. To track MD-Gata2-induced degradation in vivo it would be useful to generate an MD-*Gata2Venus* mouse model, merging our approach with the one reported by Eich et al.<sup>38</sup>. Nevertheless, in that study GATA2 was detected in IAHC cells undergoing mitosis<sup>38</sup>, providing a window of opportunity for GATA2-mediated mitotic bookmarking. The impact of GATA2 degradation at M-G1 in the displacement of multimolecular TF complexes from mitotic chromatin, and the consequences for the development of leukaemia remain to be investigated.

In summary, we provided evidence that definitive haematopoiesis is dependent on mitotic bookmarking, supporting a requirement for this mechanism for lineage commitment and blood specification.

Overall, we have established the critical role of GATA2 at M-G1 transition for in vivo hematopoietic development.

**Methods****Ethical statement**

The research presented in this work complies with ethical regulations at Lund University. Animal work was approved by the Malmö · Lund Animal Experimentation Ethics Committee (Malmö · Lunds djurförsöksetiska nämnd).

**Generation of mouse models**

MD-*Gata2* and MD<sub>mut</sub>-*Gata2* mouse models were generated in collaboration with the Core Facility for Transgenic Mice from the University of Copenhagen. Briefly, the MD domain of cyclin B1 or a non-functional mutated (R42A) domain (MD<sub>mut</sub>) were inserted after the ATG start codon, located at the exon 2 of the *Gata2* gene in ESCs via transfection of two vectors: a pX458-GFP vector containing Cas9 and the 20-nucleotide gRNA (GACACAGTAGTGACCATGG) for the target location in the *Gata2* gene, together with either the MD or MD<sub>mut</sub> double-stranded DNA template sequences synthesised in a pMX plasmid (GeneArt, Thermo Fisher Scientific) (Supplementary Data 1). GFP<sup>+</sup> cells were FACS-purified, individual clones were isolated and genotyped using a combination of PCR and Sanger sequencing. Five positive ESC clones were expanded and injected into mouse morulae, and later blastocysts were transferred to surrogate females. A heterozygous mouse colony was established for the MD-*Gata2* model. Sperm from MD-*Gata2* male founders was frozen in straws and used to rederive the mouse line at the animal facility at Lund University. For genotyping, tail biopsies or embryonic tissues were individually collected, and digested with QIAamp DNA Mini Kit (Qiagen) or KAPA Express Extract Kit (Roche). Purified genomic DNA was amplified by PCR with Phusion Hot Start II High-Fidelity PCR Master Mix (Thermo Fisher Scientific), according to the manufacturer's instructions (primers in Supplementary Data 1). The same pair of primers was used to genotype CRISPR-modified ESCs. Amplified products were run in a 1% agarose gel and visualised in a ChemiDoc (Bio-Rad) with Image Lab software (version 5.2.1).

**Animal handling**

Animal experiments were performed according to the ethical permit protocol I1845/2019 approved by the Malmö · Lund Animal Experimentation Ethics Committee (Malmö · Lunds djurförsöksetiska nämnd). All animals (*Mus musculus*), including MD-*Gata2* (I29S2;C57BL/6 N), C57BL/6 J (B6), B6.SJL-*Ptprc*<sup>+/−</sup> *Pepc*<sup>+/−</sup>/BoyJ (B6.SJL) and C57BL/6JxB6.SJL mice were kept under a 12-hour light/dark cycle with access to food and water *ad libitum*. Temperature was kept at 22 °C and relative humidity at 55%.



### Molecular cloning

For live-cell imaging experiments, mCherry-GATA2/GFIIB/FOS, GATA2/GFIIB/FOS-mCherry sequences and mCherry alone were subcloned into the doxycycline-inducible pFUW-tetO<sup>25</sup> or constitutive pHAGE-MCS lentiviral vectors. For live-cell imaging and western blots with mCherry-GATA2 mutants, point mutations were inserted with specific primers in the GATA2 sequence, using QuikChange Lightning Site-Directed Mutagenesis Kit (Agilent) and cloned together with mCherry into the constitutive SFFV lentiviral vector<sup>29</sup>, using In-Fusion HD Cloning Kit (Takara), according to the manufacturer's instructions. For reprogramming experiments, individual TFs and GATA2 mutants (L359V and C373R) were subcloned into the constitutive FUW-hUbc (FUW) lentiviral vector<sup>23</sup> using In-Fusion Cloning. A similar method was used to fuse the MD or MD<sub>mut</sub> sequences upstream mTurquoise fluorescent protein, for protein degradation experiments at different cell cycle phases, or GATA2, for reprogramming experiments, and cloned into the FUW vector. H2B-mTurquoise sequence used to detect DNA in live-cell imaging experiments and mTurquoise alone, also used in protein degradation experiments were subcloned into FUW. Fusion proteins lack the stop codon of the first sequence. Plasmids and cloning primers used in this study can be found in Supplementary Data 1.

### Cell culture

HEK 293T cells (CRL-3216, ATCC), B6 mouse embryonic fibroblasts (MEFs) and HDFs (ScienCell) were maintained in Dulbecco's modified Eagle's (DMEM) medium supplemented with 10% (v/v) FBS, 2 mM L-glutamine and 10 µg/mL penicillin/streptomycin (pen/strep). K562 cells (CCL-243, ATCC) were cultured in RPMI 1640 supplemented with 10% FBS, 2 mM L-Glutamine, 1 mM MEM non-essential amino acids, 1 mM sodium pyruvate and pen/strep. All cells were maintained at 37 °C and 5% (v/v) CO<sub>2</sub>.

### Lentiviral production

HEK 293T cells were transfected with a mixture of 10 µg transfer plasmid, 7.5 µg packaging plasmid expressing the viral packaging proteins and 2.5 µg envelope plasmid encoding the VSV-G protein, together with 30 µg/mL polyethylenimine. Viral supernatants were harvested after 36, 48, and 72 hours, filtered (0.45 µm), concentrated 100-fold with Lenti-X Virus Concentrator (Takara), and stored at -80 °C. TF combinations were pool produced.

### Viral transduction and hemogenic reprogramming

Cells were cultured until 60-70% confluency and transduced with pFUW-tetO plus FUW-M2rtTA (1:1), FUW or SFFV lentiviral particles in medium with 8 µg/mL polybrene. Spin infection (800 g for 1 hour at 32 °C) was performed for K562 cells. Medium was replaced the next day and doxycycline (1 µg/mL) added when pFUW-tetO was used. For hemogenic reprogramming of HDFs, cells were transduced twice with FUW lentivirus encoding the 3 TFs or modified versions. Day 0 was considered the day of the second transduction. Cells were split 1:2 at day 4 and cultured in MyeloCult H5100 (StemCell Technologies) supplemented with 1 mM hydrocortisone (StemCell Technologies) and 1X antibiotic-antimycotic (Thermo Fisher Scientific). Medium was changed twice a week.

### Mitotic arrest

Cells for western blot were arrested in pro-metaphase 40 to 48 h post-transduction or after the addition of doxycycline with 0.2 µg/mL nocodazole (Sigma) in complete growth medium for 12–14 h. HDFs and HEK 293T arrested cells were collected by mitotic shake-off and K562 were FACS-purified. In nocodazole arrest and

release experiments, cells were arrested as described before, collected by mitotic shake-off and washed with PBS before plating. Cells were collected 2, 4, and 6 h after nocodazole release for western blot analysis. Untreated cells (asynchronous) and unreleased treated cells were also collected. HDFs were also stained for H3 serine 10 phosphorylation (H3S10p) to confirm the accumulation of cells in mitosis. Briefly, cells were spun (Shandon Cytospin 2, Marshall Scientific) onto Polysine-coated slides (Thermo Fisher Scientific) for 10 min at 1,400 rpm, fixed with 1% formaldehyde (FA) for 10 min, washed, permeabilized with 0.4% Triton X-100 and blocked with 5% normal goat serum in PBS. Cells were then incubated with anti-H3S10p primary antibody (1:400) overnight at 4 °C, washed, and incubated with goat anti-rabbit AF488 secondary antibody (1:400) for 45 min, protected from light. Slides were mounted (DAPI-containing mounting medium, Vector Laboratories) and visualised under an inverted Olympus IX70 (Olympus) microscope. See Supplementary Data 1 for antibody information.

### Subcellular protein fractionation, whole-cell protein extraction and western blotting

400,000 sorted K562 or 1-2 million transduced HEK 293T (asynchronous or mitotic) and HDFs (mitotic) were processed with the Subcellular Protein Fractionation kit for Cultured Cells (Thermo Fisher Scientific), according to the manufacturer's instructions to extract the cytoplasmic, soluble nucleus and chromatin-bound protein fractions. For whole-cell extracts, 200 µL of RIPA buffer supplemented with 1X Halt Protease Inhibitor Cocktail (Thermo Fisher Scientific), 1 mM phenylmethylsulfonyl fluoride (PMSF) and 5 mM sodium fluoride (NaF) were added per 1 × 10<sup>8</sup> cells. Samples were vortexed and placed on ice every 5 min for a total time of 20 min and centrifuged at 4000 g for 5 min. Protein fractions were diluted 1:2 in Laemmli buffer (Bio-Rad) with 5% 2-Mercaptoethanol (Sigma) and boiled at 98 °C for 10 min. Samples were run in Bolt 4-12%, Bis-Tris (Invitrogen) SDS-PAGE gel, using a Mini Gel Tank (Thermo Fisher Scientific) and Blot MOPS SDS running buffer (Invitrogen). The transfer was performed in an iBlot 2 (Thermo Fisher Scientific) dry system for 7 min. Membranes were incubated overnight at 4 °C with unconjugated primary antibodies against GATA2 (1:1000), GFIIB (1:1000), FOS (1:1000), mCherry (1:1000), Cyclin B1 (1:1000), Histone 3 (1:5000), Calnexin (1:1000) or Actin (1:2000) and with anti-rabbit horseradish peroxidase-conjugated (1:10,000) or anti-mouse horseradish peroxidase-conjugated (1:10,000) secondary antibodies (Supplementary Data 1). Membranes were incubated with ECL prime (Amersham) for 5 min and revealed in a ChemiDoc. Similar numbers of cells were used between conditions. Blots from different membranes from the same experiment were acquired and processed in parallel with similar parameters. Uncropped blots can be found in the Source Data file and in the Supplementary Information file. Bands were quantified using ImageJ (v2.1.0).

### Real-time quantitative PCR (RT-qPCR)

Total cellular RNA was extracted using TRIzol reagent (Thermo Fisher Scientific) following the manufacturer's instructions. The yield and purity of RNA samples were assessed by absorbance in Nanodrop (Thermo Fisher Scientific). 1 µg of total RNA was treated with DNase I (Roche) and retro-transcribed using SuperScript IV reverse transcriptase (Invitrogen) and Random Primers (Invitrogen), according to the manufacturer's instructions. Quantitative PCR was performed using Maxima SYBR Green/ROX Master mix (Thermo Fisher Scientific) and specific primers (Supplementary Data 1) in a QuantStudio1 Real-Time machine (Applied Biosystems). Raw data was analysed with LinReg PCR software (v2021.2)<sup>60</sup> and NO fluorescence values were calculated using the same program. Gene expression was normalised to the housekeeping gene GAPDH.

### Live-cell imaging

Widefield live-cell images of HDFs, MEFs and K562 were obtained 48 hours after transduction or addition of doxycycline in 96-well plates (Ibidi), using the CellDiscoverer 7 automated microscope (Zeiss). Random individual positions in wells were imaged for 24–48 h (37 °C, 5% CO<sub>2</sub>) in 5–10 min intervals and representative snapshots of each mitotic phase were saved from time-lapse data. The same exposure times for mCherry, Pacific Blue (H2B-mTurquoise) and phase-gradient contrast channels were used across conditions. Single mCherry-TF and TF-mCherry images from HEK 293T cells were imaged with an Olympus IX70. CellDiscoverer images were initially processed with ZEN 2 (blue edition, version 3.1) and later with ImageJ (v2.1.0). Images obtained from Olympus IX70 were processed with Adobe Photoshop CS6. Cell counting was performed using the ImageJ plugins StarDist<sup>61</sup> (for segmentation) and Trackmate<sup>62</sup> (for cell tracking) on the time-lapse series. Only mCherry-positive cells were considered for the quantification of mitotic events, and at least 5 different fields were used for quantification. Quantifications do not represent the absolute number of mitotic events or mitotic rate in the wells.

### Chromatin retention analysis

Quantification of mitotic chromatin enrichment was calculated as the ratio between the mean grey value (fluorescence intensity) in the chromatin region of interest (ROI) and the cytoplasm in cells over-expressing mCherry-TFs. Chromatin ROI was defined by delimiting chromosomes marked with H2B-mTurquoise and cytoplasm ROI was defined by delimiting the whole cell perimeter and subtracting chromatin ROI. Cells were analysed with ImageJ (v2.1.0). Mean grey values for each ROI and Log<sub>2</sub> (Chr/Cyto) were calculated for statistical analysis.

### Sample preparation for ChIP-seq

**Asynchronous cells.** A total of  $1 \times 10^7$  asynchronous K562 cells were crosslinked with 1 mL 2 mM PBS-disuccinimidyl glutarate (DSG) (Sigma) for 50 min at room temperature (RT) with occasional shaking<sup>15</sup>. Then, cells were spun down, resuspended in 10 mL PBS and crosslinked again with 1 mL FA solution (1% FA, 0.1 M NaCl, 1 mM EDTA, 50 mM HEPES in H<sub>2</sub>O, FA final concentration 1%), with agitation for 15 min at RT – double fixation (DSG + FA). FA was quenched with 0.125 M glycine for 5 min. Cells were centrifuged at 800 g at 4 °C for 10 min and washed twice with PBS 0.5% Igepal, supplemented with 100 mM PMSF. Cell pellets were snap-frozen and stored at –80 °C.

**Mitotic cells.** A total of  $1 \times 10^8$  K562 nocodazole-arrested cells were crosslinked in 2 mL 2 mM PBS-DSG for 50 min at RT, spun down and fixed with 1% FA, as described for asynchronous cells. Cells were stained for FACS with anti-phospho-Ser/Thr-Pro MPM-2 primary antibody (1:170) and anti-mouse AF647 secondary antibody (1:170) (Supplementary Data 1), as described by Campbell et al.<sup>63</sup>, with the difference that FA was quenched with 0.5 M glycine. Approximately  $5 \times 10^6$  mitotic (MPM-2<sup>+</sup>) K562 were sorted in several rounds, after doublet exclusion resulting in <10% contamination with asynchronous cells. After each sorting, cell pellets were snap-frozen, stored at –80 °C and pulled together for ChIP-seq.

### ChIP-seq

Samples were sent to Active Motif (Carlsbad, CA) for ChIP-Seq. Chromatin was isolated with a lysis buffer, followed by disruption with a Dounce homogeniser. Lysates were sonicated and DNA sheared to an average length of 300–500 bp with Active Motif's EpiShear probe sonicator. Genomic DNA (input) was prepared for asynchronous and mitotic K562 cells by treating aliquots of chromatin with RNase, proteinase K and heat for de-crosslinking, followed by SPRI beads clean up (Beckman Coulter) and quantitation by Clariostar (BMG Labtech). 40 µg of chromatin was precleared with protein A agarose beads (Invitrogen).

Genomic DNA regions of interest were isolated using 5 µg of antibody against GATA2 (Santa Cruz, sc-9008). Complexes were washed, eluted from the beads with SDS buffer, and treated with RNase and proteinase K. Crosslinks were reversed by incubation overnight at 65 °C, and ChIP DNA was purified by phenol-chloroform extraction and ethanol precipitation. Quantitative PCR (qPCR) reactions were carried out in triplicate on specific genomic regions using SYBR Green Supermix (Bio-Rad). The resulting signals were normalised for primer efficiency by carrying out qPCR for each primer pair using Input DNA. Illumina sequencing libraries were prepared from ChIP and Input DNAs on an automated system (Apollo 342, Wafergen Biosystems/Takara). After a final PCR amplification step, the resulting DNA libraries were quantified and sequenced on Illumina's NextSeq 500 (75 nt reads, single end).

### ChIP-seq data analysis

ChIP-seq analysis was performed on raw FASTQ files. FASTQ reads were aligned to the human genome (hg38) using the BWA v0.7.12 algorithm<sup>64</sup>. Only uniquely mapped reads (mapping quality  $\geq 25$ ) were used for further analysis. Alignments were extended in silico at their 3'-ends to a length of 200 bp and assigned to 32-nt bins along the genome. Mapped output files were processed through MACS v2.1.0<sup>65</sup> and Genrich v0.6.1 (<https://github.com/jsh58/Genrich>) software to determine peaks. Peaks that were on the ENCODE blacklist of known false ChIP-Seq peaks were removed. Peak annotation was performed using ChIPseeker R library<sup>66</sup>. For genome tracks, bigwig files were created from bam files with deepTools<sup>67</sup> and explored using the UCSC Genome Browser (<https://genome.ucsc.edu/>). Heatmaps were produced with deepTools in the reference-point mode where each feature was aligned at GATA2 summits and tiled the flanking up- and downstream regions within  $\pm 2$  kb. Clusters were generated with K-means clustering ( $n = 3$ ) in deepTools. Functional enrichment analysis for the peaks from asynchronous, mitotic cells and mitotic clusters was performed with GREAT software<sup>68</sup> using GO BP ontology. For motif discovery, find-MotifsGenome.pl procedure with default parameters from HOMER<sup>69</sup> was used on ChIP-seq peaks separately. To find the number of GATA2 motifs in peaks we used GATA2 motif from HOCOMOCO v11, and scanned asynchronous, mitotic and mitotic clusters peaks using FIMO from MEME suite. To adjust for the uneven number of peaks in asynchronous versus mitotic cells, we randomly subsampled the number of peaks matching to mitotic condition 1000 times and then averaged the distribution. For chromatin state fold enrichment analysis, enrichment scores for GATA2 asynchronous and mitotic ChIP-seq peaks were calculated using the ChromHMM Overlap Enrichment<sup>70</sup>. ChromHMM segmentation for K562 cell line, containing 18 different chromatin states, was downloaded from the Roadmap Epigenomics Consortium website ([https://egg2.wustl.edu/roadmap/web\\_portal/](https://egg2.wustl.edu/roadmap/web_portal/)). To calculate fold change enrichment between two conditions, we normalised each of them by subtracting the minimum value in the condition and then dividing by the maximum value. To compare histone marks distribution in asynchronous and mitotic GATA2 peaks we used all histones marks available for K562 cell line at ENCODE (<https://www.encodeproject.org/>), along with DNase-seq and ATAC-seq (Supplementary Data 2). To produce profile matrix and plots, we used deepTools in the reference-point mode centred at GATA2 peak summits and tiled the flanking up- and downstream regions within  $\pm 2$  kb for histones marks and  $\pm 500$  bp for DNase-seq and ATAC-seq. By summing the difference through all bins (bin size = 50 bp), which were estimated in the previous step, we calculated the difference between asynchronous and mitotic states. To investigate motif co-occupancy we downloaded TF motifs, associated with HSPC regulators from HOCOMOCO v11, and proceeded as described above, focusing on the peaks that contained GATA2 motifs, and motifs for other TFs. For integration with other ChIP-seq datasets for other HSPC regulators<sup>38,39</sup>, we used bedtools intersect v2.30 (Supplementary Data 2). Replicates were merged by bedtools merge v2.30 when available.

### scRNA-seq sample preparation

A total of 20,000 live (DAPI-) single cells undergoing hemogenic reprogramming were FACS-purified at different time points (day 4 and day 6) following transduction with either MD-GATA2 plus GF1B and FOS, or MD<sub>mut</sub>-GATA2 plus GF1B and FOS, using human dermal fibroblast (HDFs) from two different donors (2 biological replicates). Untransduced HDFs were used as reprogramming controls. Sorted samples (Supplementary Data 3) were loaded in a Chromium Next GEM Chip G (10x Genomics) and run in a Chromium Controller (10x Genomics), according to the manufacturer's instructions. scRNA-seq libraries were prepared with Dual Index Chromium Next GEM Single Cell 3' Kit v3.1 (10x Genomics) according to the manufacturer's instructions. Library size and quality check was performed using High Sensitivity D1000 ScreenTape with High Sensitivity D1000 Reagents (Agilent) in a 4200 TapeStation System (Agilent), according to the manufacturer's protocol. Index libraries were pooled and sequenced on a NovaSeq 6000 System (Illumina) using the NovaSeq 6000 S4 Reagent Kit (200 cycles) v1.5 (Illumina).

### scRNA-seq data analysis

Thirty two thousand seven hundred and seventy-three single cells with an approximate median of UMI counts 60,000 per cell were generated (R1 read: technical, length: 28 bp; R2 read: biological, length: 90 bp). Paired-end sequencing reads were processed using publicly available 10x Genomics software – Cell Ranger v6.0.1<sup>31</sup>. Firstly, we used cellranger mkfastq to convert binary base call files to FASTQ files. Next, we applied cellranger count to FASTQ files and performed alignment to human (hg38, GRCh38.p14) genome assemblies using STAR v2.7.9a<sup>32</sup>. The sparse expression matrix generated by cellranger analysis pipeline was used as input to Seurat R library v4, and cells and genes that passed quality control thresholds were included according to the following criteria: 1) total number of UMIs detected per sample greater than 5000; 2) number of genes detected in each single cell greater than 1000; 3) percentage of counts in mitochondrial genes less than 7.5%. To account for technical variation, we performed batch integration. Firstly, we normalised each batch separately using “Log-Normalize” with the scale factor of 10,000 and identified 5000 variable features. Next, we performed batch integration by finding corresponding anchors between the batch using 30 dimensions. We selected the first 30 principal components for subsequent UMAP visualisation. For differential expression analysis between cell states, we used Seurat v4 FindMarkers function using Wilcoxon test with logfc.threshold = 0.1, min.pct = 0.25, BH-adjusted  $p < 0.05$ . We further checked how many differentially expressed genes are bookmarked by GATA2 and contain motifs by other HSPC regulators, by scanning mitotic peaks using FIMO from MEME suite and associating them with differentially expressed genes.

### Embryo and hematopoietic tissue isolation

Uteruses from pregnant heterozygous MD-*Gata2* females (8 to 12-weeks old), at indicated developmental stages, were collected and embryos separated from maternal tissue in individual dishes containing PBS 2% FBS, using tweezers. Yolk sacs (E9.5), the caudal region of the embryo proper containing the aorta-gonad-mesonephros (AGM) regions (E10.5 and E11.5), foetal livers (E10.5) and placentas (E10.5 and E11.5) were isolated. To isolate the embryo caudal region (simplified as “AGM”), embryos were cut below the heart and abdominal tissue, including foetal liver, limbs and tail were removed. Embryos were imaged before dissection and hematopoietic tissues were collected after head dissection, which was used for genotyping. Tissues were kept in PBS 2% FBS on ice if not dissociated immediately.

### CFU assays

Embryonic tissues were dissociated in 0.1% (w/v) type I collagenase (Thermo Fisher Scientific), 1% P/S, 10% FBS in PBS (dissociation buffer).

Placentas in 2 mL of dissociation buffer were mechanically disrupted by passing three times through an 18 G needle and incubated at 37 °C, 5% CO<sub>2</sub> for 45 min. Following incubation, placentas were disrupted again with a 21 G needle and incubated for an additional 45 min. Finally, cell suspensions were passed through a 23 G needle, filtered (50 µm), washed and pelleted at 300 g for 5 min. Individual yolk sacs, AGMs and foetal livers in 1 mL dissociation buffer were mechanically disrupted by pipetting with a P1000 and incubated for 15 min at 37 °C, 5% CO<sub>2</sub>, pipetted again with a P200 and incubated again for 15 min. After incubation, cell suspensions were filtered into a new tube, washed and pelleted. Red blood cells (RBC) were lysed with 1x BD Pharm Lyse (BD Bioscience) for 5 min at RT protected from light. After washing, cells were resuspended in Iscove's Modified Dulbecco's Medium (IMDM) (Cytiva) with 2% FBS and resuspended in MethoCult GF M3434 (StemCell Technologies). Placental cells were plated as 0.33 embryo equivalents (ee, triplicates) and yolk sacs, AGMs and foetal livers as 0.5 ee (duplicates). Hematopoietic colonies were scored after 6-7 days of culture.

### Bone marrow isolation for LSK and LSK-SLAM HSC sorting

To quantify allelic expression in MD heterozygous mice and to perform competitive transplantations, bone marrow (BM) was harvested from tibias and femurs by crushing. Cell suspensions were collected with PBS 2% FBS, filtered through a 40 µm cell strainer, washed and pelleted. RBC lysis was performed with BD Pharm Lyse for 8 min at RT protected from light. Whole BM was enriched by magnetic-activated cell sorting for c-kit, using CD117 MicroBeads (Miltenyi), according to the manufacturer's instructions for subsequent FACS.

### FACS

To purify mitotic populations for western blot, K562 cells were sorted according to DNA content, after mitotic arrest. Vybrant DyeCycle Violet DNA permeable stain (Invitrogen) was added directly to cells in growth medium to a final concentration of 5 µM and incubated at 37 °C for 30 min, protected from light. 400,000 K562 cells within G2/M (4N) gate were sorted immediately after staining for subcellular protein fractionation. For western blot and RT-qPCR analysis, 100-200,000 mCh-TF transduced HDFs were sorted and whole-cell extractions or RNA were collected. For cell cycle-dependent protein degradation experiments, mAzamiGreen positive HEK 293T cells expressing the FUCCI<sup>66</sup> vector were sorted before transduction with mTurquoise lentivirus. mTurquoise positive cells were sorted and cultured before flow cytometry analysis. MD-*Gata2* BMs isolated for LSK sorting were stained with APC-c-kit (1:100), PE-Sca-1 (1:100), PE-Cy5-Lineage: CD3e/B220/Gr1/Mac1/Ter119 (0.5:100 each) for 20 min on ice. LineageSca1<sup>+</sup>c-kit<sup>+</sup> (LSK) cells were sorted for mRNA extraction. MD-*Gata2* BMs isolated for LSK-SLAM HSC sorting were stained with APCe780-c-kit (1:50), BV421-Sca-1 (1:200), FITC-CD48 (1:200), PECy7-CD150 (1:200), PE-CD45.1 (1:100), APC-CD45.2 (1:100) and PE-Cy5-Lineage: CD3e/B220/Gr1/Mac1/Ter119 (0.5:100 each) for 20 min on ice. Mitotic K562 for ChIP-seq analysis were sorted after double-fixation and MPM-2 staining as mentioned in “Sample preparation for ChIP-seq”. Cells were sorted with either FACSArialII or FACSArialII (BD Biosciences).

### mRNA isolation and RT-PCR

mRNA from BM LSK sorted cells was isolated with 300 µL TRIzol (Invitrogen), reverse transcribed to cDNA with SuperScript IV Reverse Transcriptase (Invitrogen) and amplified by PCR using Phusion Hot Start II, according to the manufacturer's instructions (primers in Supplementary Data 1). PCR products were run in a 1% agarose gel and visualised in a ChemiDoc.

### Transplantation and bleedings

For transplantations assays with embryonic tissue, E11.5 MD-*Gata2* placentas from all genotypes were dissociated as described for CFU

assays with the exception that RBC lysis was not performed, and cells were resuspended in 350  $\mu$ L PBS 2% FBS. 11 to 14-weeks old B6.SJL (CD45.1) or C57BL/6JxB6.SJL (CD45.1/2) males were sublethally irradiated with 600 cGy (Gammacell 40 Exactor), 6 hours before injection. Mice were warmed for 10 min and each recipient was injected (0.5 mL 29 G syringe, Terumo) in the tail vein with 300  $\mu$ L placenta cell suspensions (1 ee). Bleedings were performed at 4 weeks, 3, and 6 months after injections as follows: blood was collected from the tail vein, spun down and resuspended in 200  $\mu$ L NH<sub>4</sub>Cl. After a 5 min incubation at RT in the dark, cells were spun for 5 min at 300 g, washed in 200  $\mu$ L PBS 2% FBS for flow cytometry analysis. At the 6-month mark, mice were sacrificed, and BM was collected from the left leg and ilium by crushing to assess donor chimerism. For competitive transplantations, 200 FACS-purified LSK-SLAM HSCs (LineageSca-1<sup>+</sup>Kit<sup>+</sup>CD150<sup>+</sup>CD48<sup>-</sup>) from 11 to 13-weeks old male competitor CD45.1 SLJ mice and from 9 to 13-weeks old male MD/WT or WT/WT *Mdca-Gata2* mice (CD45.2) were mixed 1:1 and injected into lethally irradiated (900 cGy) 9 to 13-weeks old female recipients (CD45.1/2), together with 200,000 support whole bone marrow cells (CD45.1/2). Blood and bone marrow analyses were performed as described before.

### Whole-embryo bleedings

E10.5 and E11.5 embryos involved by the yolk sac were carefully separated from placenta at RT with fine tweezers to avoid damaging the yolk sac, washed with PBS and placed in individual wells with PBS to bleed. At this point, yolk sacs were open to allow blood to spread in the well for 10 min. After that, both embryo and yolk sac were removed, blood suspensions were passed through a 40  $\mu$ m strainer into a FACS tube and centrifuged 5 min at 300 g before flow cytometry analysis.

### Flow cytometry analysis

Cells undergoing hemogenic reprogramming were dissociated, pelleted, and incubated with PE-CD9 and PE-Cy7-CD49f antibodies diluted 1:100 in PBS 2% FBS at 4 °C for 20 min, together with mouse serum 1% (v/v). Single live (DAPI<sup>-</sup>) cells were analysed. Cells expressing Fucci vector and mTurquoise fluorescent proteins were analysed directly after collection. Mouse-derived blood for donor-contribution analysis was stained with FITC-CD45.1 (1:100), PE-CD45.2 (1:100), APC-B220/CD3 $\epsilon$  (0.4:100 each), PECy5-B220/Mac1/Gr1 (0.4:100 each), for 20 min on ice. BMs isolated from mice 6 months after transplantation were treated with BD Pharm Lyse to remove RBC, washed, filtered, and stained for lineage with PeCy5-Ter119/B220/Gr1/Mac1/CD3 $\epsilon$  (1:400 each), plus PE-CD45.1 (1:100) and APC-CD45.2 (1:100) antibodies, prior to analysis. Blood cell suspensions from whole-embryo bleedings were incubated with lineage antibodies PE-Cy5-B220/Gr1/Mac1/CD3 $\epsilon$  (1:400 each), 7AAD (dead cell exclusion) and the erythroblast development markers FITC-CD71 and APC-Ter119<sup>67</sup> (1:100 each). For EMP analysis, single-cell E9.5 yolk sac suspensions were stained with DAPI, PE-Ter119, APC-eF780-c-kit, FITC-CD41 and APC-CD16/32 (1:100 each), as previously reported<sup>68</sup>. Nocodazole arrest efficiency of HEK 293T and HDFs was assessed by propidium iodide (PI) staining after fixation with 70% ice-cold ethanol. Prior to analysis, ethanol was washed, and cells resuspended in PI buffer (50  $\mu$ g/mL PI, 100  $\mu$ g/mL RNase A, 0.5% of 10% NP-40) for 20 min on ice and 10 min at RT. To check mitotic arrest of K562 for ChIP-seq, asynchronous and nocodazole treated cells were double fixed, stained with MPM-2 (see “Sample preparation for ChIP-seq”) and resuspended in PI buffer prior to analysis. Cells were analysed in LSR FORTessa, LSR FORTessa x20 or LSRRI (BD Biosciences). Flow cytometry results were collected using BD FACSDiva (v9.0) and analysed using FlowJo software (FLOWJO LLC, version 10.6.1).

### Whole-embryo mounting and immunohistochemistry

E9.5 and E10.5 embryos were separated from maternal tissue in PBS (+ Ca/Mg) 10% FBS and heads were isolated for genotyping. Then, embryos were fixed in 4% FA for 60–90 min and rinsed 3 times in 1 mL of PBS for 5 minutes (each wash) at RT. Samples were placed in successively higher concentrations of methanol in PBS on ice for 10 min (50%, 75% and 100%) and stored at -20 °C prior to immunostaining. Embryos were rehydrated in 50% methanol and washed in PBS and incubated in staining buffer (0.4% Triton-X, 2% FCS in PBS) overnight at 4 °C on a shaking rack. Each embryo was incubated for 8 h with gentle rotation at RT with 100–200  $\mu$ L antibody solution containing either goat anti-CD31 and rabbit anti-RUNX1, or goat anti-CD31 and rabbit anti-RUNX1, plus rat anti-c-kit primary antibodies (1:200 each). Then, embryos were washed in staining buffer overnight at 4 °C on a shaking rack and incubated with the secondary antibody AF594 anti-rabbit (1:800), AF647 anti-goat (1:800) and AF488 anti-rat (1:400) solution for 8 h, gently rotating at RT. See Supplementary Data 1 for more information on antibodies. After a final wash in 1 mL staining buffer overnight at 4 °C, embryos were dehydrated in 50% and 100% methanol and then cleared in 50% and 100% BABB (one part benzyl alcohol with two parts benzyl benzoate). Embryos were then mounted into Fastwells (Sigma) pre-attached to a slide with a coverslip and sealed with another coverslip. Confocal scans were performed using an upright LSM 900 microscope (Zeiss) and the resulting images were processed and analysed using Imaris x64 v9.5.1 (Oxford Instruments). Hematopoietic clusters (CD31<sup>+</sup>RUNX1<sup>+</sup> or CD31<sup>+</sup>RUNX1<sup>+</sup>c-kit<sup>+</sup>) were manually counted. CD31<sup>+</sup>RUNX1<sup>+</sup>c-kit<sup>+</sup> clusters were only used for quantification purposes.

### Statistics and reproducibility

Comparisons between groups were performed by one-way ANOVA followed by Bonferroni's multiple comparison test, two-way ANOVA followed by Fisher's LSD test or Kruskal-Wallis test followed by uncorrected Dunn's test, or two-tailed Mann-Whitney (for non-parametric data) with GraphPad Prism 9 software.  $\alpha = 0.5$ . Seurat v4 FindMarkers function using two-sided Wilcoxon Rank Sum test with logfc.threshold = 0.1, min.pct = 0.25 and adjusted p-value, based on bonferroni correction <0.05, was used for differential expression analysis between cell states. See figure legends for more details. Exact *p* values are shown when relevant. No statistical method was used to predetermine sample size. No data were excluded from the analyses. Mice were randomly assigned to test groups in transplantation experiments. In vitro experiments were not randomised. CFU colonies were scored blindly.

### Reporting summary

Further information on research design is available in the Nature Portfolio Reporting Summary linked to this article.

### Data availability

Data supporting this work is available upon request. Source data are provided with this paper. ChIP-seq and scRNA-seq data has been deposited in the Gene Expression Omnibus (GEO) with accession codes GSE207551, and GSE221691, respectively. Processed data was mapped to the human genome assembly (hg38, GRCh38.p14). Public datasets used in this study can be accessed under accession numbers GSM733680, GSM7336569, GSM733658, GSM733692, GSM733714, GSM733776, GSM733778, GSM733651, GSM733675, GSM733786, GSM733653, GSM733777, GSM803540, GSE96253, GSM803384, GSM777644, GSM1010820, GSE170378, GSE172523 for Histones ChIP-seq, TFs ChIP-seq, DNase-seq and ATAC-seq in K562 from ENCODE project; GSM1278240, GSM1278241, GSM1278242 for TFs ChIP-seq in Proerythroblast from Pinello *et al.*, 2013<sup>39</sup>. ChIP-seq and scRNA-seq data generated in this study are provided in Supplementary Data 2 and

Supplementary Data 3, respectively. All other data is provided in the Source Data file. Source data are provided with this paper.

### Code availability

This paper does not report original code. Any additional information required to reanalyse the data reported in this paper is available upon request.

### References

- Martínez-Balbás, M. A., Dey, A., Rabindran, S. K., Ozato, K. & Wu, C. Displacement of sequence-specific transcription factors from mitotic chromatin. *Cell* **83**, 29–38 (1995).
- Terasaki, M. et al. A new model for nuclear envelope breakdown. *Mol. Biol. Cell* **12**, 503–510 (2001).
- Palozola, K. C. et al. Mitotic transcription and waves of gene reactivation during mitotic exit. *Science* **358**, 119–122 (2017).
- Djeghloul, D. et al. Identifying proteins bound to native mitotic ESC chromosomes reveals chromatin repressors are important for compaction. *Nat. Commun.* **11**, 1–15 (2020).
- Soares, M. A. F., Oliveira, R. A. & Castro, D. S. Function and regulation of transcription factors during mitosis-to-G1 transition. *Open Biol.* **12**, 1–11 (2022).
- Festuccia, N., Gonzalez, I., Owens, N. & Navarro, P. Mitotic bookmarking in development and stem cells. *Development* **144**, 3633–3645 (2017).
- Palozola, K. C., Lerner, J. & Zaret, K. S. A changing paradigm of transcriptional memory propagation through mitosis. *Nat. Rev. Mol. Cell Biol.* **20**, 55–64 (2019).
- Raccaud, M. & Suter, D. M. Transcription factor retention on mitotic chromosomes: regulatory mechanisms and impact on cell fate decisions. *FEBS Lett.* **592**, 878–887 (2017).
- Young, D. W. et al. Mitotic retention of gene expression patterns by the cell fate-determining transcription factor Runx2. *PNAS* **104**, 3189–3194 (2007).
- Verdeguer, F. et al. A mitotic transcriptional switch in polycystic kidney disease. *Nat. Med.* **16**, 106–110 (2010).
- Kadauke, S. et al. Tissue-specific mitotic bookmarking by hematopoietic transcription factor GATA1. *Cell* **150**, 725–737 (2012).
- Caravaca, J. M. et al. Bookmarking by specific and nonspecific binding of FoxA1 pioneer factor to mitotic chromosomes. *Genes Dev.* **27**, 251–260 (2013).
- Teves, S. S. et al. A dynamic mode of mitotic bookmarking by transcription factors. *Elife* **5**, 1–24 (2016).
- Deluz, C. et al. A role for mitotic bookmarking of SOX2 in pluripotency and differentiation. *Genes Dev.* **30**, 2538–2550 (2016).
- Festuccia, N. et al. Mitotic binding of *Esrrb* marks key regulatory regions of the pluripotency network. *Nat. Cell Biol.* **18**, 1139–1148 (2016).
- Liu, Y. et al. Widespread mitotic bookmarking by histone marks and transcription factors in pluripotent stem cells. *Cell Rep.* **19**, 1283–1293 (2017).
- Soares, M. A. F. et al. Hierarchical reactivation of transcription during mitosis-to-G1 transition by Brn2 and Ascl1 in neural stem cells. *Genes Dev.* **35**, 1020–1034 (2021).
- Yang, Z., He, N. & Zhou, Q. Brd4 recruits p-TEFb to chromosomes at late mitosis to promote g1 gene expression and cell cycle progression. *Mol. Cell Biol.* **28**, 967–976 (2008).
- Dzierzak, E. & Bigas, A. Blood development: hematopoietic stem cell dependence and independence. *Cell. Stem Cell.* **22**, 639–651 (2018).
- Medvinsky, A., Rybtsov, S. & Taoudi, S. Embryonic origin of the adult hematopoietic system: advances and questions. *Development* **138**, 1017–1031 (2011).
- Zovein, A. C. et al. Fate tracing reveals the endothelial origin of hematopoietic stem cells. *Cell. Stem Cell.* **3**, 625–636 (2008).
- Boisset, J.-C. et al. In vivo imaging of haematopoietic cells emerging from the mouse aortic endothelium. *Nature* **464**, 116–120 (2010).
- Pereira, C. F. et al. Induction of a hemogenic program in mouse fibroblasts. *Cell. Stem Cell.* **13**, 205–218 (2013).
- Pereira, C. F. et al. Hematopoietic reprogramming in vitro informs in vivo identification of hemogenic precursors to definitive hematopoietic stem cells. *Dev. Cell.* **36**, 525–539 (2016).
- Gomes, A. M. et al. Cooperative transcription factor induction mediates hemogenic reprogramming. *Cell Rep.* **25**, 2821–2835 (2018).
- Silvério-Alves, R., Gomes, A. M., Kurochkin, I., Moore, K. A. & Pereira, C.-F. Hemogenic reprogramming of human fibroblasts by enforced expression of transcription factors. *J. Vis. Exp.* **153**, 1–8 (2019).
- Yang, H. Y. & Evans, T. Distinct roles for the two cGATA-1 finger domains. *Mol. Cell Biol.* **12**, 4562–4570 (1992).
- Kazenwadel, J. et al. GATA2 is required for lymphatic vessel valve development and maintenance. *J. Clin. Invest.* **125**, 2979–2994 (2015).
- Katsumura, K. R. et al. Human leukemia mutations corrupt but do not abrogate GATA-2 function. *Proc. Natl Acad. Sci.* **115**, 10109–10118 (2018).
- Chong, C. E. et al. Differential effects on gene transcription and hematopoietic differentiation correlate with GATA2 mutant disease phenotypes. *Leukemia* **32**, 194–202 (2018).
- Zhang, S. et al. Gain-of-function mutation of GATA-2 in acute myeloid transformation of chronic myeloid leukemia. *PNAS* **105**, 2076–2081 (2008).
- Festuccia, N. et al. Transcription factor activity and nucleosome organization in mitosis. *Genome Res.* **29**, 250–260 (2019).
- Yzaguirre, A. D., de Bruijn MFTR & Speck, N. A. The role of runx1 in embryonic blood cell formation. *Advances in Experimental Medicine and Biology*. 962, (47–64. Springer, Singapore, 2017).
- Karlsson, G. et al. The tetraspanin cd9 affords high-purity capture of all murine hematopoietic stem cells. *Cell Rep.* **4**, 642–648 (2013).
- Wilson, N. K. et al. Combinatorial transcriptional control in blood stem/progenitor cells: Genome-wide analysis of ten major transcriptional regulators. *Cell. Stem Cell.* **7**, 532–544 (2010).
- Calvanese, V. et al. Mapping human haematopoietic stem cells from haemogenic endothelium to birth. *Nature* **604**, 534–540 (2022).
- Robert-Moreno, Á., Espinosa, L., de la Pompa, J. L. & Bigas, A. RBPjk-dependent Notch function regulates *Gata2* and is essential for the formation of intra-embryonic hematopoietic cells. *Development* **132**, 1117–1126 (2005).
- Dunham, I. et al. An integrated encyclopedia of DNA elements in the human genome. *Nature* **489**, 57–74 (2012).
- Pinello, L., Xu, J., Orkin, S. H. & Yuan, G. C. Analysis of chromatin-state plasticity identifies cell-type-specific regulators of H3K27me3 patterns. *Proc. Natl Acad. Sci. USA* **111**, E344–E353 (2014).
- Barski, A. et al. High-resolution profiling of histone methylations in the human genome. *Cell* **129**, 823–837 (2007).
- Vincent-Fabert, C. et al. PLZF mutation alters mouse hematopoietic stem cell function and cell cycle progression. *Blood* **127**, 1881–1885 (2016).
- Goode, D. K. et al. Dynamic gene regulatory networks drive hematopoietic specification and differentiation. *Dev. Cell.* **36**, 572–587 (2016).
- Tsai, F.-Y. et al. An early haematopoietic defect in mice lacking the transcription factor GATA-2. *Nature* **371**, 221–226 (1994).
- De Bruijn MFTR, Ma. X., Robin, C., Ottersbach, K., Sanchez, M. J. & Dzierzak, E. Hematopoietic stem cells localize to the endothelial cell layer in the midgestation mouse aorta. *Immunity* **16**, 673–683 (2002).

45. de Pater, E., Kaimakis, P. & Vink, C. S. Gata2 is required for HSC generation and survival. *J. Exp. Med.* **210**, 2843–2850 (2013).
46. Rodrigues, N. P. et al. Haploinsufficiency of GATA-2 perturbs adult hematopoietic stem-cell homeostasis. *Blood* **106**, 477–485 (2005).
47. Raccaud, M. et al. Mitotic chromosome binding predicts transcription factor properties in interphase. *Nat. Commun.* **10**, 1–16 (2019).
48. Tien, F. et al. GATA2 zinc finger 1 mutations are associated with distinct clinico-biological features and outcomes different from GATA2 zinc finger 2 mutations in adult acute myeloid leukemia. *Blood Cancer J.* **8**, 1–13 (2018).
49. Bates, D. L., Chen, Y., Kim, G., Guo, L. & Chen, L. Crystal structures of multiple gata zinc fingers bound to dna reveal new insights into dna recognition and self-association by GATA. *J. Mol. Biol.* **381**, 1292–1306 (2008).
50. Burda, P., Laslo, P. & Stopka, T. The role of PU.1 and GATA-1 transcription factors during normal and leukemogenic hematopoiesis. *Leukemia* **24**, 1249–1257 (2010).
51. Hsiung, C. C. S. et al. A hyperactive transcriptional state marks genome reactivation at the mitosis–G1 transition. *Genes Dev.* **30**, 1423–1439 (2016).
52. Soufi, A. & Dalton, S. Cycling through developmental decisions: how cell cycle dynamics control pluripotency, differentiation and reprogramming. *Development* **143**, 4301–4311 (2016).
53. Ulloa, B. A. et al. Definitive hematopoietic stem cells minimally contribute to embryonic hematopoiesis. *Cell Rep.* **36**, 1–17 (2021).
54. Chen, M. J. et al. Erythroid/myeloid progenitors and hematopoietic stem cells originate from distinct populations of endothelial cells. *Cell. Stem Cell.* **9**, 541–552 (2011).
55. Hadland, B. K. et al. A requirement for Notch1 distinguishes 2 phases of definitive hematopoiesis during development. *Blood* **104**, 3097–3105 (2004).
56. Rodrigues, N. P., Tipping, A. J., Wang, Z. & Enver, T. GATA-2 mediated regulation of normal hematopoietic stem/progenitor cell function, myelodysplasia and myeloid leukemia. *Int. J. Biochem Cell Biol.* **44**, 457–460 (2012).
57. Koga, S. et al. Cell-cycle-dependent oscillation of GATA2 expression in hematopoietic cells. *Blood* **109**, 4200–4208 (2007).
58. Eich, C. et al. In vivo single cell analysis reveals Gata2 dynamics in cells transitioning to hematopoietic fate. *J. Exp. Med.* **215**, 233–248 (2018).
59. Rosa, F. F. et al. Single-cell transcriptional profiling informs efficient reprogramming of human somatic cells to cross-presenting dendritic cells. *Sci. Immunol.* **7**, 1–18 (2022).
60. Ramakers, C., Ruijter, J. M., Deprez, R. H. L. & Moorman, A. F. Assumption-free analysis of quantitative real-time polymerase chain reaction (PCR) data. *Neurosci. Lett.* **339**, 62–66 (2003).
61. Schmidt, U., Weigert, M., Broaddus, C. & Myers, G. Cell detection with star-convex polygons. *Lect. Notes Computer Sci. (Including Subser. Lect. Notes Artif. Intell. Lect. Notes Bioinforma.)* **11071**, 265–273 (2018).
62. Ershov D. et al. Bringing TrackMate in the era of machine-learning and deep-learning. Preprint at *bioRxiv*. 2021.
63. Campbell, A. E., Hsiung, C. C. S. & Blobel, G. A. Comparative analysis of mitosis-specific antibodies for bulk purification of mitotic populations by fluorescence-activated cell sorting. *Biotechniques* **56**, 90–94 (2014).
64. Li, H. & Durbin, R. Fast and accurate short read alignment with Burrows-Wheeler transform. *Bioinformatics* **25**, 1754–1760 (2009).
65. Zhang, Y. et al. Model-based analysis of ChIP-Seq (MACS). *pdf. Genome Biol.* **9**, 1–9 (2008).
66. Yu, G., Wang, L. G. & He, Q. Y. ChIP seeker: An R/Bioconductor package for ChIP peak annotation, comparison and visualization. *Bioinformatics* **31**, 2382–2383 (2015).
67. Ramirez, F. et al. deepTools2: a next-generation web server for deep-sequencing data analysis. *Nucleic Acids Res.* **44**, W160–W165 (2016).
68. McLean, C. Y. et al. GREAT improves functional interpretation of cis-regulatory regions. *Nat. Biotechnol.* **28**, 495–501 (2010).
69. Heinz, S. et al. Simple combinations of lineage-determining transcription factors prime cis-regulatory elements required for macrophage and b cell identities. *Mol. Cell.* **38**, 576–589 (2010).
70. Ernst, J. & Kellis, M. ChromHMM: automating chromatin-state discovery and characterization. *Nat. Methods* **9**, 215–216 (2012).
71. Zheng, G. X. Y. et al. Massively parallel digital transcriptional profiling of single cells. *Nat. Commun.* **8**, 14049 (2017).
72. Dobin, A. et al. STAR: ultrafast universal RNA-seq aligner. *Bioinformatics* **29**, 15–21 (2013).

## Acknowledgements

We thank the members of the Cell Reprogramming in Haematopoiesis and Immunity Laboratory for useful discussions. We thank Dr. Sjaak Philipsen (Erasmus MC, Netherlands) for kindly providing the GATA2 deletion constructs, as well as Dr. Gerd Blobel (University of Pennsylvania, USA) for the MD-GATA1 and MD<sub>mut</sub>-GATA1 plasmids and sequences. We also thank Dame Amanda Fisher (Imperial College London, UK) for her critical input. We thank the Center for Translational Genomics and Clinical Genomics Lund (SciLifeLab) for providing sequencing services and Lund University Bioimaging Center for microscopy assistance. We also thank Lund Stem Cell Center FACS Facility for cell sorting, and the Centre for Comparative Medicine for animal facilities, particularly Rosa-Linda Meza and Sofia Ekbjörn for handling the mouse models used in this study. This project has received funding (C.-F.P.) from the Olle Engkvist Foundation (194-0694), FCT (2022.02338.PTDC) and Plano de Recuperação e Resiliência de Portugal pelo fundo *NextGenerationEU* (C644865576-00000005). We would like to acknowledge the Knut and Alice Wallenberg foundation, the Medical Faculty at Lund University and Region Skåne for financial support. R.S.-A. received funding from the Royal Physiographic Society of Lund. Research in the de Bruijn group was supported by a program in the MRC Molecular Haematology Unit Core award (MC\_UU\_00016/02). C.V.E. is supported by a Marie Curie postdoctoral fellowship (101067501). R.S.-A. and A.G.F. are supported by FCT scholarships with references PD/BD/135725/2018 and SFRH/BD/133233/2017, respectively.

## Author contributions

R.S.-A. and C.-F.P. were responsible for conceptualisation and experimental design. R.S.-A., J.H., L.T. and A.L. cloned fusion proteins, performed live-cell imaging, immunofluorescence, and western blotting. C.V.E. performed RT-qPCR experiments and quantification of mitotic events. R.S.-A. performed homogenic reprogramming experiments and flow cytometry analysis. R.S.-A. and A.G.F. FACS-purified cells for protein degradation and ChIP-seq experiments. J.M.-G. and R.B. designed and generated the MD/MDmut-GATA2 mouse models. R.S.-A., A.R. and J.L. performed transplantation assays and interpreted the data. R.S.-A. isolated and dissociated embryonic tissues. M.N., C.R. and M.F.T.R.B. performed whole-embryo microscopy and M.N. quantified hematopoietic clusters. I.K. analysed ChIP-seq and scRNA-seq data. R.S.-A. and C.-F.P. wrote the manuscript. All authors contributed to data interpretation and manuscript revision.

## Funding

Open access funding provided by Lund University.

## Competing interests

The authors declare no competing interests.

**Additional information**

**Supplementary information** The online version contains supplementary material available at <https://doi.org/10.1038/s41467-023-40391-x>.

**Correspondence** and requests for materials should be addressed to Carlos-Filipe Pereira.

**Peer review information** *Nature Communications* thanks the anonymous reviewer(s) for their contribution to the peer review of this work. A peer review file is available.

**Reprints and permissions information** is available at <http://www.nature.com/reprints>

**Publisher's note** Springer Nature remains neutral with regard to jurisdictional claims in published maps and institutional affiliations.

**Open Access** This article is licensed under a Creative Commons Attribution 4.0 International License, which permits use, sharing, adaptation, distribution and reproduction in any medium or format, as long as you give appropriate credit to the original author(s) and the source, provide a link to the Creative Commons license, and indicate if changes were made. The images or other third party material in this article are included in the article's Creative Commons license, unless indicated otherwise in a credit line to the material. If material is not included in the article's Creative Commons license and your intended use is not permitted by statutory regulation or exceeds the permitted use, you will need to obtain permission directly from the copyright holder. To view a copy of this license, visit <http://creativecommons.org/licenses/by/4.0/>.

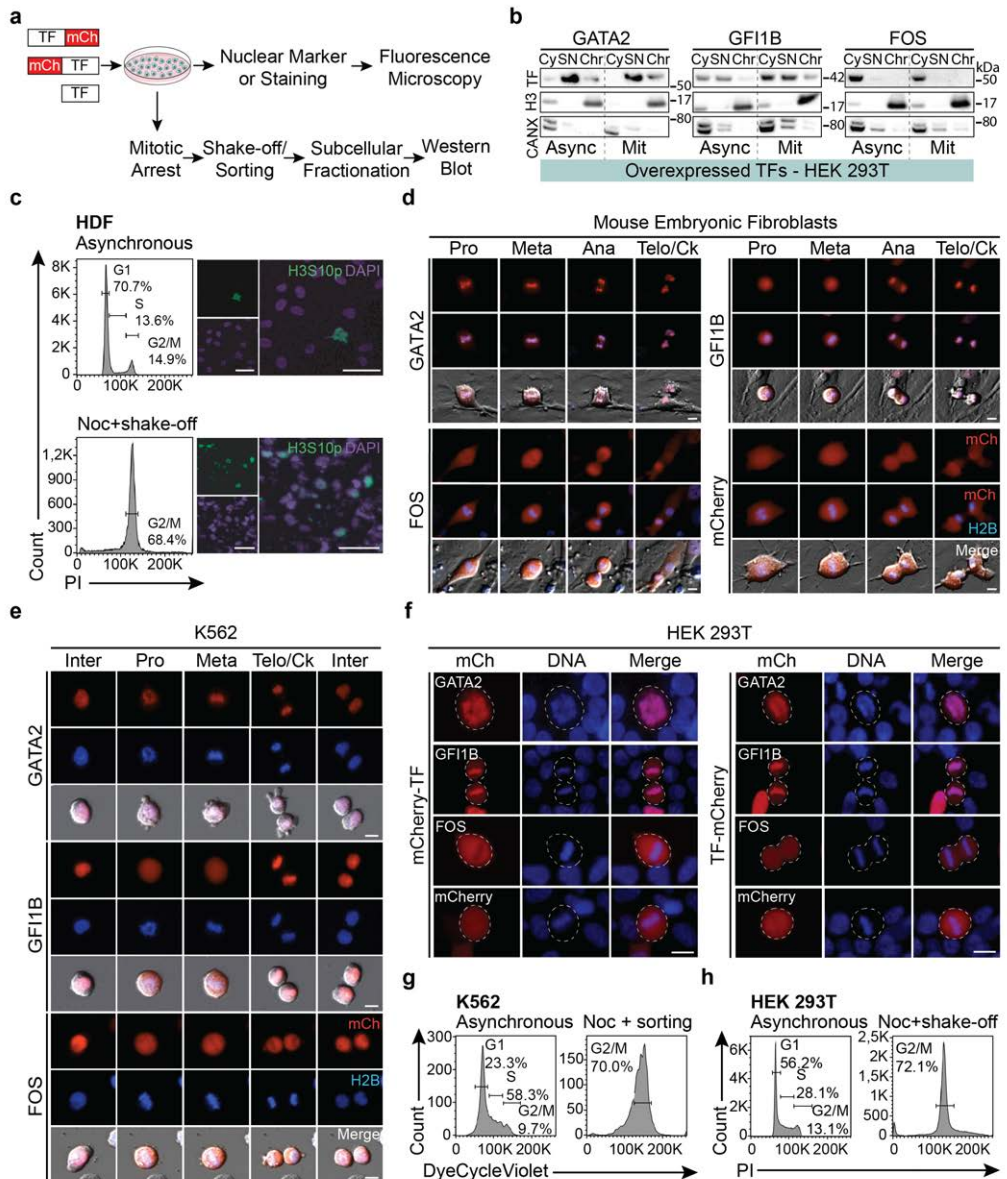
© The Author(s) 2023





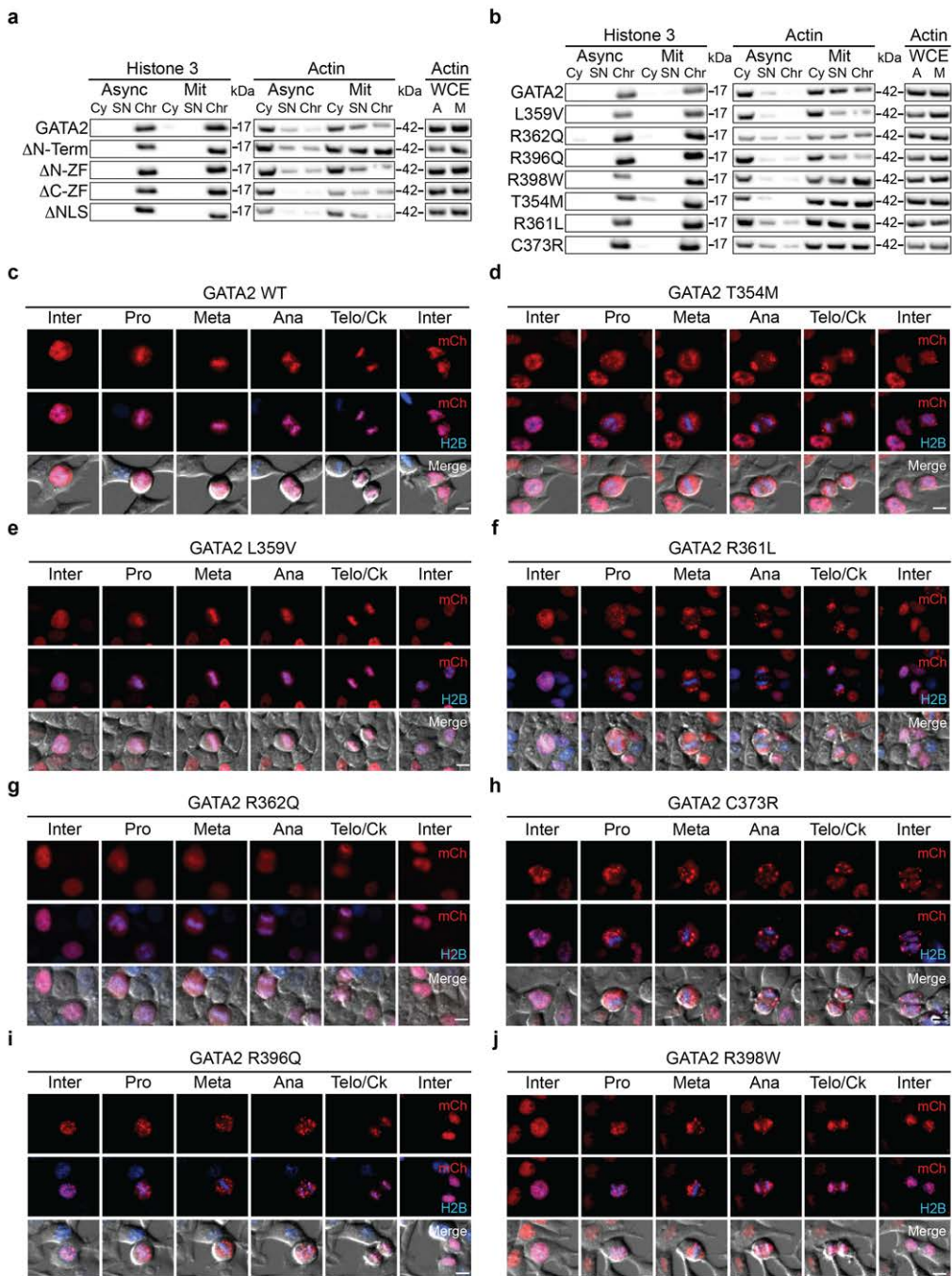
## Supplementary Information

### GATA2 mitotic bookmarking is required for definitive haematopoiesis



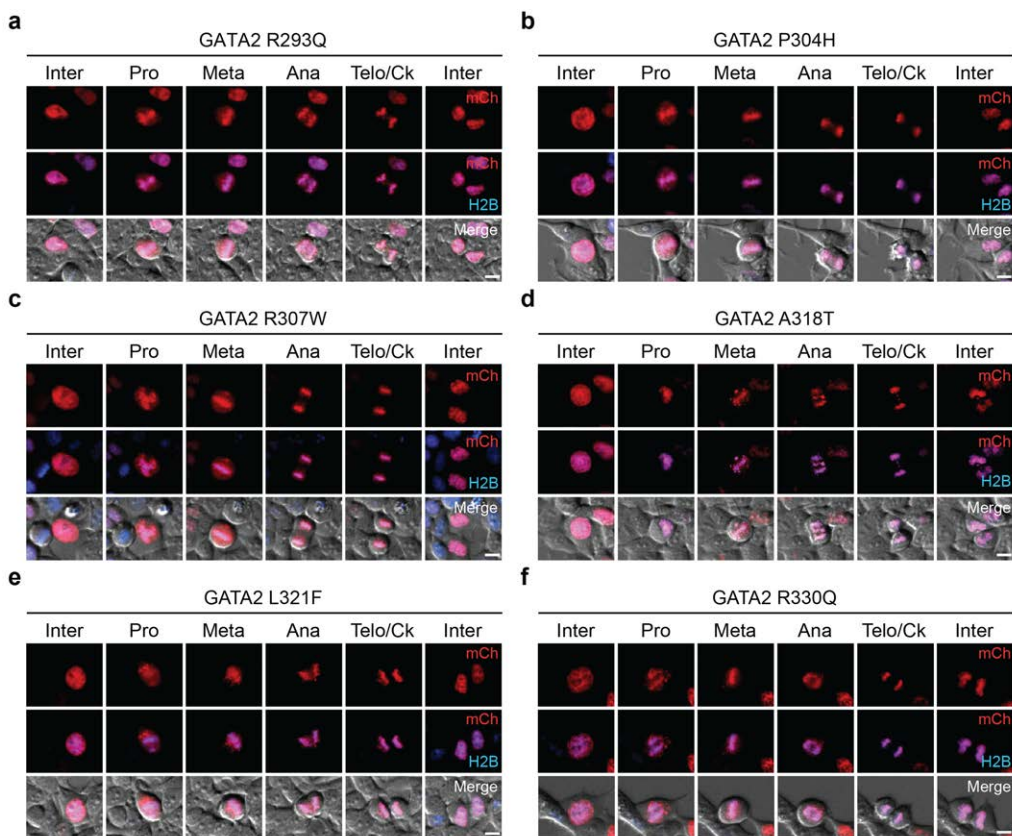
**Supplementary Fig. 1. GATA2, GF11B and FOS chromatin retention in mitotic cells. a,** Strategy to assess mitotic chromatin retention. Individual transcription factors (TFs) were fused to mCherry (mCh) fluorescent protein upstream or downstream TF sequence and mouse embryonic

fibroblasts, human dermal fibroblasts (HDFs), K562 or HEK 293T cells analysed by live-cell imaging. In parallel, HDFs, K562 or HEK 293T cells were arrested in pro-metaphase with nocodazole followed by subcellular protein fractionation and protein levels were detected by western blot. **b**, TF expression in cytoplasmic (Cy), soluble nucleus (SN) and chromatin-bound (Chr) protein fractions of asynchronous (Async) and mitotic (Mit) HEK 293T cells, after overexpression of the indicated TF. Calnexin (CANX) and histone 3 (H3) represent loading controls. Western blots were performed once. kDa, kilodaltons. **c**, Flow cytometry cell cycle analysis (left) and immunofluorescence (right) for the mitotic marker histone H3 phosphorylated at serine 10 (H3S10p) in asynchronous and mitotic HDFs after nocodazole (Noc) treatment and mitotic shake-off. Nuclei were stained with DAPI. Scale bar = 100  $\mu$ m. Experiment was performed once. **d**, Live-cell images of mouse embryonic fibroblasts overexpressing mCh-TF fusion proteins during mitosis (Pro – prophase, Meta – metaphase, Telo/Ck – Telophase/Cytokinesis). DNA content is represented by histone 2B (H2B)-mTurquoise signal. Scale bar = 10  $\mu$ m. Mitotic events: n(GATA2)=31, n(FOS)=36, n(GFI1B)=31, n(mCherry)=19. **e**, Live-cell images of K562 cells overexpressing mCh-GATA2 or mCh-GFI1B fusions during interphase (Inter) and mitosis. Mitotic events: n(GATA2)=28, n(FOS)=35, n(GFI1B)=74. Scale bar = 10  $\mu$ m. **f**, Live-cell images of HEK 293T cells overexpressing mCherry fused to the N-terminal (mCherry-TF) or C-terminal (TF-mCherry) of the 3 TFs during mitosis. Hoechst marks DNA. Scale bar = 10  $\mu$ m. **g**, Flow cytometry cell cycle analysis of asynchronous and nocodazole (Noc) treated K562 cells with the permeable DNA stain Vybrant DyeCycle Violet. For western blot quantifications, live mitotic cells were FACS sorted using the indicated G2/M gate. **h**, Cell cycle analysis of asynchronous and nocodazole (Noc) arrested HEK 293T cells after mitotic shake-off. Experiment was performed once. PI – propidium iodide.

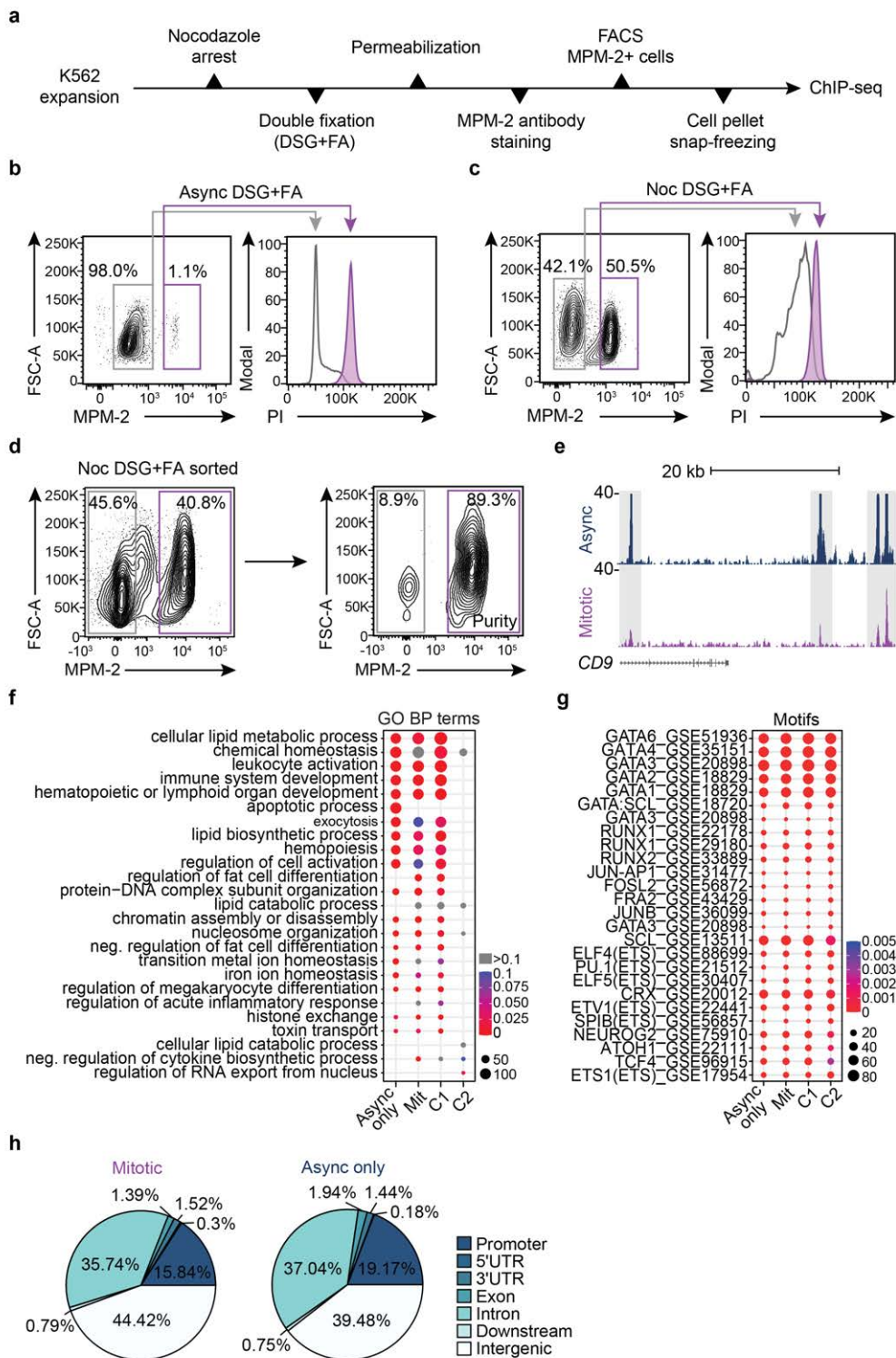


**Supplementary Fig. 2. Chromatin retention of GATA2 is reduced by mutations in the C-terminal zinc finger (C-ZF).** a, b, Western blot analysis of actin and histone 3 loading controls

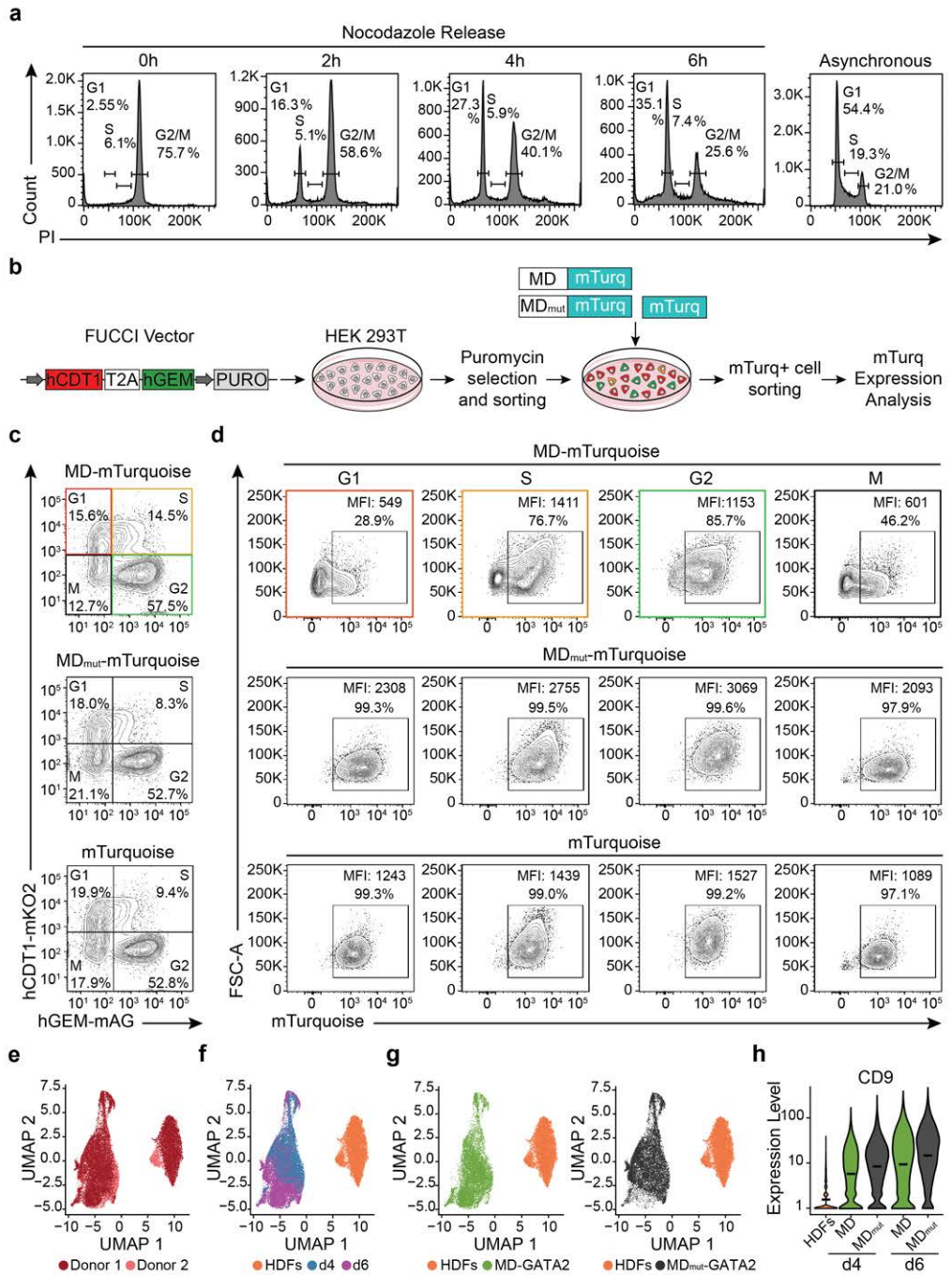
for mCherry-GATA2 deletion constructs (**a**) and mutant proteins (**b**) in whole-cell extracts (WCE) and protein fractionations of asynchronous (A, Async) and mitotic (M, Mit) HEK 293T cells. Bands were acquired using the same exposure times for asynchronous and mitotic cells, depending on the antibody and protein isolation method. Western blots were repeated at least three times. Cy, cytoplasmic protein fraction. SN, soluble nucleus protein fraction. Chr, chromatin-bound protein fraction. kDA, kilodaltons. **c-j**, Live-cell images of HEK 293T cells overexpressing mCherry (mCh)-GATA2 (red) wild-type (WT) (**c**) and GATA2 proteins mutated in C-ZF in positions T354M (**d**), L359V (**e**), R361L (**f**), R362Q (**g**), C373R (**h**), R396Q (**i**) and R398W (**j**) in interphase (Inter) and mitosis (Pro – prophase, Meta – metaphase, Telo/Ck – Telophase/Cytokinesis). The first letter represents the wild-type amino acid, followed by the position and the replaced amino acid. DNA is marked by histone 2B (H2B)-mTurquoise (blue). Scale bars = 10  $\mu$ m. Mitotic events: n(GATA2)=219, n(T354M)=724, n(L359V)=78, n(R361L)=165, n(R362Q)=18, n(C373R)=360, n(R396Q)=151, n(R398W)=147.



**Supplementary Fig. 3. Chromatin retention of GATA2 is not impacted by mutations in the N-terminal zinc finger (N-ZF).** **a-f**, Live-cell images of HEK 293T cells overexpressing mCherry (mCh)-GATA2 (red) proteins mutated in N-ZF in positions R293Q (**a**), P304H (**b**), R307W (**c**), A318T (**d**), L321F (**e**), R330Q (**f**) in interphase (Inter) and mitosis (Pro – prophase, Meta – metaphase, Telo/Ck – Telophase/Cytokinesis). The first letter represents the wild-type amino acid, followed by the position and the replaced amino acid. DNA is marked by histone 2B (H2B)-mTurquoise (blue). Scale bars = 10  $\mu$ m. Mitotic events: n(R293Q)=73, n(P304H)=151, n(R307W)=172, n(A318T)=296, n(L321F)=290, n(R330Q)=92.



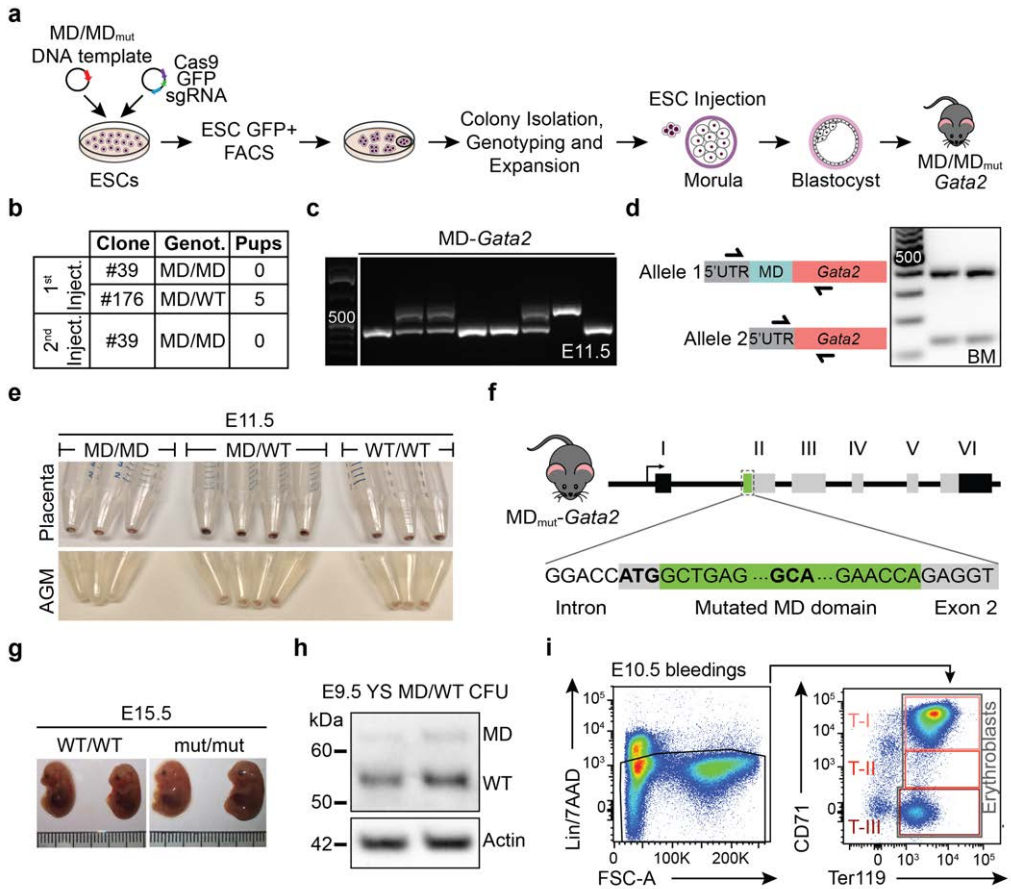
**Supplementary Fig. 4. Sorting strategy for Chromatin Immunoprecipitation followed by sequencing (ChIP-seq) of mitotic K562 cells and complementary analyses.** **a**, Outline of mitotic K562 fixation and FACS sorting steps. K562 were arrested with 0.2  $\mu\text{g}/\text{mL}$  nocodazole for 12-14h and fixed with 2mM Di(N-succinimidyl) glutarate (DSG) before fixation with 1% formaldehyde (FA). After that, cells were permeabilized and stained with anti-phospho-Ser/Thr-Pro MPM-2 primary antibody and anti-mouse AF647 secondary antibody. MPM-2 antibody recognizes several phosphorylated proteins during mitosis. Cells positive for MPM-2 were FACS sorted, washed and cell pellets were snap-frozen for ChIP. **b**, Quantification of interphasic and mitotic K562 cells after double fixation. Mitotic cells were identified in the 4N peak according to propidium iodide (PI) staining. **c**, Quantification of interphasic and mitotic K562 cells after nocodazole treatment and double fixation. **d**, Gating strategy to sort MPM-2 positive nocodazole treated K562 cells after double fixation. Mitotic cell purity after sorting is shown. **e**, Gene tracks for GATA2 binding sites at *CD9 locus*. Bookmarked sites are highlighted in grey. **f**, Gene Ontology (GO) biological processes (BP) for the top 1,000 gene-related peaks in non-bookmarked genes in asynchronous cells (Async only), mitotic (Mit) and mitotic clusters 1 (C1) and 2 (C2). Categories that contain more than 5 peaks per category are displayed. Coloured scale represents the adjusted  $p$ -value and the circle size the number of peaks per group. **g**, Motif discovery analysis for GATA2 target sites per group of peaks. Coloured scale represents the adjusted  $p$ -value and the circle size the percentage of peaks containing a particular motif. **h**, Gene body distribution of Mit and Async only GATA2 binding sites.



**Supplementary Fig. 5. Protein degradation driven by the mitotic degradation (MD) domain of cyclin B1 delays hemogenic reprogramming. a, Cell cycle analysis of asynchronous and**

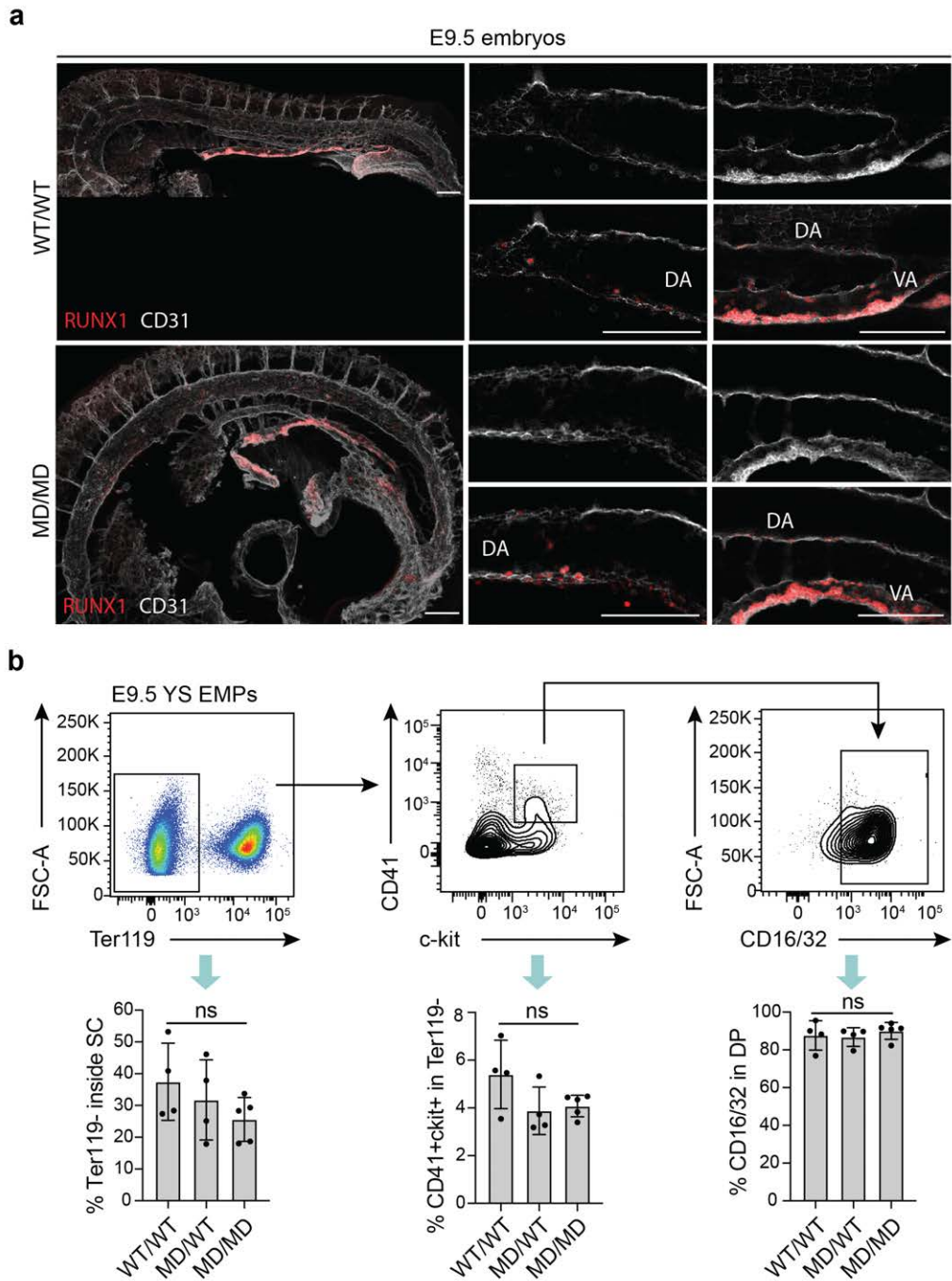


nocodazole treated HEK 293T cells before (0h) and 2, 4 and 6 hours (h) after release from nocodazole arrest. PI – propidium iodide. Percentage of cells in G1, S and G2/M phases of the cell cycle are indicated. **b**, Experimental strategy to assess mTurquoise (mTurq) protein degradation when fused to the MD domain or a mutated non-functional version (MD<sub>mut</sub>). HEK 293T cell line stably expressing a fluorescent ubiquitination-based cell cycle indicator (FUCCI) vector was generated by transduction with a FUCCI lentiviral vector, encoding a puromycin (Puro) resistance gene. After puromycin selection and purification of GFP<sup>+</sup> cells by FACS, cells were transduced with lentiviral vectors encoding MD-mTurquoise, MD<sub>mut</sub>-mTurquoise or mTurquoise. mTurquoise<sup>+</sup> cells were FACS sorted, plated and mTurquoise expression was measured 48 hours later by flow cytometry. hCDT1 – human CDT1 fused to mKusabira-Orange2 (mKO2). hGEM – human Geminin fused to mAzamiGreen (mAG). **c**, Flow cytometry plots showing the separation of cell cycle populations: interphase – G1 (red – mKO2+mAG-), S (yellow – mKO2+mAG+) and G2 (green – mKO2-mAG+), and mitosis – M (black – mKO2-mAG-) of cells expressing MD/MD<sub>mut</sub>-mTurquoise or mTurquoise alone. **d**, Flow cytometry plots showing mTurquoise expression gated within each cell cycle phase population. MFI – mean fluorescence intensity. **e-g**, Uniform Manifold Approximation and Projection (UMAP) analysis of 32,773 single transcriptomes of FACS sorted, live (Dapi-) human dermal fibroblasts (HDFs) and HDFs undergoing hemogenic reprogramming with overexpression of GFI1B, FOS and MD-GATA2 or GFI1B, FOS and MD<sub>mut</sub>-GATA2 from two donors. **(e)** shows single cells coloured by donor (Donor 1 and Donor 2) **(f)** highlights untransduced HDFs and reprogrammed cells at day (d) 4 and d6 and **(g)** shows transduced cells with either MD-GATA2 (left) or MD<sub>mut</sub>-GATA2 (right). **h**, Expression levels of the *CD9* gene in untransduced HDFs and in MD-GATA2 or MD<sub>mut</sub>-GATA2 transduced cells at d4 and d6 of hemogenic reprogramming. Mean is represented.



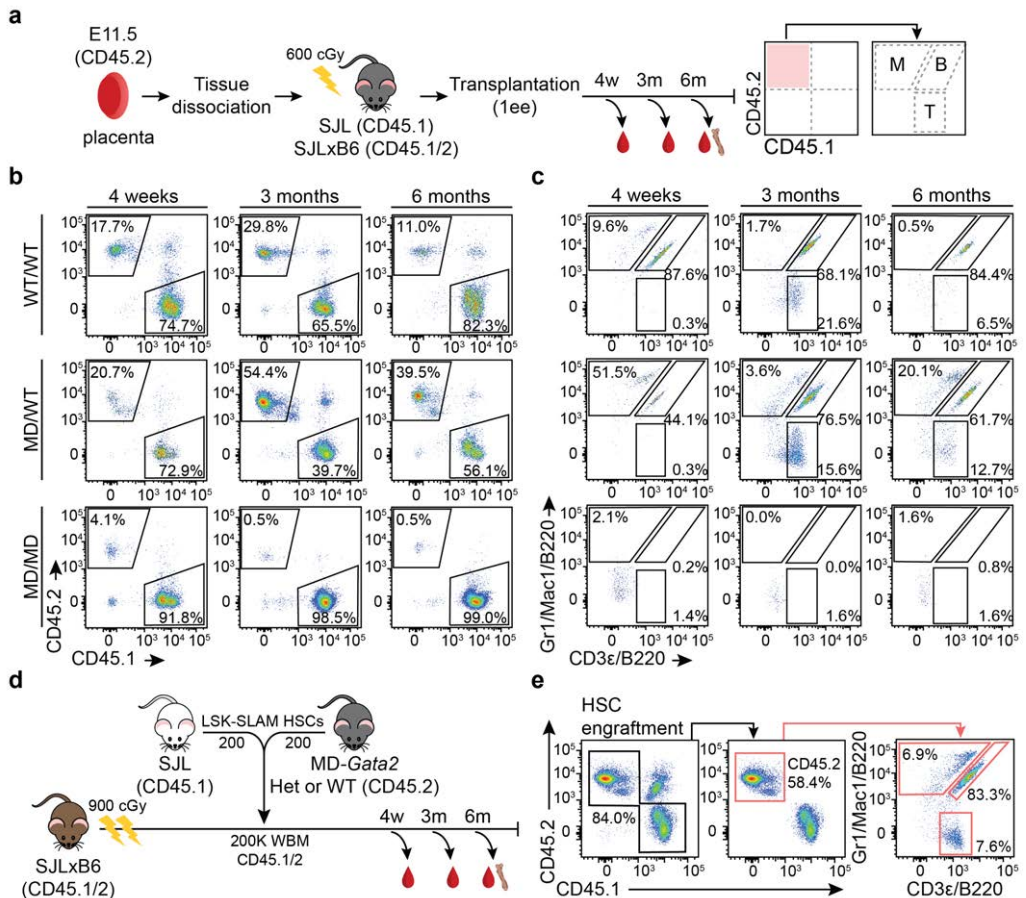
**Supplementary Fig. 6. Characterisation of MD- and MD<sub>mut</sub>-Gata2 mouse models.** **a**, Strategy to generate a mouse model to assess the role of mitotic bookmarking by GATA2 *in vivo*. The mitotic degradation (MD) domain of cyclin B1 and a mutated non-functional domain (MD<sub>mut</sub>) template sequences were delivered in a pMX plasmid to mouse embryonic stem cells (ESCs) together with a pX458-GFP vector containing a single guide (sg) RNA for *Gata2* start codon region. GFP<sup>+</sup> cells were FACS sorted, and individual clones were isolated, genotyped, expanded and injected into mouse morulae to generate both MD-*Gata2* and MD<sub>mut</sub>-*Gata2* models. **b**, Number of pups obtained after two independent morula injections with homozygous or heterozygous ESC clones for the MD insert. **c**, Genotyping of embryonic day (E) 11.5 embryos after crossing heterozygous MD-*Gata2* mice. A 630 base pairs band indicates the presence of the

insert while a lower band of 400 bps represents the wild-type (WT) *Gata2* allele. Genotyping was performed in individual embryos or adult mice before each experiment. **d**, Gene expression of the MD and *Gata2* WT alleles. mRNA of sorted LSK cells from bone marrow (BM) heterozygous mice were isolated, reverse transcribed and amplified by PCR. The stronger, heavier band corresponds to the MD sequence. Experiment was performed once with cells from 3 different adult heterozygous mice. Representative results for two mice are shown. **e**, Representative pictures of placenta pellets and caudal regions isolated from single E11.5 embryos after tissue dissociation. **f**, Scheme showing the insertion of the MD<sub>mut</sub> domain after the ATG of the *Gata2* gene in exon 2. **g**, Representative images of MD<sub>mut</sub>-*Gata2* embryos at E15.5. Scale bar = 1 mm. **h**, Western blot analysis of heterozygous MD-GATA2 E9.5 yolk sac-derived hematopoietic colonies after 6 days of culture. Bands corresponding to MD-GATA2 (MD) and wild-type (WT) proteins are shown. Experiment was performed once with cells from 4 different embryos. Representative results for two embryos are shown. kDa, kilodaltons. **i**, Representative flow cytometry plots of erythroblast quantification after whole embryo bleeding to assess erythroid output. MD-*Gata2* embryonic blood was stained with lineage antibodies (B220/CD3ε/Mac1/Gr1) and the erythroblast markers CD71 and Ter119. Live lineage negative cells (Lin-7AAD-) were gated into three types of erythroblasts from immature to more mature red blood cells (Type I-III) according to the expression of CD71 and Ter119. The grey gate includes all erythroblasts.



**Supplementary Fig. 7. Haematopoiesis is not impaired in MD-*Gata2* homozygous embryos at embryonic day 9.5.** a, Immunohistochemistry images of whole mounted E9.5 WT and MD

homozygous embryos showing vasculature expressing RUNX1 (red) and CD31 (white), highlighting the dorsal aorta (DA) and vitelline arteries (VA). Scale bars = 100  $\mu$ m. **b**, E9.5 yolk sac (YS) erythro-myeloid progenitor (EMPs) staining. Yolk sacs from E9.5 embryos were isolated, dissociated and stained with Ter119, c-kit, FITC-CD41 and CD16/32. EMPs were defined as Ter119-CD41<sup>+</sup>c-kit<sup>+</sup>CD16/32<sup>+</sup>. Representative plots with gating strategy (left) and percentage of each respective cell population (right) are shown (n=4). SC – single cells. DP – double positive. Mean $\pm$ SD is represented. Statistical significance was analysed by one-way ANOVA followed by Bonferroni's multiple comparison test. ns – nonsignificant.



**Supplementary Fig. 8. Embryonic and adult transplantation strategies to assess the role of GATA2 at mitosis-to-G1 transition for HSPC generation and maintenance.** **a**, E11.5 placentas were isolated, dissociated and transplanted as one embryo equivalent (ee) into sub-lethally irradiated B6.SJL (CD45.1) or C57BL/6JxB6.SJL (CD45.1/2) mice. Mice were bled 4 weeks (w), 3 months (m), and 6 months after transplantation to assess donor engraftment (CD45.2+) and contribution to myeloid (M), B-cell (B) and T-cell (T) lineages. Hosts' bone marrow cells from the left leg and ilium bones were isolated at the experimental end-point of 6 months and analysed in a similar manner. **b**, Representative flow cytometry plots with the gating strategy to evaluate donor chimerism (CD45.2+). Only mice with donor chimerism above the 1% threshold were considered in this analysis. **c**, Gating strategy for assessing the percentage of myeloid

(Gr1+Mac1+), B- (B220+) and T- (CD3ε+) donor-derived cells. **d**, Competitive transplantation strategy to address function of adult bone marrow HSCs. Two hundred Lineage-Sca-1<sup>+</sup>Kit<sup>+</sup>CD150<sup>+</sup>CD48<sup>-</sup> LSK-SLAM HSCs from a competitor CD45.1 SLJ mouse or from MD/WT or WT/WT MD-*Gata2* mice were FACS purified, mixed 1:1 and injected into lethally irradiated CD45.1/2 hosts, together with 200,000 support whole bone marrow (WBM) cells. Blood was collected for analysis 4w, 3m and 6m after transplantation to assess donor engraftment (CD45.2+) and contribution to myeloid, B-cell and T-cell lineages. Recipients' bone marrow was analysed at the experimental end-point of 6 months. **e**, Representative gating strategy to evaluate donor chimerism (CD45.2+) and for assessing the percentage of myeloid (Gr1+Mac1+), B- (B220+) and T- (CD3ε+) donor-derived cells.







## About the author

---



Rita Alves received her bachelor's degree in biomedical sciences from the University of Aveiro (Portugal) in 2015. Captivated by the fields of cellular and molecular biology, Rita joined the Pereira Lab at the University of Coimbra (Portugal) for her master's degree in Biochemistry, where she explored cell fate conversions, particularly somatic cell reprogramming into hematopoietic stem cells. This ignited her passion for direct cell reprogramming as a platform for studying complex developmental processes. In 2018, she moved to Sweden to continue her studies in the same group and pursue a PhD at the Department of Laboratory Medicine, Lund University, with focus on investigating the molecular mechanisms underpinning hematopoietic stem cell generation.

